Advances in High Energy Physics

Dark Matter and Dark Energy in General Relativity and Modified Theories of Gravity

Lead Guest Editor: Irina Radinschi
Guest Editors: Farook Rahaman, Cesar A. Vasconcellos, Saibal Ray, and Theophanes Grammenos

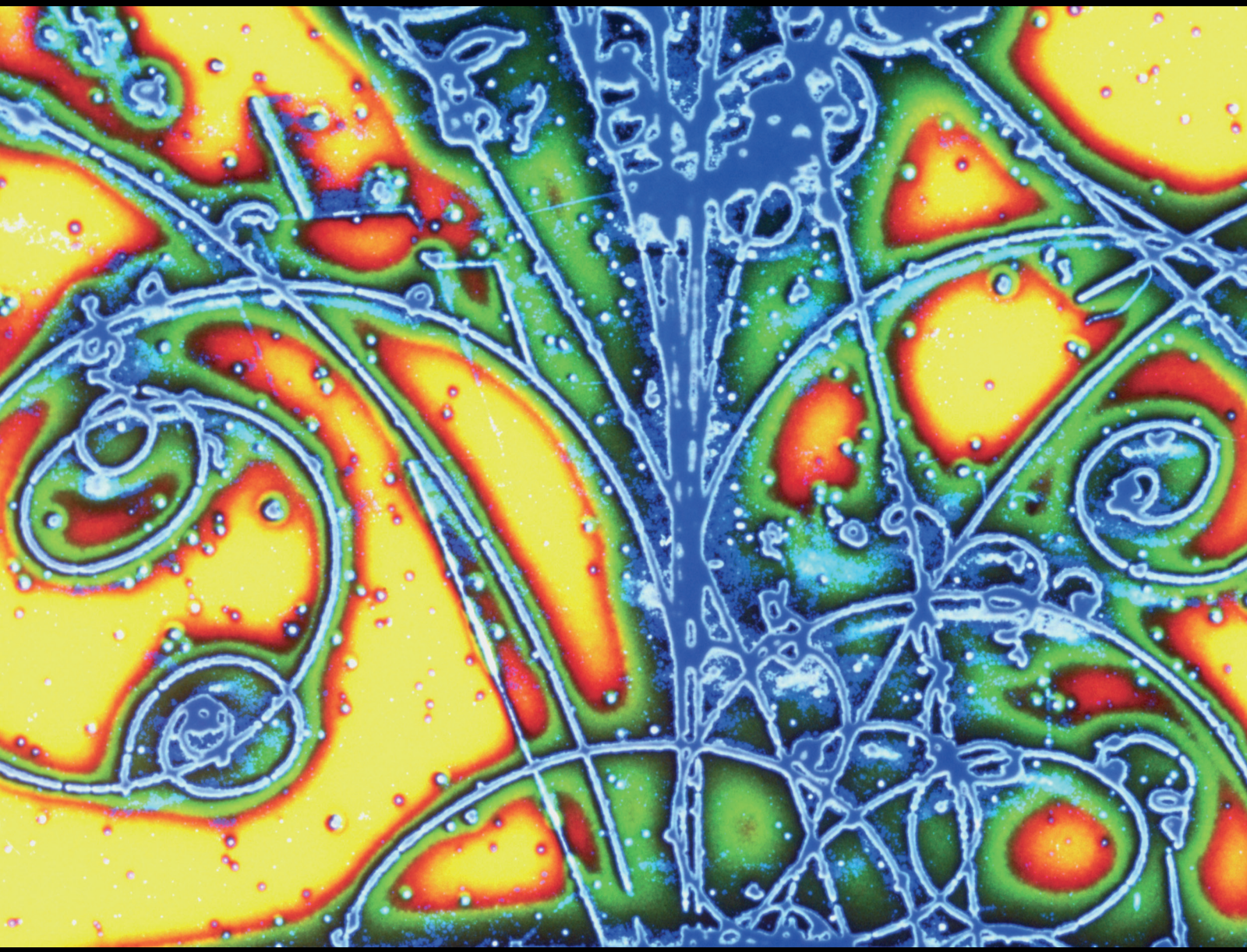

Dark Matter and Dark Energy in General Relativity and Modified Theories of Gravity

Advances in High Energy Physics

Dark Matter and Dark Energy in General Relativity and Modified Theories of Gravity

Lead Guest Editor: Irina Radinschi
Guest Editors: Farook Rahaman, Cesar A. Vasconcellos, Saibal Ray, and Theophanes Grammenos

Contents

Expression of Concern on "Antigravity, an Answer to Nature's Phenomena including the Expansion of the Universe"
Advances in High Energy Physics
Expression of Concern (1 page), Article ID 9380814, Volume 2021 (2021)

Emergence of Warm Inflation in Curved Space-Time between Accelerating Branes
Aroonkumar Beesham
Research Article (15 pages), Article ID 3963279, Volume 2020 (2020)

Generalized Phenomenological Models of Dark Energy
Prasenjit Paul and Rikpratik Sengupta
Research Article (8 pages), Article ID 5249839, Volume 2020 (2020)

Phase Structure and Quasinormal Modes of AdS Black Holes in Rastall Theory
De-Cheng Zou, Ming Zhang, and Ruihong Yue
Research Article (9 pages), Article ID 8039183, Volume 2020 (2020)

Effects of Quintessence Dark Energy on the Action Growth and Butterfly Velocity
Hossein Ghaffarnejad, Mohammad Farsam, and Emad Yaraie
Research Article (7 pages), Article ID 9529356, Volume 2020 (2020)

Antigravity, an Answer to Nature's Phenomena including the Expansion of the Universe
C. K. Gamini Piyadasa
Review Article (5 pages), Article ID 9315491, Volume 2020 (2020)

Modeling Dark Sector in Horndeski Gravity at First-Order Formalism
F. F. Santos, R. M. P. Neves, and F. A. Brito
Research Article (8 pages), Article ID 3486805, Volume 2019 (2019)

Modified Fermions Tunneling Radiation from Nonstationary, Axially Symmetric Kerr Black Hole
Jin Pu, Kai Lin, Xiao-Tao Zu, and Shu-Zheng Yang
Research Article (7 pages), Article ID 5864042, Volume 2019 (2019)

Review on the Pseudocomplex General Relativity and Dark Energy
Peter O. Hess
Review Article (11 pages), Article ID 1840360, Volume 2019 (2019)

Perihelion Advance and Trajectory of Charged Test Particles in Reissner-Nordstrom Field via the Higher-Order Geodesic Deviations
Malihe Heydari-Fard, Saeed Fakhry, and Seyedeh Nahid Hasani
Research Article (10 pages), Article ID 1879568, Volume 2019 (2019)

Cosmological Analysis of Modified Holographic Ricci Dark Energy in Chern-Simons Modified Gravity
Sarfraz Ali and M. Jamil Amir
Research Article (9 pages), Article ID 3709472, Volume 2019 (2019)

Hindawi
Advances in High Energy Physics
Volume 2021, Article ID 9380814, 1 page
https://doi.org/10.1155/2021/9380814

Expression of Concern

Expression of Concern on "Antigravity, an Answer to Nature's Phenomena including the Expansion of the Universe"

Advances in High Energy Physics

Received 21 September 2020; Accepted 21 September 2020; Published 17 April 2021

Advances in High Energy Physics would like to express concern with the article titled "Antigravity, an Answer to Nature's Phenomena including the Expansion of the Universe" [1], which reviews the author's previous studies.

Following the publication of the review article, concerns have been identified that the discussion is qualitative and without any concrete model supporting the ideas presented. The concept that clouds experience anti-gravity proportional to the temperature of water droplets appears unsustainable, as well as the idea that thermal energy produced by the stars can explain the accelerating universe. Both ideas lack a concrete model, and it is unlikely that such a model can exist. If the observations presented in the article are assumed to be correct, a model would be required to test the hypothesis. The possibility of such testing is doubtful. We additionally note that the author's previous work, reviewed in the article, has not been cited by other researchers.

References

[1] C. K. Piyadasa Gamini, "Antigravity, an answer to Nature's phenomena including the expansion of the universe," *Advances in High Energy Physics*, vol. 2020, Article ID 9315491, 5 pages, 2020.

Hindawi
Advances in High Energy Physics
Volume 2020, Article ID 3963279, 15 pages
https://doi.org/10.1155/2020/3963279

Research Article

Emergence of Warm Inflation in Curved Space-Time between Accelerating Branes

Aroonkumar Beesham

Faculty of Natural Sciences, Mangosuthu University of Technology, 511 Griffiths Mxenge Highway, Umlazi, Durban 4031, South Africa

Correspondence should be addressed to Aroonkumar Beesham; abeesham@yahoo.com

Received 5 August 2019; Revised 19 January 2020; Accepted 24 January 2020; Published 21 February 2020

Guest Editor: Saibal Ray

It appears that having our own brane to somehow interact with other branes could give rise to quite an interesting system and that interaction could lead to some observable effects. We consider the question of whether or not these signatures of interaction between the branes can be observed. To answer this question, we investigate the effect induced by the inflaton in the WMAP7 data using the warm inflationary model. In this model, slow-roll and perturbation parameters are given in terms of the inflaton thermal distribution. We show that this distribution depends on the orbital radius of the brane motion under the interaction potential of other branes in extra dimensions. Thus, an enhancement in the brane inflation can be a signature of an orbital motion in extra dimensions, and consequently, some signals of other branes can be detected by observational data. According to experimental data, the $N \simeq 50$ case leads to $n_s \simeq 0.96$, where N and n_s are the number of e-folds and the spectral index, respectively. This standard case may be found in the range $0.01 < R_{\text{tensor-scalar}} < 0.22$, where $R_{\text{tensor-scalar}}$ is the tensor-scalar ratio. We find that at this point, the radial distance between our brane and another brane is $R = (1.5\,\text{GeV})^{-1}$ in intermediate and $R = (0.02225\,\text{GeV})^{-1}$ in logamediate inflation.

1. Introduction

Recently, it was argued that the boundary conditions to be imposed on the quantum state of the whole multiverse could be such that brane universes could be created in entangled pairs [1]. Also, the consideration of entanglement between the quantum states of two or more brane universes in a multiverse scenario provides us with a completely new paradigm that opens the door to novel approaches for traditionally unsolved problems in cosmology, more precisely, the problems of the cosmological constant, the arrow of time, and the choice of boundary conditions, amongst others [2]. Some authors have tried to find direct evidence of the existence of other brane universes using a dark energy model [3, 4]. Also, some researchers show that other branes are made observable for us through interaction with our own brane [5]. In their paper, the orbital radius of our brane in extra dimensions can be described according to the interaction potential of other branes. In some scenarios, the properties of the interaction potential are calculated for a composite quantum state of two branes whose states are quantum mechanically correlated [1, 2]. It appears that having our own brane to somehow interact with other branes could give rise to quite an interesting system and that interaction could lead to an orbital motion in extra dimensions.

This scenario is very close to the well-known DGP model. Dvali et al. [6] proposed a new braneworld model, named the DGP model, having two branches. One branch is known as the accelerating branch, i.e., the accelerating phase of the universe can be explained without adding a cosmological constant or dark energy, whereas the latter one represents the decelerating branch. In this paper, we generalize this model and show that by the acceleration of branes, some extra fields emerge. These fields dissolve into branes and lead to inflation.

For this reason, these fields could be considered candidates for inflation.

The main question is the possibility of considering the properties of other branes against observational data. The warm inflationary model helps us to perform precision tests of the universal extra dimensional models and explore the new physics against observational data. In this scenario, after the period of inflation, the radiation of the universe becomes dominant and the reheating epoch will not happen. The results of this model are compatible with the WMAP7 and Planck data [7]. In this theory, slow-roll and perturbation parameters are given in terms of the thermal distribution of the inflaton. On the other hand, this distribution is given in terms of the orbital radius of the brane motion [5] in extra dimensions. As the interaction potential increases, the effect of the inflaton radiation from the horizon that appears in the brane-antibrane system on the universe's inflation becomes systematically more effective because at higher energies, there exist more channels for inflaton production and its decay into particles.

The outline of the paper is as follows. In Section 2, we consider the effect of the orbital radius of the brane motion under the interaction potential of the other branes on the thermal distribution of inflatons. In Section 3, using the warm inflationary model, we analyze the signature of other branes against observational data. The last section is devoted to a summary and conclusion.

2. The Thermal Distribution of Inflatons near the Appeared Horizon in the Brane-Antibrane System

Previously, the dynamical behavior of a pair of Dp and anti-Dp branes which move parallel to each other in the region that the brane and antibrane annihilation will not occur was considered [5]. Also, the orbital radius of the brane motion due to the interaction potential in extra dimensions was studied. Using these results, we calculate the thermal distribution of inflatons near the horizon that appears in the brane-antibrane system and show that the thermal distribution of inflatons can be given in terms of the orbital radius of the brane motion in extra dimensions.

The d-dimensional metric in the brane-antibrane system is expressed as

$$ds^2 = g_{\mu\nu}dx^\mu dx^\nu + g_{\rho\sigma}dx^\rho dx^\sigma + g_{ab}dx^a dx^b, \tag{1}$$

where $g_{\mu\nu}$ and $g_{\rho\sigma}$ are the p-dimensional metrics along the Dp and anti-Dp branes, respectively, and g_{ab} is the $(d\text{-}2p)$ dimensional metric along the transverse coordinates.

Now, let us consider the wave equation of the inflaton in extra dimensions between two branes:

$$\left\{-\frac{\partial^2}{c^2\partial\chi^2} + \frac{\partial^2}{\partial r^2}\right\}B = 0, \tag{2}$$

where χ and r are the transverse coordinates between the two branes. This equation corresponds to flat space-time. The interaction potential between the Dp brane and the anti-Dp brane in extra dimensions is of the type [5]

$$V(R) \sim \frac{64\pi^2\mu^4}{27}, \tag{3}$$

where $\mu^4 = (27/32\pi^2)T_3h^4$, $h(R) = b^4/R^4$, R is the orbital radius distance between the two branes, T_3 the brane tension, and b the curvature radius of the AdS_5 throat. This potential leads to curved space-time.

There are more models for interbrane potential; however, we make use of a symmetric model to explain the interaction between two parallel and similar branes. This helps us to understand the model better, and we could generalize it by adding more corrections due to the nonsymmetric part of potential. However, this is not the main thrust of this work.

Thus, to write the inflaton wave equation in curved space-time, we should use the following reparameterizations:

$$\begin{aligned} r &\longrightarrow \rho(r,\chi), \\ \chi &\longrightarrow \tau(r,\chi), \end{aligned} \tag{4}$$

that lead to the following inflaton wave equation:

$$\left[\left\{\left(\frac{\partial\tau}{\partial r}\right)^2 - \left(\frac{\partial\tau}{\partial\chi}\right)^2\right\}\frac{\partial^2}{c^2\partial\tau^2} + \left\{\left(\frac{\partial\rho}{\partial r}\right)^2 - \left(\frac{\partial\rho}{\partial\chi}\right)^2\right\}\frac{\partial^2}{\partial\rho^2}\right]B = 0. \tag{5}$$

We can normalize the distance between the two branes to unity by making the following choices:

$$\begin{aligned} \rho(r,\chi) &= \frac{r}{R(\chi)}, \\ \tau &= \beta c^2\int_0^\chi d\,t'\frac{R\left(\chi'\right)}{\dot{R}\left(\chi'\right)} - \beta\frac{r^2}{2}. \end{aligned} \tag{6}$$

With the above considerations, the wave equation is written as

$$(-g)^{1/2}\frac{\partial}{\partial x^\mu}\left[g^{\mu\nu}(-g)^{1/2}\frac{\partial}{\partial x^\mu}\right]B = 0, \tag{7}$$

where $x^5 = \tau$ and $x^4 = \rho$, and the metric elements are obtained as

$$\begin{aligned} g^{\tau\tau} &= -\frac{1}{\beta^2c^2}\left(\frac{R}{\dot{R}}\right)\left(\frac{1-\left(\dot{R}^2/c^2\right)\rho^2}{1+\left(\dot{R}/c^2\right)\rho^2}\right), \\ g^{44} &= R^2\left(\frac{1+\left(\dot{R}^2/c^2\right)\rho^2}{1-\left(\dot{R}/c^2\right)\rho^2}\right). \end{aligned} \tag{8}$$

The horizon of this system is located at

$$r_{\text{horizon}} = \frac{cR}{\dot{R}}, \tag{9}$$

where c is velocity of light. In Kruskal coordinates, the metric of the system becomes [8, 9]

$$\begin{aligned} ds^2 &= g_{\mu\nu}dx^\mu dx^\nu + g_{\rho\sigma}dx^\rho dx^\sigma \\ &\quad - r_{\text{horizon}}\frac{e^{-(r/r_{\text{horizon}})}}{r}d\bar{u}d\bar{v} + r^2 d\theta^2, \\ \bar{u} &= -2r_{\text{horizon}}e^{-u/2r_{\text{horizon}}},\ \bar{v} = -2r_{\text{horizon}}e^{-v/2r_{\text{horizon}}}, \\ u &= \chi - r^*,\ v = \chi + r^*, \quad r^* = -r - r_{\text{horizon}}\ln|r - r_{\text{horizon}}|. \end{aligned} \tag{10}$$

Since the Killing vector in Kruskal coordinates is given by $\partial/\partial\bar{u}$ on the past horizon H^-, the positive frequency normal mode solution in Kruskal coordinates is approximated by

$$B \propto e^{-i\omega\bar{u}}, \tag{11}$$

where ω is the inflaton energy in extra dimensions. Using this fact that $\bar{v} = 0$ on H^- [9], we can estimate the original positive frequency normal mode on the past horizon as

$$\begin{aligned} B \propto e^{-i\omega\bar{u}} &= \left(\frac{|\bar{u}|}{2r_{\text{horizon}}}\right)^{-i2r_{\text{horizon}}\omega} \\ &= \begin{cases} \left(-\bar{u}/2r_{\text{horizon}}\right)^{-i2r_{\text{horizon}}\omega}\ (\text{region I}), \\ \left(-\bar{u}/2r_{\text{horizon}}\right)^{-i2r_{\text{horizon}}r_{\text{horizon}}}\ (\text{region II}). \end{cases} \end{aligned} \tag{12}$$

In Equation (12), we can use the fact that $(-1)^{-i2r_{\text{horizon}}\omega} = e^{2r_{\text{horizon}}\omega}$. Using Equation (12), we observe that the inflaton states in the horizon satisfy the following condition [9, 10]:

$$\begin{aligned} (B_{\text{out}} - \tanh r_\omega B_{\text{in}})|\text{system}\rangle_{\text{in}\otimes\text{out}} = 0, \\ \tanh r_\omega = e^{-2r_{\text{horizon}}\omega}, \end{aligned} \tag{13}$$

which actually constitutes a boundary state. In fact, we can view Hawking radiation as the pair creation of a positive energy field that goes to infinity and a negative energy field that falls into the horizon of the brane-antibrane system. The pair is created in a particular entangled state. So the Unruh state can be viewed as an entangled thermal state. The above definition of the positive frequency solution in terms of B_{out} and B_{in} leads to the Bogoliubov transformation [8–10] for the particle creation and annihilation operators in the brane-antibrane system and Minkowski space-times in the exterior region of the system:

$$\begin{aligned} d &= \cosh r_\omega \alpha_{\text{out}} - \sinh r_\omega \alpha_{\text{in}}^\dagger, \\ d^\dagger &= \cosh r_\omega \alpha_{\text{out}}^\dagger - \sinh r_\omega \alpha_{\text{in}}, \\ \tanh r_\omega &= e^{-2\pi r_{\text{horizon}}\omega}, \end{aligned} \tag{14}$$

where $d^\dagger$ and d are the creation and annihilation operators, respectively, acting on the Minkowski vacuum, $\alpha_{\text{out}}^\dagger$ and α_{out} are the respective operators acting on the brane-antibrane vacuum outside the event horizon, and $\alpha_{\text{in}}^\dagger$ and α_{in} are the respective operators acting on the brane-antibrane vacuum inside the event horizon.

Thus, we can write the Bogoliubov transformation between the Minkowski and curved creation and annihilation operators as

$$d|\text{system}\rangle_{\text{out}\otimes\text{in}} = \left(\alpha_{\text{out}} - \tanh r_\omega \alpha_{\text{in}}^\dagger\right)|\text{system}\rangle_{\text{out}\otimes\text{in}} = 0, \tag{15}$$

which actually constitutes a boundary state. Now, we assume that the system vacuum $|\text{system}\rangle_{\text{out}\otimes\text{in}}$ is related to the flat vacuum $|0\rangle_{\text{flat}}$ by

$$|\text{system}\rangle_{\text{out}\otimes\text{in}} = F|0\rangle_{\text{flat}}, \tag{16}$$

where F is a function to be determined later.

From $[\alpha_{\text{out}}, \alpha_{\text{out}}^\dagger] = 1$, we obtain $[\alpha_{\text{out}}, (\alpha_{\text{out}}^\dagger)^m] = (\partial/\partial\alpha_{\text{out}}^\dagger)(\alpha_{\text{out}}^\dagger)^m$ and $[\alpha_{\text{out}}, F] = (\partial/\partial\alpha_{\text{out}}^\dagger)F$. Then, using Equations (15) and (16), we get the following differential equation for F:

$$\left(\frac{\partial F}{\partial\alpha_{\text{out}}^\dagger} - \tanh r_\omega \alpha_{\text{in}}^\dagger F\right) = 0, \tag{17}$$

and the solution is given by

$$F = e^{\tanh\ r_\omega \alpha_{\text{out}}^\dagger \alpha_{\text{in}}^\dagger}. \tag{18}$$

By substituting Equation (18) into Equation (16) and by properly normalizing the state vector, we get

$$\begin{aligned} |\text{system}\rangle_{\text{out}\otimes\text{in}} &= Ne^{\tanh\ r_\omega \alpha_{\text{in}}^\dagger \alpha_{\text{out}}^\dagger}|0\rangle_{\text{flat}} \\ &= \frac{1}{\cosh r_\omega}\sum_m \tanh^m r_\omega |m\rangle_{\text{out}} \otimes |\bar{m}\rangle_{\text{in}}, \end{aligned} \tag{19}$$

where $|m\rangle_{\text{in}}$ and $|\bar{m}\rangle_{\text{out}}$ are the orthonormal bases (normal mode solutions) for a particle that acts on H_{in} and H_{out}, respectively, and N is the normalization constant.

Equation (19) expresses that the states inside and outside the horizon are entangled. However, this entanglement depends on the event horizon and the horizon is given in terms of R, the orbital radius of the brane motion in the interaction potential of the other brane, $r_{\text{horizon}} = cR/R$, and consequently, the entanglement changes with the orbital radial distance between the two branes. We derive the thermal distribution for inflatons in extra dimensions as the following:

$$\begin{aligned} \langle B\rangle &= {}_{\text{out}\otimes\text{in}}\langle\text{system}|\alpha_{\text{in}}^\dagger\alpha_{\text{in}}|\text{system}\rangle_{\text{out}\otimes\text{in}} \\ &= \frac{e^{-2\pi r_{\text{horizon}}\omega}}{1 - e^{-2\pi r_{\text{horizon}}\omega}}. \end{aligned} \tag{20}$$

The above equation shows that different numbers of inflatons are produced with different probabilities inside

and outside of the apparent horizon in the brane-antibrane system. These probabilities are related to the orbital radial distance of the two branes and the energy of the inflatons.

3. Considering the Effect of Other Branes on Cosmic Inflation by Using the Warm Inflationary Model

In this section, we enter the effects of the interaction potential between the branes on the results of the derivation of slow-roll and perturbation parameters and other important parameters in the inflationary model [7]. We show that these parameters are given in terms of the orbital radial distance between the two branes and describe the shape of the interaction potential between branes. Also, using the inflationary model, we discuss the signature of interaction between branes against observational data.

Previously, it has been shown that in the FRW brane with the metric

$$ds^2 = g_{\mu\nu}dx^\mu dx^\nu = -dt^2 - a^2(t)dx^i dx_i, \tag{21}$$

the dynamics of warm inflation is presented by these equations [7]:

$$\begin{aligned}
\dot{\rho} + 3H(P+\rho) &= -\Gamma\langle\dot{B}\rangle^2,\\
\dot{\rho}_\gamma + 4H\rho_\gamma &= -\Gamma\langle\dot{B}\rangle^2,\\
H^2 &= \frac{1}{2}\left(\langle\dot{B}\rangle^2 + V(B)\right) + \frac{1}{3}\rho_\gamma,\\
V(B) &= m^2\langle B\rangle^2,
\end{aligned} \tag{22}$$

where ρ is the energy density, p is the pressure, ρ_γ is the energy density of the radiation, Γ is the dissipative coefficient, $\langle B\rangle$ is the thermal distribution of the inflaton, and the overdot ($\dot{}$) is the derivative with respect to cosmic time. In the previous section, we discussed that the thermal distribution of the inflaton can be given as a function of the orbital radial distance between branes. Using this fact, we can rewrite the above equations as

$$\begin{aligned}
\dot{\rho} + 3H(P+\rho) &= -\Gamma\left(\frac{\ddot{R}R - \dot{R}}{2\pi\omega R^2}\right)^2,\\
\dot{\rho}_\gamma + 4H\rho_\gamma &= -\Gamma\left(\frac{\ddot{R}R - \dot{R}}{2\pi\omega R^2}\right)^2,\\
H^2 &= \frac{1}{2}\left(\left(\frac{\ddot{R}R - \dot{R}}{2\pi\omega R^2}\right)^2 + V\left(R,\dot{R}\right)\right) + \frac{1}{3}\rho_\gamma,\\
V\left(R,\dot{R}\right) &= m^2\left(1 - \frac{\dot{R}}{2\pi\omega R}\right)^2.
\end{aligned} \tag{23}$$

Using quantum field theory methods [11, 12], the dissipation coefficient (Γ) in the above equations could be calculated as

$$\Gamma = \Gamma_0\frac{T^3}{\langle B\rangle^2} \sim \Gamma_0\frac{4\pi^2\omega^2T^3R^2}{\dot{R}^2}, \tag{24}$$

where T is the temperature of the thermal bath. During the inflationary epoch, the energy density ρ is more than the radiation energy density $\rho > \rho_\gamma$; however, it is comparable with the potential energy density $V(B^2)$ ($\rho \sim V$) [7]. The slow-roll approximation ($\langle\ddot{B}\rangle \le (3H + (\Gamma/3))\langle\dot{B}\rangle$) [13, 14] with the condition that inflation radiation production be quasistable ($\dot{\rho}_\gamma \le 4H\rho_\gamma, \dot{\rho}_\gamma \le \Gamma\langle\dot{B}\rangle$) leads to the following dynamic equations [7]:

$$\begin{aligned}
3H\left(1 + \frac{r}{3}\right)\langle\dot{B}\rangle &= -\frac{1}{2}V',\\
\rho_\gamma = \frac{3}{4}r\langle\dot{B}\rangle^2 &= \frac{r}{(1+(r/3))^2}\frac{V'^2}{V} = CT^4,\\
H^2 &= \frac{1}{2}V,
\end{aligned} \tag{25}$$

where $r = \Gamma/3H$ and $C = \pi^2g^*/30$ (g^* are the number of relativistic degrees of freedom). In the above equations, a prime ($'$) denotes a derivative with respect to the field **B**. Using this equation and the thermal distribution of the inflaton in Equation (20), we can obtain the dynamic equations with respect to R, the orbital radial distance between the two branes:

$$\begin{aligned}
3H\left(1 + \frac{r}{3}\right)\left(\frac{\ddot{R}R - \dot{R}}{2\pi\omega R^2}\right) &= -\frac{1}{2}V'\left(R,\dot{R}\right),\\
\rho_\gamma = \frac{3}{4}r\left(\frac{\ddot{R}R - \dot{R}}{2\pi\omega R^2}\right)^2 &= \frac{r}{(1+(r/3))^2}\frac{V'^2\left(R,\dot{R}\right)}{V\left(R,\dot{R}\right)} = CT^4,\\
H^2 &= \frac{1}{2}V\left(R,\dot{R}\right),
\end{aligned} \tag{26}$$

where the prime ($'$) denotes a derivative with respect to R. From the above equations, the temperature of the thermal bath is given by [7]

$$T = \left[-\frac{r\dot{H}}{2C(1+(r/3))}\right]^{1/4} = \left[-\frac{r\left(\ddot{R}R - \dot{R}\right)}{4C\pi\omega R^2(1+(r/3))}\right]^{1/4}. \tag{27}$$

This temperature depends on the orbital radial distance between the two branes. As the branes come close to each other, the temperature of the thermal bath increases. The reason for this is as follows: with decreasing distance between the two branes, the interaction potential increases and more inflatons radiate from the apparent horizon of the brane-antibrane system.

At this stage, we tend to calculate the dependency of slow-roll parameters on the orbital radial distance between different branes. These parameters in warm inflation are [7]

$$\epsilon = -\frac{1}{H}\frac{d}{dt}\ln(H),$$
$$\eta = -\frac{\ddot{H}}{H\dot{H}}, \tag{28}$$

where $H = \dot{a}/a$ and a is the scale factor. To calculate these parameters, we should determine the explicit form of the scale factor.

Until now, eight possible asymptotic solutions for cosmological dynamics have been proposed [15]. Three of these solutions have a noninflationary scale factor, and another three solutions give de Sitter, intermediate, and power law inflationary expansion. Finally, two cases of these solutions have asymptotic expansion with the scale factor ($a = a_0 \exp(A(\ln t)^{\lambda})$. This version of inflation is named logamediate inflation [16]. In this paper, we will study the warm tachyon inflationary model in the scenarios of intermediate and logamediate inflation.

Firstly, let us consider intermediate inflationary expansion. In this model, the expansion of the universe is between standard de Sitter inflation with the scale factor $a(t) = a_0 \exp(H_0 t)$ and power law inflation with the scale factor $a(t) = t^p, p > 1$ (slower than the first one) [17, 18]. The scale factor of this model has the form below [19–21]:

$$a = a_0 \exp\left(At^f\right), \quad 0 < f < 1, \tag{29}$$

where A is a positive constant. The number of e-folds in this case is [7]

$$N = \int_{t_1}^{t} H dt = A\left(t^f - t_1^f\right), \tag{30}$$

where t_1 is the begining time of inflation. From Equations (20), (24), (25), (26), (27), and (29), we obtain the Hubble parameter as

$$\begin{aligned} H &= fA\left(\frac{\ln\langle B\rangle - \ln\langle B_0\rangle}{\bar{\omega}}\right)^{(8(f-1))/(5f+2)} \\ &= fA\left(\frac{\ln\left(\left(e^{-2\pi r_{\text{horizon}}\omega}\right)/\left(1-e^{-2\pi r_{\text{horizon}}\omega}\right)\right) - \ln\left(\left(e^{-2\pi r_{0,\text{horizon}}\omega}\right)/\left(1-e^{-2\pi r_{0,\text{horizon}}\omega}\right)\right)}{\bar{\omega}}\right)^{(8(f-1))/(5f+2)} \\ &\sim fA\left(\frac{-2\pi\omega(r_{\text{horizon}} - r_{0,\text{horizon}}) + \ln\left(\left(1-e^{-2\pi r_{0,\text{horizon}}\omega}\right)/\left(1-e^{-2\pi r_{\text{horizon}}\omega}\right)\right)}{\bar{\omega}}\right)^{(8(f-1))/(5f+2)} \\ &\sim fA\left(\frac{2\pi\omega\left(\left(R_0/\dot{R}_0\right) - \left(R/\dot{R}\right)\right) + \ln\left(\left(1-e^{-2\pi\left(R_0/\dot{R}_0\right)\omega}\right)/\left(1-e^{-2\pi\left(R/\dot{R}\right)\omega}\right)\right)}{\bar{\omega}}\right)^{(8(f-1))/(5f+2)}, \\ B &= B_0 \exp\left(\bar{\omega}^{(5f+2)/8}\right), \end{aligned} \tag{31}$$

where $\bar{\omega} = \left((6/\Gamma_0)(2C/3)^{3/4}\right)^{1/2}\left((8(fA)^{5/8}(1-f)^{1/8})/(5f+2)\right)$ and Γ_0 is constant. This equation insists that the evolution of our brane universe is affected by the number of inflatons that are radiated from the apparent horizon of the brane-antibrane system and it changes with an increase or decrease in the orbital radial distance between the two branes.

The important slow-roll parameters ϵ and η are given by

$$\begin{aligned} \epsilon &= \frac{1-f}{fA}\left(\frac{\ln\langle B\rangle - \ln\langle B_0\rangle}{\bar{\omega}}\right)^{-(8f/(5f+2))} \\ &= \frac{1-f}{fA}\left(\frac{\ln\left(\left(e^{-2\pi r_{\text{horizon}}\omega}\right)/\left(1-e^{-2\pi r_{\text{horizon}}\omega}\right)\right) - \ln\left(\left(e^{-2\pi r_{0,\text{horizon}}\omega}\right)/\left(1-e^{-2\pi r_{0,\text{horizon}}\omega}\right)\right)}{\bar{\omega}}\right)^{-(8f/(5f+2))} \\ &\sim \frac{1-f}{fA}\left(\frac{-2\pi\omega(r_{\text{horizon}} - r_{0,\text{horizon}}) + \ln\left(\left(1-e^{-2\pi r_{0,\text{horizon}}\omega}\right)/\left(1-e^{-2\pi r_{\text{horizon}}\omega}\right)\right)}{\bar{\omega}}\right)^{-(8f/(5f+2))} \\ &\sim \frac{1-f}{fA}\left(\frac{2\pi\omega\left(\left(R_0/\dot{R}_0\right) - \left(R/\dot{R}\right)\right) + \ln\left(\left(1-e^{-2\pi\left(R_0/\dot{R}_0\right)\omega}\right)/\left(1-e^{-2\pi\left(R/\dot{R}\right)\omega}\right)\right)}{\bar{\omega}}\right)^{-(8f/(5f+2))}, \end{aligned}$$

$$\begin{aligned}\eta &= \frac{2-f}{fA}\left(\frac{\ln\langle B\rangle - \ln\langle B_0\rangle}{\bar{\omega}}\right)^{-(8f/(5f+2))} \\ &= \frac{2-f}{fA}\left(\frac{\ln\left(\left(e^{-2\pi r_{\text{horizon}}\omega}\right)/\left(1-e^{-2\pi r_{\text{horizon}}\omega}\right)\right) - \ln\left(\left(e^{-2\pi r_{0,\text{horizon}}\omega}\right)/\left(1-e^{-2\pi r_{0,\text{horizon}}\omega}\right)\right)}{\bar{\omega}}\right)^{-(8f/(5f+2))} \\ &\sim \frac{2-f}{fA}\left(\frac{-2\pi\omega(r_{\text{horizon}} - r_{0,\text{horizon}}) + \ln\left(\left(1-e^{-2\pi r_{0,\text{horizon}}\omega}\right)/\left(1-e^{-2\pi r_{\text{horizon}}\omega}\right)\right)}{\bar{\omega}}\right) \\ &\sim \frac{2-f}{fA}\left(\frac{2\pi\omega\left(\left(R_0/\dot{R}_0\right) - \left(R/\dot{R}\right)\right) + \ln\left(\left(1-e^{-2\pi\left(R_0/\dot{R}_0\right)\omega}\right)/\left(1-e^{-2\pi\left(R/\dot{R}\right)\omega}\right)\right)}{\bar{\omega}}\right)^{-(8f/(5f+2))},\end{aligned} \tag{32}$$

respectively. These parameters depend on the orbital radial distance between the branes. With a decrease in this distance, more inflatons are radiated from the apparent horizon of the system, the slow-roll parameters increase, and, as a result, the universe inflates more.

The energy density of radiation in this case has the following form:

$$\begin{aligned}\rho_\gamma &= 3(1-f)fA\left(\frac{\ln\langle B\rangle - \ln\langle B_0\rangle}{\bar{\omega}}\right)^{(8f-2)/(5f+2)} \\ &= 3(1-f)fA\left(\frac{\ln\left(\left(e^{-2\pi r_{\text{horizon}}\omega}\right)/\left(1-e^{-2\pi r_{\text{horizon}}\omega}\right)\right) - \ln\left(\left(e^{-2\pi r_{0,\text{horizon}}\omega}\right)/\left(1-e^{-2\pi r_{0,\text{horizon}}\omega}\right)\right)}{\bar{\omega}}\right)^{(8f-2)/(5f+2)} \\ &\sim 3(1-f)fA\left(\frac{-2\pi\omega(r_{\text{horizon}} - r_{0,\text{horizon}}) + \ln\left(\left(1-e^{-2\pi r_{0,\text{horizon}}\omega}\right)/\left(1-e^{-2\pi r_{\text{horizon}}\omega}\right)\right)}{\bar{\omega}}\right)^{(8f-2)/(5f+2)} \\ &\sim 3(1-f)fA\left(\frac{2\pi\omega\left(\left(R_0/\dot{R}_0\right) - \left(R/\dot{R}\right)\right) + \ln\left(\left(1-e^{-2\pi\left(R_0/\dot{R}_0\right)\omega}\right)/\left(1-e^{-2\pi\left(R/\dot{R}\right)\omega}\right)\right)}{\bar{\omega}}\right)^{(8f-2)/(5f+2)}.\end{aligned} \tag{33}$$

According to this result, the radiation energy density is given in terms of the orbital radius of the brane motion in extra dimensions. As the interaction potential increases, the effect of the inflaton radiation from the apparent horizon in the brane-antibrane system on cosmic inflation becomes systematically more effective because at higher energies, there exist more channels for inflaton production.

Using Equations (30) and (31), the number of e-folds between the two fields B_1 and $\mathbf{B}$ is given by

$$\begin{aligned}N &= A\left[\left(\frac{\ln\langle B\rangle - \ln\langle B_0\rangle}{\bar{\omega}}\right)^{-(8f/(5f+2))} - \left(\frac{\ln\langle B_1\rangle - \ln\langle B_0\rangle}{\bar{\omega}}\right)^{-(8f/(5f+2))}\right] \\ &= A\left[\left(\frac{\ln\left(\left(e^{-2\pi r_{\text{horizon}}\omega}\right)/\left(1-e^{-2\pi r_{\text{horizon}}\omega}\right)\right) - \ln\left(\left(e^{-2\pi r_{0,\text{horizon}}\omega}\right)/\left(1-e^{-2\pi r_{0,\text{horizon}}\omega}\right)\right)}{\bar{\omega}}\right)^{-(8f/(5f+2))}\right. \\ &\quad \left. - \left(\frac{\ln\left(\left(e^{-2\pi r_{1,\text{horizon}}\omega}\right)/\left(1-e^{-2\pi r_{1,\text{horizon}}\omega}\right)\right) - \ln\left(\left(e^{-2\pi r_{0,\text{horizon}}\omega}\right)/\left(1-e^{-2\pi r_{0,\text{horizon}}\omega}\right)\right)}{\bar{\omega}}\right)^{-(8f/(5f+2))}\right] \\ &\sim A\left[\left(\frac{-2\pi\omega(r_{\text{horizon}} - r_{0,\text{horizon}}) + \ln\left(\left(1-e^{-2\pi r_{0,\text{horizon}}\omega}\right)/\left(1-e^{-2\pi r_{\text{horizon}}\omega}\right)\right)}{\bar{\omega}}\right)^{-(8f/(5f+2))}\right.\end{aligned}$$

$$- \left(\frac{-2\pi\omega(r_{1,\text{horizon}} - r_{0,\text{horizon}}) + \ln\left(\left(1 - e^{-2\pi r_{0,\text{horizon}}\omega}\right)/\left(1 - e^{-2\pi r_{1,\text{horizon}}\omega}\right)\right)}{\bar{\omega}} \right)^{-(8f/(5f+2))} \Bigg]$$

$$\sim A \left[\left(\frac{2\pi\omega\left(\left(R_0/\dot{R}_0\right) - \left(R/\dot{R}\right)\right) + \ln\left(\left(1 - e^{-2\pi\left(R_0/\dot{R}_0\right)\omega}\right)/\left(1 - e^{-2\pi\left(R/\dot{R}\right)\omega}\right)\right)}{\bar{\omega}} \right)^{-(8f/(5f+2))} \right.$$

$$\left. - \left(\frac{2\pi\omega\left(\left(R_0/\dot{R}_0\right) - \left(R_1/\dot{R}_1\right)\right) + \ln\left(\left(1 - e^{-2\pi\left(R_0/\dot{R}_0\right)\omega}\right)/\left(1 - e^{-2\pi\left(R_1/\dot{R}_1\right)\omega}\right)\right)}{\bar{\omega}} \right)^{-(8f/(5f+2))} \right]. \tag{34}$$

This equation depends on $\langle B_1 \rangle$ and $\langle B_0 \rangle$. To obtain the explicit form of the number of e-folds in terms of the orbital radius distance between the branes, we should find the relation between $\langle B_1 \rangle$ and $\langle B_0 \rangle$. At the begining of the inflation period where $\varepsilon = 1$, the inflaton in terms of constant parameters of the model is

$$\begin{aligned} \langle B_1 \rangle &= \langle B_0 \rangle \exp\left(\bar{\omega} \left(\frac{1-f}{fA} \right)^{(5f+2)/8f} \right) \longrightarrow \frac{e^{-2\pi r_{1,\text{horizon}}\omega}}{1 - e^{-2\pi r_{1,\text{horizon}}\omega}} \\ &= \frac{e^{-2\pi r_{0,\text{horizon}}\omega}}{1 - e^{-2\pi r_{0,\text{horizon}}\omega}} \exp\left(\bar{\omega} \left(\frac{1-f}{fA} \right)^{(5f+2)/8f} \right) \\ &\longrightarrow (r_{1,\text{horizon}})^{-1} \sim (r_{0,\text{horizon}})^{-1} \exp \\ &\cdot \left(\bar{\omega} \left(\frac{1-f}{fA} \right)^{(5f+2)/8f} \right) - 1. \end{aligned} \tag{35}$$

From the above equations, we obtain the inflaton ($\mathbf{B}(t)$) and the distance between the two branes ($R(t)$) in terms of the number of e-folds:

$$\begin{aligned} \langle B(t) \rangle &= \langle B_0 \rangle \exp\left(\bar{\omega} \left(\frac{N}{A} + \frac{1-f}{fA} \right)^{(5f+2)/8f} \right) \\ &\longrightarrow \frac{e^{-2\pi r_{\text{horizon}}\omega}}{1 - e^{-2\pi r_{1,\text{horizon}}\omega}} \\ &= \frac{e^{-2\pi r_{0,\text{horizon}}\omega}}{1 - e^{-2\pi r_{0,\text{horizon}}\omega}} \exp\left(\bar{\omega} \left(\frac{N}{A} + \frac{1-f}{fA} \right)^{(5f+2)/8f} \right) \\ &\longrightarrow (r_{\text{horizon}})^{-1} \sim (r_{0,\text{horizon}})^{-1} \exp \\ &\cdot \left(\bar{\omega} \left(\frac{N}{A} + \frac{1-f}{fA} \right)^{(5f+2)/8f} \right) - 1 \longrightarrow R(t) \\ &= R_0 \exp\left(- \int dt r_{\text{horizon}}(N, t) \right). \end{aligned} \tag{36}$$

This equation shows that the orbital radial distance between the brane universes depends on the number of e-folds. This means that as the distance between the branes decreases, more inflatons are created near the apparent horizon of the brane-antibrane system, and the number of e-folds increases.

In Figure 1, we present the number of e-folds N for the intermediate scenario as a function of R^{-1}, where R is the orbital radial distance between branes. In this plot, we choose $R_0 = 0.45(\text{GeV})^{-1}$, $\omega = 4.6(\text{GeV})$, $\dot{R}_0 = 0.01$, $\dot{R} = 0.1$, $A = 1$, and $f = 1/2$. It is clear that the number of e-folds N is much larger for a smaller orbital radial distance between the branes. This is because as the distance between the branes becomes smaller, the temperature becomes larger and the thermal radiation of the inflatons enhances.

Now, we will consider tensor and scalar perturbations that appear during the inflationary period for the warm inflation model. These perturbations may leave an imprint in the CMB anisotropy and on the LSS [22–26]. The power spectrum and spectral index are characteristic of each fluctuation: $\Delta_R^2(k)$ and n_s for scalar perturbations and $\Delta_T^2(k)$ and n_T for tensor perturbations. In warm and cool inflation models, the scalar power spectrum is given by [7]

$$\Delta_R^2 = \left(\frac{H}{\langle \dot{B} \rangle} \langle \delta B \rangle \right)^2, \tag{37}$$

where the thermal fluctuation in the warm inflation model yields [22–26]

$$\langle \delta B \rangle = \left(\frac{\Gamma H T^2}{(4\pi)^3} \right)^{1/4}. \tag{38}$$

Using Equations (20), (36), (37), and (38), we calculate the scalar power spectrum as

$$\begin{aligned}
\Delta_R^2 &= -\left(\frac{\Gamma_0^3}{36(4\pi)^3}\right)^{1/2}\frac{H^{3/2}}{\dot{H}} = \left(\frac{\Gamma_0^3}{36(4\pi)^3}\right)^{1/2}\left(\frac{3^{11}(fA)^{15}(1-f)^3}{(2C)^{11}}\right)^{1/8}\langle B\rangle^3\left(\frac{\ln\langle B\rangle - \ln\langle B_0\rangle}{\bar{\omega}}\right)^{-((15f-18)/(5f+2))} \\
&= \left(\frac{\Gamma_0^3}{36(4\pi)^3}\right)^{1/2}\left(\frac{3^{11}(fA)^{15}(1-f)^3}{(2C)^{11}}\right)^{1/8}\left(\frac{e^{-2\pi r_{\text{horizon}}\omega}}{1-e^{-2\pi r_{\text{horizon}}\omega}}\right)^3 \\
&\quad\times\left(\frac{\ln\left(\left(e^{-2\pi r_{\text{horizon}}\omega}\right)/\left(1-e^{-2\pi r_{\text{horizon}}\omega}\right)\right) - \ln\left(\left(e^{-2\pi r_{0,\text{horizon}}\omega}\right)/\left(1-e^{-2\pi r_{0,\text{horizon}}\omega}\right)\right)}{\bar{\omega}}\right)^{-((15f-18)/(5f+2))} \\
&\sim \left(\frac{\Gamma_0^3}{36(4\pi)^3}\right)^{1/2}\left(\frac{3^{11}(fA)^{15}(1-f)^3}{(2C)^{11}}\right)^{1/8}\left(\frac{e^{-2\pi r_{\text{horizon}}\omega}}{1-e^{-2\pi r_{\text{horizon}}\omega}}\right)^3 \\
&\quad\times\left(\frac{-2\pi\omega(r_{\text{horizon}}-r_{0,\text{horizon}}) + \ln\left(\left(1-e^{-2\pi r_{0,\text{horizon}}\omega}\right)/\left(1-e^{-2\pi r_{\text{horizon}}\omega}\right)\right)}{\bar{\omega}}\right)^{-((15f-18)/(5f+2))} \\
&\sim \left(\frac{\Gamma_0^3}{36(4\pi)^3}\right)^{1/2}\left(\frac{3^{11}(fA)^{15}(1-f)^3}{(2C)^{11}}\right)^{1/8}\left(\frac{e^{-2\pi\left(R/\dot{R}\right)\omega}}{1-e^{-2\pi\left(R/\dot{R}\right)\omega}}\right)^3 \\
&\quad\times\left(\frac{2\pi\omega\left(\left(R_0/\dot{R}_0\right)-\left(R/\dot{R}\right)\right) + \ln\left(\left(1-e^{-2\pi\left(R_0/\dot{R}_0\right)\omega}\right)/\left(1-e^{-2\pi\left(R/\dot{R}\right)\omega}\right)\right)}{\bar{\omega}}\right)^{-((15f-18)/(5f+2))},
\end{aligned} \tag{39}$$

where k is the comoving wavenumber. With the wavenumber $k = k_0 = 0.002\,\text{Mpc}^{-1}$, the combined measurement from WMAP+BAO+SN of Δ_R^2 is reported by the WMAP7 data [27–29] as

$$\Delta_R^2 = (2.455 \pm 0.096)\times 10^{-19}. \tag{40}$$

Using this equation and Equation (39), and choosing ($A = 1$, $f = 1/2$, $\dot{R} = 0.1$, $\omega = 4.6(\text{GeV})$, and $\Gamma_0 = 1$), we obtain the radial distance between our brane and another brane, $R = (1.5\,\text{GeV})^{-1}$.

This result is consistent with previous calculations [30].

Another important perturbation parameter is the spectral index n_s which is given by

$$\begin{aligned}
n_s - 1 &= -\frac{dln\Delta_R^2}{dlnk} = \frac{15f-18}{8fA}\left(\frac{\ln\langle B\rangle - \ln\langle B_0\rangle}{\bar{\omega}}\right)^{-8f/(5f+2)} \\
&= \frac{15f-18}{8fA}\left(\frac{\ln\left(\left(e^{-2\pi r_{\text{horizon}}\omega}\right)/\left(1-e^{-2\pi r_{\text{horizon}}\omega}\right)\right) - \ln\left(\left(e^{-2\pi r_{0,\text{horizon}}\omega}\right)/\left(1-e^{-2\pi r_{0,\text{horizon}}\omega}\right)\right)}{\bar{\omega}}\right)^{-8f/(5f+2)} \\
&\sim \frac{15f-18}{8fA}\left(\frac{-2\pi\omega(r_{\text{horizon}}-r_{0,\text{horizon}}) + \ln\left(\left(e^{-2\pi r_{0,horizon}\omega}\right)/\left(1-e^{-2\pi r_{horizon}\omega}\right)\right)}{\bar{\omega}}\right)^{-8f/(5f+2)} \\
&\sim \frac{15f-18}{8fA}\left(\frac{-2\pi\omega\left(\left(R_0/\dot{R}_0\right)-\left(R/\dot{R}\right)\right) + \ln\left(\left(1-e^{-2\pi\left(R_0/\dot{R}_0\right)\omega}\right)/\left(1-e^{-2\pi\left(R/\dot{R}\right)\omega}\right)\right)}{\bar{\omega}}\right)^{-8f/(5f+2)},
\end{aligned} \tag{41}$$

where we have used the thermal distribution in Equation (20). In Figure 2, we show the results for the spectral index in the intermediate scenario as a function of R^{-1}, where R is the orbital radial distance between the branes. In this plot, we choose $R_0 = 0.45(\text{GeV})^{-1}$, $\omega = 4.6(\text{GeV})$, $\dot{R}_0 = 0.01$, $\dot{R} = 0.1$, $A = 1$, and $f = 1/2$. As can be seen from Figure 2, the spectral index decreases rapidly when the distance between the branes increases. By comparing Figures 1 and 2, we find that the $N \simeq 50$ case leads to $n_s \simeq 0.96$. This result is compatible with the observational data [7, 27–29, 31, 32]. At this point, the radial distance between our brane and another brane is $R = (1.5\,\text{GeV})^{-1}$.

Using Equation (20), we can calculate the tensor power spectrum and its spectral index as

$$\begin{aligned}
\Delta_T^2 &= \frac{2H^2}{\pi^2} = \frac{2(fA)^2}{\pi^2}\left(\frac{\ln\langle B\rangle - \ln\langle B_0\rangle}{\bar{\omega}}\right)^{(16(f-1))/(5f+2)} \\
&= \frac{2(fA)^2}{\pi^2}\left(\frac{\ln\left(\left(e^{-2\pi r_{\text{horizon}}\omega}\right)/\left(1-e^{-2\pi r_{\text{horizon}}\omega}\right)\right) - \ln\left(\left(e^{-2\pi r_{0,\text{horizon}}\omega}\right)/\left(1-e^{-2\pi r_{0,\text{horizon}}\omega}\right)\right)}{\bar{\omega}}\right)^{(16(f-1))/(5f+2)} \\
&\sim \frac{2(fA)^2}{\pi^2}\left(\frac{-2\pi\omega(r_{\text{horizon}} - r_{0,\text{horizon}}) + \ln\left(\left(1-e^{-2\pi r_{0,\text{horizon}}\omega}\right)/\left(1-e^{-2\pi r_{\text{horizon}}\omega}\right)\right)}{\bar{\omega}}\right)^{(16(f-1))/(5f+2)} \\
&\sim \frac{2(fA)^2}{\pi^2}\left(\frac{2\pi\omega\left(\left(R_0/\dot{R}_0\right) - \left(R/\dot{R}\right)\right) + \ln\left(\left(1-e^{-2\pi\left(R_0/\dot{R}_0\right)\omega}\right)/\left(1-e^{-2\pi\left(R/\dot{R}\right)\omega}\right)\right)}{\bar{\omega}}\right)^{(16(f-1))/(5f+2)},
\end{aligned} \tag{42}$$

$$\begin{aligned}
n_{\text{T}} &= -2\varepsilon = -\frac{2-2f}{fA}\left(\frac{\ln\langle B\rangle - \ln\langle B_0\rangle}{\bar{\omega}}\right)^{-8f/(5f+2)} \\
&= -\frac{2-2f}{fA}\left(\frac{\ln\left(\left(e^{-2\pi r_{\text{horizon}}\omega}\right)/\left(1-e^{-2\pi r_{\text{horizon}}\omega}\right)\right) - \ln\left(\left(e^{-2\pi r_{0,\text{horizon}}\omega}\right)/\left(1-e^{-2\pi r_{0,\text{horizon}}\omega}\right)\right)}{\bar{\omega}}\right)^{-8f/(5f+2)} \\
&\sim -\frac{2-2f}{fA}\left(\frac{-2\pi\omega(r_{\text{horizon}} - r_{0,\text{horizon}}) + \ln\left(\left(1-e^{-2\pi r_{0,\text{horizon}}\omega}\right)/\left(1-e^{-2\pi r_{\text{horizon}}\omega}\right)\right)}{\bar{\omega}}\right)^{-8f/(5f+2)} \\
&\sim -\frac{2-2f}{fA}\left(\frac{2\pi\omega\left(\left(R_0/\dot{R}_0\right) - \left(R/\dot{R}\right)\right) + \ln\left(\left(1-e^{-2\pi\left(R_0/\dot{R}_0\right)\omega}\right)/\left(1-e^{-2\pi\left(R/\dot{R}\right)\omega}\right)\right)}{\bar{\omega}}\right)^{-8f/(5f+2)}.
\end{aligned} \tag{43}$$

These perturbations depend on the orbital radial distance between the branes. As we discussed before, these perturbations have a direct effect on the cosmic microwave background (CMB). Thus, we can observe the signature of interaction between the branes by means of observational data.

Another important parameter is the tensor-scalar ratio that has the following form:

$$\begin{aligned}
R_{\text{tensor-scalar}} &= -\left(\frac{144(4\pi)^3(fA)^4}{\Gamma_0^3\pi^4T^2}\right)^{1/2}\dot{H}H^{1/2} = \left(\frac{144(4\pi)^3(fA)^4}{\Gamma_0^3\pi^4}\right)^{1/2}\left(\frac{3^{11}(fA)^{15}(1-f)^3}{(2C)^{11}}\right)^{1/8}\times\langle B\rangle^3\left(\frac{\ln\langle B\rangle - \ln\langle B_0\rangle}{\bar{\omega}}\right)^{(f+2)/(5f+2)} \\
&= \left(\frac{144(4\pi)^3(fA)^4}{\Gamma_0^3\pi^4}\right)^{1/2}\left(\frac{3^{11}(fA)^{15}(1-f)^3}{(2C)^{11}}\right)^{1/8}\left(\frac{e^{-2\pi r_{\text{horizon}}\omega}}{1-e^{-2\pi r_{\text{horizon}}\omega}}\right)^3 \\
&\quad\times\left(\frac{\ln\left(\left(e^{-2\pi r_{\text{horizon}}\omega}\right)/\left(1-e^{-2\pi r_{\text{horizon}}\omega}\right)\right) - \ln\left(\left(e^{-2\pi r_{0,\text{horizon}}\omega}\right)/\left(1-e^{-2\pi r_{0,\text{horizon}}\omega}\right)\right)}{\bar{\omega}}\right)^{(f+2)/(5f+2)} \\
&\sim \left(\frac{144(4\pi)^3(fA)^4}{\Gamma_0^3\pi^4}\right)^{1/2}\left(\frac{3^{11}(fA)^{15}(1-f)^3}{(2C)^{11}}\right)^{1/8}\left(\frac{e^{-2\pi r_{\text{horizon}}\omega}}{1-e^{-2\pi r_{\text{horizon}}\omega}}\right)^3 \\
&\quad\times\left(\frac{-2\pi\omega(r_{\text{horizon}} - r_{0,\text{horizon}}) + \ln\left(\left(1-e^{2\pi r_{0,\text{horizon}}\omega}\right)/\left(1-e^{2\pi r_{\text{horizon}}\omega}\right)\right)}{\bar{\omega}}\right)^{(f+2)/(5f+2)} \\
&\sim \left(\frac{144(4\pi)^3(fA)^4}{\Gamma_0^3\pi^4}\right)^{1/2}\left(\frac{3^{11}(fA)^{15}(1-f)^3}{(2C)^{11}}\right)^{1/8}\left(\frac{e^{-2\pi\left(R/\dot{R}\right)\omega}}{1-e^{-2\pi\left(R/\dot{R}\right)\omega}}\right)^3 \\
&\quad\times\left(\frac{2\pi\omega\left(\left(R_0/\dot{R}_0\right) - \left(R/\dot{R}\right)\right) + \ln\left(\left(1-e^{-2\pi\left(R_0/\dot{R}_0\right)\omega}\right)/\left(1-e^{-2\pi\left(R/\dot{R}\right)\omega}\right)\right)}{\bar{\omega}}\right)^{(f+2)/(5f+2)}.
\end{aligned} \tag{44}$$

In Figure 3, we present the tensor-scalar ratio in the intermediate scenario as a function of R^{-1}, where R is the orbital radial distance between the branes. In this plot, we choose $R_0 = 0.45(\mathrm{GeV})^{-1}$, $\omega = 4.6(\mathrm{GeV})$, $\dot{R}_0 = 0.01$, $\dot{R} = 0.1$, $C = 70$, $\Gamma_0 = 1$, $A = 1$, and $f = 1/2$. We observe that as the orbital radius distance between branes increases, the tensor-scalar ratio increases. By comparing Figures 2 and 3, we notice that the standard case $n_s \simeq 0.96$ may be found in $0.01 < R_{\text{tensor-scalar}} < 0.22$, which agrees with the observational data [7, 27–29, 31, 32]. At this stage, the radial distance between our brane and another brane is $R = (1.5\mathrm{GeV})^{-1}$.

Now, we would like to consider the signature of interaction between branes in the context of logamediate inflation with the scale factor

$$a(t) = a_0 \exp\left(A[\ln t]^{\lambda}\right), \tag{45}$$

where A is a constant parameter. This model is converted to power law inflation for the $\lambda = 1$ case. This scenario is applied in a number of scalar-tensor theories [16]. The effective potential of this solution is used in dark energy models [33], supergravity, Kaluza-Klein theories, and superstring models [16, 34]. The number of e-folds in this case is given by [7]

$$N = \int_{t_1}^{t} H dt = A\left([\ln t]^{\lambda} - [\ln t_1]^{\lambda}\right), \tag{46}$$

where t_1 is the beginning time of inflation. From Equations (20), (24), (25), (26), (27), and (45), we may find the inflaton **B** and also the orbital radial distance between the two branes:

$$\begin{aligned}
\ln\langle B\rangle - \ln\langle B_0\rangle = \tilde{\omega}\Xi(t) &\longrightarrow \ln\frac{e^{-2\pi r_{\text{horizon}}\omega}}{1-e^{-2\pi r_{\text{horizon}}\omega}} \\
&\quad - \ln\frac{e^{-2\pi r_{0,\text{horizon}}\omega}}{1-e^{-2\pi r_{0,\text{horizon}}\omega}} \\
&= \tilde{\omega}\Xi(t) \longrightarrow -2\pi\omega(r_{\text{horizon}} - r_{0,\text{horizon}}) \\
&\quad + \ln\frac{1-e^{-2\pi r_{0,\text{horizon}}\omega}}{1-e^{-2\pi r_{\text{horizon}}\omega}} \sim \tilde{\omega}\Xi(t) \\
&\longrightarrow \left(2\pi\omega\left(\frac{R_0}{\dot{R}_0} - \frac{R}{\dot{R}}\right)\right. \\
&\quad \left. + \ln\frac{1-e^{-2\pi\left(R_0/\dot{R}_0\right)\omega}}{1-e^{-2\pi\left(R/\dot{R}\right)\omega}}\right) \sim \tilde{\omega}\Xi(t),
\end{aligned} \tag{47}$$

where $\tilde{\omega} = \left((6/\Gamma_0)(2C/3)^{3/4}\right)^{1/2}\left((-4)^{5\lambda+3}(\lambda A)^5\right)^{1/8}$ and $\Xi(t) = \gamma[(5\lambda+3)/8, \ln t/4]$ is the incomplete gamma function [35, 36]). The potential in terms of the orbital radial distance between the two branes is presented as

$$\begin{aligned}
V &= \frac{2\lambda^2 A^2\left[\ln\left(\Xi^{-1}((\ln\langle B\rangle - \ln\langle B_0\rangle)/\tilde{\omega})\right)\right]^{2\lambda-2}}{\left(\Xi^{-1}((\ln\langle B\rangle - \ln\langle B_0\rangle)/\tilde{\omega})\right)^2} \\
&= \left(\frac{2\lambda^2 A^2\left[\ln\left(\Xi^{-1}\left(\left(2\pi\omega\left(\left(R_0/\dot{R}_0\right) - \left(R/\dot{R}\right)\right) + \ln\left(\left(1-e^{-2\pi\left(R_0/\dot{R}_0\right)\omega}\right)/\left(1-e^{-2\pi\left(R/\dot{R}\right)\omega}\right)\right)\right)/\tilde{\omega}\right)\right)\right]^{2\lambda-2}}{\left(\Xi^{-1}\left(\left(2\pi\omega\left(\left(R_0/\dot{R}_0\right) - \left(R/\dot{R}\right)\right) + \ln\left(\left(1-e^{-2\pi\left(R_0/\dot{R}_0\right)\omega}\right)/\left(1-e^{-2\pi\left(R/\dot{R}\right)\omega}\right)\right)\right)/\tilde{\omega}\right)\right)}\right)^2.
\end{aligned} \tag{48}$$

This equation shows that the inflatonic potential on our brane depends on the orbital radial distance and the interaction potential between the two branes. In fact, the interaction between branes causes inflation of our universe.

Now, we obtain the slow-roll parameters of the model in this case:

$$\begin{aligned}
\epsilon &= \frac{\left[\ln\left(\Xi^{-1}\left(\left(2\pi\omega\left(\left(R_0/\dot{R}_0\right) - \left(R/\dot{R}\right)\right) + \ln\left(\left(1-e^{-2\pi\left(R_0/\dot{R}_0\right)\omega}\right)/\left(1-e^{-2\pi\left(R/\dot{R}\right)\omega}\right)\right)\right)/\tilde{\omega}\right)\right)\right]^{1-\lambda}}{\lambda A}, \\
\eta &= \frac{2\left[\ln\left(\Xi^{-1}\left(\left(2\pi\omega\left(\left(R_0/\dot{R}_0\right) - \left(R/\dot{R}\right)\right) + \ln\left(\left(1-e^{-2\pi\left(R_0/\dot{R}_0\right)\omega}\right)/\left(1-e^{-2\pi\left(R/\dot{R}\right)\omega}\right)\right)\right)/\tilde{\omega}\right)\right)\right]^{1-\lambda}}{\lambda A}.
\end{aligned} \tag{49}$$

In this case, like the intermediate case, as the distance between the branes decreases, more inflatons are created in the brane-antibrane system, the slow-roll parameters increase, and the universe inflates.

Using Equations (20), (46), and (47), the number of e-folds between the two fields B_1 and $\mathbf{B}(\mathrm{t})$ can be obtained as

$$\begin{aligned} N &= A\left(\left[\ln\left(\Xi^{-1}\left(\frac{\left(2\pi\omega\left(\left(R_0/\dot{R}_0\right)-\left(R/\dot{R}\right)\right)+\ln\left(\left(1-e^{-2\pi\left(R_0/\dot{R}_0\right)\omega}\right)/\left(1-e^{-2\pi\left(R/\dot{R}\right)\omega}\right)\right)\right)}{\tilde{\omega}}\right)\right)\right]^{\lambda}\right. \\ &\left.-\left[\ln\left(\Xi^{-1}\left(\frac{\left(2\pi\omega\left(\left(R_0/\dot{R}_0\right)-\left(R/\dot{R}\right)\right)+\ln\left(\left(1-e^{-2\pi\left(R_0/\dot{R}_0\right)\omega}\right)/\left(1-e^{-2\pi\left(R_1/\dot{R}_1\right)\omega}\right)\right)\right)}{\tilde{\omega}}\right)\right)\right]^{\lambda}\right) \\ &= A\left(\left[\ln\left(\Xi^{-1}\left(\frac{\left(2\pi\omega\left(\left(R_0/\dot{R}_0\right)-\left(R/\dot{R}\right)\right)+\ln\left(\left(1-e^{-2\pi\left(R_0/\dot{R}_0\right)\omega}\right)/\left(1-e^{-2\pi\left(R/\dot{R}\right)\omega}\right)\right)\right)}{\tilde{\omega}}\right)\right)\right]^{\lambda}-[\lambda A]^{\lambda/(1-\lambda)}\right), \end{aligned} \tag{50}$$

where R_1 is the the orbital radial distance between the two branes at the begining of the inflationary epoch when $\epsilon = 1$. Using the above equation, the orbital radial distance between the two branes in the inflationary period could be obtained in terms of the number of e-folds as

$$R - R_0 = \frac{\tilde{\omega}\dot{R}^2\dot{R}_0^2}{2\pi\omega}\Xi\left(\exp\left(\frac{N}{A}+(\lambda A)^{\lambda/(1-\lambda)}\right)^{1/\lambda}\right). \tag{51}$$

This equation shows that, in this case, like the intermediate case, the number of e-fields depends on the orbital radial distance between the branes. This is because as the distance between the branes decreases, the number of inflatons, which has direct effects on the number of e-folds, increases.

Also, the scalar and tensor power spectra in this case are given by

$$\begin{aligned} \Delta_R^2 &= \left(\frac{\Gamma_0^3}{36(4\pi)^3}\right)^{1/2}\left(\frac{3^{11}(\lambda A)^{15}}{(2C)^{11}}\right)^{1/8}\left(\frac{e^{-2\pi r_{\mathrm{horizon}}\omega}}{1-e^{-2\pi r_{\mathrm{horizon}}\omega}}\right)^{-3} \\ &\times\exp\left(-\frac{15}{8}\left[\ln\left(\Xi^{-1}\left(\frac{\left(2\pi\omega\left(\left(R_0/\dot{R}_0\right)-\left(R/\dot{R}\right)\right)+\ln\left(\left(1-e^{-2\pi\left(R_0/\dot{R}_0\right)\omega}\right)/\left(1-e^{-2\pi\left(R/\dot{R}\right)\omega}\right)\right)\right)}{\tilde{\omega}}\right)\right)\right]\right) \\ &\times\left[\left[\ln\left(\Xi^{-1}\left(\frac{\left(2\pi\omega\left(\left(R_0/\dot{R}_0\right)-\left(R/\dot{R}\right)\right)+\ln\left(\left(1-e^{-2\pi\left(R_0/\dot{R}_0\right)\omega}\right)/\left(1-e^{-2\pi\left(R/\dot{R}\right)\omega}\right)\right)\right)}{\tilde{\omega}}\right)\right)\right]^{\lambda}\right]^{15(\lambda-1)/8\lambda} \\ &\times\exp\left(-3\tilde{\omega}\Xi\left(\exp\left(\ln\left(\Xi^{-1}\left(\frac{\left(2\pi\omega\left(\left(R_0/\dot{R}_0\right)-\left(R/\dot{R}\right)\right)+\ln\left(\left(1-e^{-2\pi\left(R_0/\dot{R}_0\right)\omega}\right)/\left(1-e^{-2\pi\left(R/\dot{R}\right)\omega}\right)\right)\right)}{\tilde{\omega}}\right)\right)\right)\right)\right), \\ \Delta_T^2 &= \frac{2\lambda^2 A^{\left[\ln\left(\Xi^{-1}\left(\left(2\pi\omega\left(\left(R_0/\dot{R}_0\right)-\left(R/\dot{R}\right)\right)+\ln\left(\left(1-e^{-2\pi\left(R_0/\dot{R}_0\right)\omega}\right)/\left(1-e^{-2\pi\left(R/\dot{R}\right)\omega}\right)\right)\right)/\tilde{\omega}\right)\right)\right]^{2-2\lambda}}}{\pi^2\left(\Xi^{-1}\left(\left(2\pi\omega\left(\left(R_0/\dot{R}_0\right)-\left(R/\dot{R}\right)\right)+\ln\left(\left(1-e^{-2\pi\left(R_0/\dot{R}_0\right)\omega}\right)/\left(1-e^{-2\pi\left(R/\dot{R}\right)\omega}\right)\right)\right)/\tilde{\omega}\right)\right)^2}. \end{aligned} \tag{52}$$

These spectra in the context of logamediate inflation, like intermediate inflation, change with an increase or decrease in the orbital radial distance between the branes. The spectral index in this case has the following forms:

$$n_s - 1 = -\frac{15(\lambda-1)}{8\lambda A}\left[\left[\ln\left(\Xi^{-1}\left(\frac{\left(2\pi\omega\left(\left(R_0/\dot{R}_0\right)-\left(R/\dot{R}\right)\right)+\ln\left(\left(1-e^{-2\pi\left(R_0/\dot{R}_0\right)\omega}\right)/\left(1-e^{-2\pi\left(R/\dot{R}\right)\omega}\right)\right)\right)}{\tilde{\omega}}\right)\right)\right]^{\lambda}\right]^{-1},$$
$$n_{\mathrm{T}} = -\frac{2\left[\ln\left(\Xi^{-1}\left(\left(2\pi\omega\left(\left(R_0/\dot{R}_0\right)-\left(R/\dot{R}\right)\right)+\ln\left(\left(1-e^{-2\pi\left(R_0/\dot{R}_0\right)\omega}\right)/\left(1-e^{-2\pi\left(R/\dot{R}\right)\omega}\right)\right)\right)/\tilde{\omega}\right)\right)\right]^{1-\lambda}}{\lambda A}. \tag{53}$$

In Figures 4 and 5, we present the number of e-folds N and the spectral index for the logamediate inflation scenario as a function of R^{-1}, where R is the orbital radial distance between the branes. In these plots, we choose $R_0 = 0.45\ (\mathrm{GeV})^{-1}$, $\omega = 4.6(\mathrm{GeV})$, $\dot{R}_0 = 0.01$, $\dot{R} = 0.1$, $\lambda = 10$, $A = 1$, and $f = 1/2$. In this case, like the intermediate case, we find that the number of e-folds N and the spectral index are much larger for smaller orbital radial distance between branes. This is because as the distance between the branes becomes smaller, the temperature becomes larger and the thermal radiation of the inflatons enhances.

Finally, we could find the tensor-scalar ratio in terms of the orbital radial distance between two branes:

$$\begin{aligned}R_{\text{tensor-scalar}} = {} & \left(\frac{144(4\pi)^3}{\Gamma_0^3\pi^4}\right)^{1/2}\left(\frac{(2C)^{11}(\lambda A)}{3^{11}}\right)^{1/8}\left(\frac{e^{-2\pi r_{0,\text{horizon}}\omega}}{1-e^{-2\pi r_{0,\text{horizon}}\omega}}\right)^3 \\ & \times \exp\left(-\frac{1}{8}\left[\ln\left(\Xi^{-1}\left(\frac{\left(2\pi\omega\left(\left(R_0/\dot{R}_0\right)-\left(R/\dot{R}\right)\right)+\ln\left(\left(1-e^{-2\pi\left(R_0/\dot{R}_0\right)\omega}\right)/\left(1-e^{-2\pi\left(R/\dot{R}\right)\omega}\right)\right)\right)}{\tilde{\omega}}\right)\right)\right]\right) \\ & \times \left[\left[\ln\left(\Xi^{-1}\left(\frac{\left(2\pi\omega\left(\left(R_0/\dot{R}_0\right)-\left(R/\dot{R}\right)\right)+\ln\left(\left(1-e^{-2\pi\left(R_0/\dot{R}_0\right)\omega}\right)/\left(1-e^{-2\pi\left(R/\dot{R}\right)\omega}\right)\right)\right)}{\tilde{\omega}}\right)\right)\right]^{\lambda}\right]^{-31(\lambda-1)/8\lambda} \\ & \times \exp\left(3\tilde{\omega}\Xi\left[\exp\left(\ln\left(\Xi^{-1}\left(\frac{\left(2\pi\omega\left(\left(R_0/\dot{R}_0\right)-\left(R/\dot{R}\right)\right)+\ln\left(\left(1-e^{-2\pi\left(R_0/\dot{R}_0\right)\omega}\right)/\left(1-e^{-2\pi\left(R/\dot{R}\right)\omega}\right)\right)\right)}{\tilde{\omega}}\right)\right)\right]\right).\end{aligned} \tag{54}$$

In Figure 6, we present the tensor-scalar ratio in the logamediate scenario as a function of R^{-1}, where R is the orbital radial distance between the branes. In this plot, we choose $R_0 = 0.45(\mathrm{GeV})^{-1}$, $\omega = 4.6(\mathrm{GeV})$, $\dot{R}_0 = 0.01$, $\dot{R} = 0.1$, $C = 70$, $\Gamma_0 = 1$, $\lambda = 10$, $A = 1$, and $f = 1/2$. In this case, like the intermediate case, with an increase in the orbital radial distance between branes, the tensor-scalar ratio increases. By comparing Figures 5 and 6, we notice that the standard case $n_s \simeq 0.96$ may be found in $0.01 < R_{\text{tensor-scalar}} < 0.22$, which agrees with the observational data [7, 27–29, 31, 32]. At this stage, the radial distance between our brane and another brane is $R = (0.02225\ \mathrm{GeV})^{-1}$.

4. Summary and Discussion

In this research, we calculate the thermal distribution of inflatons near the apparent horizon in a brane-antibrane system and show that the energy density, slow-roll parameters, number of e-folds, and perturbation parameters can be given in terms of the orbital radius of the brane motion in extra dimensions. According to our results, when the distance between branes increases, the number of e-folds and the spectral index for both the intermediate and logamediate models decrease rapidly; however, the tensor-scalar ratio increases. This is because as the separate distance between branes decreases, the interaction potential increases, and at higher energies, there exist more channels for inflaton production near the apparent horizon in the brane-antibrane system; consequently, the effect of inflaton radiation from this horizon on cosmic inflation becomes systematically more effective. We find that the $N \simeq 50$ case leads to $n_s \simeq 0.96$. This standard case may be found in $0.01 < R_{\text{tensor-scalar}} < 0.22$, which agrees with the observational data [7, 27–29, 31, 32] (we note that some new observational data

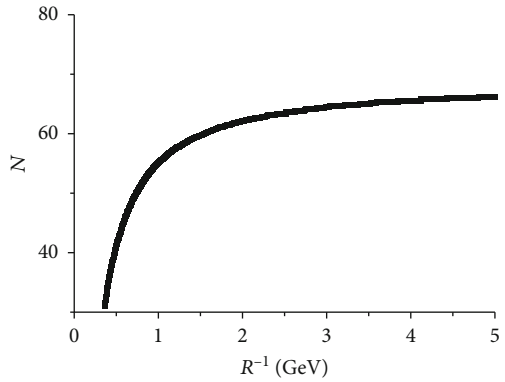

Figure 1: The number of e-folds N for the intermediate scenario as a function of the R^{-1} for $R_0 = 0.45(\text{GeV})^{-1}$, $\omega = 4.6(\text{GeV})$, $\dot{R}_0 = 0.01$, $\dot{R} = 0.1$, $A = 1$, and $f = 1/2$.

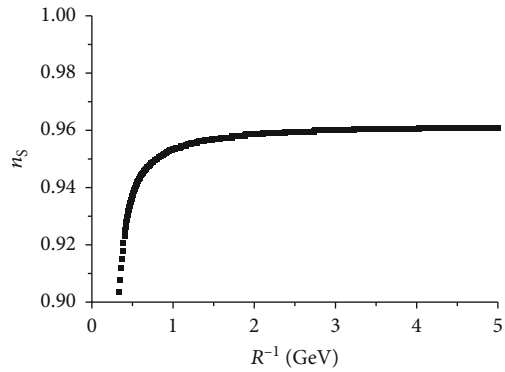

Figure 2: The spectral index in the intermediate scenario as a function of R^{-1} for $R_0 = 0.45(\text{GeV})^{-1}$, $\omega = 4.6(\text{GeV})$, $\dot{R}_0 = 0.01$, $\dot{R} = 0.1$, $A = 1$, and $f = 1/2$.

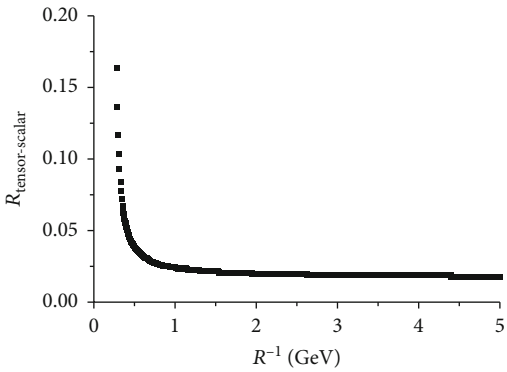

Figure 3: The tensor-scalar ratio in the intermediate scenario as a function of R^{-1} for $R_0 = 0.45(\text{GeV})^{-1}$, $\omega = 4.6(\text{GeV})$, $\dot{R}_0 = 0.01$, $\dot{R} = 0.1$, $A = 1$, and $f = 1/2$.

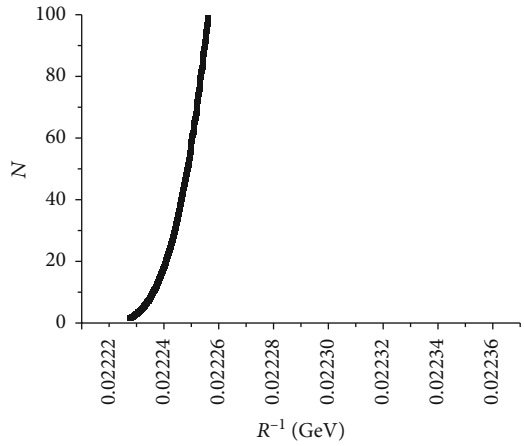

Figure 4: The number of e-folds N in the logamediate inflation scenario as a function of R^{-1} for $R_0 = 0.45(\text{GeV})^{-1}$, $\omega = 4.6(\text{GeV})$, $\dot{R}_0 = 0.01$, $\dot{R} = 0.1$, $\lambda = 10$, $A = 1$, and $f = 1/2$.

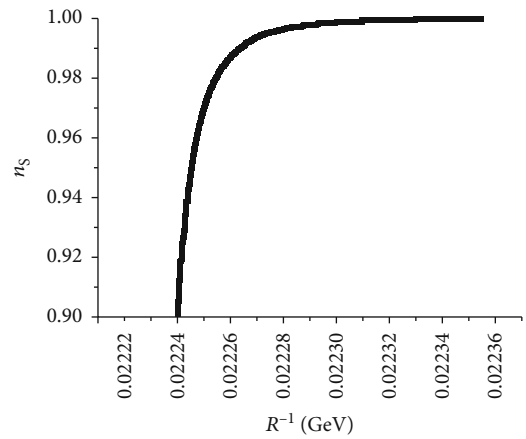

Figure 5: The spectral index in the logamediate inflation scenario as a function of R^{-1} for $R_0 = 0.45(\text{GeV})^{-1}$, $\omega = 4.6(\text{GeV})$, $\dot{R}_0 = 0.01$, $\dot{R} = 0.1$, $\lambda = 10$, $A = 1$, and $f = 1/2$.

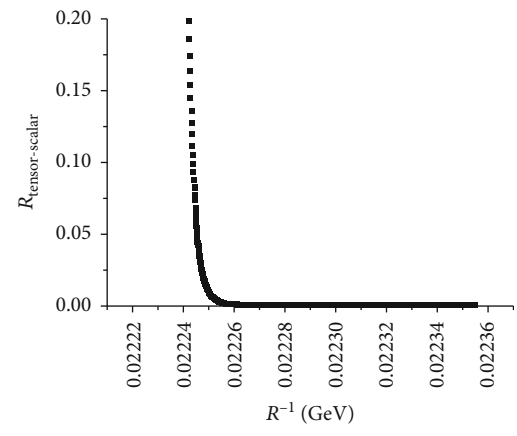

Figure 6: The tensor-scalar ratio in the logamediate inflation scenario as a function of R^{-1} for $R_0 = 0.45(\text{GeV})^{-1}$, $\omega = 4.6(\text{GeV})$, $\dot{R}_0 = 0.01$, $\dot{R} = 0.1$, $\lambda = 10$, $A = 1$, and $f = 1/2$.

has been obtained, but we believe that our models will fit this as well. This work in under progress). At this point, the radial distance between our brane and another brane is $R = (1.5\,\mathrm{GeV})^{-1}$ in the intermediate model and $R = (0.02225\,\mathrm{GeV})^{-1}$ in the logamediate model.

Data Availability

No data were used to support this study.

Conflicts of Interest

The author declares that there is no conflict of interest regarding the publication of this paper.

Acknowledgments

This work is based on the research supported wholly/in part by the National Research Foundation of South Africa (Grant Number: 118511).

References

[1] S. Robles-Perez and P. F. González-Diaz, "Quantum state of the multiverse," *Physics Review D*, vol. 81, no. 8, article 083529, 2010.

[2] P. F. Gonzlez-Diaz and S. Robles-Perez, "The entangled accelerating universe," *Physics Letters*, vol. B679, pp. 298–301, 2009.

[3] A. Sepehri, S. Shoorvazi, and M. E. Zomorrodian, "The quantum entanglement between colorful dark energy universes in a colorful multiverse," *Canadian Journal of Physics*, vol. 91, no. 3, pp. 256–259, 2013.

[4] A. Sepehri, T. Ghaffary, and M. E. Zomorrodian, "Measurement of strong coupling constant from transverse momentum," *Canadian Journal of Physics*, vol. 87, no. 11, pp. 1151–1158, 2009.

[5] Y.-Z. Ma, Q.-G. Huang, and X. Zhang, "Confronting brane inflation with Planck and pre-Planck data," *Physical Review D*, vol. 87, no. 10, article 103516, 2013.

[6] G. Dvali, G. Gabadaze, and M. Porrati, "4D gravity on a brane in 5D Minkowski space," *Physics Letters B*, vol. 485, no. 1-3, pp. 208–214, 2000.

[7] M. Bastero-Gil and A. Berera, "Warm inflation model building," *International Journal of Modern Physics A*, vol. 24, no. 12, pp. 2207–2240, 2009.

[8] N. D. Birrell and P. C. W. Davies, *Quantum Fields in Curved Space*, Cambridge University Press, New York, NY, USA, 1982.

[9] D. Ahn, "Final state boundary condition of the Schwarzschild black hole," *Physics Review D*, vol. 74, no. 8, article 084010, 2006.

[10] A. Sepehri and S. Shoorvazi, "The signature of string ball near surface horizon of cylindrical Universe," *Astrophysics and Space Science*, vol. 344, no. 2, pp. 521–527, 2013.

[11] M. Bastero-Gil, A. Berera, and R. O. Ramos, "Dissipation coefficients from scalar and fermion quantum field interactions," *Journal of Cosmology and Astroparticle Physics*, vol. 1109, p. 33, 2011.

[12] M. Bastero-Gil, A. Berera, R. O. Ramos, and J. G. Rosa, "General dissipation coefficient in low-temperature warm inflation," *Journal of Cosmology and Astroparticle Physics*, vol. 1301, p. 16, 2013.

[13] A. Berera, "Warm inflation," *Physical Review Letters*, vol. 75, no. 18, pp. 3218–3221, 1995.

[14] A. Berera, "Interpolating the stage of exponential expansion in the early universe: possible alternative with no reheating," *Physical Review D*, vol. 55, pp. 3346–3357, 1997.

[15] J. D. Barrow, "Varieties of expanding universe," *Classical and Quantum Gravity*, vol. 13, no. 11, pp. 2965–2975, 1996.

[16] J. D. Barrow, "Slow-roll inflation in scalar-tensor theories," *Physical Review D*, vol. 51, no. 6, pp. 2729–2732, 1995.

[17] M. B.-G. A. Berera, "Warm inflation dynamics in the low temperature regime," *Physical Review D*, vol. 76, no. 4, article 043515, 2007.

[18] J. Yokoyama and K. Maeda, "On the dynamics of the power law inflation due to an exponential potential," *Physics Letters B*, vol. 207, no. 1, pp. 31–35, 1988.

[19] J. D. Barrow, "Graduated inflationary universes," *Physics Letters B*, vol. 235, no. 1-2, pp. 40–43, 1990.

[20] J. D. Barrow and A. R. Liddle, "Perturbation spectra from intermediate inflation," *Physics Review D*, vol. 47, no. 12, pp. 5219–R5223, 1993.

[21] J. D. Barrow and P. Saich, "The behaviour of intermediate inflationary universes," *Physics Letters B*, vol. 249, pp. 406–410, 1990.

[22] A. H. Guth and S. Y. Pi, "Fluctuations in the new inflationary universe," *Physical Review Letters*, vol. 49, no. 15, pp. 1110–1113, 1982.

[23] V. F. Mukhanov and G. V. Chibisov, "Quantum fluctuations and a nonsingular universe," *Pisma Zhurnal Eksperimentalnoi i Teoreticheskoi Fiziki*, vol. 33, p. 549, 1981.

[24] S. W. Hawking, "The development of irregularities in a single bubble inflationary universe," *Physics Letters B*, vol. 115, no. 4, pp. 295–297, 1982.

[25] A. A. Starobinsky, "Dynamics of phase transition in the new inflationary universe scenario and generation of perturbations," *Physics Letters B*, vol. 117, pp. 175–178, 1982.

[26] J. M. Bardeen, P. J. Steinhardt, and M. S. Turner, "Spontaneous creation of almost scale-free density perturbations in an inflationary universe," *Physical Review D*, vol. 28, pp. 679–693, 1983.

[27] E. Komatsu, K. M. Smith, J. Dunkley et al., "Seven-year Wilkinson Microwave Anisotropy Probe (WMAP) observations: cosmological interpretation," https://arxiv.org/abs/1001.4538.

[28] B. Gold, N. Odegard, J. L. Weiland et al., "Seven-Year Wilkinson Microwave Anisotropy Probe (WMAP) observations: galactic foreground emission," http://arxiv.org/abs/1001.4555.

[29] D. Larson, J. Dunkley, G. Hinshaw et al., "Seven-Year Wilkinson Microwave Anisotropy Probe (WMAP) observations: power spectra and WMAP-derived parameters," http://arxiv.org/abs/1001.4635.

[30] G. Belanger, A. Belyaev, M. Brown, M. Kakizaki, and A. Pukhov, "Testing minimal universal extra dimensions using Higgs boson searches at the LHC," *Physics Review D*, vol. 87, article 016008, 2013.

[31] Planck Collaboration, "*Planck* early results. XXII. The submillimetre properties of a sample of Galactic cold clumps," *Astronomy & Astrophysics*, vol. 536, article A22, 2011.

[32] The Planck Collaboration, "The scientific programme of Planck," https://arxiv.org/abs/astro-ph/0604069.

[33] P. J. E. Peebles and B. Ratra, "The cosmological constant and dark energy," *Reviews of Modern Physics*, vol. 75, no. 2, pp. 559–606, 2003.

[34] P. G. Ferreira and M. Joyce, "Cosmology with a primordial scaling field," *Physical Review D*, vol. 58, no. 2, article 023503, 1998.

[35] M. Abramowitz and I. A. Stegun, *Handbook of Mathematical Functions with Formulas, Graphs, and Mathematical Tables*, Dover, 9th edition, 1972.

[36] G. Arfken, "The incomplete gamma function and related functions," in *Mathematical Methods for Physicists*, Academic Press, 3rd edition, 1985.

Hindawi
Advances in High Energy Physics
Volume 2020, Article ID 5249839, 8 pages
https://doi.org/10.1155/2020/5249839

Research Article

Generalized Phenomenological Models of Dark Energy

Prasenjit Paul[1] **and Rikpratik Sengupta**[2]

[1]*Department of Physics, Indian Institute of Engineering Science and Technology, Shibpur, India*
[2]*Department of Physics, Government College of Engineering and Ceramic Technology, Kolkata, 700010 West Bengal, India*

Correspondence should be addressed to Prasenjit Paul; prasenjit071083@gmail.com

Received 30 July 2019; Accepted 28 November 2019; Published 20 February 2020

Academic Editor: Luca Stanco

It was first observed at the end of the last century that the universe is presently accelerating. Ever since, there have been several attempts to explain this observation theoretically. There are two possible approaches. The more conventional one is to modify the matter part of the Einstein field equations, and the second one is to modify the geometry part. We shall consider two phenomenological models based on the former, more conventional approach within the context of general relativity. The phenomenological models in this paper consider a Λ term firstly a function of $\ddot{a}/a$ and secondly a function of ρ, where a and ρ are the scale factor and matter energy density, respectively. Constraining the free parameters of the models with the latest observational data gives satisfactory values of parameters as considered by us initially. Without any field theoretic interpretation, we explain the recent observations with a dynamical cosmological constant.

1. Introduction

Type Ia high-redshift supernova observations indicate that the universe is presently accelerating [1, 2]. This is mostly thought to be due to the presence of some unknown fluid known as dark energy. Soon after the first cosmological solution to the Einstein field equations (EFE), Einstein had put an additional Λ term (known as the cosmological constant) which produced a repulsive effect, in order to modify the EFE so that the cosmological solution could lead to a static universe. He later called the introduction of this term to be the greatest blunder of his life. However, after observations suggested an accelerating universe, there was a revived interest in the Λ term as a possible candidate for the dark energy. Theoretically, the cosmological constant is assumed to be the contribution from vacuum energy given by $\Lambda = 8\pi G\rho_{\text{vac}}$, arising out of quantum vacuum fluctuations of some fundamental field. Although the calculated value of ρ_{vac} turns out to be much larger than the value of Λ determined from observations, but there is no theoretical argument of making the ρ_{vac} term vanish to exactly zero [3]. So Λ models are favored for dark energy (DE). Λ has also been thought to be generated from a particle creation effect or dynamical scalar field [4]. If we consider that the Λ term is responsible for the dark energy, whatever is the generation mechanism, it is clear that contrary to Einstein, Λ is not a constant but a dynamical cosmological term [5].

DE is also sometimes considered without the presence of any fluid or Λ term, just as a consequence of the modification of the geometric part or the left hand side of the EFE, but such efforts are not possible in the context of standard general relativity (GR) [6, 7]. There are also dynamically evolving scalar field models which have been used to describe DE. The popular dynamical physical field models that have been utilized for this purpose are quintessence [8–11], k-essence [12–17], phantom [18], and tachyonic field [19–26]. Phenomenological models of a dynamical Λ term are also being popularly considered candidates of DE. "Phenomenological" simply means that there is no derivation of the dynamical Λ term from any underlying quantum field theory. Such models may be categorized into three types: (i) kinematic, (ii) hydrodynamic, and (iii) field theoretic. The first means that Λ is a function of time or scale factor $a(t)$. The second means that Λ is treated as a barotropic fluid with

some equation of state (EOS). The third means that Λ is treated as a new physical classical field with phenomenological Lagrangian. We will be concerned here with (i) and (ii) only. Such kinematic and hydrodynamic models have been treated in some depth before. A dynamical model with $\Lambda = \alpha H^2$, where $H(t) = \dot{a}/a$, has been explored by Mukhopadhyay et al. [27]. A similar model with $\dot{\Lambda} \sim H^3$ has been considered in [28, 29]. The main motivation of considering $\Lambda \sim \ddot{a}/a$ and $\Lambda \sim \rho$ is to prove that these two dynamical models are equivalent for both open and closed universes in addition to the flat space, which has already been proved previously. The value of Λ obtained theoretically from particle physics is several orders of magnitude greater than the observed value for Λ, if Λ has to be considered dark energy. This is explained in various models as it is obtained that $\Lambda \sim 1/t^2$ for flat space-time and it is presently very small but nonzero, and this fact is well supported by our models.

The most frequently used forms of Λ for phenomenological models are $\Lambda = \alpha(\dot{a}/a)^2$, $\Lambda = \beta(\ddot{a}/a)$, and $\Lambda = 8\pi G\gamma\rho$, where α, β, and γ are constants whose values can be constrained from observations. In general, the sign constraints on β and γ are imposed in order to ensure a positive value of the matter density parameter Ω_m. The first type of model has been considered by [30–37]. The second model has been dealt with by [5, 38–40]. The third type of model has been considered by [41]. The equivalence of these three forms has been shown by Ray et al. [42, 43], connecting the free parameters of the models with the matter density and vacuum energy density parameters in the first paper and by application of numerical methods in the later one. This paper is basically an in-depth extension of the work done by Mukhopadhyay et al. [44] where they have considered the first type of model and obtained cosmological solutions for any possible value of the curvature constant and equation of state parameter ω. They have also analysed the physical features of the solutions. We shall do the same for the second and third models and also compare our results to the latest observational data constraining our free parameters. The constraints are found to be exactly compatible with our initial considerations.

The paper is organized as follows. In the second section, we consider the mathematical model in the background of an isotropic and homogeneous Friedmann–Lemaître–Robertson–Walker (FLRW) space-time, which is the generally used cosmological metric in GR. We calculate the various cosmological and physical parameters for the two different phenomenological models in consideration. In the next section, we constrain the free parameters associated with the models based on recent observational data. The final section summarizes the physical insights of the results we have obtained.

2. Mathematical Model

The Einstein field equation (EFE) in the presence of a cosmological constant, $\Lambda(t)$, is given by

$$G^{\mu\nu} = -8\pi G\left[T^{\mu\nu} - \frac{\Lambda}{8\pi G}g^{\mu\nu}\right], \tag{1}$$

where we shall take the cosmological constant as a function of time in order to account for the dark energy. We obtain the EFE for the cosmological FLRW metric:

$$ds^2 = -dt^2 + \left[\frac{dr^2}{1-kr^2} + r^2\left(d\theta^2 + \sin^2\theta d\phi^2\right)\right], \tag{2}$$

which yields the equations

$$\left(\frac{\dot{a}}{a}\right)^2 + \frac{k}{a^2} = \frac{8\pi G\rho}{3} + \frac{\Lambda}{3}, \tag{3}$$

$$\left(\frac{\ddot{a}}{a}\right) = -\frac{4\pi G(\rho + 3p)}{3} + \frac{\Lambda}{3}, \tag{4}$$

where $a(t)$ and k are the scale factor and curvature constant, respectively.

The energy-momentum conservation gives

$$8\pi G(p+\rho)\left(\frac{\dot{a}}{a}\right) = -\frac{8\pi G}{3}\dot{\rho} - \frac{\dot{\Lambda}}{3}. \tag{5}$$

We consider the barotropic fluid with equation of state (EOS) of the form:

$$p = \omega\rho, \tag{6}$$

where ω denotes the EOS parameter which can assume specific values during the evolution of the universe for different phases. By plugging this relation in equation (4), the energy density is obtained as

$$\rho = \frac{3}{4\pi G(1+3\omega)}\left(\frac{\Lambda}{3} - \frac{\ddot{a}}{a}\right). \tag{7}$$

Substituting equation (6) into equation (4) multiplied by a factor of $2/(1+3\omega)$ and adding equation (3) to it, we get the differential equation

$$\left(\frac{\dot{a}}{a}\right)^2 + \frac{k}{a^2} + \frac{2}{1+3\omega}\left(\frac{\ddot{a}}{a}\right) = \left(\frac{1+\omega}{1+3\omega}\right)\Lambda. \tag{8}$$

The above equation describes the cosmological dynamics for a barotropic fluid in the presence of the cosmological constant Λ.

2.1. Solutions for Phenomenological Model $\Lambda \sim \ddot{a}/a$. In this phenomenological model, we consider $\Lambda = \beta(\ddot{a}/a)$, where $\beta < 0$ which is justified in the light of the latest observational data [45] as shown in Section 3. Using this form of Λ in equation (8), we obtain

$$\frac{\ddot{a}}{a} = -\frac{(1+3\omega)}{2-(1+\omega)\beta}\frac{\dot{a}}{a} - \frac{(1+3\omega)k}{2-(1+\omega)\beta}\frac{1}{a\dot{a}}. \tag{9}$$

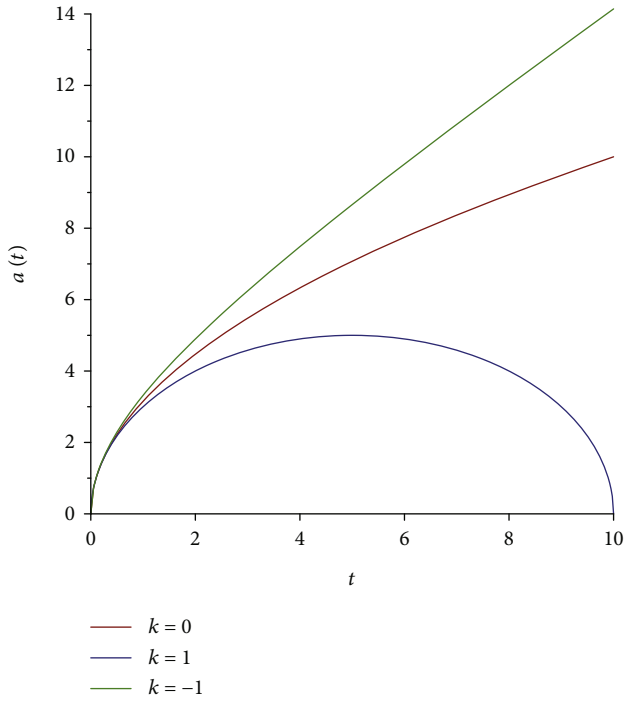

Figure 1: Plot of $a(t)$ versus t for different values of k.

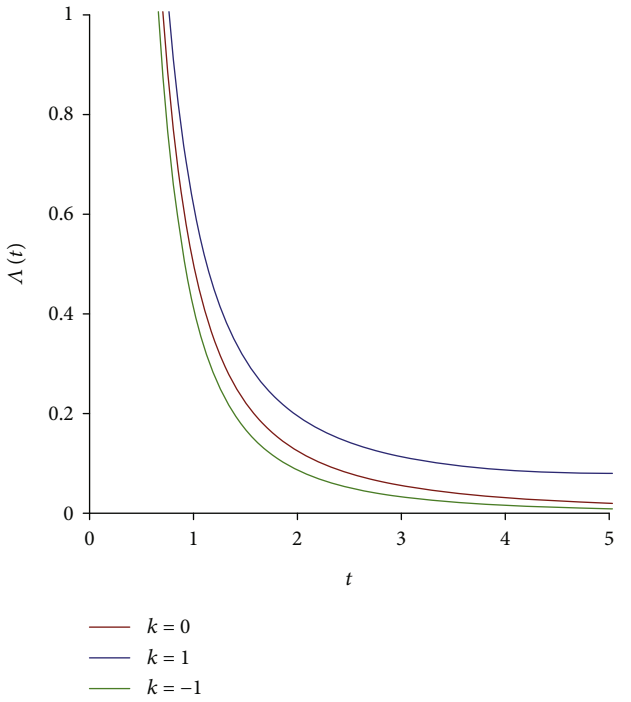

Figure 2: Plot of $\Lambda(t)$ versus t for different values of k.

This equation can be simplified to

$$a\dot{a}\frac{d}{dt}\left[\ln\left(\dot{a}a^{-A}\right)\right] = Ak, \tag{10}$$

where $A = -((1+3\omega)/(2-(1+\omega)\beta))$. We choose $A = -1$ [?], such that $\omega = (1-\beta)/(3+\beta)$. Any arbitrary value can be taken. We take $A = -1$ and later $B = -1$ so that the differential equation can be solved analytically and complex numerical calculations may be avoided.

The above equation now takes the form

$$a\dot{a}\frac{d}{dt}\left[\ln\left(\dot{a}a\right)\right] = -k. \tag{11}$$

The scale factor turns out to be

$$a(t) = \sqrt{A_0 t + A_1 - kt^2}, \tag{12}$$

where A_0 and A_1 are integration constants.

As we are considering a universe evolving from a singularity, $a(t=0) = 0$. This gives $A_1 = 0$. So

$$a(t) = \sqrt{A_0 t - kt^2}. \tag{13}$$

We show the evolution of the scale factor with time for different values of k in Figure 1. As expected, we obtain flat, open, and closed universes for $k = 0$, $k = -1$, and $k = 1$, respectively. The Hubble parameter is computed as

$$H(t) = \frac{A_0 - 2kt}{2\left(A_0 t - kt^2\right)}. \tag{14}$$

The cosmological constant is given by

$$\Lambda(t) = -\frac{\beta {A_0}^2}{4\left(A_0 t - kt^2\right)^2}. \tag{15}$$

The variation of the cosmological parameter λ with time is shown in Figure 2 and is found to be monotonically decreasing for all considered values of k. The energy density is given by

$$\rho(t) = \frac{(3-\beta)}{16\pi G}\frac{A_0^2}{\left(A_0 t - kt^2\right)^2}. \tag{16}$$

The variation of the scale factor and cosmological constant with time has been plotted for $k = 0, \pm 1$ in Figures 1 and 2.

We obtain a closed universe for $k = 1$ and an open universe for $k = -1$ as expected.

The density parameters for matter, a cosmological constant, and curvature, respectively, can be computed for this phenomenological model as

$$\Omega_m = \frac{8\pi G\rho}{3H^2} = -\frac{4\beta}{3}\left[\frac{k\left(A_0 t - kt^2\right)}{\left(A_0 - 2kt^2\right)^2} + \frac{1}{4}\right], \tag{17}$$

$$\Omega_\Lambda = \frac{\Lambda}{3H^2} = \frac{4(3+\beta)}{3}\left[\frac{k\left(A_0 t - kt^2\right)}{\left(A_0 - 2kt^2\right)^2} + \frac{1}{4}\right], \tag{18}$$

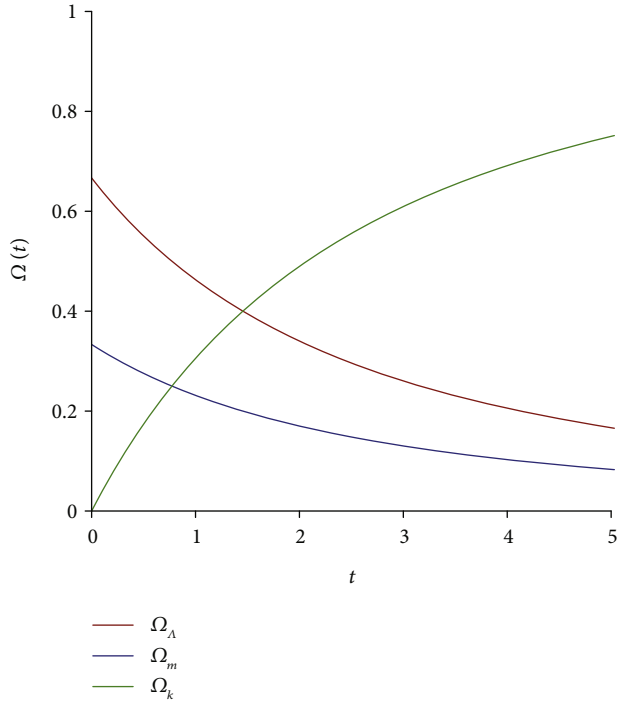

Figure 3: Plot of $\Omega(t)$ versus t for $k = -1$.

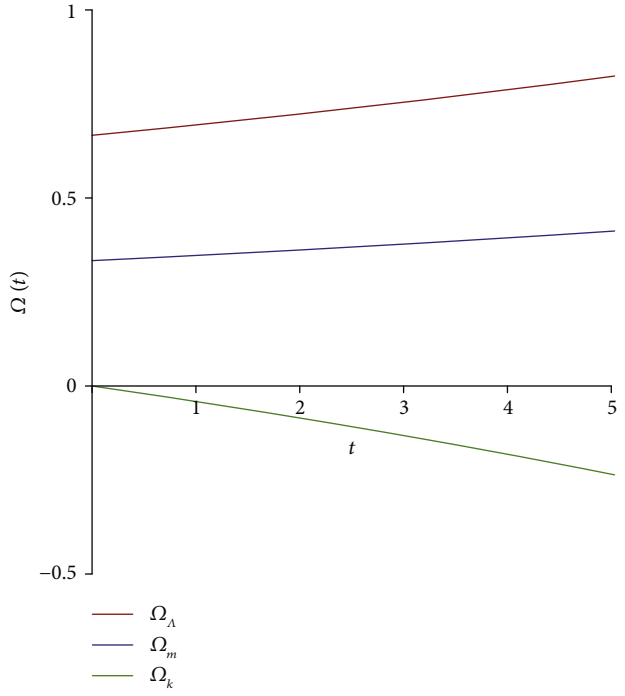

Figure 4: Plot of $\Omega(t)$ versus t for $k = +1$.

$$\Omega_k = -\frac{k}{a^2H^2} = -\frac{4k\left(A_0 t - kt^2\right)}{\left(A_0 - 2kt^2\right)^2}. \tag{19}$$

We plot the time evolution of the density parameters for all contributing components, i.e., matter, curvature, and dark energy, for $k = -1$ in Figure 3. The contribution to the density parameter due to curvature increases while contributions due to Λ and matter decrease, but the overall density parameter due to all three components remains the same.

We also plot the time evolution of the density parameters for matter, curvature, and dark energy for $k = 1$ in Figure 4. The contribution to the density parameter due to curvature decreases and is *negative* while contributions due to Λ and matter increase, but again the overall density parameter remains the same.

For the flat space ($k = 0$), we see from the above expressions that the sum total of the density parameters of the above components is equal to 1, such that $\Omega_k = 0$, $\Omega_\Lambda = -(\beta/3)$, and $\Omega_m = (3 + \beta)/3$.

Also, for both the limiting cases, $t \longrightarrow 0$ and ∞, the sum total of the density parameters is equal to 1. In these two cases, both Ω_m and Ω_Λ become independent of k. Hence, for both early and late times, the universe exhibits similar behaviour as far as the k dependency of Ω_m and Ω_Λ is concerned.

In general, it can be observed on taking the sum of equations (17)–(19) that

$$\Omega_m + \Omega_\Lambda + \Omega_k = 1. \tag{20}$$

This analytical approach is consistent with the observational constraints $\Omega = 1 \pm 0.016$ [45].

2.2. Solutions for the Phenomenological Model $\Lambda \sim \rho$. In this phenomenological model, we consider $\Lambda = 8\pi G\rho\gamma$, where $\gamma > 0$ which is consistent with the observation as can be seen in Section 3. Using this form of Λ in equation (8), we obtain

$$\frac{\ddot{a}}{\dot{a}} = -\frac{(1 + 3\omega - 2\gamma)}{2(1 + \gamma)}\frac{\dot{a}}{a} - \frac{(1 + 3\omega - 2\gamma)}{2(1 + \gamma)}\frac{k}{a\dot{a}}. \tag{21}$$

This equation can be simplified to

$$a\dot{a}\frac{d}{dt}\left[\ln\left(\dot{a}a^{-B}\right)\right] = Bk, \tag{22}$$

where $B = (1 + 3\omega - 2\gamma)/2(1 + \gamma)$. We choose $B = -1$, such that $\omega = (4\gamma + 1)/3$.

The above equation now takes the form

$$a\dot{a}\frac{d}{dt}\left[\ln\left(\dot{a}a\right)\right] = -k. \tag{23}$$

The scale factor turns out to be

$$a(t) = \sqrt{A_0{}'t + A_1' - kt^2}, \tag{24}$$

where $A_0{}'$ and $A_1{}'$ are integration constants.

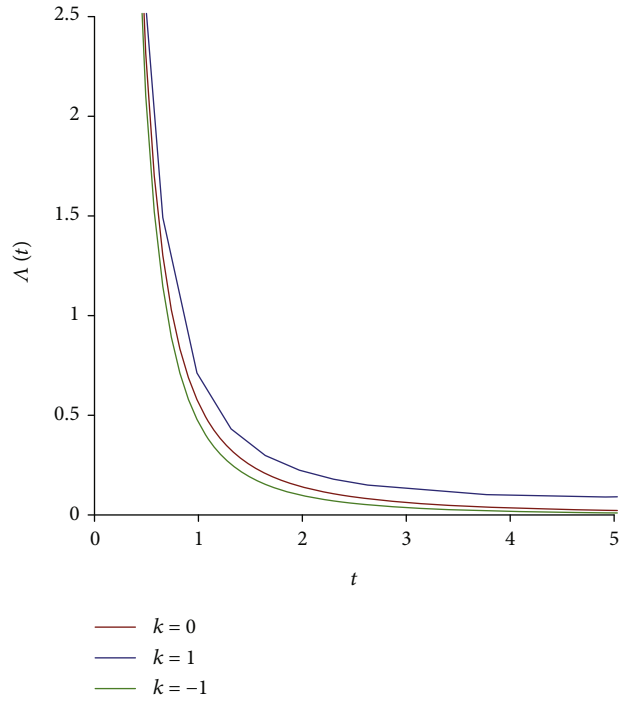

Figure 5: Plot of $\Lambda(t)$ versus t for different values of k.

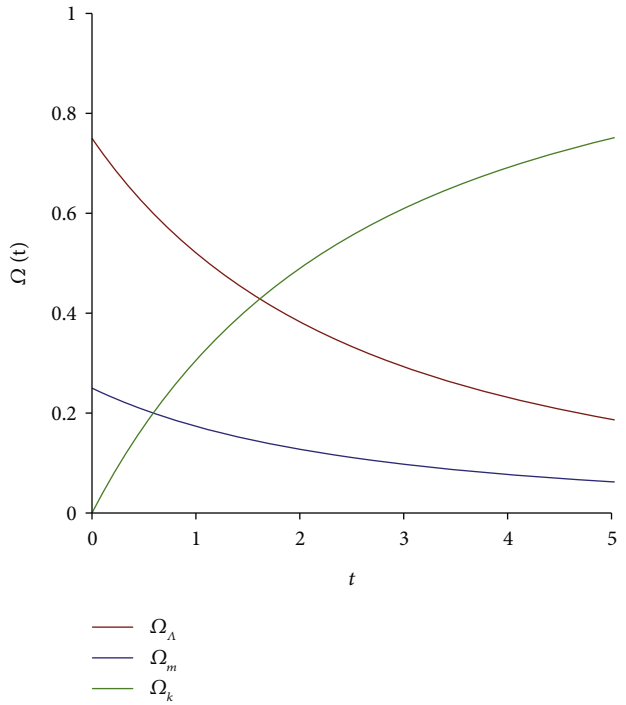

Figure 6: Plot of $\Omega(t)$ versus t for $k = -1$.

As we are considering a universe evolving from a singularity, $a(t = 0) = 0$. This gives $A_1' = 0$. So

$$a(t) = \sqrt{A_0' t - kt^2}. \tag{25}$$

The Hubble parameter is computed as

$$H(t) = \frac{A_0' - 2kt}{2\left(A_0' t - kt^2\right)}. \tag{26}$$

The cosmological constant is given by

$$\Lambda(t) = -\frac{3\gamma A_0'^2}{2(1 + 3\omega - 2\gamma)\left(A_0' t - kt^2\right)^2}. \tag{27}$$

Time evolution of the cosmological constant is plotted in Figure 5 and is found to be monotonically decreasing for all considered values of k, similar to the β model. The energy density is given by

$$\rho(t) = \frac{3}{16\pi G(1 + 3\omega - 2\gamma)} \frac{A_0'^2}{\left(A_0' t - kt^2\right)^2}. \tag{28}$$

Variation of the scale factor $a(t)$ is the same as shown in Figure 1.

The density parameters for matter, a cosmological constant, and curvature, respectively, can be computed in a similar manner as the above for this phenomenological model as

$$\begin{aligned}
\Omega_m &= \frac{4\gamma}{1 + \gamma}\left[\frac{k\left(A_0' t - kt^2\right)}{\left(A_0' - 2kt^2\right)^2} + \frac{1}{4}\right], \\
\Omega_\Lambda &= \frac{4}{1 + \gamma}\left[\frac{k\left(A_0' t - kt^2\right)}{\left(A_0' - 2kt^2\right)^2} + \frac{1}{4}\right], \\
\Omega_k &= -\frac{k}{a^2 H^2} = -\frac{4k\left(A_0' t - kt^2\right)}{\left(A_0' - 2kt^2\right)^2}.
\end{aligned} \tag{29}$$

Similar to the previous model, we again plot the time evolution of the density parameters for all contributing components, i.e., matter, curvature, and dark energy, for $k = -1$ in Figure 6. The contribution to the density parameter due to curvature increases while contributions due to Λ and matter decrease, but the overall density parameter due to all three components remains the same; also, the time evolution of the density parameters for matter, curvature, and dark energy for $k = 1$ has been plotted in Figure 7. Similarly, as for the previous model, the contribution to the density parameter due to curvature decreases and is *negative* while contributions due to Λ and matter increase, but again the overall density parameter remains the same.

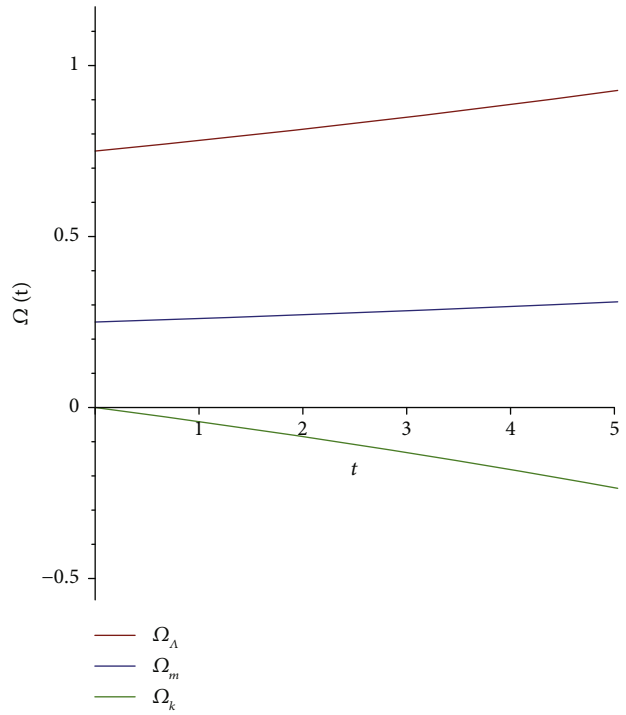

Figure 7: Plot of $\Omega(t)$ versus t for $k = +1$.

For the flat space ($k = 0$), we see from the above expressions that the sum total of the density parameters of the above components is equal to 1, such that $\Omega_k = 0$, $\Omega_m = 1/(1+\gamma)$, and $\Omega_\Lambda = \gamma/(1+\gamma)$.

In the case of $t \to 0$ and ∞, the sum total of the density parameters is equal to 1 in a similar manner as for the previous model.

In general, it can be observed on taking the sum of the above three equations that

$$\Omega_m + \Omega_\Lambda + \Omega_k = 1, \tag{30}$$

which is again consistent with [45].

3. Constraints on the Different Parameters with the Latest Observational Results

Although we deal with simple phenomenological models which are not dependent on any quantum field theory, different cosmological pictures can be reflected successfully.

Considering the cosmology of base-Λ-CDM, late universe parameters can be observed in ranges: Hubble constant $H_0 = 67.4 \pm 0.5$ km/s/Mpc and matter density parameter $\Omega_{m0} = 0.315 \pm 0.007$ [45]. Using the above ranges of Ω_{m0}, the model parameters can be constrained as $-2.076 \le \beta_0 \le -2.034$ and $2.105 \le \gamma_0 \le 2.247$. Using more recent data [46] where the present value of the Hubble parameter is given as $H_0 = 74.03 \pm 1.42$ km/s/Mpc, we obtain $-2.0717 \le \beta_0 \le -2.06$ and $1.785 \le \gamma_0 \le 1.821$.

The present value of the cosmological constant Λ_0 can be obtained using the relation $\Lambda_0 = 3H_0^2\gamma_0\Omega_{m0}$. It lies within the range $0.9 \times 10^{-35}\,\mathrm{s}^{-2} \le \Lambda_0 \le 1.042 \times 10^{-35}\,\mathrm{s}^{-2}$, which is in sync with the observation [45]. We know the quintessence equation of state as $p_Q = \omega_Q \rho_Q$, $\omega_Q = -\Omega_\Lambda = -\gamma\Omega_m$. Using the above ranges we have $-0.724 \le \omega_Q \le -0.648$. This range is in good agreement with the accepted range of ω_Q which is $-1 \le \omega_Q \le -0.6$ [45, 47, 48], although, in either of our models, we do not consider quintessence and present the range only as a qualitative check.

Also, there are upcoming observational surveys like the Euclid survey [49] which is aimed at obtaining more precise and accurate data concerning dark energy and dark matter. The survey plans to use redshift selected baryon acoustic oscillation (BAO) to study dark energy and its time evolution. The phenomenological models which consider Λ dark energy in the kinematic and hydrodynamic forms can also be constrained more stringently using precise data from this survey. This may decide the fate of these models in future study.

4. Conclusion

To summarize, the basic philosophy behind the present paper is to generalize two phenomenological models. Explicit expressions of $a(t)$, $H(t)$, $\rho(t)$, $\Lambda(t)$, and also the parameter $\Omega(t)$ corresponding to matter, curvature, and DE have been derived. Cosmic evolution of the universe from the very early time to the late time has been discussed.

The conclusions of the present work can be jotted down as follows:

(i) The models $\Lambda \sim \ddot{a}/a$ and $\Lambda \sim \rho$ are equivalent for $k = \pm 1$

(ii) Both the models exhibit usual cosmological behaviour for early and late time universes. Initially chosen values of the model parameters are found to be in good agreement with the observational data

(iii) Constraints on the different cosmological variables have been evaluated using our models, and the results are in good agreement with the observational results

Data Availability

We have not generated any data in this paper but used observational data from references [45–48].

Conflicts of Interest

The authors declare that they have no conflicts of interest.

References

[1] S. Perlmutter, G. Aldering, G. Goldhaber et al., "Measurements of Ω and Λ from 42 high-redshift supernovae," *The Astrophysical Journal*, vol. 517, no. 2, pp. 565–586, 1999.

[2] A. G. Riess, R. P. Kirshner, B. P. Schmidt et al., "BVRI light curves for 22 type Ia supernovae," *The Astrophysical Journal*, vol. 117, 1999.

[3] A. Aguirre, "Intergalactic dust and observations of type Ia supernovae," *The Astrophysical Journal*, vol. 525, no. 2, pp. 583–593, 1999.

[4] V. Sahni and A. A. Starobinsky, "The case for a positive cosmological Λ-term," *International Journal of Modern Physics D: Gravitation; Astrophysics and Cosmology*, vol. 9, no. 4, pp. 373–443, 2000.

[5] J. M. Overduin and F. I. Cooperstock, "Evolution of the scale factor with a variable cosmological term," *Physical Review D*, vol. 58, no. 4, 1998.

[6] A. Lue, "The phenomenology of Dvali-Gabadadze-Porrati cosmologies," *Physics Reports*, vol. 423, no. 1, pp. 1–48, 2006.

[7] S. Nojiri and S. D. Odintsov, "Introduction to modified gravity and gravitational alternative for dark energy," *International Journal of Geometric Methods in Modern Physics*, vol. 4, no. 1, pp. 115–145, 2007.

[8] I. Zlatev, L. Wang, and P. J. Steinhardt, "Quintessence, cosmic coincidence, and the cosmological constant," *Physical Review Letters*, vol. 82, no. 5, pp. 896–899, 1999.

[9] P. Brax and J. Martin, "Robustness of quintessence*Physical Review D*," vol. 61, no. 10, 2000.

[10] T. Barreiro, E. J. Copeland, and N. A. Nunes, "Quintessence arising from exponential potentials," *Physical Review D*, vol. 61, no. 12, 2000.

[11] A. Albrecht and C. Skordis, "Phenomenology of a realistic accelerating universe using only Planck-scale physics," *Physical Review Letters*, vol. 84, no. 10, pp. 2076–2079, 2000.

[12] C. Armendáriz-Picón, T. Damour, and V. Mukhanov, "*k*-Inflation," *Physics Letters B*, vol. 458, no. 2-3, pp. 209–218, 1999.

[13] J. Garriga and V. F. Mukhanov, "Perturbations in *k*-inflation," *Physics Letters B*, vol. 458, no. 2-3, pp. 219–225, 1999.

[14] T. Chiba, T. Okabe, and M. Yamaguchi, "Kinetically driven quintessence," *Physical Review D*, vol. 62, no. 2, 2000.

[15] C. Armendariz-Picon, V. Mukhanov, and P. J. Steinhardt, "Dynamical solution to the problem of a small cosmological constant and late-time cosmic acceleration," *Physical Review Letters*, vol. 85, no. 21, pp. 4438–4441, 2000.

[16] C. Armendariz-Picon, V. Mukhanov, and P. J. Steinhardt, "Essentials of *k*-essence," *Physical Review D*, vol. 63, no. 10, p. 103510, 2001.

[17] M. Malquarti and A. R. Liddle, "Initial conditions for quintessence after inflation," *Physical Review D*, vol. 66, no. 2, 2002.

[18] R. R. Caldwell, "A phantom menace? Cosmological consequences of a dark energy component with super-negative equation of state," *Physics Letters B*, vol. 545, no. 1-2, pp. 23–29, 2002.

[19] A. Sen, "Rolling tachyon," *Journal of High Energy Physics*, vol. 2002, no. 4, 2002.

[20] A. Sen, "Tachyon matter," *Journal of High Energy Physics*, vol. 2002, no. 7, 2002.

[21] M. R. Garousi, "Tachyon couplings on non-BPS D-branes and Dirac-Born-Infeld action," *Nuclear Physics B*, vol. 584, no. 1-2, pp. 284–299, 2000.

[22] M. R. Garousi, "On-shell S-matrix and tachyonic effective actions," *Nuclear Physics B*, vol. 647, no. 1-2, pp. 117–130, 2002.

[23] M. R. Garousi, "Slowly varying tachyon and tachyon potential," *Journal of High Energy Physics*, vol. 2003, no. 5, p. 058, 2003.

[24] E. A. Bergshoeff, M. de Roo, T. C. de Wit, E. Eyras, and S. Panda, "T-duality and actions for non-BPS D-branes," *Journal of High Energy Physics*, vol. 5, 2000.

[25] J. Kluson, "Proposal for non-Bogomol'nyi-Prasad-Sommerfield D-brane action," *Physical Review D*, vol. 62, no. 12, p. 126003, 2000.

[26] D. Kutasov and V. Niarchos, "Tachyon effective actions in open string theory," *Nuclear Physics B*, vol. 666, no. 1-2, pp. 56–70, 2003.

[27] U. Mukhopadhyay, S. Ray, A. A. Usmani, and P. P. Ghosh, "Time variable Λ and the accelerating universe," *International Journal of Theoretical Physics*, vol. 50, no. 3, pp. 752–759, 2011.

[28] S. Ray, F. Rahaman, U. Mukhopadhyay, and R. Sarkar, "Variable equation of state for generalized dark energy model," *International Journal of Theoretical Physics*, vol. 50, no. 9, pp. 2687–2696, 2011.

[29] A. A. Usmani, P. P. Ghosh, U. Mukhopadhyay, P. C. Ray, and S. Ray, "The dark energy equation of state," *Monthly Notices of the Royal Astronomical Society: Letters*, vol. 386, no. 1, pp. L92–L95, 2008.

[30] J. C. Carvalho, J. A. S. Lima, and I. Waga, "Cosmological consequences of a time-dependent Λ term," *Physical Review D*, vol. 46, no. 6, pp. 2404–2407, 1992.

[31] I. Waga, "Decaying vacuum flat cosmological models-expressions for some observable quantities and their properties," *The Astrophysical Journal*, vol. 414, p. 436, 1993.

[32] J. A. S. Lima and J. C. Carvalho, "Dirac's cosmology with varying cosmological constant," *General Relativity and Gravitation*, vol. 26, no. 9, pp. 909–916, 1994.

[33] J. M. Salim and I. Waga, "Thermodynamic constraints on a time-dependent lambda model (cosmology)," *Classical and Quantum Gravity*, vol. 10, no. 9, pp. 1767–1774, 1993.

[34] A. I. Arbab and A.-M. M. Abdel-Rahman, "Nonsingular cosmology with a time-dependent cosmological term," *Physical Review D*, vol. 50, no. 12, pp. 7725–7728, 1994.

[35] C. Wetterich, "An asymptotically vanishing time-dependent cosmological constant," *Astronomy and Astrophysics*, vol. 301, p. 321, 1995.

[36] A. I. Arbab, "Cosmological models with variable cosmological and gravitational "constants" and bulk viscous models," *General Relativity and Gravitation*, vol. 29, no. 1, pp. 61–74, 1997.

[37] T. Padmanabhan, https://arxiv.org/abs/1907.12869v1.

[38] A. I. Arbab, "Cosmic acceleration with a positive cosmological constant," *Classical and Quantum Gravity*, vol. 20, no. 1, pp. 93–99, 2003.

[39] A. I. Arbab, "Cosmological consequences of a built-in cosmological constant model," *Journal of Cosmology and Astroparticle Physics*, vol. 5, p. 008, 2003.

[40] A. I. Arbab, "The equivalence between different dark (matter) energy scenarios," *Astrophysics and Space Science*, vol. 291, no. 2, pp. 143–149, 2004.

[41] R. G. Vishwakarma, "Consequences on variable Λ-models from distant type Ia supernovae and compact radio sources," *Classical and Quantum Gravity*, vol. 18, no. 7, pp. 1159–1172, 2001.

[42] S. Ray, P. C. Ray, M. Khlopov, P. P. Ghosh, U. Mukhopadhyay, and P. Chowdhury, "Scenario of inflationary cosmology from the phenomenological Λ models," *International Journal of Theoretical Physics*, vol. 48, no. 9, pp. 2499–2510, 2009.

[43] S. Ray, U. Mukhopadhyay, and X.-H. Meng, "Accelerating universe with a dynamic cosmological term," *Gravitation and cosmology*, vol. 13, p. 142, 2007.

[44] U. Mukhopadhyay, P. C. Ray, S. Ray, and S. B. Datta Choudhury, "Generalized model for Λ− dark energy," *International Journal of Modern Physics D: Gravitation; Astrophysics and Cosmology*, vol. 18, p. 389, 2009.

[45] N. Aghanim et al., *Planck Collaboration*, https://arxiv.org/abs/1807.06209.

[46] A. G. Riess, S. Casertano, W. Yuan, L. M. Macri, and D. Scolnic, "Large Magellanic Cloud Cepheid standards provide a 1% foundation for the determination of the Hubble constant and stronger evidence for physics beyond ΛCDM," *The Astrophysical Journal*, vol. 876, no. 1, p. 85, 2019.

[47] A. Balbi, C. Baccigalupi, S. Matarrese, F. Perrotta, and N. Vittorio, "Implications for quintessence models from MAXIMA-1 and BOOMERANG-98," *The Astrophysical Journal*, vol. 547, no. 2, pp. L89–L92, 2001.

[48] P. S. Corasaniti and E. J. Copeland, "Constraining the quintessence equation of state with SnIa data and CMB peaks," *Physical Review D*, vol. 65, no. 4, 2002.

[49] R. Laureijs et al., https://arxiv.org/abs/1110.3193.

Hindawi
Advances in High Energy Physics
Volume 2020, Article ID 8039183, 9 pages
https://doi.org/10.1155/2020/8039183

Research Article

Phase Structure and Quasinormal Modes of AdS Black Holes in Rastall Theory

De-Cheng Zou,[1] **Ming Zhang**,[2] **and Ruihong Yue**[1]

[1]*Center for Gravitation and Cosmology, College of Physical Science and Technology, Yangzhou University, Yangzhou 225009, China*
[2]*Faculty of Science, Xi'an Aeronautical University, Xi'an 710077, China*

Correspondence should be addressed to De-Cheng Zou; dczou@yzu.edu.cn

Received 6 June 2019; Revised 26 July 2019; Accepted 19 August 2019; Published 22 January 2020

Guest Editor: Farook Rahaman

We discuss the $P-V$ criticality and phase transition in the extended phase space of anti-de Sitter(AdS) black holes in four-dimensional Rastall theory and recover the Van der Waals (VdW) analogy of small/large black hole (SBH/LBH) phase transition when the parameters ω_s and ψ satisfy some certain conditions. Later, we further explore the quasinormal modes (QNMs) of massless scalar perturbations to probe the SBH/LBH phase transition. It is found that it can be detected near the critical point, where the slopes of the QNM frequencies change drastically in small and large black holes.

1. Introduction

As the most beautiful and simplest theory of gravity, Einstein's general relativity (GR) admits the covariant conservation of matter energy-momentum tensor. It is worthy to point out that the idea of the covariant conservation for spacetime symmetries has been implemented only in the Minkowski flat or weak field regime of gravity. Nevertheless, the actual nature of the spacetime geometry and the covariant conservation relation is still debated in the strong domain of gravity. In 1972, Rastall [1] demonstrated an adjustment to Einstein's equation, which results in a violation of the usual conservation law, and the energy-momentum tensor satisfies

$$T^{\mu\nu}{}_{;\mu} = \lambda R^{\nu}, \tag{1}$$

where R is the Ricci scalar and λ is the Rastall coupling parameter, which measures the potential deviation of Rastall theory from GR. This theory provides an explanation of the inflation problem, as the simplest modified gravity scenario to realize the late-time acceleration and other cosmological problems [2–5]. It is an interesting result that all electrovacuum solutions of GR automatically meet the equation of motion in the Rastall gravity. However, it failed if one introduces any nonvanishing trace matter field. Until now, many works on the various black hole solutions have been investigated in Rastall theory. The spherically symmetric black hole solutions were constructed in Refs. [6–10], the rotating black holes were in Refs. [11, 12], the thermodynamics of black holes was in Refs. [13–17], and also instability of black holes was in Refs. [18, 19].

Recently, the study of thermodynamics of AdS black holes has been generalized to the extended phase space, where the cosmological constant is related to the thermodynamic pressure [20, 21].

$$P = \frac{\Lambda}{8\pi}. \tag{2}$$

In fact, the variation of the cosmological constant is beneficial to the consistency between the first law of black hole thermodynamics and the Smarr formula. In the extended phase space, the charged AdS black hole admits a more direct and precise coincidence between the first-order small/large black hole (SBH/LBH) phase transition and Van der Waals (VdW) liquid-gas phase transition, and both systems share the same critical exponents near the critical

point [22]. More discussions in this direction can be found as well in including reentrant phase transitions and some other phase transitions [23–51].

On the other hand, in the context of the AdS/CFT correspondence, the QNMs of a $(D+1)$-dimensional asymptotically AdS black hole or brane are poles of the retarded Green's function in the D-dimensional dual conformal field theory at strong coupling [52–54]. Then, one can describe various properties of strongly coupled quark-gluon plasmas which cannot be studied by traditional perturbative methods of quantum field theory [55, 56], such as the universal value $1/4\pi$ for the ratio of viscosity to the entropy density in quark-gluon plasma via various gravitational backgrounds [57]. In the dual-field theory, thermodynamic phase transition of black holes corresponds to the onset of instability of a black hole. It is naturally considered that QNMs of black holes are connected with thermodynamic phase transitions of strongly coupled field theories [58]. A lot of discussions have been focused on this topic, and more and more evidence has been found between thermodynamical phase transitions and QNMs [50, 59–70]. Recently, the extended phase space thermodynamics for $P-V$ criticality and phase transition of d-dimensional AdS black holes in perfect fluid background have been investigated in Ref. [17], which shows the existence of Van der Waals analogy of SBH/LBH phase transition. Motivated by the result, in this paper, we use the QNM frequencies of a massless scalar perturbation to probe the Van der Waals-like SBH/LBH phase transition of four-dimensional AdS black holes surrounded by perfect fluid in the Rastall theory.

This paper is organized as follows. In Section 2, we review the thermodynamics of four-dimensional AdS black holes in the extended phase space and will show the analogy of the SBH/LBH phase transition with the VdW liquid-gas system. In Section 3, we will disclose that the phase transition can be reflected by the QNM frequencies of dynamical perturbations. We end the paper with conclusions and discussions in Section 4.

2. Thermodynamics and Phase Transition of AdS Black Holes

Considering (1), the field equation including the negative cosmological constant Λ reads as [17]

$$G_{\mu\nu}+\Lambda g_{\mu\nu}=k\left(T_{\mu\nu}-\lambda g_{\mu\nu}R\right), \tag{3}$$

where these field equations reduce to GR field equations in the limit of $\lambda\to 0$, κ equals to $8\pi G_N$, and G_N is the Newton gravitational coupling constant.

In four-dimensional spacetime, the energy-momentum tensor $T_{\mu\nu}$ of perfect fluid reads as [8, 9]

$$\begin{aligned}&\mathcal{T}^{u}{}_{u}=\mathcal{T}^{r}{}_{r}=-\rho_s(r),\\&\mathcal{T}^{\theta}{}_{\theta}=\mathcal{T}^{\varphi}{}_{\theta_{d-2}}=\frac{1}{2}(1+3\omega_s)\rho_s(r).\end{aligned} \tag{4}$$

Then, the AdS black hole solution in four-dimensional Rastall theory is [17]

$$ds^2=-f(r)dt^2+\frac{1}{f(r)}dr^2+r^2\left(d\theta^2+\sin^2\theta d\vartheta^2\right), \tag{5}$$

$$f(r)=1-\frac{2M}{r}-\frac{N_s}{r\xi}+\frac{r^2}{R_\Lambda^2}, \tag{6}$$

with

$$\begin{aligned}&\xi=\frac{1+3\omega_s-6\psi(1+\omega_s)}{1-3\psi(1+\omega_s)},\quad \psi=k\lambda,\\&\frac{1}{R_\Lambda^2}=-\frac{\Lambda}{3(1-4\psi)},\end{aligned} \tag{7}$$

where R_Λ is the curvature radius in the Rastall gravity and ω_s is the state parameter of fluid. M and N_s are two integration constants representing the black hole mass and surrounding field structure parameter, respectively. The subscript "s" denotes the surrounding field, like the dust, radiation, quintessence, cosmological constant, or phantom field.

Moreover, the integration constant N_s is related to the energy density ρ_s [9, 17]:

$$\rho_s=-\frac{3W_sN_s}{\kappa r^{(3(1+\omega_s)-12\psi(1+\omega_s))/(1-3\psi(1+\omega_s))}}, \tag{8}$$

with

$$W_s=-\frac{(1-4\psi)(\psi(1+\omega_s)-\omega_s)}{(1-3\psi(1+\omega_s))^2}. \tag{9}$$

Regarding the weak energy condition representing the positivity of any kind of energy density of the surrounding field, i.e., $\rho_s\geq 0$, the following condition was imposed:

$$W_sN_s\leq 0, \tag{10}$$

which implies that for the surrounding field with geometric parameter $W_s>0$, we need $N_s<0$ and conversely for $W_s<0$, we need $N_s>0$ [9]. When N_s vanishes, (6) reduces to vacuum AdS black hole solution in the Rastall gravity:

$$f(r)=1-\frac{2M}{r}+\frac{r^2}{R_\Lambda^2}. \tag{11}$$

In the limit of $\psi\to 0$, namely, $\lambda\to 0$, the covariant derivative of energy-momentum tensor vanishes and the Rastall gravity becomes the Einstein gravity. We can recover the Schwarzschild-AdS black hole from (3):

$$\begin{aligned}&f(r)=1-\frac{2M}{r}+\frac{r^2}{R^2},\\&\frac{1}{R^2}=-\frac{\Lambda}{3}.\end{aligned} \tag{12}$$

Table 1: The positive values of critical points in the case of $\rho_s \geq 0$.

$N_s > 0 \cup W_s < 0$	$\omega_s < -1 \cup \frac{1}{3+3\omega_s} < \psi < \frac{1}{4}$	$-1 < \omega_s < \frac{1}{3} \cup \frac{\omega_s}{1+\omega_s} < \psi < \frac{1+3\omega_s}{6+6\omega_s}$	None
$N_s > 0 \cup W_s < 0$	$\omega_s < -1 \cup \frac{1}{4} < \psi < \frac{2+3\omega_s}{9+9\omega_s}$	$-1 < \omega_s \leq \frac{1}{3} \cup \psi < \frac{\omega_s}{1+\omega_s}$	$\omega_s > \frac{1}{3} \cup \psi < \frac{1}{3+3\omega_s}$

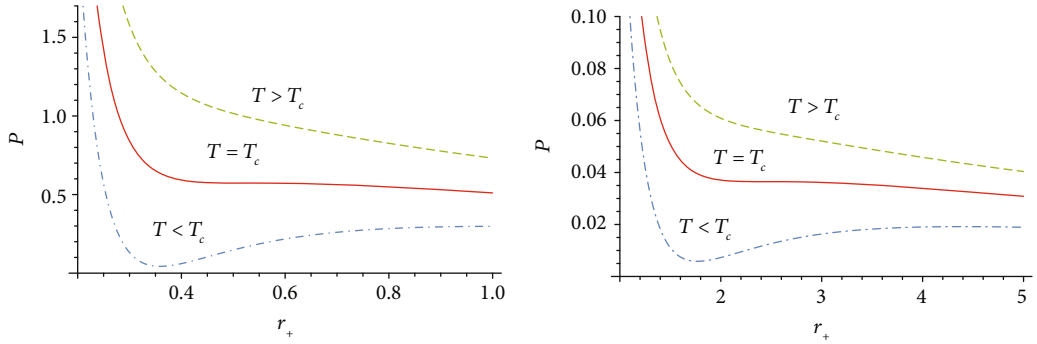

(a) $\omega_s = -2/3$ (b) $\omega_s = 1/3$

Figure 1: The $P - r_+$ diagrams of four-dimensional AdS black holes with $\psi = -5/2$ and $N_s = -1$. The upper dashed line corresponds to the idea gas phase behavior for $T > T_c$. The critical temperature case $T = T_c$ is denoted by the solid line. The line below is with temperatures smaller than the critical temperature. We have $T_c = 0.1610$ in (a) and $T_c = 0.0433$ in (b).

In terms of horizon radius r_+, mass M, Hawking temperature T, and entropy S of the AdS black holes can be written, respectively, as

$$M = \frac{r_+}{2}\left(1 - \frac{N_s}{r_+^{\xi}} + \frac{r_+^2}{R_\Lambda^2}\right),$$
$$T = \frac{1}{4\pi}\left(\frac{1}{r_+} + \frac{3r}{R_\Lambda^2} + \frac{(\xi-1)N_s}{r_+^{1+\xi}}\right), \quad (13)$$
$$S = \pi r_+^2.$$

In the extended phase space, the cosmological constant is related to the thermodynamic pressure with

$$P = -\frac{\Lambda}{8\pi} = \frac{3(1-4\psi)}{8\pi R_\Lambda^2}, \quad (14)$$

we can obtain the equation of state:

$$P = \frac{(1-4\psi)}{2r_+}\left[T - \frac{1}{4\pi r_+} - \frac{(\xi-1)N_s}{4\pi r_+^{1+\xi}}\right], \quad (15)$$

from the Hawking temperature (13).

As usual, a critical point occurs when P has an inflection point:

$$\left.\frac{\partial P}{\partial r_+}\right|_{T=T_c, r_+=r_c} = \left.\frac{\partial^2 P}{\partial r_+^2}\right|_{T=T_c, r_+=r_c} = 0. \quad (16)$$

The corresponding critical values are obtained as

$$r_c = \left[\frac{(1-\xi)(1+\xi)(2+\xi)N_s}{2}\right]^{1/\xi},$$
$$T_c = \frac{\xi}{2\pi(1+\xi)r_c}, \quad (17)$$
$$P_c = \frac{(1-4\psi)\xi}{8\pi r_c^2(2+\xi)}.$$

The subscript "c" denotes the values of the physical quantities at the critical points. Evidently, the critical parameters r_c, T_c, and P_c depend on the values of ω_s (in [7]), N_s, and ψ. Regarding the weak energy condition $\rho_s > 0$, we summarize the corresponding constraint conditions of the positive critical values r_c, T_c, and P_c in Table 1.

For instance, we plot the $P - r$ isotherm diagram for the quintessence surrounding field ($\omega_s = -2/3$) [71] and radiation surrounding field ($\omega_s = 1/3$) [72] in the region of $-1 < \omega_s \leq 1/3 \cup \psi < \omega_s/(1+\omega_s)$ in Figure 1. The dotted line corresponds to the "idea gas" phase behavior when $P > P_c$, and the VdW-like SBH/LBH phase transition appears in the system when $P < P_c$.

The behavior of the Gibbs free energy G is important to determine the thermodynamic phase transition. The free energy G obeys the following thermodynamic relation $G = M - TS$ with

$$G = \frac{r_+}{4} - \frac{2P\pi r_+^3}{3(1-4\psi)} - \frac{(1+\xi)N_s}{4r_+^{\xi-1}}. \quad (18)$$

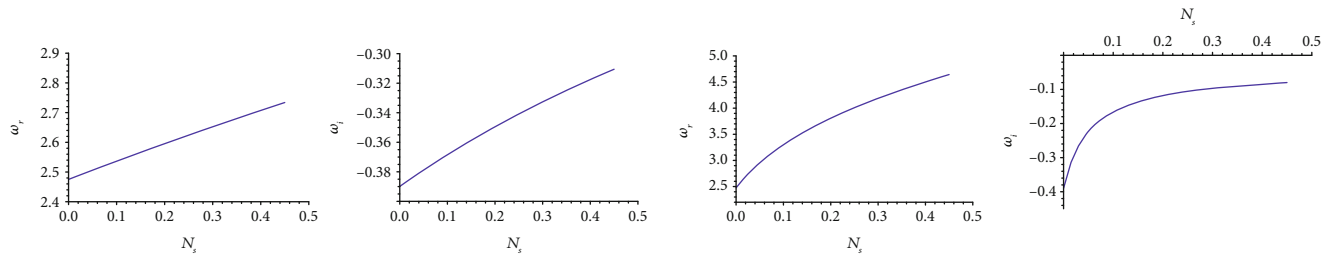

(a) $\omega_s = -2/3$ (b) $\omega_s = 1/3$

FIGURE 2: For $n = 0$, (a) real quasinormal frequency and (b) negative imaginary quasinormal frequency as functions of N_s around the AdS black hole with $r_+ = 0.2$, $R_\Lambda = 1$, and $\psi = -5/2$ in the Rastall gravity.

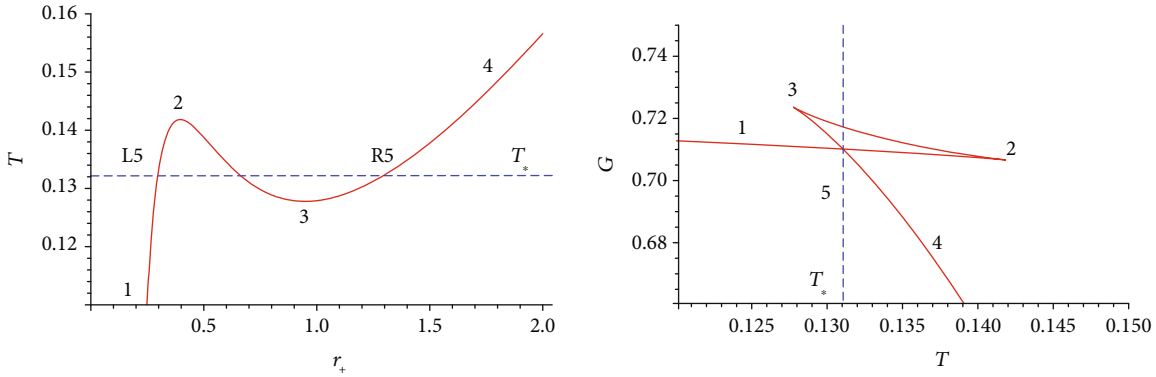

FIGURE 3: The $T - r_+$ and $G - T$ diagrams of four-dimensional AdS black holes with $\psi = -5/2$, $N_s = -1$, $\omega_s = -2/3$, and $P = 0.3283$.

Here, r_+ is understood as a function of pressure and temperature ($r_+ = r_+(P, T)$), via the equation of state (15).

3. Perturbations of AdS Black Holes in Rastall Gravity

Now, we study a massless scalar field perturbation on the four-dimensional AdS black holes surrounded by perfect fluid. The test scalar field satisfies the Klein-Gordon equation:

$$\frac{1}{\sqrt{-g}}\partial_\mu\left(\sqrt{-g}g^{\mu\nu}\partial_\nu\Phi(r,t,\theta,\vartheta)\right) = 0. \tag{19}$$

Assuming the scalar field with

$$\Phi(t,r,\theta,\vartheta) = \sum_{lm}\frac{\phi(r)}{r}Y_{lm}(\theta,\vartheta)e^{-i\omega t}, \tag{20}$$

the radial perturbed equation is

$$\left(\frac{d^2}{dr_*^2} + \omega^2 - V(r)\right)\phi(r) = 0, \tag{21}$$

where r_* is the tortoise coordinate, defined by $dr/dr_* = f(r)$. The effective potential $V(r)$ reads as

$$V(r) = f(r)\left(\frac{f'(r)}{r} + \frac{l(l+1)}{r^2}\right), \tag{22}$$

where l is the angular momentum eigenvalue related to the angular momentum operator L^2. We only consider the case of $l = 0$ in this paper.

At the AdS boundary $r \to +\infty$, the generalized potential $V(r)$ diverges, which leads to $\phi(r) \to 0$.

Near the horizon r_+, the scalar field needs to satisfy the ingoing boundary condition, $\phi(r) \sim (r - r_+)^{i\omega/4\pi T}$. Following the same path in Refs. [50, 68–70], we define $\phi(r)$ as $\varphi(r)$ $\exp[-i\int(\omega/f(r))r]$, where $\exp[-i\int(\omega/f(r))dr]$ asymptotically approaches to the ingoing wave near the horizon; then, (21) becomes

$$\varphi''(r) + \varphi'(r)\left(\frac{f'(r)}{f(r)} - \frac{2i\omega}{r} + \frac{2}{r}\right) - \frac{2i\omega}{rf(r)}\varphi(r) = 0. \tag{23}$$

In the limit of $r \to r_+$, we can set $\varphi(r) = 1$ and we have $\varphi(r) = 0$ when $r \to \infty$.

It is worthy to point out that without surrounding perfect fluid ($N_S = 0$), the vacuum AdS black hole solution (11) in the

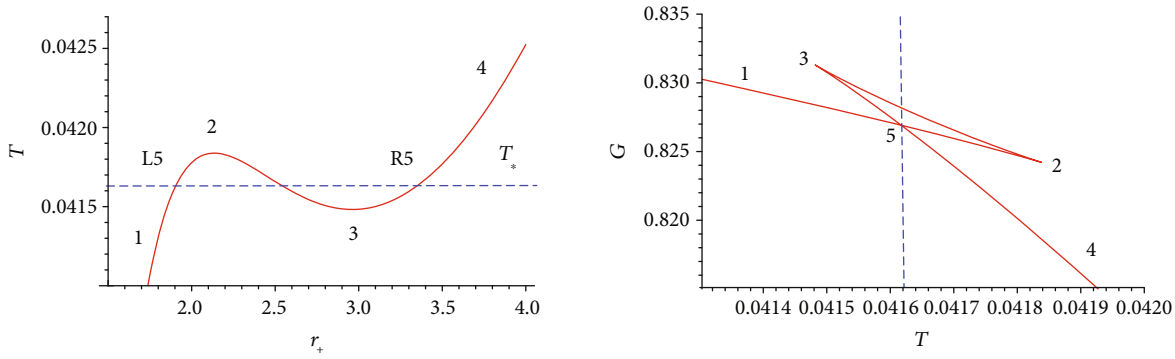

FIGURE 4: The $T - r_+$ and $G - T$ diagrams of four-dimensional AdS black holes with $\psi = -5/2$, $N_s = -1$, $\omega_s = 1/3$, and $P = 0.0328$.

Rastall gravity has the similar form with the Schwarzschild-AdS black hole solution in GR. Under the $l = 0$ scalar field perturbation, the quasinormal modes of Schwarzschild-AdS black hole with the AdS radius $R = 1$ have been computed in Ref. [73], where $n = 0$ fundamental frequency of Schwarzschild-AdS black hole with $r_+ = 0.2$ equals to $2.47511 - 0.38990i$. For the AdS black hole solution (6) in the Rastall gravity, we also set $R_\Lambda = 1$ and evaluate the effect of N_s on the quasinormal frequency, as shown in Figure 2. In the limit of $N_s \to 0$, these QNMs coincide with the fundamental mode $2.47511 - 0.38990i$, which plays the role of a starting point.

By choosing the pressure $P < P_c$, the $T - r_+$ and $G - T$ diagrams of four-dimensional AdS black holes are plotted in Figures 3 and 4. In that case, an inflection point occurs, which displays that the behavior is reminiscent of the Van der Waals system. Notice that the similar diagrams have been presented in Refs. [68, 70], where the point "5" represents coexistence of small and large black hole and the solid lines "1-5" or "1-L5" and "5-4" or "R5-4" separately denote small and large black holes (see Figures 3 and 4). In addition, the points "L5" and "R5" share the same Gibbs free energy and temperature with $T_* \approx 0.13105$ for $\omega_s = -2/3$ and $T_* \approx 0.04162$ for $\omega_s = 1/3$.

On the other hand, the QNM frequencies of massless scalar perturbation against the small and large black holes are shown in Table 2. For the small black hole phase $T < T_*$, the absolute values of the imaginary part of QNM frequencies decrease, while the real part of frequencies increase with the shrink of the horizon radius from T. In the large black hole phase $T < T_*$, the QNM frequencies are characterized by larger real oscillation frequency and larger damping with the increase in the horizon radius. These QNM frequencies for small and large black hole phases are also plotted in Figures 5 and 6. The arrow denotes the increase in the horizon radius r_+.

In addition, the mass M of Schwarzschild AdS black hole from (12) is given as

$$M = \frac{r_+^3}{2R^2} + \frac{r_+}{2}. \tag{24}$$

TABLE 2: The QNM frequencies of (a) ($\omega_s = -2/3$) and (b) ($\omega_s = 1/3$) with the change of temperature T and horizon radius r_+. The italic values denote the small black hole phase, while the rest of the values correspond to the large black hole phase.

(a)

T	r_+	ω
0.1250	*0.275*	*1.66875-0.02303I*
0.1270	*0.280*	*1.66643-0.02462I*
0.1288	*0.285*	*1.66407-0.02629I*
0.1304	*0.290*	*1.66167-0.02804I*
0.1311	1.245	1.97363-0.78752I
0.1312	1.250	1.97610-0.78863I
0.1313	1.255	1.97859-0.78974I
0.1314	1.260	1.98110-0.79083I

(b)

T	r_+	ω
0.040759	*1.700*	*1.15336-0.219889I*
0.041069	*1.750*	*1.14943-0.221412I*
0.041308	*1.800*	*1.14140-0.223724I*
0.041488	*1.850*	*1.13570-0.224786I*
0.041634	3.3525	1.93148-0.263925I
0.041636	3.3550	1.93191-0.263982I
0.041638	3.3575	1.93236-0.264036I
0.041640	3.3600	1.93281-0.264086I

In the limit $r_+ \to 0$, the mass M vanishes and (12) reduces to the pure AdS space:

$$f_{\mathrm{AdS}}(r) = 1 + \frac{r^2}{R^2}, \qquad \frac{1}{R^2} = -\frac{\Lambda}{3}. \tag{25}$$

In other words, the quasinormal modes of small Schwarzschild AdS black holes ($r_+ \to 0$) can tend to the

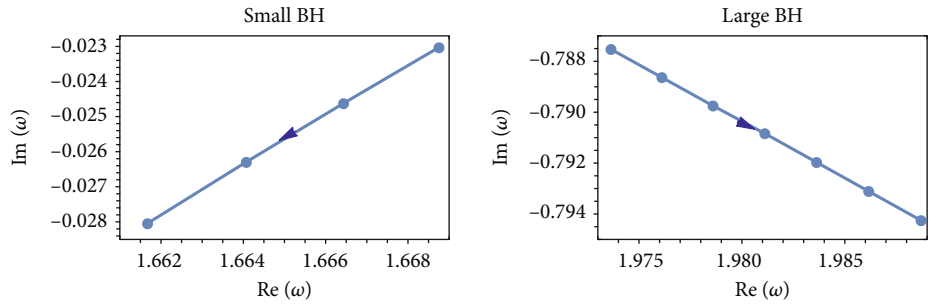

FIGURE 5: The real and imaginary parts of frequencies for large and small black holes with $\omega_s = -2/3$. The arrow denotes the increase in r_+.

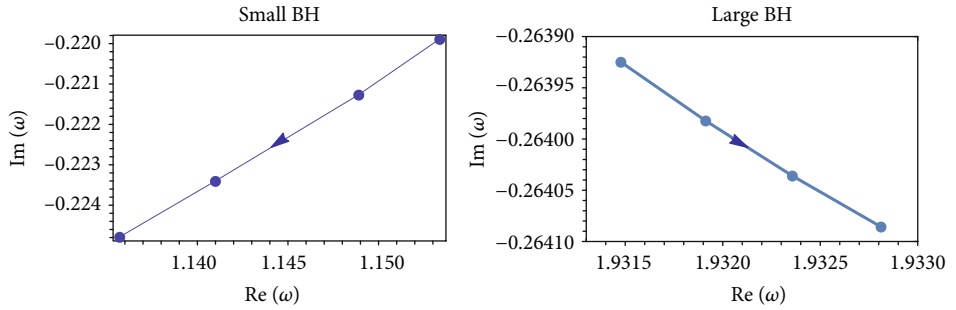

FIGURE 6: The real and imaginary parts of frequencies for large and small black holes with $\omega_s = 1/3$. The arrow denotes the increase in r_+.

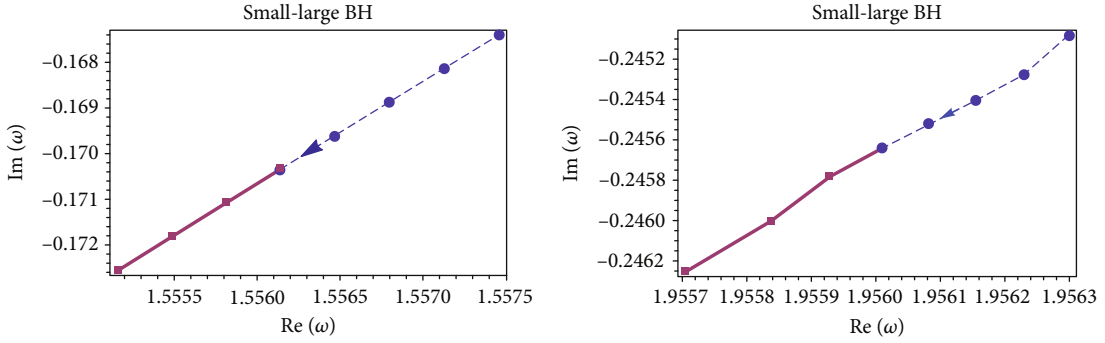

(a) $\omega_s = -2/3$ (b) $\omega_s = 1/3$

FIGURE 7: The real and imaginary parts of QNM frequencies for large (dashed) and small (solid) black holes. The arrow denotes the increase in the horizon radius.

purely normal modes of empty AdS spacetime, which has been proven by Konoplya in Ref. [74]. With regard to the AdS black hole (6) in the Rastall theory, the mass is obtained:

$$M_{\text{Ras}} = \frac{r_+^3}{2R_\Lambda^2} + \frac{r_+}{2} - \frac{N_s}{r_+^{\xi-1}}. \tag{26}$$

Evidently, the mass of AdS black hole is divergent in the limit $r_+ \to 0$. Then, this solution (6) cannot reduce the pure AdS space:

$$f_{\text{RAdS}}(r) = 1 + \frac{r^2}{R_\Lambda^2}, \tag{27}$$

because of the existence of $N_s \neq 0$. Therefore, the quasinormal modes of small AdS black holes ($r_+ \to 0$) cannot also tend to the purely AdS spectrum in the Rastall gravity.

In addition, at the critical position $P = P_c$, a second-order phase transition occurs. The QNM frequencies of the small and large black hole phases are shown in Figure 7. The QNM frequencies of two black hole phases display the similar trend of decay as increases in the horizon radius r_+. In fact, this phenomenon has also emerged in some other gravity theories [50, 68–70].

4. Concluding Remarks

In the four-dimensional Rastall theory, we reviewed the $P - V$ criticality and phase transition of AdS black holes

in the extended phase space. Considering the weak energy condition of energy density $\rho_s \geq 0$, we derived five proper regions for the parameters ω_s and ψ, where the VdW-like SBH/LBH phase transition could happen for the AdS black holes. Later, we further calculated the QNMs of massless scalar perturbations to probe the SBH/LBH phase transition of AdS black holes surrounded by two special fields: radiation and quintessence fields, respectively. These results reveal that when the SBH/LBH phase transition happens, the slopes of the QNM frequencies change drastically in the small and large black hole phases with the increase in r_+. In other words, the thermodynamic SBH/LBH phase transition has been exactly reflected by the variations of QNM frequencies for corresponding small and large black holes in the four-dimensional Rastall theory.

Nevertheless, this phenomenon does not appear at the critical isobaric phase transitions, where the QNM frequencies for both small and large black holes share the same behavior. This implies that the QNM frequencies are not suitable to probe the black hole phase transition in the second order.

In four-dimensional Rastall gravity, charged Kiselev-like black holes surrounded by perfect fluid have been obtained by Heydarzade and Darabi [9]. It would be interesting to derive charged AdS black hole solutions in the Rastall gravity. Then, we can recover the possible relation between the thermodynamical phase transition and QNM frequencies. Similar discussions for the charged AdS black holes in the Rastall gravity coupled with a nonlinear electric field also deserve a new work in the future.

Data Availability

The data used to support the findings of this study are included within the article.

Conflicts of Interest

The authors declare that they have no conflicts of interest.

Acknowledgments

This work is supported by the National Natural Science Foundation of China under Grant Nos. 11605152, 11675139, and 51802247 and the Natural Science Foundation of Jiangsu Province (Grant No. BK20160452)

References

[1] P. Rastall, "Generalization of the Einstein theory," *Physical Review D*, vol. 6, no. 12, pp. 3357–3359, 1972.

[2] H. Moradpour, Y. Heydarzade, F. Darabi, and I. G. Salako, "A generalization to the Rastall theory and cosmic eras," *European Physical Journal C: Particles and Fields*, vol. 77, no. 4, p. 259, 2017.

[3] H. Moradpour, "Thermodynamics of flat FLRW universe in Rastall theory," *Physics Letters B*, vol. 757, pp. 187–191, 2016.

[4] I. G. Salako, M. J. S. Houndjo, and A. Jawad, "Generalized Mattig's relation in Brans–Dicke–Rastall gravity," *International Journal of Modern Physics D*, vol. 25, no. 7, article 1650076, 2016.

[5] C. E. M. Batista, J. C. Fabris, O. F. Piattella, and A. M. Velasquez-Toribio, "Observational constraints on Rastall's cosmology," *The European Physical Journal C*, vol. 73, no. 5, article 2425, 2013.

[6] Y. Heydarzade, H. Moradpour, and F. Darabi, "Black hole solutions in Rastall theory," *Canadian Journal of Physics*, vol. 95, no. 12, pp. 1253–1256, 2017.

[7] K. Lin and W. L. Qian, "Neutral regular black hole solution in generalized Rastall gravity," *Chinese Physics C*, vol. 43, no. 8, article 083106, 2019.

[8] S. Chen, B. Wang, and R. Su, "Hawking radiation in ad-dimensional static spherically symmetric black hole surrounded by quintessence," *Physical Review D*, vol. 77, no. 12, article 124011, 2008.

[9] Y. Heydarzade and F. Darabi, "Black hole solutions surrounded by perfect fluid in Rastall theory," *Physics Letters B*, vol. 771, pp. 365–373, 2017.

[10] K. Lin, Y. Liu, and W. L. Qian, "Higher dimensional power-Maxwell charged black holes in Einstein and Rastall gravity," *General Relativity and Gravitation*, vol. 51, no. 5, p. 62, 2019.

[11] R. Kumar and S. G. Ghosh, "Rotating black hole in Rastall theory," *The European Physical Journal C*, vol. 78, no. 9, p. 750, 2018.

[12] Z. Xu and J. Wang, "Kerr-Newman-AdS black hole surrounded by scalar field matter in Rastall gravity," https://arxiv.org/abs/1711.04542.

[13] H. Moradpour and I. G. Salako, "Thermodynamic analysis of the static spherically symmetric field equations in Rastall theory," *Advances in High Energy Physics*, vol. 2016, Article ID 3492796, 5 pages, 2016.

[14] M. Cruz, S. Lepe, and G. Morales-Navarrete, "A thermodynamics revision of Rastall gravity," https://arxiv.org/abs/1904.11945.

[15] I. P. Lobo, H. Moradpour, J. P. Morais Graca, and I. G. Salako, "Thermodynamics of black holes in Rastall gravity," *International Journal of Modern Physics D*, vol. 27, no. 7, article 1850069, 2018.

[16] K. Bamba, A. Jawad, S. Rafique, and H. Moradpour, "Thermodynamics in Rastall gravity with entropy corrections," *The European Physical Journal C*, vol. 78, no. 12, p. 986, 2018.

[17] M. S. Ali, "Ehrenfest scheme for *P-V* criticality of the *d*-dimensional-AdS black holes surrounded by perfect fluid in Rastall theory," https://arxiv.org/abs/1901.04318.

[18] J. P. Morais Graca and I. P. Lobo, "Scalar QNMs for higher dimensional black holes surrounded by quintessence in Rastall gravity," *The European Physical Journal C*, vol. 78, no. 2, p. 101, 2018.

[19] J. Liang, "Quasinormal modes of the Schwarzschild black hole surrounded by the quintessence field in Rastall gravity," *Communications in Theoretical Physics*, vol. 70, no. 6, p. 695, 2018.

[20] B. P. Dolan, "Pressure and volume in the first law of black hole thermodynamics," *Classical and Quantum Gravity*, vol. 28, no. 23, article 235017, 2011.

[21] B. P. Dolan, "The cosmological constant and black-hole thermodynamic potentials," *Classical and Quantum Gravity*, vol. 28, no. 12, article 125020, 2011.

[22] D. Kubiznak and R. B. Mann, "$P - V$ criticality of charged AdS black holes," *Journal of High Energy Physics*, vol. 2012, p. 33, 2012.

[23] M. Chabab, H. El Moumni, S. Iraoui, and K. Masmar, "Phase transitions and geothermodynamics of black holes in dRGT massive gravity," *The European Physical Journal C*, vol. 79, no. 4, p. 342, 2019.

[24] K. Bhattacharya and B. R. Majhi, "Thermogeometric study of van der Waals like phase transition in black holes: an alternative approach," https://arxiv.org/abs/1903.10370.

[25] A. Haldar and R. Biswas, "Geometrothermodynamic analysis and P–V criticality of higher dimensional charged Gauss–Bonnet black holes with first order entropy correction," *General Relativity and Gravitation*, vol. 51, no. 2, p. 35, 2019.

[26] H. Yazdikarimi, A. Sheykhi, and Z. Dayyani, "Critical behavior of Gauss-Bonnet black holes via an alternative phase space," https://arxiv.org/abs/1903.09020.

[27] W. Xu, C. Y. Wang, and B. Zhu, "Effects of Gauss-Bonnet term on the phase transition of a Reissner-Nordström-AdS black hole in (3+1) dimensions," *Physical Review D*, vol. 99, no. 4, article 044010, 2019.

[28] Y. P. Hu, H. A. Zeng, Z. M. Jiang, and H. Zhang, "P-V criticality in the extended phase space of black holes in Einstein-Horndeski gravity," https://arxiv.org/abs/1812.09938.

[29] A. Dehyadegari, B. R. Majhi, A. Sheykhi, and A. Montakhab, "Universality class of alternative phase space and Van der Waals criticality," *Physics Letters B*, vol. 791, pp. 30–35, 2019.

[30] M. Jamil, B. Pourhassan, A. Övgün, and İ. Sakallı, "PV criticality of Achucarro-Ortiz black hole in the presence of higher order quantum and GUP corrections," https://arxiv.org/abs/1811.02193.

[31] S. Gunasekaran, R. B. Mann, and D. Kubiznak, "Extended phase space thermodynamics for charged and rotating black holes and Born-Infeld vacuum polarization," *Journal of High Energy Physics*, vol. 1211, p. 110, 2012.

[32] S. H. Hendi and M. H. Vahidinia, "Extended phase space thermodynamics and $P–V$ criticality of black holes with a nonlinear source," *Physical Review D*, vol. 88, no. 8, article 084045, 2013.

[33] R. Zhao, H.-H. Zhao, M.-S. Ma, and L.-C. Zhang, "On the critical phenomena and thermodynamics of charged topological dilaton AdS black holes," *The European Physical Journal C*, vol. 73, no. 12, article 2645, 2013.

[34] D. C. Zou, S. J. Zhang, and B. Wang, "Critical behavior of Born-Infeld AdS black holes in the extended phase space thermodynamics," *Physical Review D*, vol. 89, no. 4, article 044002, 2014.

[35] D. C. Zou, Y. Liu, and B. Wang, "Critical behavior of charged Gauss-Bonnet-AdS black holes in the grand canonical ensemble," *Physical Review D*, vol. 90, no. 4, article 044063, 2014.

[36] R. G. Cai, L. M. Cao, L. Li, and R. Q. Yang, "P-V criticality in the extended phase space of Gauss-Bonnet black holes in AdS space," *Journal of High Energy Physics*, vol. 2013, p. 5, 2013.

[37] M. H. Dehghani, S. Kamrani, and A. Sheykhi, "$P–V$ criticality of charged dilatonic black holes," *Physical Review D*, vol. 90, no. 10, article 104020, 2014.

[38] R. A. Hennigar, W. G. Brenna, and R. B. Mann, "$P – v$ criticality in quasitopological gravity," *Journal of High Energy Physics*, vol. 2015, p. 77, 2015.

[39] M. Zhang, D. C. Zou, and R. H. Yue, "Reentrant phase transitions and triple points of topological AdS black holes in Born-Infeld-massive gravity," *Advances in High Energy Physics*, vol. 2017, Article ID 3819246, 11 pages, 2017.

[40] A. Övgün, "P-v criticality of a specific black hole in f(R) gravity coupled with Yang-Mills field," *Advances in High Energy Physics*, vol. 2018, Article ID 8153721, 7 pages, 2018.

[41] P. Cheng, S. W. Wei, and Y. X. Liu, "Critical phenomena in the extended phase space of Kerr-Newman-AdS black holes," *Physical Review D*, vol. 94, no. 2, article 024025, 2016.

[42] J. X. Mo, G. Q. Li, and X. B. Xu, "Combined effects of f(R) gravity and conformally invariant Maxwell field on the extended phase space thermodynamics of higher-dimensional black holes," *European Physical Journal C: Particles and Fields*, vol. 76, no. 10, p. 545, 2016.

[43] M. S. Ma, L. C. Zhang, H. H. Zhao, and R. Zhao, "Phase transition of the higher dimensional charged Gauss-Bonnet black hole in de Sitter spacetime," *Advances in High Energy Physics*, vol. 2015, Article ID 134815, 2015.

[44] J. X. Mo and W. B. Liu, "P-V criticality of conformal anomaly corrected AdS black holes," *Advances in High Energy Physics*, vol. 2015, Article ID 206963, 7 pages, 2015.

[45] H. Xu, W. Xu, and L. Zhao, "Extended phase space thermodynamics for third-order Lovelock black holes in diverse dimensions," *European Physical Journal C: Particles and Fields*, vol. 74, no. 9, article 3074, 2014.

[46] W. Xu, H. Xu, and L. Zhao, "Gauss–Bonnet coupling constant as a free thermodynamical variable and the associated criticality," *European Physical Journal C: Particles and Fields*, vol. 74, no. 7, article 2970, 2014.

[47] A. M. Frassino, D. Kubiznak, R. B. Mann, and F. Simovic, "Multiple reentrant phase transitions and triple points in Lovelock thermodynamics," *Journal of High Energy Physics*, vol. 2014, p. 80, 2014.

[48] S. W. Wei and Y. X. Liu, "Triple points and phase diagrams in the extended phase space of charged Gauss-Bonnet black holes in AdS space," *Physical Review D*, vol. 90, no. 4, article 044057, 2014.

[49] N. Altamirano, D. Kubiznak, R. B. Mann, and Z. Sherkatghanad, "Thermodynamics of rotating black holes and black rings: phase transitions and thermodynamic volume," *Galaxies*, vol. 2, no. 1, pp. 89–159, 2014.

[50] D. C. Zou, R. Yue, and M. Zhang, "Reentrant phase transitions of higher-dimensional AdS black holes in dRGT massive gravity," *The European Physical Journal C*, vol. 77, no. 4, p. 256, 2017.

[51] H. F. Li, H. H. Zhao, L. C. Zhang, and R. Zhao, "Clapeyron equation and phase equilibrium properties in higher dimensional charged topological dilaton AdS black holes with a nonlinear source," *European Physical Journal C: Particles and Fields*, vol. 77, no. 5, p. 295, 2017.

[52] E. Berti, V. Cardoso, and A. O. Starinets, "Quasinormal modes of black holes and black branes," *Classical and Quantum Gravity*, vol. 26, no. 16, article 163001, 2009.

[53] R. A. Konoplya and A. Zhidenko, "Quasinormal modes of black holes: from astrophysics to string theory," *Reviews of Modern Physics*, vol. 83, no. 3, pp. 793–836, 2011.

[54] R. A. Konoplya and A. Zhidenko, "Quasinormal modes of Gauss-Bonnet-AdS black holes: towards holographic description of finite coupling," *Journal of High Energy Physics*, vol. 2017, p. 139, 2017.

[55] P. K. Kovtun and A. O. Starinets, "Quasinormal modes and holography," *Physical Review D*, vol. 72, no. 8, article 086009, 2005.

[56] M. Luzum and P. Romatschke, "Erratum: conformal relativistic viscous hydrodynamics: applications to RHIC results at $\sqrt{s_{NN}} = 200$ GeV," *Physical Review C*, vol. 79, article 039903, 2008Phys. Rev. C 78, 034915.

[57] D. T. Son and A. O. Starinets, "Viscosity, black holes, and quantum field theory," *Annual Review of Nuclear and Particle Science*, vol. 57, no. 1, pp. 95–118, 2007.

[58] S. S. Gubser and I. Mitra, "The evolution of unstable black holes in anti-de Sitter space," *Journal of High Energy Physics*, vol. 2001, p. 18, 2001.

[59] S. Mahapatra, "Thermodynamics, phase transition and quasinormal modes with Weyl corrections," *Journal of High Energy Physics*, vol. 2016, p. 142, 2016.

[60] H. P. Nollert, "Quasinormal modes: the characteristic 'sound' of black holes and neutron stars," *Classical and Quantum Gravity*, vol. 16, no. 12, pp. R159–R216, 1999.

[61] K. D. Kokkotas and B. G. Schmidt, "Quasi-normal modes of stars and black holes," *Living Reviews in Relativity*, vol. 2, no. 1, p. 2, 1999.

[62] X. P. Rao, B. Wang, and G. H. Yang, "Quasinormal modes and phase transition of black holes," *Physics Letters B*, vol. 649, no. 5-6, pp. 472–477, 2007.

[63] X. He, B. Wang, R. G. Cai, and C. Y. Lin, "Signature of the black hole phase transition in quasinormal modes," *Physics Letters B*, vol. 688, no. 2-3, pp. 230–236, 2010.

[64] E. Berti and V. Cardoso, "Quasinormal modes and thermodynamic phase transitions," *Physical Review D*, vol. 77, no. 8, article 087501, 2008.

[65] J. Shen, B. Wang, C. Y. Lin, R. G. Cai, and R. K. Su, "The phase transition and the quasi-normal modes of black holes," *Journal of High Energy Physics*, vol. 2007, p. 37, 2007.

[66] G. Koutsoumbas, S. Musiri, E. Papantonopoulos, and G. Siopsis, "Quasi-normal modes of electromagnetic perturbations of four-dimensional topological black holes with scalar hair," *Journal of High Energy Physics*, vol. 2006, p. 6, 2006.

[67] D. C. Zou, Y. Liu, C. Y. Zhang, and B. Wang, "Dynamical probe of thermodynamical properties in three-dimensional hairy AdS black holes," *Europhysics Letters*, vol. 116, no. 4, article 40005, 2016.

[68] Y. Liu, D. C. Zou, and B. Wang, "Signature of the Van der Waals like small-large charged AdS black hole phase transition in quasinormal modes," *Journal of High Energy Physics*, vol. 2014, p. 179, 2014.

[69] M. Chabab, H. El Moumni, S. Iraoui, and K. Masmar, "Behavior of quasinormal modes and high dimension RN–AdS black hole phase transition," *European Physical Journal C: Particles and Fields*, vol. 76, no. 12, p. 676, 2016.

[70] M. Zhang and R. H. Yue, "Phase transition and quasinormal modes for spherical black holes in 5D Gauss–Bonnet gravity," *Chinese Physics Letters*, vol. 35, no. 4, article 040401, 2018.

[71] V. V. Kiselev, "Quintessence and black holes," *Classical and Quantum Gravity*, vol. 20, no. 6, pp. 1187–1197, 2003.

[72] A. Vikman, "Can dark energy evolve to the phantom?," *Physical Review D*, vol. 71, no. 2, article 023515, 2005.

[73] V. Cardoso, R. Konoplya, and J. P. S. Lemos, "Quasinormal frequencies of Schwarzschild black holes in anti–de Sitter spacetimes: a complete study of the overtone asymptotic behavior," *Physical Review D*, vol. 68, no. 4, article 044024, 2003.

[74] R. A. Konoplya, "Quasinormal modes of a small Schwarzschild–anti-de Sitter black hole," *Physical Review D*, vol. 66, no. 4, article 044009, 2002.

Hindawi
Advances in High Energy Physics
Volume 2020, Article ID 9529356, 7 pages
https://doi.org/10.1155/2020/9529356

Research Article

Effects of Quintessence Dark Energy on the Action Growth and Butterfly Velocity

Hossein Ghaffarnejad, Mohammad Farsam, and Emad Yaraie

Faculty of Physics, Semnan University, P.C. 35131-19111, Semnan, Iran

Correspondence should be addressed to Hossein Ghaffarnejad; hghafarnejad@semnan.ac.ir

Received 1 July 2019; Revised 19 August 2019; Accepted 5 September 2019; Published 20 January 2020

Guest Editor: Saibal Ray

In this work we are about to investigate the effects of quintessence dark energy on evolution of the computational complexity relating to the AdS/CFT correspondence. We use "*complexity = action*" conjecture for a charged AdS black hole surrounded by the dark energy at the quintessence regime. Then we try to find some conditions on the quintessence parameters where the Lloyd bound is satisfied in presence of affects of the quintessence dark energy on the complexity growth at the late time approximations. We compare late time approximation of the action growth by perturbed geometry in small limits of shift function. Actually we investigate the evμolution of complexity when thermofield double state on the boundaries is perturbed by local operator corresponding to a shock wave geometry as holographically. Furthermore we seek spread of local shock wave on the black hole horizon in presence of the quintessence dark energy.

1. Introduction

In the perspective of gauge/gravity duality evolution of all dynamical fields in the anti-de Sitter (AdS) gravity have dual pictures in the boundary field theories on which the gravity has been removed [1]. Actually this duality acts as a dictionary for all field theory characteristics in the language of black hole physics in AdS spacetime. One of important conjectures in the holographic context is about computational quantum complexity which implies the minimum quantum gates necessary to produce states associated with boundary complexity from the reference state. These conjectures are based on the behavior of a patch created by the light rays emitted from t_L on the left boundary and t_R on the right side of a two-sided eternal black hole, called Wheeler-DeWitt (WDW) patch [2, 3]. The old conjecture states "complexity = volume" (CV), in which the volume of a maximal space-like slice in the black hole interior that connects t_L and t_R supposed to be appropriated with computational complexity in its conformal field theory dual on the boundary [4]. This conjecture is a result of the behavior of the interior volume of black hole which grows linearly with time, so it could be translated with the growth of computational complexity on the boundary with time [5, 6]. However, if the bulk contains a shock wave the interior volume of the black hole shrinks for a finite time interval and shows an opposite behavior. In the new conjecture of "complexity = action" (CA), computational complexity of a holographic state on the boundary pictures is as the on-shell action in WDW patch. This new conjecture has some preferences with respect to the old one and solve some problems which the "CV" conjecture suffers. Lloyd showed [7] the growth rate of quantum complexity has an upper bound which is related to the average energy of the orthogonal quantum states E such that

$$\frac{d(Action)}{dt} \leq 2E. \tag{1}$$

In this new conjecture, authors of the works [2, 3] concluded that the action growth of WDW patch obeys this bound at late time approximation which is provided us to work with orthogonal states. At this approximation we can have a general and universal form of the above bound for a rotating charged black hole as follows [8].

$$\frac{d\mathcal{A}}{dt} \leq (M - \Omega J - \mu Q)_+ - (M - \Omega J - \mu Q)_-, \tag{2}$$

where + and − indicate the lowest and highest energy of states. These states for a black hole with multiple horizon happen at the most outer (r_+) and the most inner (r_-) horizons.

In the other side, shock waves near the horizon of an AdS black hole describe chaos in a thermal CFT [9–11] and could have interesting effects on the boundary complexity. From the point of view of holography dictionary the spreading of the shock wave near the horizon has butterfly effect in the boundary field theory. This effect could be seen with a sudden decay after scrambling time $t_* = (\beta/2\pi)\ln S$, in which "S" stands for the black hole entropy. It is the necessary time for the black hole as the fastest scramblers to render the density matrix of a small essentially exactly thermal subsystem. The spreading local shock waves in the bulk arise from throwing a few quanta into the horizon which corresponds to perturb thermofield double state $|TFD\rangle$ on the boundaries by local operators. The growth of spreading the shock wave on the boundary is identified with butterfly velocity "v_B" could be obtained by solving the equation of motions of perturbed geometry. Complexity growth rate and the effects of butterfly on it, are investigated on various gravity models for the bulk. In refs. [2, 3, 8] the authors investigated action growth for various AdS black holes and tested the Lloyd bound by considering the effects of charge. The growth of holographic complexity is studied in massive gravity in ref. [12], and in a more variety of other works [13–19]. On the other side, some of works have been done about studying the shock wave geometry in different gravity models in the bulk [9–11, 20, 21] and effects of them were investigated on the action growth by obtaining butterfly velocity and comparing them with other simple models [22, 23].

Motivation of studying the effect of dark energy arises from several works in holographic context. For instance Chen et al. found that quintessence dark energy can affect the s-wave and p-wave holographic superconductor [24]. In the other side, Kuang et al. studied the holographic fermionic spectrum dual to AdS black brane in 4 dimensions in the presence of quintessence dark energy and showed that this fermionic system exhibits a nonFermi liquid behavior [25]. So it would be natural to investigate other aspects of holographic effects of this quintessence dark energy such as its impact on complexity growth or its effect on the spread of chaos on boundary. Quintessence dark energy introduced by an equation of state arisen from its energy tensor has a state parameter which is varied like $-1 < \omega < -1/3$. This state parameter which is a factor to explain the accelerating expansion of the universe, could define various regimes and could be fixed by regarding some cosmological observations. Here we like to study effects of this factor on the holographic complexity of a AdS black hole which is perturbed with a shock wave matter field. It can help us to get more profound understanding from the entropy of the black hole in presence of the quintessence dark energy by attention to some related bounds like Lloyd bound. Also it could help us to have more information about quintessence state parameter to get a better understanding of late time acceleration of the universe. Furthermore it could be interesting how the spreading of a chaos could be sensitive for changes of ω. This could give a comprehensive and statistical study for different regimes of the used gravity theory during the evolution of the action. Moreover, from [26] we know free parameter a emerged from quintessence energy tensor should be considered as thermodynamic variable and so its physical insight needs to investigation more. So as next work we are interested to study dual CFT perspective of this variable to approach to goal of this article.

In the present work we consider the effects of quintessence dark energy on the AdS black holes geometry, and therefore we will see how it changes the action growth rate and butterfly velocity in the shock wave geometry. Quintessence dark energy is a canonical scalar field which is one of the successful theories to explain the acceleration phase of the universe [27–29]. In this model which was first introduced by Kiselev [30] an additional energy-momentum tensor of quintessence counterpart must be added to the Einstein equation as $\mathcal{G} = \kappa\left(T_{matter} + T_{\text{quintessence}}\right) = \kappa\mathcal{T}$. The effects of quintessence have been studied in a wide range of works and thermodynamics of the various black holes have been investigated when they are surrounded by the dark energy [30–35]. It would be challenging to see how it affects the holographic characteristics as well. Layout of this work is as follows.

We first study the action growth in the presence of quintessence dark energy in Section 2. Then we discuss about conditions where the Lloyd bound [7] could be hold with new charge associated with this new field. In Section 3 we calculate the butterfly velocity related to the spreading of perturbation and compare the action growth in the presence of a local shock wave geometry in the gravity model under consideration. Section 4 denotes to concluding remarks and outlook of the work.

2. The Rate of Action Growth in Presence of the Dark Energy

We consider RN-AdS black hole surrounded by the quintessence dark energy in four dimensional curved space time. It could be described by the following action functional.

$$\mathcal{S} = \mathcal{S}_{bk} + \mathcal{S}_{bd}. \tag{3}$$

where the first part is related with the bulk action contains Einstein-Maxwell Lagrangian density defined in the AdS spacetime as follows.

$$\mathcal{S}_{bk} = \frac{1}{16\pi G}\int_{bulk} d^4x\left(\sqrt{-g}\left[R - 2\Lambda - F^{\mu\nu}F_{\mu\nu}\right] + \mathcal{L}_q\right). \tag{4}$$

In the above action the cosmological constant is related to the AdS space radius L by $\Lambda = -3/L^2$ in four dimension. The second term in the action (4), $\mathcal{L}_q$ implies on the lagrangian of the quintessence dark energy as a barotropic perfect fluid defined by [36]

$$\mathcal{L}_q = -\rho c^2\left(1 + \omega\ln\left(\frac{\rho}{\rho_0}\right)\right), \tag{5}$$

in which c is the light speed and ρ_0 is integral constant which is come from singularity cut-off. Also the quintessence dark energy barotropic index satisfies $-1 < \omega < -1/3$. It comes from the quintessence dark energy equation of state as $p = \omega\rho c^2$ in which ρ is energy density and p is corresponding isotropic pressure.

In the other side the Gibbons-Hawking-York (GHY) boundary part of the action term within the WDW patch at the late time approximation is defined by

$$\mathcal{S}_{bd} = \frac{1}{8\pi G}\int_{\text{boundary}} d^3x\,\sqrt{-h}K, \tag{6}$$

where h stands for the determinant of induced metric on the boundary of AdS bulk and K represents the trace of extrinsic curvature. We should note the authors of the work [37] showed that "CA" conjecture suffers from some ambiguities related to the null surface's parametrization and they found joint and boundary terms which are absent in this proposal. However authors of the works [38, 39] proved that the action growth at late time approximation does not need these extra terms. So for the present work, all other boundary terms and joint terms vanish at late time approximation.

In general, a line element for spherically symmetric static geometry in the Schwarzschild coordinates could be given by

$$ds^2 = -f(r)dt^2 + \frac{dr^2}{f(r)} + r^2\vec{dx}_2^{\,2}, \tag{7}$$

with the following solution in presence of the quintessence dark energy effect [30].

$$f(r) = 1 - \frac{2M}{r} - \frac{\Lambda r^2}{3} + \frac{q_E^2}{r^2} - \frac{a}{r^{3\omega+1}}, \tag{8}$$

where the positive constant "a" treats as normalization factor for density of the quintessence dark energy via $\rho = -3a\omega/2r^{3(\omega+1)}$. The electromagnetic tensor field $F_{\mu\nu}$ is defined by 4-vector potential A_μ as $F_{\mu\nu} = \partial_\mu A_\nu - \partial_\nu A_\mu$. This is a gauge field and so for a spherically symmetric static metric (7) we can take its form as spherically symmetric time independent function for simplicity reasons as follows.

$$A = A_t dt = -q_E\left(\frac{1}{r} - \frac{1}{r_+}\right)dt. \tag{9}$$

Substituting the metric solution (7) with (8) one can calculate the Ricci scalar as

$$R = 4\Lambda + \frac{3a\omega(3\omega-1)}{r^{3(\omega+1)}}. \tag{10}$$

To study the evolution of WDW action of this model it is useful to depict its Penrose diagram at late time approximation. As the black hole solution (7) has multiple horizons so we must consider its behavior between the lowest and the highest energy which happen at r_- and r_+, respectively. In Figure 1, we depicted the evolution of WDW patch for black hole containing the multiple horizons at late time approximation [40]. By increasing the time on the boundary the patch terminates at location of $r = r_{meet}(t_L, t_R)$ for all charged black holes. Time transition says us that the action growth at late time approximation only relates to the dark blue region behind the future horizon in Figure 1. Of course, the tiny part above the meet line is in second order δ^2 which is negligible.

Now by studying time dependence behavior of total action (3) in the quintessence regime of dark energy, we can evaluate holographic complexity growth. By considering the Ricci scalar (10) and the quintessence lagrangian density (5) one can calculate the action growth of the bulk such that

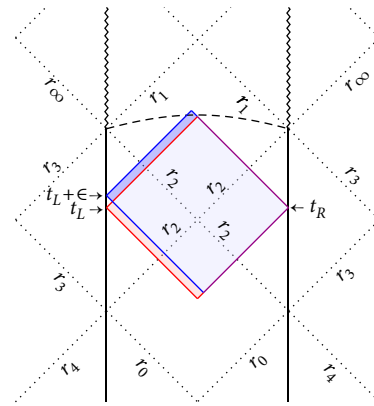

FIGURE 1: Penrose diagram for a two sided black hole with multiple horizons in which WDW patch evolves at late time approximation and terminates at meet point with $t_L = t_R$ and $t = 0$. r_0 is the null spatial infinity and the wavy lines indicate the singularities at $r = 0$, also r_∞ stands for $r = -\infty$.

$$\frac{d\mathcal{S}_{bk}}{dt} = \frac{1}{16\pi G}\int\int_{r_-}^{r_+} r^2\left(2\Lambda + \frac{3a\omega(3\omega-1)}{r^{3(\omega+1)}} + \frac{2q_E^2}{r^4} + \lambda(\omega)\frac{1}{r^{3\omega+1}} + \mu(\omega)\frac{\ln(r)}{r^{3\omega+1}}\right)dr\,d\Omega_2, \tag{11}$$

in which

$$\lambda(\omega) = -\frac{3a\omega}{2}(1 + \omega\,\ln(-\omega)),$$
$$\mu(\omega) = \frac{9a\omega^2(\omega+1)}{2}, \tag{12}$$

and we put $\rho_0 \equiv 3a/2$. It is simple to show $\lambda(\omega) > 0$ and $\mu(\omega) > 0$ in quintessence regime $-1 < \omega < -1/3$ as follows. By setting $\Omega_2/4\pi G = 1$ (11) reads

$$\frac{d\mathcal{S}_{bk}}{dt} = -\frac{1}{2L^2}\left(r_+^3 - r_-^3\right) - \frac{q_E^2}{2}\left(\frac{1}{r_+} - \frac{1}{r_-}\right) - \frac{a(3\omega-1)}{4}\left(\frac{1}{r_+^{3\omega}} - \frac{1}{r_-^{3\omega}}\right) - \frac{1}{12\omega}\left(\lambda + \frac{\mu}{3\omega}\right)\left(\frac{1}{r_+^{3\omega}} - \frac{1}{r_-^{3\omega}}\right) - \frac{\mu}{12\omega}\left(\frac{\ln(r_+)}{r_+^{3\omega}} - \frac{\ln(r_-)}{r_-^{3\omega}}\right). \tag{13}$$

It is also easy to see $(\lambda + (\mu/3\omega)) > 0$ for quintessence regime $-1 < \omega < -1/3$.

To obtain the action growth of the boundary part we must evaluate the extrinsic curvature associated to the metric solution (7) for which we have

$$K = \frac{1}{r^2}\frac{\partial}{\partial r}\left(r^2\sqrt{f(r)}\right) = \frac{2}{r}\sqrt{f(r)} + \frac{f'(r)}{2\sqrt{f(r)}}, \tag{14}$$

where the prime $\prime$ notes to derivative with respect to "r". By this definition time derivative of the second part of the action (3) leads to the following form.

$$\begin{aligned}\frac{d\mathcal{S}_{bd}}{dt} &= \frac{1}{8\pi G}\int_{\text{boundary}} d\Omega_2\left(\sqrt{-h}K\right)\\ &= \left[rf(r)+\frac{r^2 f^{'}(r)}{4}\right]_{r_-}^{r_+}\\ &= (r_+-r_-)+\frac{3}{2L^2}\left(r_+^3-r_-^3\right)+\frac{q_E^2}{2}\left(\frac{1}{r_+}-\frac{1}{r_-}\right)\\ &\quad+\frac{3a(\omega-1)}{4}\left(\frac{1}{r_+^{3\omega}}-\frac{1}{r_-^{3\omega}}\right).\end{aligned} \tag{15}$$

Adding (13) and (15) we obtain total growth action for quintessence RN-AdS black hole such as follows.

$$\begin{aligned}\frac{d\mathcal{S}}{dt} &= (r_+-r_-)+\frac{r_+^3-r_-^3}{L^2}-\frac{a}{2}\left(\frac{1}{r_+^{3\omega}}-\frac{1}{r_-^{3\omega}}\right)\\ &\quad-\frac{1}{12\omega}\left(\lambda+\frac{\mu}{3\omega}\right)\left(\frac{1}{r_+^{3\omega}}-\frac{1}{r_-^{3\omega}}\right)\\ &\quad-\frac{\mu}{12\omega}\left(\frac{\ln(r_+)}{r_+^{3\omega}}-\frac{\ln(r_-)}{r_-^{3\omega}}\right).\end{aligned} \tag{16}$$

Solving the horizon equation $f(r_\pm)=0$ one can obtain the following expressions for charge and mass of the RN-AdS black hole.

$$q_E^2 = r_+r_-\left[1+\frac{1}{L^2}\frac{r_+^3-r_-^3}{r_+-r_-}-a\frac{r_+^{-3\omega}-r_-^{-3\omega}}{r_+-r_-}\right], \tag{17}$$

$$\begin{aligned}M &= \frac{1}{2}\Bigg[(r_++r_-)+\frac{1}{L^2}\frac{r_+^4-r_-^4}{r_+-r_-}\\ &\quad+\frac{a}{2}\frac{r_+}{r_-^{3\omega}(r_+-r_-)}\left(\frac{r_-}{r_+}-\left(\frac{r_-}{r_+}\right)^{3\omega}\right)\Bigg].\end{aligned} \tag{18}$$

By attention to these expressions the total growth rate (17) could be rewritten as follows.

$$\begin{aligned}\frac{d\mathcal{S}}{dt} &= -q_E^2\left(\frac{1}{r_+}-\frac{1}{r_-}\right)+\frac{a}{2}\left(\frac{1}{r_+^{3\omega}}-\frac{1}{r_-^{3\omega}}\right)\\ &\quad-\frac{1}{12\omega}\left(\lambda+\frac{\mu}{3\omega}\right)\left(\frac{1}{r_+^{3\omega}}-\frac{1}{r_-^{3\omega}}\right)\\ &\quad-\frac{\mu}{12\omega}\left(\frac{\ln(r_+)}{r_+^{3\omega}}-\frac{\ln(r_-)}{r_-^{3\omega}}\right).\end{aligned} \tag{19}$$

Looking to the works presented by Brown et al. [2, 3], one can infer there are some extra terms due to the presence of quintessence dark energy. If we rewrite this expression with respect to thermodynamic variables we find

$$\begin{aligned}\frac{d\mathcal{S}}{dt} &= (M-\mu_+q_E-\mathcal{A}_+a)-(M-\mu_-q_E-\mathcal{A}_-a)\\ &\quad-\frac{1}{12\omega}\left(\lambda+\frac{\mu}{3\omega}\right)\left(\frac{1}{r_+^{3\omega}}-\frac{1}{r_-^{3\omega}}\right)\\ &\quad-\frac{\mu}{12\omega}\left(\frac{\ln(r_+)}{r_+^{3\omega}}-\frac{\ln(r_-)}{r_-^{3\omega}}\right),\end{aligned} \tag{20}$$

in which $\mu_\pm = q_E/r_\pm$ stands for chemical potential, $\mathcal{A}_\pm = -1/2r_\pm^{3\omega}$ is conjugated potential for parameter "a". As we expect for $a=0$ the second line in the above result vanishes. If we take "E" for the average energy of the quantum states then the rate of quantum complexity satisfies the Lloyd bound [7] as

$$\frac{d\mathcal{C}}{dt} \le \frac{2E}{\pi\hbar}. \tag{21}$$

This satisfaction arises from the conditions $\mu>0, \lambda>0$ and $\lambda+\mu/3\omega>0$ which are mentioned in the above for the quintessence regime $-1<\omega<-1/3$.

3. Butterfly Effect with Shock Wave Geometry

The shock wave geometry happens when our black hole solution is perturbed by a small amount of energy. Study of the shock wave geometry can be done by calculating the butterfly velocity which is the velocity of shock wave near the horizon. To do so we first rewrite the black hole solution (7) in the Kruskal coordinates system such that

$$ds^2 = -2H(u,v)dudv+h(u,v)\overrightarrow{dx}_2^{\,2}, \tag{22}$$

where we defined

$$H(u,v) = -\frac{4}{uv}\frac{f(r)}{\left[f'(r_h)\right]^2}, \tag{23}$$

and $h(u,v)=r^2$ where and from now on we mark outer horizon by r_h instead of r_+ for simplicity reasons. As we know that there are the following relationship between the null Kruskal coordinates and the spherical coordinates.

$$\begin{aligned}u &= e^{(2\pi/\beta)\left(-t+r_*(r)\right)},\\ v &= -e^{(2\pi/\beta)\left(t+r_*(r)\right)},\end{aligned} \tag{24}$$

with the thermodynamic parameter $\beta=1/k_BT$ in which T is temperature and k_B is the Boltzmann constant. Also $r_* = \int dr/f(r)$ called as the tortoise spatial radial coordinate. For neighborhood of the exterior horizon r_h the tortoise coordinate is approximated with the following form.

$$r_* \approx \frac{1}{f'(r_h)}\ln\left(\frac{r-r_h}{r_h}\right)+\cdots. \tag{25}$$

Now by rewriting the metric (22) in the new coordinates we can study the effects of disturbance as a shock wave geometry. Actually when a scalar operator w acts on the boundary at $t_w<0$ this shock wave creates. If t_w be large enough then this shock creates a particle of null matter which travels along $u=0$ in the bulk. Suppose that the metric has form like (22) for $u<0$ but it is changed to a perturbed metric in which v is replaced by $v+\alpha\left(x^i\right)$ [8]. $\alpha\left(x^i\right)$ is called the (red) shift function which shows a boundary perturbation in the direction of x^i. This shift function creates some similarities for WDW patch with unperturbed geometry at late time approximation which is studied in previous section. In fact when the shift function takes some large values then the light rays of WDW patch run into the past singularity which is similar to early time approximation,

since for small shift function similar to the late time approximation, these light rays meet each other behind the past horizon [3]. Applying some new transformations as

$$\begin{aligned} U &= u, \\ V &= v + \theta(u)\alpha\left(x^i\right), \\ X^i &= x^i, \end{aligned} \tag{26}$$

in which $\theta(u)$ represents the Heaviside step function, the metric line element (22) then takes the new form as follows.

$$\begin{aligned} ds^2 = &-2H(U,V)dUdV + h(U,V)\vec{dx}_2^{\,2} \\ &+ 2H(U,V)\alpha\left(X^i\right)\delta(U)dU^2, \end{aligned} \tag{27}$$

where $\delta(U)$ denotes to the well known "Dirac" delta function. It is simple to see for $u = U < 0$ the above metric reduces to old one (22).

The injected null matter stress-energy tensor, T_{matter}, can be written before the injection of disturbance into the boundary as (22) which in the Kruskal coordinates become

$$\frac{1}{\kappa}\mathcal{G}_{\{u,v\}} = T_{\text{matter}} = 2T_{uv}dudv + T_{uu}du^2 + T_{vv}dv^2 + T_{ij}\vec{dx}_2^{\,2}, \tag{28}$$

where $\mathcal{G}$ is the Einstein tensor. After injection this tensor could be expressed in the new coordinates such that

$$\begin{aligned} \frac{1}{\kappa}\mathcal{G}_{\{U,V\}} = T_{\text{matter}} = &2\left(T_{UV} - T_{VV}\alpha\left(X^i\right)\delta(U)\right)dUdV + T_{VV}dV^2 \\ &+ \left(T_{UU} + T_{VV}\alpha^2\left(X^i\right)\delta^2(U)\right. \\ &\left.-2T_{UV}\alpha\left(X^i\right)\delta(U)\right)dU^2 + T_{ij}\vec{dx}_2^{\,2}. \end{aligned} \tag{29}$$

By attention to [11, 41] one can consider a massless particle at $u = 0$ which moves in the v-direction with the speed of light, the stress-energy tensor of this particle which is corresponds to the shock wave stress-energy tensor is:

$$T_{(shock)UU} = \frac{E}{L^4}e^{(2\pi/\beta)t}a(X)\delta(U), \tag{30}$$

where E is a dimensionless constant and $a(X)$ is a local source of perturbation which for simplicity reasons we take to be as Dirac delta function, i.e. $a(X) = \delta(X)$. By considering the stress-energy tensor of this disturbance the Einstein equation reads $(1/\kappa)\mathcal{G} = T_{\text{matter}} + T_{\text{shock}}$ which should be solved. This equation at the leading order term near the horizon can be solved as follows.

$$\alpha(t, x_i) \sim e^{-\xi\left(|x_i| - v_B t\right)}, \tag{31}$$

where,

$$\xi = \sqrt{\frac{f'(r_h)h'(r_h)}{2}}, \tag{32}$$

and v_B given by

$$v_B = \frac{2\pi}{\beta\xi} = \sqrt{\frac{f'(r_h)}{2h'(r_h)}}. \tag{33}$$

is called as "butterfly velocity". In fact, this velocity as it is mentioned before is the spread of the local perturbation on the boundary of space-time. In our case $h(r) = r^2$ and so the butterfly velocity (33) reads

$$v_B = \sqrt{\frac{\pi T}{r_h}}. \tag{34}$$

Regarding the quintessence dark energy counterpart in the present work we see that the butterfly velocity is depend on the quintessence parameters such as normalization factor a and the state parameter ω. It could be calculated by attention to Hawking temperature $T = f'(r_h)/4\pi$ as

$$v_B = \frac{1}{2}\sqrt{\frac{1}{r_h^2} + \frac{3}{L^2} - \frac{q_E^2}{r_h^4} + \frac{3a\omega}{r_h^{3\omega+3}}} \tag{35}$$

in which r_h is the outer horizon. To study the action growth in this perturbed geometry two parts must be included: the action of WDW patch behind the (I) past and (II) future horizons. By attention to [3, 22] these two parts are defined respectively by

$$\begin{aligned} \mathcal{S}_{\text{future}} &= \frac{2M}{L\lambda_L}\int \ln e^{\lambda_L\left(|t_w| - t_* + t_L - \left(|x|/v_B\right)\right)}dx, \\ \mathcal{S}_{\text{past}} &= \frac{2M}{L\lambda_L}\int \ln e^{\lambda_L\left(|t_w| - t_* - t_R - \left(|x|/v_B\right)\right)}dx, \end{aligned} \tag{36}$$

at which λ_L is the Lyapunov exponent proportional to the Hawking temperature and L is the length of the transverse direction x. The upper bound of this coordinate called maximal transverse coordinate is $|x| = v_B\left(|t_w| - t_* - t_R\right)$ that guarantees the emergence of shock wave effect. Time dependence of the action of WDW patch yields:

$$\begin{aligned} \mathcal{S}_{\text{WDW}} &= \mathcal{S}_{\text{future}} + \mathcal{S}_{\text{past}} \\ &= 2M\left(t_L + t_R\right) + 2\mathcal{A}Mv_B\left(|t_w| - t_* - t_R\right)^2, \end{aligned} \tag{37}$$

where $\mathcal{A}$ is amplitude of shock wave in (31). As we can see by disturbing the geometry the perturbation spreads on the horizon and the action growth get corrected by an extra term which has linear dependence to the speed of perturbation. As the shock wave initially starts from the left side boundary of our two sided black hole and reaches the right side so the extra part depends only on t_R. By vanishing any perturbation term $\mathcal{A} \to 0$ one can re-derive non-perturbative situation which has same rate of growth with respect to both t_L and t_R.

Now it would be useful to study the effect of dark energy on the butterfly velocity for the same gravity model. As we can see dark energy leads to an extra term to v_B which is addressed as the last term in (35). Since $-1 < \omega < -1/3$ so this term has negative sign. Horizon radius r_h as we know is a solution of $f(r_h) = 0$. In a charged black hole solution with no dark energy around it we should set $a = 0$ in the equation (8) as

$$\widetilde{f}(r) = 1 - \frac{2\widetilde{M}}{r} - \frac{\Lambda r^2}{3} + \frac{\widetilde{q}_E^2}{r^2}. \tag{38}$$

and so the corresponding butterfly velocity $\widetilde{v}_B$ will be obtain from (35) without the last term and with different horizon radius $\widetilde{r}_h$ obtained from $\widetilde{f}(\widetilde{r}_h) = 0$. From (8) and (38) it is

simple to conclude that for fixed mass $M = \widetilde{M}$ and fixed charge $q_E = \widetilde{q}_E$ we have $f(r) < \widetilde{f}(r)$ because $f(r) = \widetilde{f}(r) - a/r^{3\omega+1}$. This equation is situated properly for any horizon radius such as the horizon of quintessence solution, namely $f(r_h) < \widetilde{f}(r_h)$. Since $f(r_h) = 0$ then $\widetilde{f}(r_h) > 0$ and because $\widetilde{f}(\widetilde{r}_h) = 0$ so it leads to $\widetilde{f}(r_h) > \widetilde{f}(\widetilde{r}_h)$. This means the horizon radius of charged black hole solution must be greater when it is surrounded by the dark energy, $r_h > \widetilde{r}_h$. The latter statement can be checked easily as follows: To do so we must be expand Taylor series expansion of the positive function $\widetilde{f}(r_h) > 0$ about the horizon radius in absence of the quintessence dark energy $\widetilde{r}_h$ which leading order term is obtained as

$$\widetilde{f}(r_h) \approx 4\pi\widetilde{T}(r_h - \widetilde{r}_h) + O(2) \tag{39}$$

in which we used the horizon equation of the black hole in absence of the quintessence $\widetilde{f}(\widetilde{r}_h) = 0$ and corresponding the Hawking radiation temperature $4\pi\widetilde{T} = \widetilde{f}'(\widetilde{r}_h)$. Regarding positivity condition on $\widetilde{f}(r)$, $\widetilde{T}$ and $\widetilde{f}(r_h)$ then the equation (39) satisfy the statement $r_h > \widetilde{r}_h$. Substituting $a = 0$ and assuming $\widetilde{q}_E = q_E$ the equation (35) leads to the following form:

$$4\widetilde{v}_B^2 = \frac{1}{\widetilde{r}_h^2} + \frac{3}{L^2} - \frac{q_E^2}{\widetilde{r}_h^4}. \tag{40}$$

for which $\widetilde{r}_h \geq \widetilde{r}_h^{(0)}$ with

$$\widetilde{r}_h^{(0)} = \frac{\sqrt{1 + 12q_E^2/L^2} - 1}{6/L^2}. \tag{41}$$

For small values of charge $qE/L << 1$ the above minimal horizon radius reaches to the following limit.

$$\widetilde{r}_h^{(0)} \to |q_E|. \tag{42}$$

In this limit one can write the butterfly velocity (35) as follows.

$$4v_B^2 \approx 4\widetilde{v}_B^2 + \frac{3a\omega}{|q_E|^{3\omega+3}}, \tag{43}$$

where

$$4\widetilde{v}_B^2 = \frac{3}{L^2}. \tag{44}$$

By attention to the conditions $a > 0$ and $-1 < \omega < -1/3$ one can compare (43) and (44) to infer $v_B < \widetilde{v}_B$. It means that the complexity action spreads on the AdS black hole horizon with slower (faster) butterfly velocity in presence (absence) of the quintessence dark energy. In the other side when ω is decreased and get closer to smallest value $\omega = -1$, then the gap of the butterfly velocity arisen by dark energy get more decreased and for which we have $4v_B^2 \to 3/L^2 - 3a$ with $a < 1/L^2$. In short one can infer that by decreasing value of the quintessence state equation parameter the butterfly velocity and so the complexity decreased.

4. Concluding Remarks

We studied the complexity growth rate by using "CA" conjecture [2, 3] for a simple model of gravity when its AdS black hole solution is surrounded by quintessence dark energy [30]. The effects of this kind of dark energy is investigated earlier in various works [29–34] and it seems challenging to see how it affects the holographic characteristics. We found some extra terms related to the quintessence dark energy are added to the total action growth. Also it is proved that by attention to the conjugated potential for the quintessence parameter the Lloyd bound [7] is satisfied for all parameter states defined in regime of the quintessence dark energy.

We also investigate the action growth of this model for shock wave geometry [9]. Actually when the boundary is perturbed by a small amount of energy, the geometry in the bulk is affected. The local shock wave spreads near the horizon with the "butterfly velocity" which could be obtained by the equation of motion for the new stress-energy tensor. In fact its form is same as of the old stress tensor but with an extra term which comes from the shock wave and has only UU component. It is due to a massless particle moving at null hypersurface $u = 0$ with the speed of light. We showed that the effect of the quintessence dark energy causes to spread the shock wave with slower butterfly velocity near the horizon, so the complexity growth would be slower as well.

Data Availability

In fact we do not use Experimental Data in our work. It is free of experimental date and is a purely theoretical research.

Conflicts of Interest

The authors declare that they have no conflicts of interest.

References

[1] J. Maldacena, "The large N limit of superconformal field theories and supergravity," *Advances in Theoretical and Mathematical Physics*, vol. 2, no. 2, pp. 231–252, 1998.

[2] A. R. Brown, D. A. Roberts, L. Susskind, B. Swingle, and Y. Zhao, "Holographic Complexity Equals Bulk Action?" *Physical Review Letters*, vol. 116, p. 191301, 2016.

[3] A. R. Brown, D. A. Roberts, L. Susskind, B. Swingle, and Y. Zhao, "Complexity, action, and black holes," *Physical Review*, vol. 93, no. 8, 2016.

[4] D. Stanford and L. Susskind, "Complexity and shock wave geometries," *Physical Review*, vol. 90, no. 12, 2014.

[5] L. Susskind, "Addendum to computational complexity and black hole horizons," *Fortschritte der Physik*, vol. 64, no. 1, pp. 44–48, 2016.

[6] L. Susskind, "The typical-state paradox: diagnosing horizons with complexity," *Fortschritte de Physik*, vol. 64, no. 1, pp. 84–91, 2016.

[7] S. Lloyd, "Ultimate physical limits to computation," *Nature*, vol. 406, no. 6799, pp. 1047–1054, 2000.

[8] R.-G. Cai, S.-M. Ruan, S.-J. Wang, R.-Q. Yang, and R.-H. Peng, "Action growth for AdS black holes," *Journal of High Energy Physics*, vol. 2016, no. 9, Article ID 161, 2016.

[9] S. H. Shenker and D. Stanford, "Black holes and the butterfly effect," *Journal of High Energy Physics*, vol. 2014, no. 3, 2014.

[10] S. H. Shenker and D. Stanford, "Multiple Shocks," *Journal of High Energy Physics*, vol. 1412, p. 046, 2014, https://arxiv.org/abs/1312.3296.

[11] D. A. Roberts, D. Stanford, and L. Susskind, "Localized shocks," *Journal of High Energy Physics*, vol. 2015, no. 3, 2015.

[12] W. J. Pan and Y. C. Huang, "Holographic complexity and action growth in massive gravities," *Physics Review*, vol. 95, no. 12, Article ID 126013, 2017.

[13] R.-G. Cai, M. Sasaki, and S.-J. Wang, "Action growth of charged black holes with a single horizon," *Physical Review*, vol. 95, no. 12, Article ID 124002, 2017.

[14] M. Alishahiha, A. F. Astaneh, A. Naseh, and M. H. Vahidinia, "On complexity for f(R) and critical gravity," *Journal of High Energy Physics*, vol. 2017, no. 5, Article ID 009, 2017.

[15] W.-D. Guo, S.-W. Wei, Y.-Y. Li, and Y.-X. Liu, "Complexity growth rates for AdS black holes in massive gravity and f(R) gravity," *European Physical Journal*, vol. 77, Article ID 904, 2017.

[16] Y. S. An and R. H. Peng, "The effect of dilaton on the holographic complexity growth," *Physical Review*, vol. 97, Article ID 066022, 2018.

[17] A. Ovgun and K. Jusufi, "Complexity growth rates for AdS black holes with dyonic/ nonlinear charge/ stringy hair/ topological defects," 2018, https://arxiv.org/abs/1801.09615.

[18] E. Yaraie, H. Ghaffarnejad, and M. Farsam, "Complexity growth and shock wave geometry in AdS-Maxwell-power-Yang-Mills theory," *The European Physical Journal*, vol. 78, no. 11, Article ID 967, 2018.

[19] S. H. Hendi and B. Bahrami Asl, "Complexity of the Einstein-Born-Infeld-Massive Black holes," 2018, https://arxiv.org/abs/1810.04792.

[20] E. Perlmutter, "Bounding the space of holographic CFTs with chaos," *Journal of High Energy Physics*, vol. 2016, no. 10, Article ID 069, 2016.

[21] M. Alishahiha, A. Davody, A. Naseh, and S. F. Taghavi, "On butterfly effect in higher derivative gravities," *Journal of High Energy Physics*, vol. 2016, no. 11, Article ID 032, 2016.

[22] Y.-G. Miao and L. Zhao, "Complexity/Action duality of the shock wave geometry in a massive gravity theory," *Physical Review*, vol. 97, Article ID 024035, 2018.

[23] S. A. Hosseini Mansoori and M. M. Qaemmaqami, "Complexity growth, butterfly velocity and black hole thermodynamics," 2017, https://arxiv.org/abs/1711.09749.

[24] S. Chen, Q. Pan, and J. Jing, "Holographic superconductors in quintessence AdS black hole spacetime," *Classical and Quantum Gravity*, vol. 30, no. 14, Article ID 145001, 2013.

[25] X.-M. Kuang and J.-P. Wu, "Effect of quintessence on holographic fermionic spectrum," *The European Physical Journal*, vol. 77, no. 10, Article ID 670, 2017.

[26] G.-Q. Li, "Effects of dark energy on PV criticality of charged AdS black holes," *Physics Letters*, vol. 735, pp. 256–260, 2014.

[27] S. Tsujikawa, "Quintessence: a review," *Class Quantum Gravity*, vol. 30, p. 214003, 2013, https://arxiv.org/abs/1304.1961.

[28] L. H. Ford, "Cosmological-constant damping by unstable scalar fields," *Physical Review*, vol. 35, no. 8, pp. 2339–2344, 1987.

[29] Y. Fujii, "Origin of the gravitational constant and particle masses in a scale invariant scalar-tensor theory," *Physical Review*, vol. 26, no. 10, pp. 2580–2588, 1982.

[30] V. V. Kiselev, "Quintessence and black holes," *Classical and Quantum Gravity*, vol. 20, no. 6, pp. 1187–1197, 2003.

[31] S. Chen, B. Wang, and R. Su, "Hawking radiation in a d-dimensional static spherically-symmetric black Hole surrounded by quintessence," *Physical Review*, vol. 77, no. 12, Article ID 124011, 2008.

[32] Y. H. Wei and Z. H. Chu, "Thermodynamic properties of a Reissner-Nordstroem quintessence black hole," *Chinese Physical Letters*, vol. 28, Article ID 100403, 2011.

[33] S. Fernando, "Schwarzschild black hole surrounded by quintessence: Null geodesics," *General Relativity and Gravitation*, vol. 44, no. 7, pp. 1857–1879, 2012.

[34] B. B. Thomas and M. Saleh, "Thermodynamics and phase transition of the Reissner-Nordstroem black hole surrounded by quintessence," *General Relativity and Gravitation*, vol. 44, no. 9, pp. 2181–2189, 2012.

[35] H. Ghaffarnejad, E. Yaraie, and M. Farsam, "Quintessence reissner nordstrom anti de sitter black holes and joule thomson effect," *International Journal of Theoretical Physics*, vol. 57, no. 6, pp. 1671–1682, 2018.

[36] M. Olivier and T. Harko, "New derivation of the Lagrangian of a perfect fluid with a barotropic equation of state," *Physical Review*, vol. 86, no. 8, Article ID 087502, 2012.

[37] L. Lehner, R. C. Myers, E. Poisson, and R. D. Sorkin, "Gravitational action with null boundaries," *Physical Review*, vol. 94, no. 8, Article ID 084046, 2016.

[38] D. Carmi, S. Chapman, H. Marrochio, R. C. Myers, and S. Sugishita, "On the time dependence of holographic complexity," *Journal of High Energy Physics*, vol. 2017, no. 11, Article ID 188, 2017.

[39] R.-Q. Yang, C. Niu, C.-Y. Zhang, and K.-Y. Kim, "Comparison of holographic and field theoretic complexities for time dependent thermofield double states," *Journal of High Energy Physics*, vol. 2018, no. 2, Article ID 82, 2018.

[40] C. Gao, L. Youjun, Y. Shuang, and Y.-G. Shen, "Black hole and cosmos with multiple horizons and multiple singularities in vector-tensor theories," *Physical Review*, vol. 97, no. 10, Article ID 104013, 2018.

[41] K. Sfetsos, "Gravitational shock waves in curved space-times," *Nuclear Physics*, vol. 436, p. 721, 1995, https://arxiv.org/abs/hep-th/9408169.

Hindawi
Advances in High Energy Physics
Volume 2021, Article ID 9380814, 1 page
https://doi.org/10.1155/2021/9380814

Expression of Concern

Expression of Concern on "Antigravity, an Answer to Nature's Phenomena including the Expansion of the Universe"

Advances in High Energy Physics

Received 21 September 2020; Accepted 21 September 2020; Published 17 April 2021

Advances in High Energy Physics would like to express concern with the article titled "Antigravity, an Answer to Nature's Phenomena including the Expansion of the Universe" [1], which reviews the author's previous studies.

Following the publication of the review article, concerns have been identified that the discussion is qualitative and without any concrete model supporting the ideas presented. The concept that clouds experience anti-gravity proportional to the temperature of water droplets appears unsustainable, as well as the idea that thermal energy produced by the stars can explain the accelerating universe. Both ideas lack a concrete model, and it is unlikely that such a model can exist. If the observations presented in the article are assumed to be correct, a model would be required to test the hypothesis. The possibility of such testing is doubtful. We additionally note that the author's previous work, reviewed in the article, has not been cited by other researchers.

References

[1] C. K. Piyadasa Gamini, "Antigravity, an answer to Nature's phenomena including the expansion of the universe," *Advances in High Energy Physics*, vol. 2020, Article ID 9315491, 5 pages, 2020.

Hindawi
Advances in High Energy Physics
Volume 2020, Article ID 9315491, 5 pages
https://doi.org/10.1155/2020/9315491

Review Article

Antigravity, an Answer to Nature's Phenomena including the Expansion of the Universe

C. K. Gamini Piyadasa

Electrical and Computer Engineering, University of Manitoba, 75, Chancellors Circle, Winnipeg, MB R3T 5V6, Canada

Correspondence should be addressed to C. K. Gamini Piyadasa; gaminickg@gmail.com

Received 18 March 2019; Accepted 6 September 2019; Published 7 January 2020

Guest Editor: Farook Rahaman

The gravitational attraction force being proportional to the mass has been experimentally shown for several hundred years now, but no gravitational repulsion has been identified within the accepted scientific reasoning. Here, we show that the gravitational repulsion force, similar to the gravitational attraction among particles has also been in existence in nature but, yet to be recognized. The results of experiments are shown in detail and are discussed in the recent series of-publications. It is also shown here that this gravitational repulsion force is proportional to the temperature which is an indicator of thermal energy of the particle, similar to the gravitational attraction that is proportional to the mass of the particle. The situations where heavy particles such as iodine, tungsten, and thorium in vacuum move against gravitational force have already been shown qualitatively. The increase in time-of-fall of water droplets (slowing down of fall) with rise in temperature is also quantitatively discussed. This article discusses two major phenomena observable in nature, clouds and the expansion of universe, which could be more preciously explained by the concept of antigravity.

1. Introduction

Gravity is a one of the fundamental forces identified in nature, formulated by Sir Isaac Newton in 1728 as: The law of universal gravitation [1]. However, the concept of gravitational repulsion has neither been discerned nor identified within the prevailing scientific laws and concepts until recent past [2–5]. The gravitational attraction is proportional to the mass which has been experimentally proved for several hundred years.

The idea of this short communication is to discuss observations and results published in three consecutive journal articles published by the author and extend its manifestation to explain two major physical processes in nature.

Manuscript 1 has shown [2] the upward movement of heavy particles in vacuum, in a situation where, all factors which are believed to be causing the upward movement of particles against the gravitational pull in air: viz—buoyancy and the lift force, are eliminated by experimental design. Manuscript [2] shows that iodine particles move against gravitational pull when they get heated in a vacuum as shown in Figure 1. It also cites an example from electronic vacuum tubes (also called electronic valves) where evaporated tungsten and thorium particles from the heater moves upwards, despite the gravitational pull and the strong radial electric fields and deposits in the top of the glass container.

Manuscript 2 discusses [3] the movement of heated water droplets in still air against the gravitational pull. Thermal image (Figures 2(a) and 2(b)) of the path of heated condensed water droplets reveals that, even though the temperature gradient does not support (Figure 2(c)) the formation of convection air currents, the condensed water droplets slow down its motion, turn around, and then move upward against gravitational pull.

Manuscript 3 [4] shows the upward movement of heated water droplets inside an ice cylinder (Figure 3(a)) which intentionally inhibits air convection. Secondly, the manuscript also shows the measurements related to the time-of-fall of a heavy water droplet (Figure 3(b)). Two droplets with mass 4 mg and 9 mg were used in the temperature range of 10°C–60°C.

In considering the equilibrium of the rising and falling water-droplet in still air, attention has been given to all relevant factors—force of gravity, buoyancy, surface evaporation [6, 7] and force due to the temperature profile in air [8, 9].

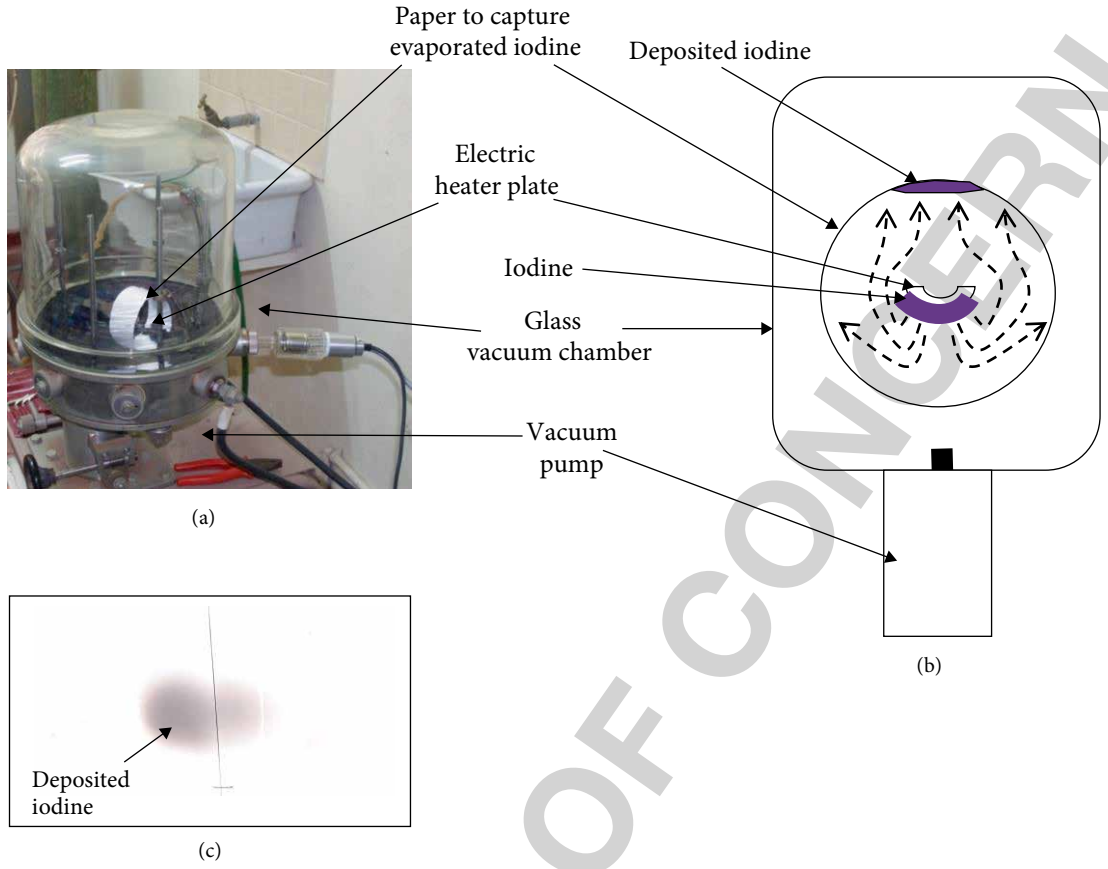

FIGURE 1: Figure extracted from reference [2]—Experimental set-up to observe movement of heat-evaporated iodine vapor in vacuum. (a) Vacuum deposition chamber. (b) A layer of iodine was gradually heat evaporated (ejected downward direction) inside the vacuum chamber. The electrical heater plate itself covers the iodine particles moving directly in upward direction. The iodine source was surrounded with a paper jacket in order to capture the deposition geometry of iodine. The paper was placed 50 mm radially away from the iodine source. Pressure in the chamber was $\sim 1 \times 10^{-5}$ mbar, average mean free path is greater than 6.6 m, and air density was approximately 12.6 ng m^{-3}. Pressure at the top (P_{top}) of the chamber was higher than at the bottom (P_{bottom}), $P_{\text{top}} > P_{\text{bottom}}$. (c) Photograph of deposited iodine on the inner top part of the paper. Reprinted from "Antigravity—Is it already under our nose?" by C. K. G. Piyadasa, 2011, Canadian Journal of Pure and Applied Sciences, Vol. 5, No. 2, pp. 1586, Reprinted by permission of SENRA Academic Publishers, 5919 129 B.

Here, it is experimentally demonstrated that there exists a cryptic force (upward force) which increases with temperature where a linear increase in time-of-fall (slowing down) is observed.

2. Discussion

As a summary of the content of these publications (Figure 4), it is concluded that there is a repulsion force, against the direction of gravitational pull, and further that this repulsion force is proportional to the temperature which is a parameter of the thermal energy of the particle, similar to the gravitational attraction that is proportional to the mass of the particles.

Referring to the results shown in the three manuscripts, Figure 4 summarizes the following relationship between two arbitrary particles with masses m_1, m_2, temperatures T_1, T_2 and specific heat capacities C_1, C_2.

Conventional gravitational law reveals that

$$\text{Attraction force} \propto \text{mass}\,(m_1, m_2). \tag{1}$$

The findings in experiments state that

$$\text{Repulsion force} \propto \text{thermal energy}\,(H_1, H_2). \tag{2}$$

Thermal energy, H is expressed in the following expression

$$H = m \times C \times T. \tag{3}$$

Therefore, resultant forces acting on an object (as in water droplet in manuscript 2, Expe. 2) are proportional to the mass and heat energy of objects. Generalizing expressions 1 and 2.

$$\begin{aligned}&\text{Resultant force between any two arbitrary objects}\\ &= F_{att} \sim F_{rep} \propto f(\text{mass, heat energy}).\end{aligned} \tag{4}$$

For the objects with mass m_1, m_2 and thermal energy H_1, H_2 respectively, the above expression can be rewritten as

$$\text{Resultant force} = F_{att} \sim F_{rep} \propto f(m_1, m_2, H_1, H_2). \tag{5}$$

Similar to gravitational acceleration g, due to the attraction force of earth, a gravitational deceleration can also be proposed due to thermal energy.

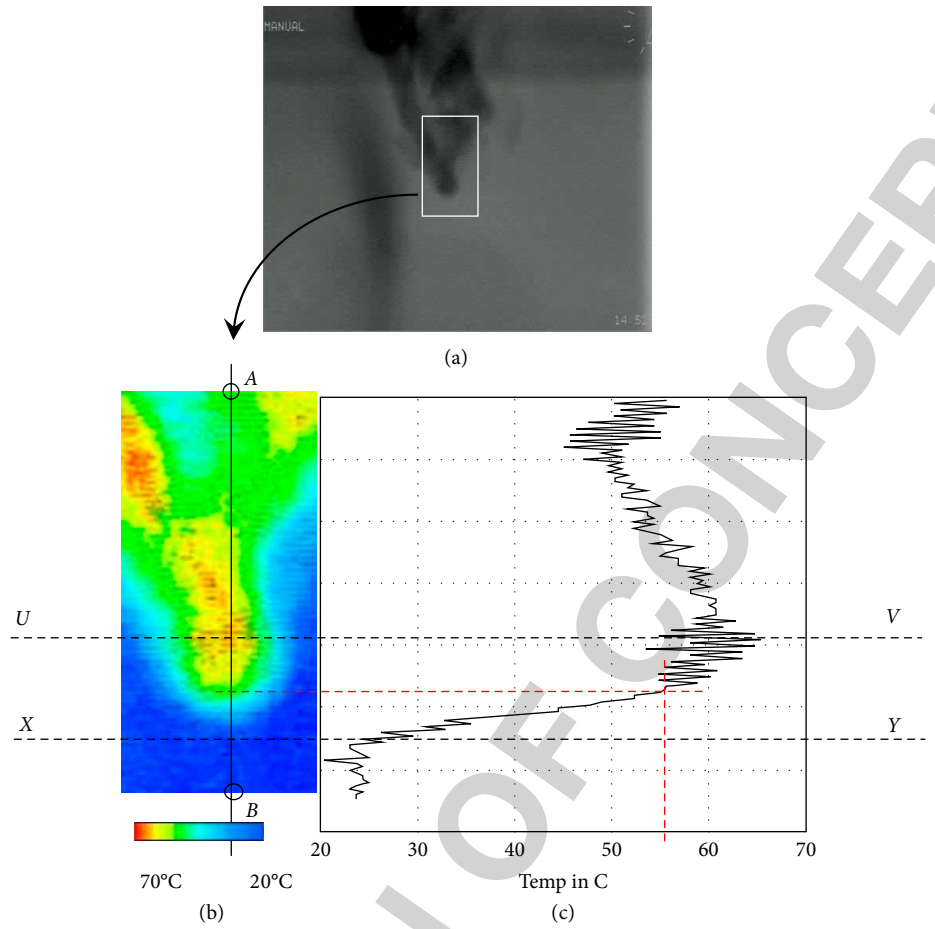

Figure 2: Figure extracted from reference [3]—Thermal image of the turnaround point (TAP) of the stream of the condensed steam droplets (CSD) and the vertical temperature distribution of the middle of TAP area. (a) Thermal image of downward projected CSD taken from the cryogenically cooled third generation forward looking infrared (FLIR) thermal camera (3–5μm). (b) Temperature distribution at the droplet turning around area. Color gradient is proportional to the temperature as shown in the plate below (c) temperature distribution along the line AB in (b). Reprinted from "Will rising water droplets change science?" by C. K. G. Piyadasa, 2011, Canadian Journal of Pure and Applied Sciences, Vol. 6, No. 2, pp. 1995, Reprinted by permission of SENRA Academic Publishers, 5919 129 B Street Surrey, British Columbia, Canada V3X 0C5.

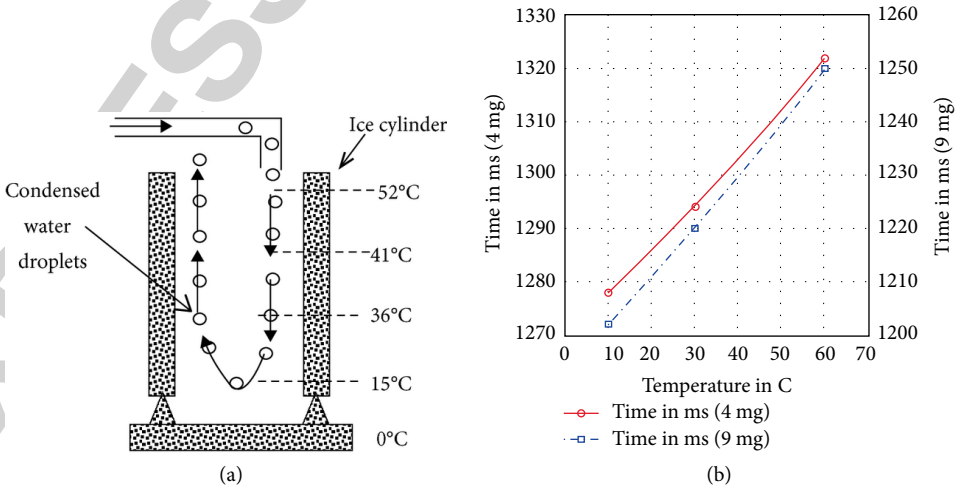

Figure 3: Results from the Manuscript 3 [4]. (a) Motion of condensed water droplets in the ice cylinder where the environment supports no convection currents. (b) Time-of-fall of water droplet increases with the increase in droplet temperature. Time-of-fall of two water droplets in a 5.913 m long metal tube was measured. Temperature of droplets was changed from 10°C to 60°C. Time delays of 44 ms and 48 ms were measured for 4 mg and 9 mg droplets for the temperature range of 10°C–60°C, respectively.

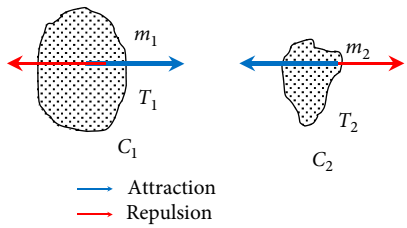

Figure 4: Forces acting in between two arbitrary particles with masses m_1, m_2, temperatures T_1, T_2, and specific heat capacities C_1, C_2. There exist attraction (blue arrows) and repulsion forces (red arrows) between them.

The gravitational force is considered a weak force in classical physics. Any gravitational interaction could be considered the resultant effect of the gravitational and antigravitational forces inherent in the two bodies under consideration; hence, the gravitational force manifests itself as a weak force.

In this proposal, repulsive force depends not only on C and T but also on mass (Equation 3). Thermal energy is stored in mass/matter and therefore the repulsive force is invariably linked with the mass. Therefore, it is reasonable to connect this repulsive force with "gravitational repulsion" or "anti-gravity". Further, what we have witnessed here is a "rising up" against gravity, it is logical to bring in this antigravity factor. It is also worthwhile noting that no other concept of general physics could explain the observations, upward motion of iodine molecules (nm scale) in vacuum, rise of water-droplets (in μm scale) and the delay of fall of water-droplets (in mm scale) with the rise in temperature against the direction of gravitational pull (i.e., this force acts on against the gravitational pull).

A detailed mathematical analysis will follow this conceptual paper in the time to come.

Concept of antigravity can be used to effectively interpret many phenomena. In this manuscript, the following two natural phenomena that represent two different scopes clouds and the expanding universe are selected for discussion. A cloud represents a relatively small system compared to the expanding universe.

2.1. Clouds. Clouds are floating even though they contain water-droplets [10] (condensed water-droplets) which are 899 times denser than the surrounding air at the altitude 1000 m and at temperature 8.5°C. This ratio (density of water and air) becomes 1667 times at altitude of 7000 m (Physics fact book https://hypertextbook.com/facts/2007/AllenMa.shtml, The Engineering tool box https://www.engineeringtoolbox.com/standard-atmosphere-d_604.html) where temperature is around −40°C.

The main argument here, in cloud-physics, is that it is only because the updraft (convection currents) in the cloud counteracts the fall of the cloud particles [11–13]. It is also worth mentioning that there exists a down draft similar to updraft in clouds [14, 15].

However, the mist and the fog forming at the ground level, in still (or undisturbed) air where no updraft (convection currents) exists, have the same composition as in a cloud. Mist and fog usually form on a calm night when the air is too cold to hold all its moisture. Volume mean diameter (VMD) of fog droplets are observed up to about 65 μm [16, 17] and in mist the VMD tends to be a little higher than fog. In another words, mist is heavier and lies closer to the ground. The separation among these droplets is relatively large compared to their size. The number density of these droplets is around 25 droplets per cubic centimeter [16]. In these situations, no updraft exists even though they (mist & fog) have the same composition as in a cloud. This is further observable in still or in slowly moving clouds on a high mountain, especially in the morning where the ground is nearly frozen where no convection or updraft exists.

The repulsive force against the gravitational pull of the water droplets is shown in the second and third manuscript. This repulsive property of water droplets against the earth's gravitational pull is also shown in Figures 2 and 3. This concludes that there exists a repulsive force (with earth) as well as gravitational attraction force to the particle depending on their thermal energy and the mass where the water droplets are in equilibrium.

In addition to attractive and repulsive forces of water-droplets of a cloud with earth, there exist attraction and repulsive forces among water droplets within the cloud. These forces acting inside the cloud explain the accumulative (flocking together) nature of the cloud which has not been explained by the classical theories. The equilibrium of these two forces will confine the droplets to a certain area as a floccule. The repulsiveness does not allow shrinking and finally collapsing the cloud. The attractive force keeps the droplets together without dispersion.

Some other observations can be spotted if we think very carefully.

For example, the high concentration of Chlorofluorocarbon (CFC—120.9 amu) molecules observed in high altitudes (17–50 km) could also be attributed to the antigravity force, although it is generally explained as a result of diffusion. CFC is four times heavier than average air (average air molecule is 28.84 amu).

Another similar phenomenon in which the classical theories fail to explain is the rising of water droplets when hot water is thrown horizontally in the air in extremely cold weather. The hot water breaks in to tiny droplets as soon as it gets in to free air, and these tiny droplets move upwards against the gravitational attraction (see video in Supplementary Materials (available here)). The repulsion among hot water molecules in the water breaks up the water masses. These particles then move against earth's gravitational field due to its thermal energy (antigravity force) as experimentally shown by the author in his second and third manuscripts.

2.2. Expanding Universe. Further, even in the observation of an "expanding/accelerating universe", the galaxies are moving apart from each other despite the strong gravitational forces among massive systems. At present two main theories, big bang theory and dark energy, try to interpret this expansion of the universe but these interpretations are not very promising. If only attraction force due to the gravitational force exists, the universe must shrink together and finally collapse. Instead, it is expanding and the galaxies are repelling each other. Hence, it is logical to sense a repulsive force among celestial bodies in the universe. This idea was recently published elsewhere [18] as "Antigravity could replace dark energy as cause of universe's

Hindawi
Advances in High Energy Physics
Volume 2019, Article ID 3486805, 8 pages
https://doi.org/10.1155/2019/3486805

Research Article

Modeling Dark Sector in Horndeski Gravity at First-Order Formalism

F. F. Santos,[1] R. M. P. Neves,[1] and F. A. Brito[1,2]

[1]*Departamento de Física, Universidade Federal da Paraíba, Caixa Postal 5008, 58051-970 João Pessoa PB, Brazil*
[2]*Departamento de Física, Universidade Federal de Campina Grande, Caixa Postal 10071, 58109-970 Campina Grande PB, Brazil*

Correspondence should be addressed to F. A. Brito; fabrito@df.ufcg.edu.br

Received 2 July 2019; Revised 20 August 2019; Accepted 26 November 2019; Published 17 December 2019

Guest Editor: Cesar A. Vasconcellos

We investigate a cosmological scenario by finding solutions using first-order formalism in the Horndeski gravity that constrains the superpotential and implies that no free choice of scalar potential is allowed. Despite this, we show that a de Sitter phase at late-time cosmology can be realized, where the dark energy sector can be identified. The scalar field equation of state tends to the cosmological scenario at present time and allows us to conclude that it can simulate the dark energy in the Horndeski gravity.

1. Introduction

Ever since Einstein proposed the General Relativity, it has been supported by strong observational evidence in many astrophysical scenarios, namely, Eddington's measurement of the deflection of light in 1919 and recent direct observation of gravitational waves by the LIGO collaboration [1, 2]. However, we still have fundamental problems that are not well-understood in General Relativity such as dark matter, dark energy, and the inflationary phase of the Universe. In recent years, models have been proposed involving modifications of General Relativity [3, 4]. In such modifications, some of its essential properties are maintained such as a second order of the equations of motion arising from a diffeomorphism-invariant action and keeping the Lorentz invariance. Due to these assumptions, the additional propagating degrees of freedom into the gravity sector consist of including additional fields (scalars, vectors, or tensors) [5]. These modifications of the gravity theory taking into account nonminimal couplings between geometry and matter become one of the mainstream of modified gravity theories, and the applications of the nonminimal couplings of matter with gravity provide a way to solve the cosmological constant problem [6, 7] and accelerated expansion of the Universe [8, 9]—see also alternative theories, for instance, involving late-time [10, 11] and early-time acceleration (inflation) [12] in the context of supergravity.

Recent investigations about Einstein gravity have called attention for the coupling of the theory to scalar fields [13]. These efforts led to the development of the well-known Galileons that are scalar-tensor theories [14]. Indeed, these studies have led to the rediscovery of the Horndeski gravity.

The Horndeski gravity was originally discovered in 1974 [5, 15–18]. It is a general single scalar field-tensor theory with second-order field equations and second-order energy-momentum tensor. The Lagrangian-producing second-order equations of motion as discussed in [4, 16, 18–22] include four arbitrary functions of the scalar field and its kinetic term [3, 23]. The term that we are interested in includes a nonminimal coupling between the standard scalar kinetic term and the Einstein tensor. Besides the cosmological interest, recent investigation has also called attention in astrophysics, such as the search for black hole solutions which develop Hawking-Page phase transitions at a critical temperature [18]. Other examples of spherically symmetric solutions in Horndeski theory in the context of the solar system and further astrophysical scenarios can also be found, for instance, in the study of perihelion shift and light bending [24] and in

the issues involving properties of spinning gyroscope and the Gravity Probe B experiment [25]. Some applications in astrophysical compact objects have also been considered in [26, 27].

An interesting problem in the cosmological scenario is the cosmological constant problem that is related to the discrepancy between the natural scale and its measured value. As discussed in [28], it is possible to address this problem by using a self-tuning mechanism, which has been analyzed in the original Horndeski theory for the so-called Fab Four theory [29, 30]. However, more analyses of the cosmological self-tuning and the local solutions in the context beyond Horndeski theories can be found in [31].

In the cosmological scenario, the Horndeski cosmological models are able to screen the vacuum energy coming from any field theory in a space that should be a de Sitter vacuum [32, 33]. In these models, we can understand that the current accelerated expansion of the Universe is a dynamical result evolution of a de Sitter attractor [34]. In this sense, the Horndeski models involving a de Sitter critical point for any kind of material content may provide a mechanism to alleviate the cosmological problem [35]. Thus, the models involving nonminimal derivative couplings to gravity have been explored in a variety of extended theories of gravity [36]. These models show peculiar features, for example, an essential mixing of scalar and tensor kinetic terms, named kinetic braiding, and possessing a rich cosmological phenomenology that includes a late-time asymptotic de Sitter state that allows a phantom-divide line crossing with neither ghost nor gradient instabilities.

In this work, we consider the Horndeski theory in the cosmological context by using the first-order equation formalism that was presented recently for Horndeski gravity in a brane world scenario [17]. We investigate the second-order equations through the first-order formalism because, in general, one simplifies the study of analytical or numerical solutions. Moreover, the first-order equation formalism is a fundamental tool in the renormalization group (RG) flow in holographic cosmology [37–40]. In our case, we consider the Friedmann equations without curvature and assume dark energy dominance. In particular, the inflationary context was analyzed by considering a power-law potential and using the dynamical system method to investigate the possible asymptotical regimes of the model [41]. It was shown that for sloping potentials, there exists a quasi-de-Sitter phase corresponding to the early inflationary Universe. In our investigations, by considering numerical methods, we show that kink-type solutions of first-order equations represent a de Sitter Universe. We address several important issues in cosmological observables, such as the Hubble function, the deceleration parameter, and the dark energy equation of state. We investigate their evolution at small redshifts for a general scalar potential written in terms of a superpotential. Furthermore, as shown in [42], the Horndeski action in the Friedmann frame without scalar potential cannot describe the dark matter and dark energy, due the instability, and also by constraint of gravity waves, the scalar field on the background evolution is negligible, and the presence of this field becomes unnecessary for explaining the dark matter and dark energy. In our case, however, the nature of the scalar potential in the Horndeski gravity in the Friedmann frame is much more satisfactory for describing dark energy.

The paper is organized as follows. In Section II, we present the first-order formalism in Horndeski theory with a scalar potential given in terms of an implicit superpotential obtained numerically. In Section III, we use the numerical method to find cosmological solutions that represent a de Sitter Universe. In Section IV, we discuss the following cosmological observables: the Hubble function, the deceleration parameter, and the dark energy equation of state at small redshifts. Finally, in Section V, we present our conclusions.

2. The Horndeski Gravity with a Scalar Potential

In our present investigation, we shall address the study of Friedmann-Robertson-Walker (FRW) solutions in the framework of the Horndeski gravity [13, 15–18, 43] in which action with a scalar potential reads

$$I\left[g_{\mu\nu},\phi\right]=\int\sqrt{-g}d^4x\left[kR-\frac{1}{2}\Big(\alpha g_{\mu\nu}-\eta G_{\mu\nu}\Big)\nabla^\mu\phi\nabla^\nu\phi-V(\phi)\right]. \tag{1}$$

Note that we have a nonminimal scalar-tensor coupling where we can define a new field $\dot{\phi}\equiv\psi$. This field has dimension of $(\text{mass})^2$ and the parameters α and η control the strength of the kinetic couplings; α is dimensionless and η has dimension of $(\text{mass})^{-2}$. Thus, the Einstein-Horndeski field equations can be formally written as in the usual way:

$$G_{\mu\nu}=\frac{1}{2k}T_{\mu\nu}, \tag{2}$$

where $T_{\mu\nu}=\alpha T^1_{\mu\nu}-g_{\mu\nu}V(\phi)+\eta T^2_{\mu\nu}$ with $k=(16\pi G)^{-1}$, and the scalar field equation is given by

$$\nabla_\mu[(\alpha g^{\mu\nu}-\eta G^{\mu\nu})\nabla_\nu\phi]=V_\phi. \tag{3}$$

We shall adopt the notation $f_{\phi\phi\cdots\phi}(\phi)\equiv d^nf(\phi)/d\phi^n$. In particular, $V_\phi\equiv dV/d\phi$. The aforementioned energy-momentum tensors $T^1_{\mu\nu}$ and $T^2_{\mu\nu}$ take the following form:

$$\begin{aligned}
T^1_{\mu\nu}&=\nabla_\mu\phi\nabla_\nu\phi-\frac{1}{2}g_{\mu\nu}\nabla_\lambda\phi\nabla^\lambda\phi,\\
T^2_{\mu\nu}&=\frac{1}{2}\nabla_\mu\phi\nabla_\nu\phi R-2\nabla_\lambda\phi\nabla\Big({}_\mu\phi R^\lambda_\nu\Big)-\nabla^\lambda\phi\nabla^\rho\phi R_{\mu\lambda\nu\rho}\\
&\quad-\Big(\nabla_\mu\nabla^\lambda\phi\Big)(\nabla_\nu\nabla_\lambda\phi)+\big(\nabla_\mu\nabla_\nu\phi\big)\Box\phi\\
&\quad+\frac{1}{2}G_{\mu\nu}(\nabla\phi)^2-g_{\mu\nu}\left[-\frac{1}{2}\Big(\nabla^\lambda\nabla^\rho\phi\Big)\big(\nabla_\lambda\nabla_\rho\phi\big)\right.\\
&\quad\left.+\frac{1}{2}(\Box\phi)^2-\big(\nabla_\lambda\phi\nabla_\rho\phi\big)R^{\lambda\rho}\right].
\end{aligned} \tag{4}$$

Here, we are interested in investigating the cosmological implications of theories with extended nonminimal derivative couplings. Considering the flat FRW metric of the form

$$ds^2 = -dt^2 + a^2(t)\delta_{ij}dx^i dx^j, \tag{5}$$

the scalar field depends on the cosmic time only, and computing the tt-component of the Einstein-Horndeski field equation (2) gives

$$3\dot{a}(t)^2\left(4k - 3\eta\psi^2(t)\right) - a^2(t)\left[\alpha\psi^2(t) + 2V(\phi)\right] = 0. \tag{6}$$

The Friedmann equation can be readily found from this equation and reads as

$$H^2 = \frac{\alpha\dot{\phi}^2 + 2V(\phi)}{3\left(4k - 3\eta\dot{\phi}^2\right)}. \tag{7}$$

Now, we use the first-order formalism by assuming [11, 44, 45]

$$\begin{aligned} H &= W(\phi), \quad H \equiv \frac{\dot{a}}{a}, \\ \dot{\phi} &= -W_\phi(\phi), \end{aligned} \tag{8}$$

where the superpotential $W(\phi)$ plays a central role. Through these equations and equation (7), we can write the scalar potential as follows:

$$V(\phi) = \frac{3}{2}W^2\left(4k - 3\eta W_\phi^2\right) - \frac{\alpha}{2}W_\phi^2. \tag{9}$$

Notice the scalar potential is similar to that found in the brane world scenario [17]. Now, we proceed with the xx-yy -zz-components of equation (2) which are given by

$$\begin{aligned} &\dot{a}^2(t)\left(\eta\psi^2(t) - 4k\right) + a(t)\left[\ddot{a}(t)\left(2\eta\psi^2(t) - 8k\right)\right. \\ &\quad \left. + 4\eta\dot{a}(t)\psi(t)\dot{\psi}(t)\right] + a^2(t)\left[\alpha\psi^2(t) + 2V(\phi)\right] = 0. \end{aligned} \tag{10}$$

The scalar field equation (3) in the FRW background is written in the form

$$\ddot{\phi} + 3H\dot{\phi} + \frac{6\eta\dot{\phi}H\dot{H}}{\alpha + 3\eta H^2} + \frac{V_\phi(\phi)}{\alpha + 3\eta H^2} = 0, \tag{11}$$

and for $V_\phi = 0$ reduces to the form found in [22]. Now, combining equation (6) with equation (10), we can write a differential equation for the superpotential:

$$2WW_{\phi\phi} + W_\phi^2 + 3W^2 - \beta = 0, \tag{12}$$

where $\beta = (1 - \alpha)/\eta$. There is a family of analytical solutions for the homogeneous case $\beta = 0$ given in terms of trigonometric functions:

$$W(\phi) = \left(-C_1 \sin\left(\frac{3}{2}\phi\right) + C_2 \cos\left(\frac{3}{2}\phi\right)\right)^{2/3}. \tag{13}$$

From equation (8), we can find an approximated solution, for $C_1 = 0$ and $C_2 = 1$; e.g., the limit of one of the functions is very small. Here, we assume $\phi \approx 1$ for a cosmological time around a time scale t^*, to find an acceptable cosmological solution for the accelerating Universe:

$$\begin{aligned} \phi &\approx 2.41t - \phi_0, \\ a(t) &\approx \exp\left(0.17t\right). \end{aligned} \tag{14}$$

As we shall see below, for arbitrary values of $\beta \neq 0$, we should apply numerical methods to find exact solutions for equations (8) and (12).

3. Numerical Solutions

The pair of first-order equations can be solved numerically for a broader range of Horndeski parameter values as long as we assume appropriate boundary conditions. In Figure 1, we show the behavior of the scalar field with a "kink" profile (a) and scale factor (b) associated with the FRW solutions for $\beta = 23.5$ with $\alpha = 0.06$ and $\eta = 0.04$ (blue curve) and $\beta = 15.3$ with $\alpha = 0.08$ and $\eta = 0.06$ (red curve). These regimes of small η and $\alpha \neq 1$ are required to produce acceptable cosmological solutions. Of course, these choices of parameters lead to a nonhomogeneous limit of equation (12) where no analytical solutions are known. Thus, we shall find such cosmological solutions by using numerical methods. In the present case, we have applied the Runge-Kutta method to first-order equation (8) for $a(t)$ and $\phi(t)$ and second-order equation (12) for $W(\phi)$. The boundary conditions we used here were the following: $W(0) = 1$, $W'(0) = 1$, and $\phi(0) = 0$.

4. Cosmological Observables

In this section we investigate cosmological observables in our cosmological setup in Horndeski gravity. Several studies in this context have already been considered and shown to produce successful models [21, 22, 46], as, for example, in the description of dark energy [22].

We extend these earlier studies in the context of the first-order formalism, which is in the direction of connecting them with cosmological scenarios in fundamental theories such as supergravity and string theory where de Sitter solutions are hard to find. One of the recent approaches in order to overcome such difficulty is the holographic renormalization group (RG) flow which is written in terms of first-order equations for a given superpotential [37–40]. The first-order formalism has also been applied, e.g., in $f(R)$ and $f(R, T)$ gravity [47, 48], but to the best of our knowledge, this is the first time where it is investigated in Horndeski cosmology. In our study, the scalar potential cannot be arbitrary since it depends on the superpotential that obeys a differential equation which constrains the possible cosmological scenarios. Despite this, as we shall see below, there exists some

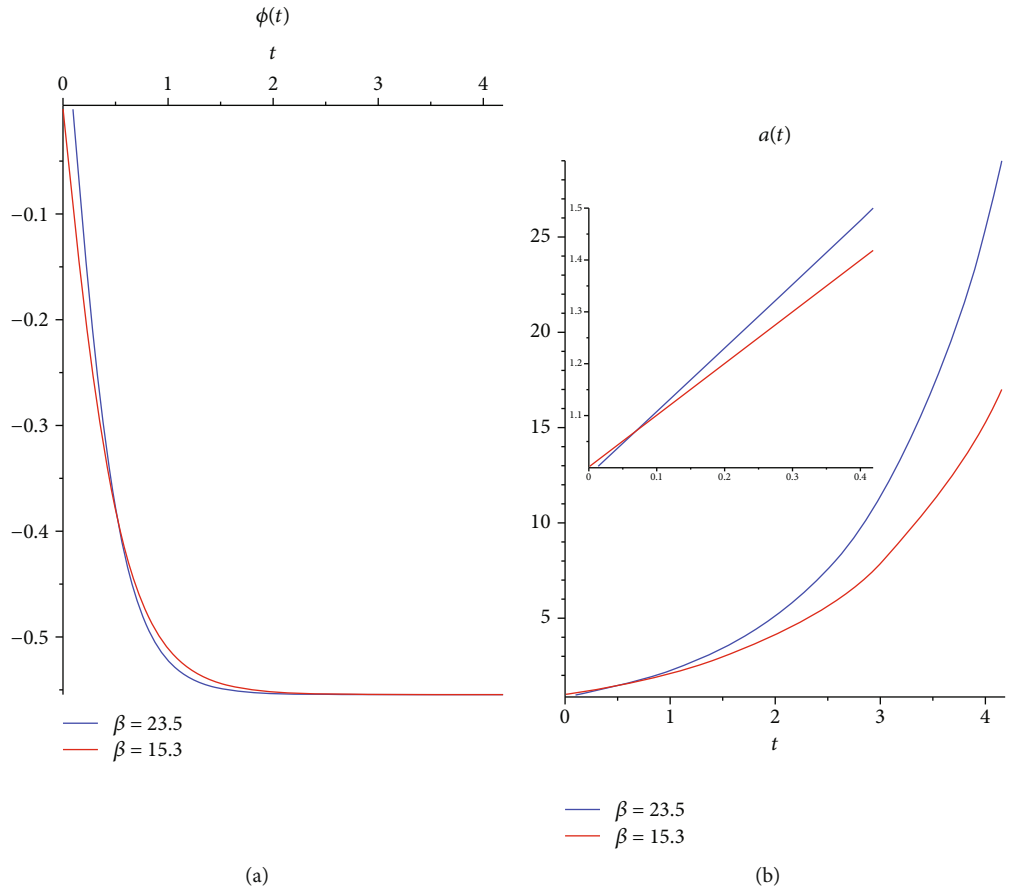

FIGURE 1: The behavior of the solutions of equation (8): $\phi(t)$ (a) for $\beta = 23.5$, with $\alpha = 0.06$ and $\eta = 0.04$ (blue curve), and $\beta = 15.3$, with $\alpha = 0.08$ and $\eta = 0.06$ (red curve); $a(t)$ (b) for the same values of parameters. The inset shows the behavior of $a(t)$ at smaller times. Particularly, $a(0) = 1$, for $\beta = 15.3$ (red curve), where $t = 0$ does not mean the Big Bang. Instead, it means the time at which our formalism starts to describe the present phase of the Universe.

restricted values of parameters that allow describing the current acceleration of the Universe. Thus, we shall assume a dark energy dominance described by the scalar field dynamics at small redshifts.

Let us first focus on the equation of state.

Then, by using the energy-momentum tensor of equation (2) defined as

$$T_{\mu\nu} = \frac{\alpha}{2k} T^1_{\mu\nu} - g_{\mu\nu} V(\phi) + \frac{\eta}{2k} T^2_{\mu\nu}, \tag{15}$$

the tt and xx-yy-zz-components define the effective dark energy sector with energy density and pressure:

$$\rho_{\mathrm{DE}} \equiv T_{tt} = \frac{\alpha\dot{\phi}^2}{4k} + \frac{V(\phi)}{2k} + \frac{9\eta H^2 \dot{\phi}^2}{4k}, \tag{16}$$

$$\begin{aligned} p_{\mathrm{DE}} \equiv T_{xx} = {} & \frac{\alpha\dot{\phi}^2}{4k} - \frac{V(\phi)}{2k} \\ & - \frac{\eta}{2k}\left[\frac{1}{2}\dot{\phi}^2\left(3H^2 + 2\dot{H}\right) + 2H\dot{\phi}\ddot{\phi}\right], \end{aligned} \tag{17}$$

where $T_{xx} = T_{yy} = T_{zz}$. To check consistency, it is interesting to see that using equations (8) and (9), the energy density satisfies $\rho_{\mathrm{DE}} = 3H^2$, as expected. Thus, the dark energy equation of the state is given by

$$\begin{aligned} \omega_{\mathrm{DE}} &= \frac{p_{\mathrm{DE}}}{\rho_{\mathrm{DE}}} \\ &= \frac{\alpha\dot{\phi}^2 - 2V(\phi) - 2\eta\left[(1/2)\dot{\phi}^2\left(3H^2 + 2\dot{H}\right) + 2H\dot{\phi}\ddot{\phi}\right]}{\alpha\dot{\phi}^2 + 2V(\phi) + 9\eta H^2\dot{\phi}^2}. \end{aligned} \tag{18}$$

In terms of the dark energy density and pressure, the scalar field equation can be written in the standard form through the energy-momentum conservation, $\nabla_\mu T^\mu_\nu = 0$, that implies

$$\dot{\rho}_{\mathrm{DE}} + 3H(p_{\mathrm{DE}} + \rho_{\mathrm{DE}}) = 0. \tag{19}$$

This result (19) is in agreement with [46]. We may now compute another interesting cosmological quantity called

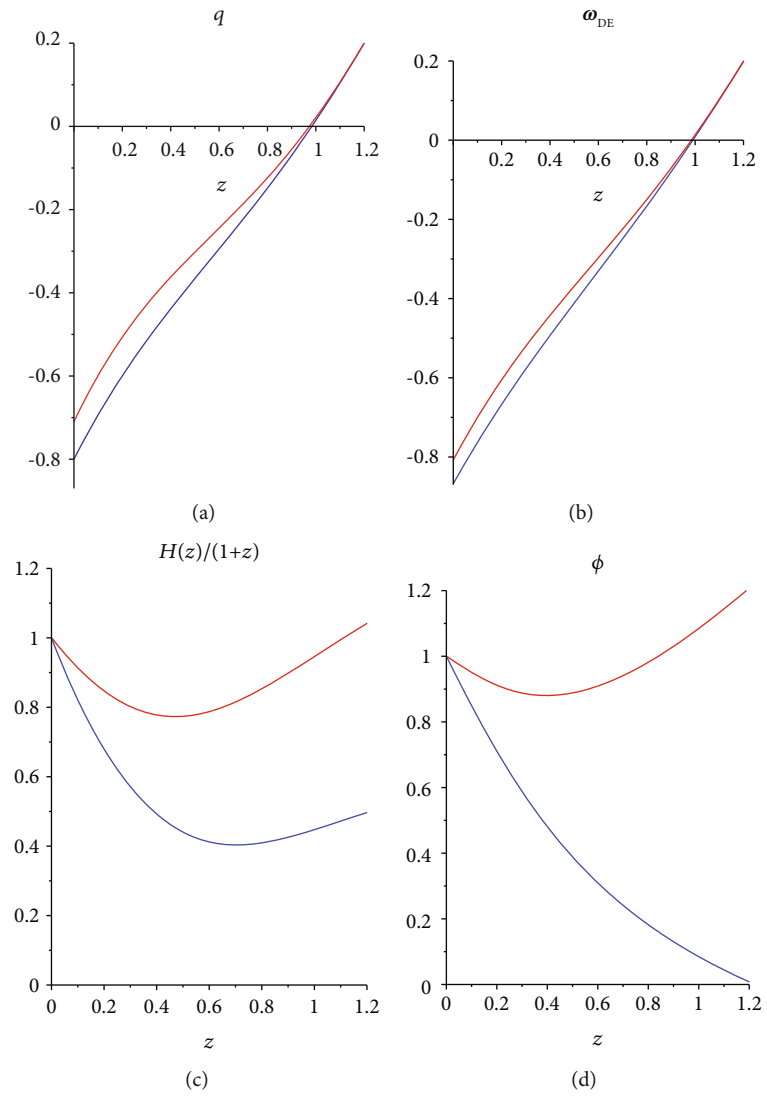

FIGURE 2: The decelerate parameter q (21) (a) and dark energy equation of state ω_{DE} (25) (b) for $\beta = 23.5$, with $\alpha = 0.06$ and $\eta = 0.04$ (blue curve), and $\beta = 15.3$, with $\alpha = 0.08$ and $\eta = 0.06$ (red curve). The Hubble parameter H (c) and scalar field ϕ (d) with the same values of parameters. All the cosmological observables are given as functions of the redshift z.

decelerate parameter q, which indicates how the Universe expansion is accelerating and is given by the equation

$$q = -\left(1 + \frac{\dot{H}}{H^2}\right). \tag{20}$$

Furthermore, combining equation (19) with $\rho_{DE} = 3H^2$, we can write a useful relationship between the deceleration parameter and the equation of state as follows:

$$q = \frac{1}{2}(1 + 3\omega_{DE}). \tag{21}$$

From this point, we shall make use of the dimensionless redshift parameter z in place of time variable t in our cosmological setup since it is used to compare theoretical with observational results. The redshift parameter is defined as

$$1 + z = \frac{1}{a}. \tag{22}$$

Thus, time derivatives can now be expressed as

$$\frac{d}{dt} = -H(z)(1+z)\frac{d}{dz}, \tag{23}$$

and the first-order equation (8) can simply be rewritten in the new variable z in the form

$$\begin{aligned} H(z) &= W(\phi(z)), \\ \phi'(z) &= -\frac{W_\phi(z)}{(1+z)W(z)}. \end{aligned} \tag{24}$$

The numerical results are also computed for equation (18) given in terms of the superpotential

$$\omega_{\mathrm{DE}} = -1 + \frac{2\alpha}{3}\frac{W_\phi^2}{W} + 2\eta W_\phi^2 + \frac{\eta W_\phi^4}{3W^2} + \frac{4\eta W_\phi^2 W_{\phi\phi}}{3W}. \quad (25)$$

We summarize as follows. According to Figure 2(b) the dark energy equation of state ω_{DE} (25) acquires values near −0.87 (blue curve).

Notice that our cosmological observables here were calculated only in the scalar-tensor sector of the Horndeski gravity given by the action (1) with no matter contribution. This sector alone is unable to take into account all phases of the Universe at high redshifts. Thus, we addressed only the dark energy (scalar) dominance at low redshifts. But investigations considering matter contribution to extension of this theory with several scalar potentials were already considered in [46]. Such a similar investigation in our model is out of the scope of this paper and can be addressed elsewhere. On the other hand, an inflationary phase can be found for a constant superpotential $W = H_0$ that satisfies (12). The first-order equation (8) gives the solution $a(t) = a_0 \exp(H_0 t)$ and $\phi = \text{const.}$, which characterizes an exponential inflation with equation of state $\omega = -1$.

Moreover from equation (25) and using the exact solution of the superpotential given by equation (13), we can see that the equation of state $\omega_{\mathrm{DE}} < -1$, since in the assumed limit $\phi \approx 1$, this function is dominated by the following term:

$$\omega_{\mathrm{DE}} = -\frac{5}{9}\left[\frac{1}{\cos((3/2)\phi)}\right]^{8/3} < -1. \quad (26)$$

This is one of the advantages of the Horndeski gravity, where a phantom-like behavior is obtained even though the scalar field has canonical dynamics. This effect is simply achieved due to the nonminimal coupling of the scalar field to gravity in the gravitational extension of the Einstein-Horndeski gravity [46]. It is important to address the phantom cosmology issues since recent observational data [49] have shown the possibility of $\omega_{\mathrm{DE}} < -1$.

The Hubble function in Figure 2(c) develops an increasing behavior between the onset at $z = 0.6$ and $z = 0$ (blue curve). This fact indicates a dark energy phase dominance starting in a relatively recent time of the cosmological evolution of the Universe. The scalar field in Figure 2(d) evolves accordingly, approaching a constant at $z = 0$ (blue curve and red curve) which represents a de Sitter Universe [46].

Furthermore, as we can see from Figure 2(a) that $q(0) = -0.8$ or -0.7 is consistent with supernova observations that reveal $q(0) = -0.1 \pm 0.4$ [50].

5. Conclusions

In the present study, we have taken the advantage of the first-order formalism in the Horndeski cosmology. This formalism applied to Horndeski gravity as well as to $f(R)$ and $f(R, T)$ theories [47, 48] is concerned in reducing the equations of motion to first-order equations, which simplifies the solution of the problem from both analytical and numerical perspectives. Besides, the first-order formalism plays an important role in RG flow in holographic cosmology [37–40]. Our numerical solutions showed a good agreement with the current phase of the Universe, where the Hubble parameter as a function of the redshift has a behavior similar to the one found in [49]. By using first-order formalism supported by a constrained superpotential in the Horndeski gravity for the FRW background, we have shown by using numerical methods that late-time cosmology is well described by the scalar field. The solutions correspond to an accelerating Universe for small redshifts, which is in agreement with the current observational data that is usually associated with a phenomenon driven by a dark energy fluid. The scalar field nonminimally coupled to the gravity sector produces kink-type solutions which render a de Sitter Universe at late-time cosmology, reproducing a dark energy scenario in Horndeski gravity at first-order formalism.

Data Availability

The data used to support the findings of this study are available from the corresponding author upon request.

Conflicts of Interest

The authors declare that they have no conflicts of interest.

Acknowledgments

We would like to thank CNPq, CAPES, and CNPq/PRONEX, for partial financial support. FAB acknowledges support from CNPq (Grant no. 312104/2018-9). We also thank M. Rinaldi for useful discussions in the early stages of this work.

References

[1] G. Papallo, *Causality and the Initial Value Problem in Modified Gravity*, University of Cambridge, 2019.

[2] B. P. Abbott, R. Abbott, T. D. Abbott et al., "Observation of gravitational waves from a binary black hole merger," *Physical Review Letters*, vol. 116, no. 6, p. 061102, 2016.

[3] M. Zumalacárregui and J. García-Bellido, "Transforming gravity: from derivative couplings to matter to second-order scalar-tensor theories beyond the Horndeski Lagrangian," *Physical Review D*, vol. 89, no. 6, p. 064046, 2014.

[4] A. Cisterna, M. Hassaine, J. Oliva, and M. Rinaldi, "Axionic black branes in the k-essence sector of the Horndeski model," *Physical Review D*, vol. 96, no. 12, p. 124033, 2017.

[5] L. Heisenberg, "A systematic approach to generalisations of general relativity and their cosmological implications," *Physics Reports*, vol. 796, no. 1, pp. 1–113, 2019.

[6] A. D. Dolgov and M. Kawasaki, "Realistic cosmological model with dynamical cancellation of vacuum energy," 2003, *arXiv preprint astro-ph/0307442*.

[7] S. Mukohyama and L. Randall, "Dynamical approach to the cosmological constant," *Physical Review Letters*, vol. 92, no. 21, p. 211302, 2004.

[8] S. I. Nojiri and S. D. Odintsov, "Gravity assisted dark energy dominance and cosmic acceleration," *Physics Letters B*, vol. 599, no. 3-4, pp. 137–142, 2004.

[9] G. Allemandi, A. Borowiec, M. Francaviglia, and S. D. Odintsov, "Dark energy dominance and cosmic acceleration in first-order formalism," *Physical Review D*, vol. 72, no. 6, p. 063505, 2005.

[10] F. A. Brito, F. F. Cruz, and J. F. N. Oliveira, "Accelerating universes driven by bulk particles," *Physical Review D*, vol. 71, no. 8, article 083516, 2005.

[11] D. Bazeia, F. A. Brito, and F. G. Costa, "First-order framework and domain-wall/brane-cosmology correspondence," *Physics Letters B*, vol. 661, no. 2-3, pp. 179–185, 2008.

[12] M. A. Santos, M. Benetti, J. S. Alcaniz, F. A. Brito, and R. Silva, "CMB constraints on β-exponential inflationary models," *Journal of Cosmology and Astroparticle Physics*, vol. 2018, no. 03, p. 023, 2018.

[13] F. A. Brito and F. F. Santos, "Black branes in asymptotically Lifshitz spacetime and viscosity/entropy ratios in Horndeski gravity," 2019, arXiv preprint arXiv:1901.06770.

[14] A. Nicolis, R. Rattazzi, and E. Trincherini, "Galileon as a local modification of gravity," *Physical Review D*, vol. 79, no. 6, p. 064036, 2009.

[15] G. W. Horndeski, "Second-order scalar-tensor field equations in a four-dimensional space," *International Journal of Theoretical Physics*, vol. 10, no. 6, pp. 363–384, 1974.

[16] A. Cisterna and C. Erices, "Asymptotically locally AdS and flat black holes in the presence of an electric field in the Horndeski scenario," *Physical Review D*, vol. 89, no. 8, p. 084038, 2014.

[17] F. A. Brito and F. F. Dos Santos, "Braneworlds in Horndeski gravity," 2018, arXiv preprint arXiv:1810.08196.

[18] A. Anabalon, A. Cisterna, and J. Oliva, "Asymptotically locally AdS and flat black holes in Horndeski theory," *Physical Review D*, vol. 89, no. 8, p. 084050, 2014.

[19] K. Van Acoleyen and J. Van Doorsselaere, "Galileons from lovelock actions," *Physical Review D*, vol. 83, no. 8, p. 084025, 2011.

[20] C. Deffayet, X. Gao, D. A. Steer, and G. Zahariade, "From k-essence to generalized Galileons," *Physical Review D*, vol. 84, no. 6, p. 064039, 2011.

[21] A. R. Gomes and L. Amendola, "The general form of the coupled Horndeski Lagrangian that allows cosmological scaling solutions," *Journal of Cosmology and Astroparticle Physics*, vol. 2016, no. 02, article 035, 2016.

[22] M. Rinaldi, "Mimicking dark matter in Horndeski gravity," *Physics of the Dark Universe*, vol. 16, no. 14, pp. 14–21, 2017.

[23] J. Gleyzes, D. Langlois, F. Piazza, and F. Vernizzi, "Essential building blocks of dark energy," *Journal of Cosmology and Astroparticle Physics*, vol. 2013, no. 08, article 025, 2013.

[24] S. Bhattacharya and S. Chakraborty, "Constraining some Horndeski gravity theories," *Physical Review D*, vol. 95, no. 4, p. 044037, 2017.

[25] S. Mukherjee and S. Chakraborty, "Horndeski theories confront the Gravity Probe B experiment," *Physical Review D*, vol. 97, no. 12, p. 124007, 2018.

[26] Y. Brihaye, A. Cisterna, and C. Erices, "Boson stars in biscalar extensions of Horndeski gravity," *Physical Review D*, vol. 93, no. 12, p. 124057, 2016.

[27] A. Cisterna, T. Delsate, L. Ducobu, and M. Rinaldi, "Slowly rotating neutron stars in the nonminimal derivative coupling sector of Horndeski gravity," *Physical Review D*, vol. 93, no. 8, p. 084046, 2016.

[28] E. Babichev, C. Charmousis, D. Langlois, and R. Saito, "Beyond Fab Four," *Classical and Quantum Gravity*, vol. 32, no. 24, p. 242001, 2015.

[29] C. Charmousis, E. J. Copeland, A. Padilla, and P. M. Saffin, "Self-tuning and the derivation of a class of scalar-tensor theories," *Phys. Rev. D*, vol. 85, no. 10, p. 104040, 2012.

[30] C. Charmousis, E. J. Copeland, A. Padilla, and P. M. Saffin, "General second-order scalar-tensor theory and self-tuning," *Physical Review Letters*, vol. 108, no. 5, p. 051101, 2012.

[31] E. Babichev and G. Esposito-Farese, "Cosmological self-tuning and local solutions in generalized Horndeski theories," *Physical Review D*, vol. 95, no. 2, p. 024020, 2017.

[32] P. Martin-Moruno, N. J. Nunes, and F. S. N. Lobo, "Horndeski theories self-tuning to a de Sitter vacuum," *Physical Review D*, vol. 91, no. 8, p. 084029, 2015.

[33] P. Martin-Moruno and N. J. Nunes, "Accelerating universe as a result of an adjustment mechanism," *International Journal of Modern Physics D*, vol. 24, no. 12, p. 1544018, 2015.

[34] P. Martín-Moruno, N. J. Nunes, and F. S. N. Lobo, "Attracted to de Sitter: cosmology of the linear Horndeski models," *Journal of Cosmology and Astroparticle Physics*, vol. 2015, no. 05, p. 033, 2015.

[35] P. Martin-Moruno and N. J. Nunes, "Attracted to de Sitter II: cosmology of the shift-symmetric Horndeski models," *Journal of Cosmology and Astroparticle Physics*, vol. 2015, no. 09, p. 056, 2015.

[36] C. Deffayet, O. Pujolas, I. Sawicki, and A. Vikman, "Imperfect dark energy from kinetic gravity braiding," *Journal of Cosmology and Astroparticle Physics*, vol. 2010, no. 10, p. 026, 2010.

[37] P. McFadden and K. Skenderis, "Holography for cosmology," *Physical Review D*, vol. 81, no. 2, p. 021301, 2010.

[38] D. Baumann, D. Green, and T. Hartman, "Dynamical constraints on RG flows and cosmology," 2019, arXiv preprint arXiv:1906.10226.

[39] E. Kiritsis and A. Tsouros, "de Sitter versus anti de Sitter flows and the (super)gravity landscape," 2019, arXiv preprint arXiv:1901.04546.

[40] E. Kiritsis, "Asymptotic freedom, asymptotic flatness and cosmology," *Journal of Cosmology and Astroparticle Physics*, vol. 2013, no. 11, article 011, 2013.

[41] M. A. Skugoreva, S. V. Sushkov, and A. V. Toporensky, "Publisher's note: cosmology with nonminimal kinetic coupling and a power-law potential [Phys. Rev. D88, 083539 (2013)]," *Physical Review D*, vol. 88, no. 10, 2013.

[42] A. Casalino and M. Rinaldi, "Testing Horndeski gravity as dark matter with hi_class," *Physics of the Dark Universe*, vol. 23, no. 100243, p. 100243, 2019.

[43] X. H. Feng, H. S. Liu, H. Lü, and C. N. Pope, "Black hole entropy and viscosity bound in Horndeski gravity," *Journal of High Energy Physics*, vol. 2015, no. 11, article 2590, 2015.

[44] D. Bazeia, C. B. Gomes, L. Losano, and R. Menezes, "First-order formalism and dark energy," *Physics Letters B*, vol. 633, no. 4-5, pp. 415–419, 2006.

[45] D. Bazeia, L. Losano, J. J. Rodrigues, and R. Rosenfeld, "First-order formalism for dark energy and dust," *European Physical Journal C: Particles and Fields*, vol. 55, no. 1, pp. 113–117, 2008.

[46] T. Harko, F. S. N. Lobo, E. N. Saridakis, and M. Tsoukalas, "Cosmological models in modified gravity theories with

extended nonminimal derivative couplings," *Physical Review D*, vol. 95, no. 4, p. 044019, 2017.

[47] V. I. Afonso, D. Bazeia, R. Menezes, and A. Y. Petrov, "f(R)-Brane," *Physics Letters B*, vol. 658, no. 1-3, pp. 71–76, 2007.

[48] P. H. R. S. Moraes and J. R. L. Santos, "A complete cosmological scenario from $f(R,T^{\phi})$ gravity theory," *The European Physical Journal C*, vol. 76, no. 2, 2016.

[49] N. Aghanim, Y. Akrami, M. Ashdown et al., "Planck 2018 results. VI. Cosmological parameters," 2018, arXiv preprint arXiv:1807.06209.

[50] A. G. Riess, A. V. Filippenko, P. Challis et al., "Observational evidence from supernovae for an accelerating universe and a cosmological constant," *The Astronomical Journal*, vol. 116, no. 3, pp. 1009–1038, 1998.

Hindawi
Advances in High Energy Physics
Volume 2019, Article ID 5864042, 7 pages
https://doi.org/10.1155/2019/5864042

Research Article

Modified Fermions Tunneling Radiation from Nonstationary, Axially Symmetric Kerr Black Hole

Jin Pu,[1,2] **Kai Lin**,[3] **Xiao-Tao Zu**,[1] **and Shu-Zheng Yang**[2]

[1]*School of Physics, University of Electronic Science and Technology of China, Chengdu 610054, Sichuan, China*
[2]*College of Physics and Space Science, China West Normal University, Nanchong 637002, Sichuan, China*
[3]*Hubei Subsurface Multi-Scale Imaging Key Laboratory, Institute of Geophysics and Geomatics, China University of Geosciences, Wuhan 430074, Hubei, China*

Correspondence should be addressed to Shu-Zheng Yang; szyangphys@126.com

Received 4 June 2019; Accepted 14 July 2019; Published 22 July 2019

Guest Editor: Saibal Ray

In this paper, by applying the deformed dispersion relation in quantum gravity theory, we study the correction of fermions' tunneling radiation from nonstationary symmetric black holes. Firstly, the motion equation of fermions is modified in the gravitational space-time. Based on the motion equation, the modified Hamilton-Jacobi equation has been obtained by a semiclassical approximation method. Then, the tunneling behavior of fermions at the event horizon of nonstationary symmetric Kerr black hole is investigated. Finally, the results show that, in the nonstationary symmetric background, the correction of Hawking temperature and the tunneling rate are closely related to the angular parameters of the horizon of the black hole background.

1. Introduction

Since Hawking proposed that black holes can radiate thermally like a black body in 1974 [1, 2], a series of studies have been carried out on static, stationary, and nonstationary black holes. Actually, Hawking thermal radiation is a pure thermal radiation, and the radiation spectrum formed by this radiation is a pure thermal radiation spectrum, which leads to the problem of the information loss of black holes. In order to explain the information loss paradox of black holes, Robinson, Wilczek, Kraus, and Parikh have modified Hawking pure thermal radiation spectrum and found that the information was conserved during Hawking tunneling radiation from static and stationary black holes, by considering the self-gravitational interaction and the change of curved space-time background [3–8]. Subsequently, there are a series of studies on the massive particles and fermions via tunneling radiation from black holes [9–56]. However, the actual existence of black holes in the universe should be nonstationary, so the issues, such as the thermodynamic properties and the information conservation of nonstationary black holes, and merging process of black holes, deserve to be studied in depth.

On the other hand, quantum gravity theory suggests that Lorentz symmetry may be modified at high energy. Although the dispersion relation theory at high energy has not yet been fully established, it is generally accepted that the scale of this correction term is equal to or close to the Planck scale. We have studied fermions' quantum tunneling radiation from stationary black holes by using the deformed dispersion relation and obtained the very interesting results that there was a correction in the tunneling radiation behavior [57]. However, the correction is only obtained for fermions' tunneling radiation at the event horizon of stationary black holes. Therefore, we generalize the modified dispersion relation to study the quantum tunneling radiation of nonstationary symmetric Kerr black holes in this paper and give an effective correction of thermodynamic characteristics of the black holes.

The remainder of this paper is outlined as follows. In Section 2, by applying the modified dispersion relation in quantum gravity theory, we construct new Rarita-Schwinger equation and obtain the modified Hamilton-Jacobi equation of fermions by using semiclassical approximation method. In Section 3, the quantum tunneling radiation of fermions from nonstationary symmetric Kerr black hole is modified

correctly, and the tunneling rate and Hawking temperature are modified. Section 4 ends up with some discussions and conclusions.

2. The Modified Hamilton-Jacobi Equation

Kerner and Mann studied the quantum tunneling radiation of the Dirac field using a semiclassical method [20, 21]. Subsequently, this method was extended to study quantum tunneling radiation in various black holes. Since the kinematic equation of fermions is the Dirac equation but the Dirac equation is related to the matrix equation, so a new method is proposed in the literature [22–25] to study the tunneling radiation of Dirac particles in curved space-time of static and stationary black holes. This method is that the Dirac equation is transformed into a simple matrix equation, and then this matrix equation is converted into the Hamilton-Jacobi equation in the curved space-time by applying the relationship between the gamma matrix and the space-time metric. After this Hamilton-Jacobi equation was proposed in 2009, it not only promoted the study of quantum tunneling radiation of dynamic black holes, but also effectively simplified the research work on quantum tunneling radiation of fermions. Recently, this Hamilton-Jacobi equation, combined with the modified Lorentz dispersion relation, has been generalized to effectively revise the quantum tunneling radiation of fermions from the event horizon of stationary axisymmetric Kerr-Newman de Sitter black hole and has obtained very meaningful results [57]. However, it only modifies the quantum tunneling radiation of fermions from the stationary black hole, while the real black holes existing in the universe are nonstationary, so the quantum tunneling radiation of fermions from the event horizon of the dynamic Kerr black hole is modified in this paper by considering the correction of dispersion relation.

The Lorentz dispersion relation is considered to be one of the basic relations in modern physics and related to the correlative theory research of general relativity and quantum field theory. Research on the quantum gravity theory has shown that the Lorentz relationship may be modified in the high energy field. In the study of string theory and quantum gravity theory, a dispersion relation has been proposed [58–66]:

$$P_0^2 = \overrightarrow{P}^2 + m^2 - \left(LP_0\right)^{\alpha} \overrightarrow{P}^2. \tag{1}$$

In the natural units, P_0 and P denote the energy and momentum of particles, respectively. m is the rest mass of particles and L is a constant of the Planck scale. $\alpha = 1$ is used in the Liouville-string model [62–64]. Kruglov got the modified Dirac equation in the case of $\alpha = 2$ [67]. The more general motion equation of fermions was proposed by Rarita and Schwinger and called the Rarita-Schwinger equation [68]. According to (1), we select $\alpha = 2$, so the Rarita-Schwinger equation in flat space-time is given by

$$\left(\overline{\gamma}^{\mu}\partial_{\mu} + \frac{m}{\hbar} - \sigma\hbar\overline{\gamma}^{t}\partial_{t}\overline{\gamma}^{j}\partial_{j}\right)\psi_{\alpha_1\cdots\alpha_k} = 0, \tag{2}$$

where $\overline{\gamma}^{\mu}$ is the gamma matrix in flat space-time; j and μ denote space and time coordinates, respectively. According to the relationship between the covariant derivative of the curved space-time and the derivative of the flat space-time, the Rarita-Schwinger equation in the curved space-time of nonstationary symmetric Kerr black hole can be expressed as

$$\left(\gamma^{\mu}D_{\mu} + \frac{m}{\hbar} - \sigma\hbar\gamma^{\mathrm{v}}D_{\mathrm{v}}\gamma^{j}D_{j}\right)\psi_{\alpha_1\cdots\alpha_k} = 0, \tag{3}$$

where γ^{μ} is the gamma matrix in the curved space-time, and v denotes the advanced Eddington coordinate. In (3), when $k = 0$, we have $\phi_{\alpha_1\wedge\alpha_k} = \phi$, in which case (3) represents the Dirac equation of a spin of 1/2; when $k = 1$, (3) describes the motion equation of the fermions with the spin of 3/2. However, when $m = 0$, the fermions with the spin of 3/2 describe the Gravitino particle in the supersymmetry and supergravity theory, which are a kind of fermions associated with the graviton, and the study on such particles is likely to promote the development of quantum gravity theory.

It is worth noting that (3) satisfies the following conditions:

$$\gamma^{\mu}\gamma^{\nu} + \gamma^{\nu}\gamma^{\mu} = 2g^{\mu\nu}I, \tag{4}$$

$$\gamma^{\mu}\psi_{\mu\alpha_2\cdots\alpha_k} = D_{\mu}\psi^{\mu}_{\alpha_2\cdots\alpha_k} = \psi^{\mu}_{\mu\alpha_3\cdots\alpha_k}, \tag{5}$$

where I is the unit matrix. In (3), D_{μ} is defined as

$$D_{\mu} \equiv \partial_{\mu} + \Omega_{\mu}, \tag{6}$$

where Ω_{μ} is the spin connection. In (3), coupling constant $\sigma \ll 1$, and $\sigma\hbar\gamma^{\mathrm{v}}D_{\mathrm{v}}\gamma^{j}D_{j}$ is very small quantity.

In order to study the tunneling radiation of fermions in nonstationary curved space-time, S is used to represent the action function of particles, and the wave function of fermions is written as

$$\psi_{\alpha_1\cdots\alpha_k} = \xi_{\alpha_1\cdots\alpha_k}e^{(i/\hbar)S}. \tag{7}$$

For nonstationary and axisymmetric curved space-time, there must be

$$\partial_{\varphi}S = n, \tag{8}$$

where n is the angular momentum parameter of particles' tunneling radiation and a constant for nonstationary axisymmetric black holes. Substituting (6), (7), and (8) into (3), $\hbar$ is considered as a small quantity, and the lowest order is retained, so we obtain

$$i\gamma^{\mu}\partial_{\mu}S\xi_{\alpha_1\cdots\alpha_k} + m\xi_{\alpha_1\cdots\alpha_k} + \sigma\partial_{\mathrm{v}}S\gamma^{\mathrm{v}}\gamma^{j}\partial_{j}S\xi_{\alpha_1\cdots\alpha_k} = 0. \tag{9}$$

Because of $\gamma^{\mu}\partial_{\mu}S = \gamma^{\mathrm{v}}\partial_{\mathrm{v}}S + \gamma^{j}\partial_{j}S$, (9) is abbreviated to

$$\Gamma^{\mu}\partial_{\mu}S\xi_{\alpha_1\cdots\alpha_k} + M_D\xi_{\alpha_1\cdots\alpha_k} = 0, \tag{10}$$

where

$$\begin{aligned}\Gamma^{\mu} &= \gamma^{\mu} - i\sigma\partial_{\mathrm{v}}S\gamma^{\mathrm{v}}\gamma^{\mu},\\ M_D &= m - \sigma\left(\partial_{\mathrm{v}}S\right)^2 g^{\mathrm{vv}}.\end{aligned} \tag{11}$$

We use premultiplication $\Gamma^{\nu}\partial_{\nu}S$ to (10) and get

$$\Gamma^{\nu}\partial_{\nu}S\Gamma^{\mu}\partial_{\mu}S\xi_{\alpha_1\cdots\alpha_k} + M_D\Gamma^{\nu}\partial_{\nu}S\xi_{\alpha_1\cdots\alpha_k} = 0, \tag{12}$$

where

$$\Gamma^{\nu}\Gamma^{\mu} = \gamma^{\nu}\gamma^{\mu} - 2i\sigma\partial_{\beta}S\gamma^{\beta}\gamma^{\nu}\gamma^{\mu} + \mathcal{O}\left(\sigma^2\right). \tag{13}$$

Now, after exchanging μ and ν in (12) and comparing them with (12), we get

$$\begin{aligned}&\left[\frac{\gamma^{\mu}\gamma^{\nu}+\gamma^{\nu}\gamma^{\mu}}{2}\partial_{\mu}S\partial_{\nu}S+m^{2}-2\sigma mg^{\nu\nu}\left(\partial_{\nu}S\right)^{2}\right.\\&\left.-2i\sigma\partial_{\nu}Sg^{\nu\beta}\partial_{\beta}S\gamma^{\mu}\partial_{\mu}S\right]\xi_{\alpha_{1}\cdots\alpha_{k}}+\mathcal{O}\left(\sigma^{2}\right)\\&=\left[g^{\mu\nu}\partial_{\mu}S\partial_{\nu}S+m^{2}-2\sigma mg^{\nu\nu}\left(\partial_{\nu}S\right)^{2}\right.\\&\left.-2i\sigma\partial_{\nu}Sg^{\nu\beta}\partial_{\beta}S\gamma^{\mu}\partial_{\mu}S\right]\xi_{\alpha_{1}\cdots\alpha_{k}}+\mathcal{O}\left(\sigma^{2}\right)=0.\end{aligned}\tag{14}$$

Eq. (14) is further simplified to

$$i\sigma\gamma^{\mu}\partial_{\mu}S\xi_{\alpha_{1}\cdots\alpha_{k}}+M_{\xi}\xi_{\alpha_{1}\cdots\alpha_{k}}=0,\tag{15}$$

where

$$M_{\xi}=\frac{g^{\mu\nu}\partial_{\mu}S\partial_{\nu}S+m^{2}-2\sigma mg^{\nu\nu}\left(\partial_{\nu}S\right)^{2}}{2\partial_{\nu}Sg^{\nu\beta}\partial_{\beta}S}.\tag{16}$$

We use premultiplication $-i\sigma\gamma^{\mu}\partial_{\mu}S$ for (15) and exchange μ and ν. Then, we add it to (15) and divide that by 2, so we get

$$\left[\sigma^{2}g^{\mu\nu}\partial_{\mu}S\partial_{\nu}S+M_{\xi}^{2}\right]\xi_{\alpha_{1}\cdots\alpha_{k}}=0.\tag{17}$$

This is a matrix equation, actually an eigenmatrix equation. The condition that the equation has a nontrivial solution is that the value of the determinant corresponding to its matrix is 0; that is,

$$\sigma^{2}g^{\mu\nu}\partial_{\mu}S\partial_{\nu}S+M_{\xi}^{2}=0.\tag{18}$$

Ignoring $\mathcal{O}(\sigma^{2})$, the modified Hamilton-Jacobi equation can be obtained from the above equation as

$$g^{\mu\nu}\partial_{\mu}S\partial_{\nu}S+m^{2}-2\sigma mg^{\nu\nu}\left(\partial_{\nu}S\right)^{2}=0.\tag{19}$$

Obviously, modified Hamilton-Jacobi equation (19) is entirely different from the previously well-known Hamilton-Jacobi equation, with the addition of the modified term $2\sigma mg^{\nu\nu}(\partial_{\nu}S)^{2}$. Equation (19), derived from the modified Rarita-Schwinger equation, is not affected by the specific spin and can describe the motion equation of any fermions in the semiclassical approximation method. For any fermions in nonstationary curved space-time, it is convenient to study and modify characteristics of quantum tunneling radiation of fermions as long as the properties of the curved space-time and the action S of fermions are known.

3. Fermions' Tunneling Radiation in Nonstationary Symmetric Kerr Black Hole

In the advanced Eddington coordinate, the line element of nonstationary symmetric Kerr black hole is expressed as

$$\begin{aligned}ds^{2}=&-\left(1-\frac{2Mr}{\rho^{2}}\right)dr^{2}+2d\nu dr\\&-2\frac{2Mra\sin^{2}\theta}{\rho^{2}}d\nu d\varphi-2a\sin^{2}\theta drd\varphi+\rho^{2}d\theta^{2}\\&+\left[\left(r^{2}+a^{2}\right)+\frac{2Mra^{2}\sin^{2}\theta}{\rho^{2}}\right]\sin^{2}\theta d\varphi^{2},\end{aligned}\tag{20}$$

where $\rho^{2}=r^{2}+a^{2}\cos^{2}\theta$, $M=M(\nu)$, $a=a(\nu)$. According to (20), the inverse tensors metric of the black hole is

$$g^{\mu\nu}=\begin{pmatrix}g^{00}&g^{01}&0&g^{03}\\g^{10}&g^{11}&0&g^{13}\\0&0&g^{22}&0\\g^{30}&g^{31}&0&g^{33}\end{pmatrix},\tag{21}$$

where

$$\begin{aligned}g^{00}&=\frac{a^{2}\sin^{2}\theta}{\rho^{2}},\\g^{01}&=g^{10}=\frac{r^{2}+a^{2}}{\rho^{2}},\\g^{03}&=g^{30}=\frac{a}{\rho^{2}},\\g^{13}&=g^{31}=\frac{a}{\rho^{2}},\\g^{11}&=\frac{\Delta}{\rho^{2}},\\g^{22}&=\frac{1}{\rho^{2}},\\g^{33}&=\frac{1}{\rho^{2}\sin^{2}\theta},\\\Delta&=r^{2}+q^{2}-2Mr.\end{aligned}\tag{22}$$

According to (20), the null hypersurface equation of the black hole is given by

$$g^{\mu\nu}\frac{\partial f}{\partial x^{\mu}}\frac{\partial f}{\partial x^{\nu}}=0,\tag{23}$$

Substituting (22) into (23), the equation at the event horizon of the black hole is expressed as

$$\begin{aligned}&a^{2}r_{H}^{2}\sin^{2}\theta+r_{H}^{2}-2mr_{H}+a^{2}+r_{H}^{\prime2}-2\left(r_{H}^{2}+a^{2}\right)\dot{r}_{H}\\&\quad=0,\end{aligned}\tag{24}$$

From (24), we have

$$\begin{aligned}&r_{H}\\&=\frac{M+\left[m^{2}-\left(1-2\dot{r}_{H}\right)\left(a^{2}+a^{2}\dot{r}_{H}\sin^{2}\theta+r_{H}^{\prime2}-2a^{2}\dot{r}_{H}\right)\right]^{1/2}}{1-2\dot{r}_{H}}.\end{aligned}\tag{25}$$

Obviously, the event horizon of the black hole r_{H} is associated with $a(\nu)$, $M(\nu)$, $\partial_{\nu}r|_{r=r_{H}}=\dot{r}_{H}$, and $\partial_{\theta}r|_{r=r_{H}}=r_{H}^{\prime}$. Once we know the characteristics of the event horizon of the black

hole, we can study the quantum tunneling radiation at the event horizon.

The motion equation of fermions is given by matrix equation (3). From the above research, we can conclude that the motion equation of any half-integer fermions can be reduced to (19), and (19) is the modified Hamilton-Jacobi equation, where S is the main function of Hamilton, also known as the action of fermions. Substituting (22) and (8) into (19), the motion equation of the half-integer fermions in space-time of the black hole is obtained:

$$\begin{aligned} &g^{00}\left(\frac{\partial S}{\partial \mathsf{v}}\right)^2 + 2\frac{\partial S}{\partial \mathsf{v}}\frac{\partial S}{\partial r} + 2g^{03}n\frac{\partial S}{\partial \mathsf{v}} + 2g^{13}n\frac{\partial S}{\partial r} \\ &\quad + g^{11}\left(\frac{\partial S}{\partial r}\right)^2 + g^{22}\left(\frac{\partial S}{\partial \theta}\right)^2 + g^{33}n^2 + m^2 \\ &\quad - 2\sigma m g^{00}\left(\frac{\partial S}{\partial \mathsf{v}}\right)^2 = 0. \end{aligned} \tag{26}$$

Since the space-time of the black hole is axially symmetric, n is a constant according to $n = \partial S/\partial\varphi$. Equation (26) is the motion equation of fermions in nonstationary Kerr black hole. Actually, (26) is a modified Hamilton-Jacobi equation in the nonstationary curved space-time, where $S = S(\mathsf{v}, r, \theta)$. In order to solve the equation, we need to use the general tortoise coordinate transformation as follows:

$$\begin{aligned} r_\star &= r + \frac{1}{2\kappa}\left[r - r_H\left(\mathsf{v}_0, \theta_0\right)\right], \\ \mathsf{v}_\star &= \mathsf{v} - \mathsf{v}_0, \\ \theta_\star &= \theta - \theta_0. \end{aligned} \tag{27}$$

According to (27), we have

$$\begin{aligned} \frac{\partial}{\partial r} &= \frac{2\kappa\left(r - r_H\right) + r_H}{2\kappa\left(r - r_H\right)}\frac{\partial}{\partial r_\star}, \\ \frac{\partial}{\partial \theta} &= \frac{\partial}{\partial \theta_\star} - \frac{r_H' r_H}{2\kappa\left(r - r_H\right)}\frac{\partial}{\partial r_\star}, \\ \frac{\partial}{\partial \mathsf{v}} &= \frac{\partial}{\partial \mathsf{v}_\star} - \frac{\dot{r}_H r_H}{2\kappa\left(r - r_H\right)}\frac{\partial}{\partial r_\star}. \end{aligned} \tag{28}$$

Substituting (27) and (28) into (26) and noticing

$$\begin{aligned} S &= S\left(\mathsf{v}_\star, r_\star, \theta_\star\right), \\ \frac{\partial S}{\partial \mathsf{v}_\star} &= -\omega, \\ \frac{\partial S}{\partial \theta_\star} &= p_\theta, \end{aligned} \tag{29}$$

where ω denotes the energy of fermions' tunneling radiation, p_θ is θ component of the generalized momentum of fermions, σ is a small quantity, and $\sigma\dot{r}^2$ is also a small quantity, the equation at the horizon of the black hole can be written as

$$\begin{aligned} &\frac{A}{D}\left(\frac{\partial S}{\partial r_\star}\right)^2 + 2\frac{\partial S}{\partial \mathsf{v}_\star}\frac{\partial S}{\partial r_\star} + \frac{B}{D}\frac{\partial}{\partial r_\star} + 2\kappa\left(r - r_H\right)\frac{C}{D} \\ &\quad = 0 \end{aligned} \tag{30}$$

where

$$\begin{aligned} A &= \frac{1}{2\kappa\left(r - r_H\right)}\left\{g^{00}\dot{r}_H + 2\dot{r}_H\left[2\kappa\left(r - r_H\right) + 1\right]\right. \\ &\quad + g^{11}\left[2\kappa\left(r - r_H\right) + 1\right]^2 + g^{11}\left[2\kappa\left(r - r_H\right) + 1\right]^2 \\ &\quad \left. + g^{22}r_H'^2\right\}, \\ B &= g^{22}p_\theta r_H' - g^{13}n - g^{03}n\dot{r}_H, \\ C &= g^{00}\omega^2 + g^{22}p_\theta^2 + g^{33}n + m^2 - 2\sigma m g^{00}\omega^2, \\ D &= g^{00}\dot{r}_H - g^{01} + 2\sigma m g^{00}\dot{r}_H. \end{aligned} \tag{31}$$

When $r \longrightarrow r_H$, we have

$$A\left(\frac{\partial S}{\partial r_\star}\right)^2 + 2\left(\omega - \omega_0\right)\frac{\partial S}{\partial r_\star} = 0, \tag{32}$$

where

$$A|_{r\longrightarrow r_H} = \lim_{\substack{r\longrightarrow r_H \\ \mathsf{v}\longrightarrow \mathsf{v}_0 \\ \theta\longrightarrow\theta_0}} \frac{g^{00}\dot{r}_H^2 - 2g^{01}\dot{r}_H\left[2\kappa\left(r - r_H\right) + 1\right] + g^{11}\left[2\kappa\left(r - r_H\right) + 1\right]^2 + g^{22}r_H'^2}{2\kappa\left(r - r_H\right)\left(g^{00}\dot{r}_H - g^{01} + 2\sigma m g^{00}\dot{r}_H\right)} = 1. \tag{33}$$

From $A|_{r\longrightarrow r_H} = 1$, we get

$$\begin{aligned} \omega_0\big|_{r\longrightarrow r_H} &= \frac{g^{03}n\dot{r}_H + g^{22}p_\theta\dot{r}_H - g^{13}n}{g^{00}\dot{r}_H - g^{01} + 2\sigma m g^{00}\dot{r}_H} \\ &= \frac{an\dot{r}_H + p_\theta\dot{r}_H - an}{a^2\sin^2\theta\dot{r}_H - r_H^2 - a^2 + 2\sigma m\dot{r}_H a^2\sin^2\theta} \\ &= \frac{an\dot{r}_H + p_\theta\dot{r}_H - an}{a^2\sin^2\theta\dot{r}_H - r_H^2 - a^2}\left(1 \right. \\ &\quad \left. - \frac{2\sigma m\dot{r}_H a^2\sin^2\theta}{a^2\sin^2\theta\dot{r}_H - r_H^2 - a^2} + \mathcal{O}\left(\sigma^2\right)\right). \end{aligned} \tag{34}$$

So the event horizon surface gravity is given by

$$\kappa = \frac{\left(1-2\dot{r}_H\right) r_H - M}{a^2 \sin^2\theta_0 \dot{r}_H \left(1+2\sigma m\right) - \left(r_H^2 + a^2\right)\left(1-2\dot{r}_H\right) + 4Mr_H - \left(r_H^2 + a^2\right)} = \frac{\left(1-2\dot{r}_H\right) r_H - M}{a^2 \sin^2\theta_0 \dot{r}_H \left(1+2\sigma m\right) - \left(r_H^2 + a^2\right)\left(1-2\dot{r}_H\right) + 4Mr_H} \tag{35}$$

We notice $r_H^2(1-2\dot{r}_H) - 2Mr_H + a^2(1-2\dot{r}_H + \dot{r}_H^2 \sin^2\theta_0) + r_H'^2 = 0$ and get

$$\begin{aligned}\kappa &= \frac{\left(1-2\dot{r}_H\right) r_H - M}{2Mr_H - \left(1-\dot{r}_H\right)\dot{r}_H a^2 \sin^2\theta_0 + r_H'^2 + 2\sigma m a^2 \sin^2\theta_0} \\ &= \frac{\left(1-2\dot{r}_H\right) r_H - M}{\left(1-2\dot{r}_H\right)\left[r_H^2 + a^2\left(1-\dot{r}_H \sin^2\theta_0\right)\right] + r_H'^2 + 2\sigma m a^2 \sin^2\theta_0} \\ &= \frac{\left(1-2\dot{r}_H\right) r_H - M}{\left(1-2\dot{r}_H\right)\left[r_H^2 + a^2\left(1-\dot{r}_H \sin^2\theta_0\right)\right] + r_H'^2} \times \left\{1 \right. \\ &\quad \left. - \frac{2\sigma m a^2 \sin^2\theta_0}{\left(1-2\dot{r}_H\right)\left[r_H^2 + a^2\left(1-\dot{r}_H \sin^2\theta_0\right)\right] + r_H'^2} + \mathcal{O}\left(\sigma^2\right)\right\}\end{aligned} \tag{36}$$

Obviously, the event horizon surface gravity is modified, and the modified term depends on θ_0. It means that the correction is made in different angle directions. Due to $\partial S/\partial r = [1 + 1/2\kappa(r - r_H)](\partial S/\partial r_*)$, we have

$$S = \frac{i\pi}{2\kappa}\left[\left(\omega - \omega_0\right) \pm \left(\omega - \omega_0\right)\right]. \tag{37}$$

Thus, the imaginary part of the total action and the quantum tunneling rate, respectively, are

$$ImS_+ - ImS_- = \frac{i\pi}{2\kappa}\left[\left(\omega - \omega_0\right) \pm \left(\omega - \omega_0\right)\right], \tag{38}$$

$$\Gamma = \frac{\Gamma_{emission}}{\Gamma_{absption}} = \exp\left[\frac{2\pi}{\kappa}\left(\omega - \omega_0\right)\right] \tag{39}$$

Here, as shown in (36), it is clear that κ mentioned above is the event horizon surface gravity of the black hole. So, the event horizon temperature of the black hole is given by

$$T|_{r=r_H} = \frac{\kappa}{2\pi}. \tag{40}$$

It is worth noting that the temperature (40) is the modified Hawking temperature, since κ in (40) is the modified surface gravity related to the correction term $2\sigma m a^2 \sin^2\theta_0$. Obviously, the correction of tunneling rate, surface gravity, and Hawking temperature at the event horizon of the black hole are related not only to the rates of the event horizon change $\dot{r}_H$, r_H', and $M(\mathrm{v})$ of the black hole, but also to the correction of the angle parameter θ_0.

4. Discussion

In this paper, we study the quantum tunneling radiation of fermions in nonstationary curved space-time by combining the modified Lorentz dispersion relation and obtain the modified character of quantum tunneling radiation related to the effects of the Planck scale. The modified Dirac equation proposed by Kruglov is first extended to the modified Rarita-Schwinger equation for the more general fermions, and the modified Hamilton-Jacobi equation of fermions is obtained in the semiclassical approximation method. Then, we study the quantum tunneling radiation of fermions in curved space-time of nonstationary symmetric Kerr black hole using the modified Hamilton-Jacobi equation and obtain the correction of Hawking temperature and tunneling rate of fermions. Interestingly, we found that the modified Hawking temperature at the event horizon of the black hole depends not only on the rates of the event horizon change $\dot{r}_H$, r_H', and $M(\mathrm{v})$ of the black hole, but also on the correction of the angle parameter θ_0. It means that the correction of Hawking radiation not only is the radial property of the black hole, but also is related to the angular property of the black hole.

In the study of quantum tunneling radiation of black holes, people first modified Hawking pure thermal radiation and then modified character of tunneling radiation from stationary black holes. With the research on quantum gravity effect, we combine the deformed dispersion relation to modify the tunneling radiation of nonstationary symmetric Kerr black hole effectively. We believe that the correction of tunneling radiation from other types of curved space-time will yield some interesting results. This paper only provides a method to modify quantum tunneling radiation, and further research is needed.

Data Availability

This paper is a theoretical research that does not involve data processing. No data were used to support this study.

Conflicts of Interest

The authors declare that they have no conflicts of interest.

Acknowledgments

This work is supported by the National Natural Science Foundation of China (Grants No. 11573022, No. 11805166) and by the starting funds of China West Normal University with Grants No. 17YC513 and No. 17C050.

References

[1] S. W. Hawking, "Black hole explosions?" *Nature*, vol. 248, no. 5443, pp. 30-31, 1974.

[2] S. W. Hawking, "Particle creation by black holes," *Communications in Mathematical Physics*, vol. 43, no. 3, pp. 199–220, 1975.

[3] S. P. Robinson and F. Wilczek, "Relationship between Hawking radiation and gravitational anomalies," *Physical Review Letters*, vol. 95, no. 1, Article ID 011303, 4 pages, 2005.

[4] T. Damoar and R. Ruffini, "Black-hole evaporation in the Klein-Sauter-Heisenberg-Euler formalism," *Physical Review D: Particles, Fields, Gravitation and Cosmology*, vol. 14, no. 2, p. 332, 1976.

[5] S. Sannan, "Heuristic derivation of the probability distributions of particles emitted by a black hole," *General Relativity and Gravitation*, vol. 20, no. 3, pp. 239–246, 1988.

[6] P. Kraus and F. Wilczek, "Self-interaction correction to black hole radiance," *Nuclear Physics B*, vol. 433, no. 2, pp. 403–420, 1995.

[7] M. K. Parikh and F. Wilczek, "Hawking radiation as tunneling," *Physical Review Letters*, vol. 85, no. 24, pp. 5042–5045, 2000.

[8] M. K. Parikh, "Energy conservation and hawking radiation," in *Proceedings of the Tenth Marcel Grossmann Meeting*, pp. 1585–1590, 2006.

[9] S. Hemming and E. Keski-Vakkuri, "Hawking radiation from AdS black holes," *Physical Review D: Particles, Fields, Gravitation and Cosmology*, vol. 64, no. 4, Article ID 044006, 2001.

[10] Q. Q. Jiang, S. Q. Wu, and X. Cai, "Hawking radiation from dilatonic black holes via anomalies," *Physical Review D: Particles, Fields, Gravitation and Cosmology*, vol. 76, no. 2, Article ID 064029, 2007.

[11] S. Iso, H. Umetsu, and F. Wilczek, "Anomalies, Hawking radiations, and regularity in rotating black holes," *Physical Review D: Particles, Fields, Gravitation and Cosmology*, vol. 74, no. 4, Article ID 044017, 10 pages, 2006.

[12] A. J. M. Medved, "Radiation via tunneling from a de Sitter cosmological horizon," *Physical Review D: Particles, Fields, Gravitation and Cosmology*, vol. 66, no. 12, Article ID 124009, 7 pages, 2002.

[13] J. Zhang and Z. Zhao, "Charged particles' tunnelling from the Kerr-Newman black hole," *Physics Letters B*, vol. 638, no. 2-3, pp. 110–113, 2006.

[14] K. Srinivasan and T. Padmanabhan, "Particle production and complex path analysis," *Physical Review D: Particles, Fields, Gravitation and Cosmology*, vol. 60, no. 2, Article ID 024007, 20 pages, 1999.

[15] S. Shankaranarayanan, T. Padmanabhan, and K. Srinivasan, "Hawking radiation in different coordinate settings: complex paths approach," *Classical and Quantum Gravity*, vol. 19, no. 10, pp. 2671–2687, 2002.

[16] R. Banerjee and B. R. Majhi, "A new global embedding approach to study Hawking and Unruh effects," *Physics Letters. B. Particle Physics, Nuclear Physics and Cosmology*, vol. 690, no. 1, pp. 83–86, 2010.

[17] R. Banerjee and B. R. Majhi, "Hawking black body spectrum from tunneling mechanism," *Physics Letters B*, vol. 675, p. 243, 2009.

[18] R. Banerjee and B. R. Majhi, "Quantum tunneling and trace anomaly," *Physics Letters B*, vol. 674, no. 3, pp. 218–222, 2009.

[19] R. Banerjee and S. K. Modak, "Quantum tunneling, blackbody spectrum and non-logarithmic entropy correction for lovelock black holes," *JHEP*, vol. 11, no. 073, 2009.

[20] R. Kerner and R. B. Mann, "Fermions tunnelling from black holes," *Classical and Quantum Gravity*, vol. 25, no. 9, Article ID 095014, 2008.

[21] R. Kerner and R. B. Mann, "Charged fermions tunnelling from kerr-newman black holes," *Physics Letters B*, vol. 665, no. 4, pp. 277–283, 2008.

[22] K. Lin and S. Z. Yang, "Fermion tunneling from higher-dimensional black holes," *Physical Review D: Particles, Fields, Gravitation and Cosmology*, vol. 79, no. 6, Article ID 064035, 2009.

[23] K. Lin and S. Yang, "Fermions tunneling of higher-dimensional Kerr-anti-de Sitter black hole with one rotational parameter," *Physics Letters B*, vol. 674, no. 2, pp. 127–130, 2009.

[24] K. Lin and S. Z. Yang, "Quantum tunneling from apparent horizon of rainbow-FRW universe," *International Journal of Theoretical Physics*, vol. 48, no. 7, pp. 2061–2067, 2009.

[25] K. Lin and S. Z. Yang, "A simpler method for researching fermions tunneling from black holes," *Chinese Phys. B*, vol. 20, no. 11, Article ID 110403, 2011.

[26] S. K. Modak, "Corrected entropy of BTZ black hole in tunneling approach," *Physics Letters B*, vol. 671, no. 1, pp. 167–173, 2009.

[27] S. Sarkar and D. Kothawala, "Hawking radiation as tunneling for spherically symmetric black holes: a generalized treatment," *Physics Letters. B. Particle Physics, Nuclear Physics and Cosmology*, vol. 659, no. 3, pp. 683–687, 2008.

[28] S. Zhou and W. Liu, "Hawking radiation of charged Dirac particles from a Kerr-Newman black hole," *Physical Review D: Particles, Fields, Gravitation and Cosmology*, vol. 77, no. 10, Article ID 104021, 6 pages, 2008.

[29] J. Hu and H. Yu, "Geometric phase outside a Schwarzschild black hole and the Hawking effect," *Journal of High Energy Physics*, Article ID 1209, p. 062, 2012.

[30] C. Ding, M. Wang, and J. Jing, "Particle energy and Hawking temperature," *Physics Letters. B. Particle Physics, Nuclear Physics and Cosmology*, vol. 676, no. 1-3, pp. 99–104, 2009.

[31] P. Mitra, "Hawking temperature from tunnelling formalism," *Physics Letters. B. Particle Physics, Nuclear Physics and Cosmology*, vol. 648, no. 2-3, pp. 240–242, 2007.

[32] E. T. Akhmedov, V. Akhmedova, and D. Singleton, "Hawking temperature in the tunneling picture," *Physics Letters B*, vol. 642, no. 1-2, pp. 124–128, 2006.

[33] R. Di Criscienzo, M. Nadalini, L. Vanzo, S. Zerbini, and G. Zoccatelli, "On the Hawking radiation as tunneling for a class of dynamical black holes," *Physics Letters. B. Particle Physics, Nuclear Physics and Cosmology*, vol. 657, no. 1-3, pp. 107–111, 2007.

[34] S. H. Mehdipour, "Hawking radiation as tunneling from a Vaidya black hole in noncommutative gravity," *Physical Review D: Particles, Fields, Gravitation and Cosmology*, vol. 81, no. 12, Article ID 124049, 9 pages, 2010.

[35] M. A. Rahman and M. I. Hossain, "Hawking radiation of Schwarzschild–de SITter black hole by Hamilton-Jacobi method," *Physics Letters. B. Particle Physics, Nuclear Physics and Cosmology*, vol. 712, no. 1-2, pp. 1–5, 2012.

[36] G. P. Li, J. Pu, Q. Q. Jiang, and X. T. Zu, "An application of Lorentz-invariance violation in black hole thermodynamics," *The European Physical Journal C*, vol. 77, p. 666, 2017.

[37] J. Pu and Y. Han, "Hawking radiation of the charged particle via tunneling from the Kaluza-KLEin black hole," *International Journal of Theoretical Physics*, vol. 55, no. 12, pp. 5077–5085, 2016.

[38] J. Pu and Y. Han, "Hawking radiation of the charged particle via tunneling from the reissner-nordström black hole," *International Journal of Theoretical Physics*, vol. 56, no. 8, pp. 2485–2494, 2017.

[39] J. Pu and Y. Han, "On Hawking radiation via tunneling from the Reissner-Nordström-de Sitter black hole with a global monopole," *International Journal of Theoretical Physics*, vol. 56, no. 7, pp. 2061–2070, 2017.

[40] Z. W. Feng, H. L. Li, S. Z. Yang et al., "Corrections to the thermodynamics of Schwarzschild-Tangherlini black hole and the generalized uncertainty principle," *The European Physical Journal C*, vol. 76, no. 4, p. 212, 2016.

[41] H. L. Li, Z. W. Feng, S. Z. Yang, and X. T. Zu, "The remnant and phase transition of a Finslerian black hole," *The European Physical Journal C*, vol. 78, no. 9, p. 768, 2018.

[42] X. X. Zeng, D. Y. Chen, and L. F. Li, "Holographic thermalization and gravitational collapse in a spacetime dominated by quintessence dark energy," *Physical Review D: Particles, Fields, Gravitation and Cosmology*, vol. 91, Article ID 046005, 2015.

[43] X. X. Zeng, X. M. Liu, and W. B. Liu, "Periodicity and area spectrum of black holes," *The European Physical Journal C*, vol. 72, no. 1967, 2012.

[44] X. X. Zeng and W. B. Liu, "Hawking radiation via Landauer transport model," https://arxiv.org/abs/1106.0548.

[45] X. X. Zeng, S. W. Zhou, and W. B. Liu, "Non-equilibrium Landauer transport model for Hawking radiation from a Reissner—Nordstrom black hole," *Chinese Physics B*, vol. 21, Article ID 090402, 2012.

[46] Y. W. Han, X. X. Zeng, and Y. Hong, "Thermodynamics and weak cosmic censorship conjecture of the torus-like black hole," *The European Physical Journal C*, vol. 79, p. 252, 2019.

[47] X. X. Zeng and L. F. Li, "Holographic phase transition probed by nonlocal observables," *Advances in High Energy Physics*, vol. 2016, Article ID 6153435, 2016.

[48] X. M. Liu, H. B. Shao, and X. X. Zeng, "Van der waals-like phase transition from holographic entanglement entropy in lorentz breaking massive gravity," *Advances in High Energy Physics*, vol. 2017, Article ID 6402101, 8 pages, 2017.

[49] Q.-Q. Jiang and S.-Q. Wu, "Hawking radiation from rotating black holes in anti-de Sitter spaces via gauge and gravitational anomalies," *Physics Letters. B. Particle Physics, Nuclear Physics and Cosmology*, vol. 647, no. 2-3, pp. 200–206, 2007.

[50] Q. Q. Jiang and X. Cai, "Back reaction, emission spectrum and entropy spectroscopy," *JHEP*, vol. 1011, no. 066, 2010.

[51] Q. Q. Jiang, D. Y. Chen, and D. Wen, "Remark on massive particle's de Sitter tunneling," *JCAP*, vol. 1311, no. 027, 2013.

[52] S. Z. Yang, K. Lin, J. Li, and Q. Q. Jiang, "Lorentz invariance violation andmodified hawking fermions tunneling radiation," *Adva. High Energy Phys*, vol. 2016, Article ID 7058764, 2016.

[53] Q.-Q. Jiang, "Dirac particle tunneling from black rings," *Physical Review D: Particles, Fields, Gravitation and Cosmology*, vol. 78, Article ID 044009, 2008.

[54] Q.-Q. Jiang, "Fermions tunnelling from GHS and non-extremal D1–D5 black holes," *Physics Letters B*, vol. 666, no. 5, pp. 517–521, 2008.

[55] Q. Q. Jiang, "Revisit emission spectrum and entropy quantum of the Reissner–Nordström black hole," *The European Physical Journal C*, vol. 72, no. 7, p. 2086, 2012.

[56] S. Z. Yang, "Dynamics equation of spin particles in a strong gravitational field," *J. Chinese West Normal Univ.(Nat. Sci)*, vol. 37, p. 126, 2016.

[57] S. Z. Yang and K. Lin, "Modified fermions tunneling radiation from Kerr-Newman-de Sitter black hole," *SCIENTIA SINICA Physica, Mechanica and Astronomica*, vol. 49, no. 1, Article ID 019503, 2019.

[58] G. Amelino-Camelia, "Relativity in spacetimes with short-distance structure governed by an observer-independent (Planckian) length scale," *International Journal of Modern Physics D*, vol. 11, no. 1, pp. 35–59, 2002.

[59] G. Amelino-Camelia, "Phenomenology of Planck-scale Lorentz-symmetry test theories," *New Journal of Physics* , vol. 6, p. 188, 2004.

[60] J. Magueijo and L. Smolin, "Lorentz invariance with an invariant energy scale," *Physical Review Letters*, vol. 88, no. 19, Article ID 190403, 2002.

[61] J. Magueijo and L. Smolin, "Generalized Lorentz invariance with an invariant energy scale," *Physical Review D: Particles, Fields, Gravitation and Cosmology*, vol. 67, no. 4, Article ID 044017, 2003.

[62] J. Ellis, N. E. Mavromatos, and D. V. Nanopoulos, "String theory modifies quantum mechanics," *Physics Letters B*, vol. 293, no. 1-2, pp. 37–48, 1992.

[63] J. Ellis, N. E. Mavromatos, and D. V. Nanopoulos, "A microscopic Liouville arrow of time," *Chaos, Solitons & Fractals*, vol. 10, no. 2-3, pp. 345–363, 1999.

[64] J. R. Ellis, N. E. Mavromatos, and A. S. Sakharov, "Synchrotron radiation from the Crab Nebula discriminates between models of space-time foam," *Astroparticle Physics*, vol. 20, no. 6, pp. 669–682, 2004.

[65] S. I. Kruglov, "Modified wave equation for spinless particles and its solutions in an external magnetic field," *Modern Physics Letters A*, vol. 28, Article ID 1350014, 2013.

[66] T. Jacobson, S. Liberati, and D. Mattingly, "A strong astrophysical constraint on the violation of special relativity by quantum gravity," *Nature*, vol. 424, pp. 1019–1021, 2003.

[67] S. I. Kruglov, "Modified Dirac equation with Lorentz invariance violation and its solutions for particles in an external magnetic field," *Physics Letters B*, vol. 718, no. 1, pp. 228–231, 2012.

[68] W. Rarita and J. Schwinger, "On a theory of particles with half-integral spin," *Physical Review*, vol. 60, p. 61, 1941.

Hindawi
Advances in High Energy Physics
Volume 2019, Article ID 1840360, 11 pages
https://doi.org/10.1155/2019/1840360

Review Article

Review on the Pseudocomplex General Relativity and Dark Energy

Peter O. Hess [1,2]

[1] *Instituto de Ciencias Nucleares, UNAM, Circuito Exterior, C.U., A.P. 70-543, 04510, Mexico City, Mexico*
[2] *Frankfurt Institute for Advanced Studies, Wolfgang Goethe University, Ruth-Moufang-Strasse 1, 60438 Frankfurt am Main, Germany*

Correspondence should be addressed to Peter O. Hess; hess@nucleares.unam.mx

Received 26 March 2019; Accepted 30 May 2019; Published 20 June 2019

Guest Editor: Cesar A. Vasconcellos

A review will be presented on the algebraic extension of the standard Theory of Relativity (GR) to the pseudocomplex formulation (pc-GR). The pc-GR predicts the existence of a dark energy outside and inside the mass distribution, corresponding to a modification of the GR-metric. The structure of the emission profile of an accretion disc changes also inside a star. Discussed are the consequences of the dark energy for cosmological models, permitting different outcomes on the evolution of the universe.

1. Introduction

The Theory of General Relativity (GR) [1] is one of the best tested known theories [2], mostly in solar system experiments. Also the loss of orbital energy in a binary system [3] was the first indirect proof for gravitational waves, which were finally detected in [4]. On April 10, *The Event Horizon Telescope* collaboration announced the first picture taken from the black hole in M87. This gives us an opportunity to compare results from the pc-GR to GR.

Nevertheless, the limits of GR may be reached when strong gravitational fields are present, which can lead to different interpretations of the sources of gravitational waves [5, 6].

A first proposal to extend GR was attempted by A. Einstein [7, 8] who introduced a complex valued metric $G_{\mu\nu} = g_{\mu\nu} + iF_{\mu\nu}$, with $G^*_{\mu\nu} = G_{\nu\mu}$. The real part corresponds to the standard metric, while the imaginary part defines the electromagnetic tensor. With this, A. Einstein intended to unify GR with Electrodynamics. Another motivation to extend GR is published in [9, 10], where M. Born investigated on how to recover the symmetry between coordinates and momenta, which are symmetric in Quantum Mechanics but not in GR. To achieve his goal, he introduced also a complex metric, where the imaginary part is momentum dependent. In [11] this was more elaborated, leading to the square of the length element ($c = 1$)

$$d\omega^2 = g_{\mu\nu}\left[dx^\mu dx^\nu + l^2 du^\mu du^\nu\right], \tag{1}$$

which implies maximal acceleration (see also [12]). The interesting feature is that a minimal length "l" is introduced as a *parameter* and Lorentz symmetry is, thus, automatically maintained; no deformation to small lengths is necessary!

In [13] the GR was algebraically extended to a series of variables and the solutions for the limit of weak gravitational fields were investigated. As a conclusion, only real and pseudocomplex coordinates (called in [13] *hyper-complex*) make sense, because all others show either tachyon or ghost solutions, or both. Thus, even the complex solutions do not make sense. This was the reason to concentrate on the pseudocomplex extension.

In pc-GR, all the extended theories, mentioned in the last paragraph, are contained and the Einstein equations require an energy-momentum tensor, related to vacuum fluctuations (dark energy), described by an asymmetric ideal fluid [12]. Due to the lack of a microscopic theory, this dark energy is treated phenomenologically. One possibility is to choose it such that no event horizon appears or barely still exists. The reason to do so is that, in our philosophical understanding, *no theory should have a singularity*, even a coordinate singularity

of the type of an event horizon encountered in a black hole. Though it is only a coordinate singularity, the existence of an event horizon implies that even a black hole in a nearby corner cannot be accessed by an outside observer. Its event horizon is a consequence of a strong gravitational field. Because no quantized theory of gravitation exists yet, we are led to the construction of models for the distribution of the dark energy.

In [14] the pc-GR was compared to the observation of the amplitude for the inspiral process. As found, the fall-off in r of the dark energy has to be stronger than suggested in earlier publications. We will discuss this and what will change, in the main body of the text. We also will compare EHT observations with pc-GR, taking into account the low resolution of $20\mu as$, as obtained by the EHT. The main question is if one can discriminate between GR and pc-GR.

A general principle emerges; namely, that *mass not only curves the space* (which leads to the standard GR) *but also changes the space- (vacuum-) structure in its vicinity*, which in turn leads to an important deviation from the classical solution.

The consequences will be discussed in Section 3. There, also the cosmological effects are discussed, with different outcomes for the evolution of the dark energy as function of time/radius of the universe. Another application treats the interior of a stars, where first attempts will be reported on how to stabilize a large mass. In Section 4 conclusions will be drawn.

2. Pseudocomplex General Relativity (pc-GR)

An algebraic extension of GR consists in a mapping of the real coordinates to a different type, as, for example, complex or pseudocomplex (pc) variables

$$X^\mu = x^\mu + Iy^\mu, \tag{2}$$

with $I^2 = \pm 1$ and where x^μ is the standard coordinate in space-time and y^μ is the complex component. When $I^2 = -1$ it denotes *complex* variables, while when $I^2 = +1$ it denotes pseudocomplex (pc) variables. This algebraic mapping is just *one possibility* to explore extensions of GR.

In [13] all possible extensions of real coordinates in GR were considered. It was found that only the extension to pseudocomplex coordinates (called in [13] *hyper-complex*) makes sense, because all others lead to tachyon and/or ghost solutions, in the limit of weak gravitational fields.

In what follows, some properties of pseudocomplex variables are resumed, which is important to understand some of the consequences.

(i) The variables can be expressed alternatively as

$$\begin{aligned} X^\mu &= X^\mu_+\sigma_+ + X^\mu_-\sigma_- \\ \sigma_\pm &= \frac{1}{2}(1 \pm I). \end{aligned} \tag{3}$$

(ii) The $\sigma_\pm$ satisfy the relations

$$\begin{aligned} \sigma_\pm^2 &= \sigma_\pm, \\ \sigma_+\sigma_- &= 0. \end{aligned} \tag{4}$$

(iii) Due to the last property in (4), when multiplying one variable proportional to σ_+ by another one proportional to σ_-, the result is zero; i.e., there is a *zero-divisor*. The variables, therefore, do not form a *field* but a *ring*.

(iv) In both zero-divisor components ($\sigma_\pm$) the analysis is very similar to the standard complex analysis.

In pc-GR the metric is also pseudocomplex

$$g_{\mu\nu} = g^+_{\mu\nu}\sigma_+ + g^-_{\mu\nu}\sigma_-. \tag{5}$$

Because $\sigma_+\sigma_- = 0$ in each zero-divisor component one can construct independently a GR theory.

For a consistent theory, both zero-divisor components have to be connected! One possibility is to define a modified variational principle, as done in [15]. Alternatively, one can implement a constraint; namely, a particle should always move along a real path; i.e., the pseudocomplex length element should be real.

The infinitesimal pc length element squared is given by (see also [16])

$$d\omega^2 = g_{\mu\nu}dX^\mu dX^\nu = g^+_{\mu\nu}dX^\mu_+dX^\nu_+\sigma_+ + g^-_{\mu\nu}dX^\mu_-dX^\nu_-\sigma_- \tag{6}$$

as written in the zero-divisor components. In terms of the pseudoreal and pseudoimaginary components, we have

$$\begin{aligned} d\omega^2 = {} & g^s_{\mu\nu}\left(dx^\mu dx^\nu + dy^\mu dy^\nu\right) + g^a_{\mu\nu}\left(dx^\mu dy^\nu\right. \\ & \left. + dy^\mu dx^\nu\right) + I\left[g^a_{\mu\nu}\left(dx^\mu dx^\nu + dy^\mu dy^\nu\right)\right. \\ & \left. + g^s_{\mu\nu}\left(dx^\mu dy^\nu + dy^\mu dx^\nu\right)\right], \end{aligned} \tag{7}$$

with $g^s_{\mu\nu} = (1/2)(g^+_{\mu\mu} + g^-_{\mu\nu})$ and $g^a_{\mu\nu} = (1/2)(g^+_{\mu\mu} - g^-_{\mu\nu})$. The upper indices s and a refer to a *symmetric* and *antisymmetric* combination of the metrics. The case when $g_{\mu\nu} = g^+_{\mu\nu} = g^-_{\mu\nu}$, i.e., $g^a_{\mu\nu} = 0$, leads to

$$g_{\mu\nu}\left(dx^\mu dx^\nu + dy^\mu dy^\nu\right) + Ig_{\mu\nu}\left(dx^\mu dy^\nu + dy^\mu dx^\nu\right). \tag{8}$$

Identifying $y^\mu = lu^\mu$, where l is an infinitesimal length and u^μ is the 4-velocity, one obtains the length element defined in [11]. It also contains the line element as proposed in [9, 10], where the y^μ is proportional to the momentum component p^μ of a particle. However, this identification of y^μ is only valid in a flat space, where the second term in (8) is just the scalar product of the 4-velocity ($u^\mu = dx^\mu/d\tau$) to the 4-acceleration ($y^\mu = d^2x^\mu/d\tau^2$).

The connection between the two zero-divisor components is achieved, requiring that the infinitesimal length element squared in (7) *is real*; i.e., in terms of the $\sigma_\pm$ components it is

$$\left(\sigma_+ - \sigma_-\right)\left(g^+_{\mu\nu}dX^\mu_+dX^\nu_+ - g^-_{\mu\nu}dX^\mu_-dX^\nu_-\right) = 0. \tag{9}$$

Using the standard variational principle with a Lagrange multiplier, to account for the constraint, leads to an additional contribution in the Einstein equations, interpreted as an energy-momentum tensor.

The action of the pc-GR is given by [16]

$$S = \int dx^4 \sqrt{-g}\,(\mathscr{R} + 2\alpha)\,, \tag{10}$$

where $\mathscr{R}$ is the Riemann scalar. The last term in the action integral allows to introduce the cosmological constant in cosmological models, where α has to be constant in order not to violate the Lorentz symmetry. This changes when a system with a uniquely defined center is considered, which has spherical (Schwarzschild) or axial (Kerr) symmetry. In these cases, the α is allowed to be a function in r, for the Schwarzschild solution, and a function in r and ϑ, for the Kerr solution.

The variation of the action with respect to the metric $g^{\pm}_{\mu\nu}$ leads to the equations of motion

$$\begin{aligned} &\mathscr{R}^{\pm}_{\mu\nu} - \frac{1}{2} g^{\pm}_{\mu\nu} \mathscr{R}_{\pm} = 8\pi T^{\Lambda}_{\pm\mu\nu} \\ &\text{with } T^{\Lambda}_{\pm\mu\nu} = \lambda u_\mu u_\nu + \lambda \left(\dot{y}_\mu \dot{y}_\nu \pm u_\mu \dot{y}_\nu \pm u_\nu \dot{y}_\mu \right) + \alpha g^{\pm}_{\mu\nu}, \end{aligned} \tag{11}$$

in the zero-divisor component, denoted by the independent unit-elements $\sigma_{\pm}$. These equations still contain the effects of a minimal length parameter l, as shown in [11]. Because the effects of a minimal length scale are difficult to measure, maybe not possible at all, we neglect them, which corresponds to mapping the above equations to their real part, giving

$$\mathscr{R}_{\mu\nu} - \frac{1}{2} g^{\pm}_{\mu\nu} \mathscr{R} = 8\pi T^{\Lambda}_{\mu\nu}. \tag{12}$$

The $T^{\Lambda}_{\mu\nu}$, $\mathscr{R}^{\pm}_{\mu\nu}$ is real and is now given by [16]

$$T^{\Lambda}_{\mu\nu,R} = \left(\rho_\Lambda + p^{\Lambda}_{\vartheta} \right) u_\mu u_\nu + p^{\Lambda}_{\vartheta} g_{\mu\nu} + \left(p^{\Lambda}_{r} - p^{\Lambda}_{\vartheta} \right) k_\mu k_\nu, \tag{13}$$

where p^{Λ}_{ϑ} and radial p^{Λ}_{r} are the tangential and pressure, respectively. For an isotropic fluid we have $p^{\Lambda}_{\vartheta} = p^{\Lambda}_{r} = p^{\Lambda}$. The u^μ are the components of the 4-velocity of the elements of the fluid and k^μ is a space-like vector ($k_\mu k^\mu = 1$) in the radial direction. It satisfies the relation $u_\mu k^\mu = 0$. The fluid is anisotropic due to the presence of y_μ. The λ and α are related to the pressures as [16]

$$\begin{aligned} \lambda &= 8\pi\widetilde{\lambda}, \\ \alpha &= 8\pi\widetilde{\alpha} \\ \widetilde{\lambda} &= \left(p^{\Lambda}_{\vartheta} + \rho_\Lambda \right), \\ \widetilde{\alpha} &= p^{\Lambda}_{\vartheta}, \\ \widetilde{\lambda} y_\mu y_\nu &= \left(p^{\Lambda}_{r} - p^{\Lambda}_{\vartheta} \right) k_\mu k_\nu. \end{aligned} \tag{14}$$

The reason why the dark energy outside a mass distribution has to be an anisotropic fluid is understood contemplating the *Tolman-Oppenheimer-Volkov* (TOV) equations [17] for an isotropic fluid: The TOV equations relate the derivative of the dark-energy pressure with respect to r (for an isotropic fluid, the tangential pressure has to be the same as the radial pressure, i.e., $p^{\Lambda}_{\vartheta} = p^{\Lambda}_{r} = p^{\Lambda}$) to the dark energy density ρ_Λ. Assuming the isotropic fluid and that the equation of state for the dark energy is $p^{\Lambda} = -\rho_\Lambda$, the factor $(p^{\Lambda} + \rho_\Lambda)$ in the TOV equation for dp^{Λ}/dr is zero; i.e., the pressure derivative is zero. As a result the pressure is constant and with the equation of state also the density is constant, which leads to a contradiction. Thus, the fluid has to be anisotropic, due to an additional term, allowing the pressure to fall off as a function on increasing distance. The additional term in the radial pressure dp^{Λ}_{r}/dr, added to the TOV equation, is given by $(2/r)\Delta p^{\Lambda} = (2/r)(p^{\Lambda}_{\vartheta} - p^{\Lambda}_{r})$ [18].

For the density one has to apply a phenomenological model, due to the lack of a quantized theory of gravity. What helps is to recall one-loop calculations in gravity [19], where vacuum fluctuations result due to the non-zero back ground curvature (Casimir effect). Results are presented in [20], where at large distances the density falls off approximately as $1/r^6$. The semiclassical Quantum Mechanics [19] was applied, which assumes a *fixed* back-ground metric and is thus only valid for weak gravitational fields (weak compared to the solar system). Near the Schwarzschild radius the field is very strong which is exhibited by a singularity in the energy density, which is proportional to $1/(1 - 2m/r)^2$, with m a constant mass parameter [20].

Because we treat the vacuum fluctuations as a classical ideal anisotropic fluid, we are free to propose a different fall-off of the negative energy density, which is finite at the Schwarzschild radius. In earlier publications the density did fall-off proportional to $1/r^5$. However, in [14] it is shown that this fall-off has to be stronger. Thus, in this contribution we will also discuss a variety of fall-offs as a function of a parameter n, i.e., proportional to B_n/r^{n+2}, where B_n describes the coupling of the dark energy to the mass.

With the assumed density, the metric for the Kerr solution changes to [21, 22]

$$\begin{aligned} g_{00} &= -\frac{r^2 - 2mr + a^2\cos^2\vartheta + B_n/\left((n-1)(n-2)\,r^{n-2}\right)}{r^2 + a^2\cos^2\vartheta}, \\ g_{11} &= \frac{r^2 + a^2\cos^2\vartheta}{r^2 - 2mr + a^2 + B_n/\left((n-1)(n-2)\,r^{n-2}\right)}, \\ g_{22} &= r^2 + a^2\cos^2\vartheta, \\ g_{33} &= \left(r^2 + a^2\right)\sin^2\vartheta \\ &\quad + \frac{a^2\sin^4\vartheta\left(2mr - B_n/\left((n-1)(n-2)\,r^{n-2}\right)\right)}{r^2 + a^2\cos^2\vartheta}, \\ g_{03} &= \frac{-a\sin^2\vartheta 2mr + a\left(B_n/\left((n-1)(n-2)\,r^{n-2}\right)\right)\sin^2\vartheta}{r^2 + a^2\cos^2\vartheta}, \end{aligned} \tag{15}$$

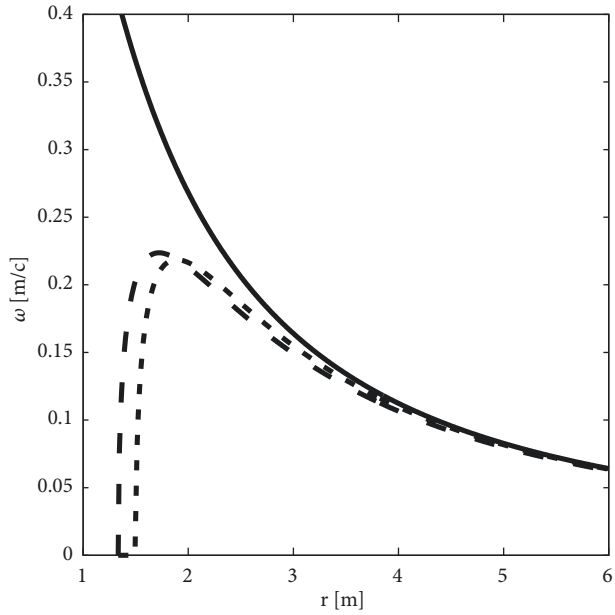

Figure 1: The orbital frequency of a particle in a circular orbit for the case GR (upper curve) and for $n = 3$ (long dashed curve) and $n = 4$ (short dashed curve) [12, 25].

where $0 \leq a \leq m$ is the spin parameter of the Kerr solution and $n = 3, 4, \ldots$. For $n = 2$ the old ansatz is achieved. The Schwarzschild solution is obtained, setting $a = 0$. The parameter $B_n = b_n m^n$ measures the coupling of the dark energy to the central mass. The definition of n here is related to the n_N in [14] by $n_N = n - 1$.

When no event horizon is demanded, the parameter B_n has a lower limit given by

$$B_n > \frac{2(n-1)(n-2)}{n}\left[\frac{2(n-1)}{n}\right]^{n-1} \mathrm{m}^n = b_{\max}\mathrm{m}^n. \quad (16)$$

For the equal sign, an event horizon is located at

$$r_h = \frac{2(n-1)}{n}\mathrm{m}, \quad (17)$$

e.g., 4/3 for $n = 3$ and 3/2 for $n = 4$.

3. Applications

3.1. Motion of a Particle in a Circular Orbit. In [23] the motion of a particle in a circular orbit was investigated. This section was first discussed in [24, 25].

The main results are resumed in Figures 1 and 2. In Figure 1 the orbital frequency, in units of c/m, is depicted versus the radial distance r, in units of m, for a rotational parameter of $0.9m$. The function for the orbital frequency, in prograde orbits, is given by

$$\omega_n = \frac{1}{a + \sqrt{2r/h_n(r)}}$$
$$h_n(r) = \frac{2}{r^2} - \frac{nB_n}{(n-1)(n-2)r^{n+1}}. \quad (18)$$

The upper curve in Figure 1 corresponds to GR while the two lower ones correspond to pc-GR with $n = 3$ (dashed curve) and $n = 4$ (dotted curve). The curve shows a maximum at

$$r_{\omega_{\max}} = \left[\frac{n(n+2)b_{\max}}{6(n-1)(n-2)}\right]^{1/(n-1)} \mathrm{m}, \quad (19)$$

which, for $b_n = b_{\max}$ as given in (16), is independent of the value of a, after which it falls off toward the center and reaches zero at r_h (Eq. (17)), which is *independent* on the rotational parameter a. After the maximum the curve falls off toward smaller r. These features will be important for the understanding of the emission structure of an accretion disc (see next subsection).

As one can see, the difference between $n = 3$ and $n = 4$ is minimal and, thus, will not change the qualitative results as obtained for $n = 3$ in former publications. The position of the maximum, which gives the position of the dark ring discussed below, is approximately the same in both cases. For $b_n \longrightarrow 0$ the curve approaches the one for GR.

In Figure 2 the last stable orbit, for $n = 3$, is plotted versus the rotational parameter a. The solid enveloping curve is the result for GR. For $a = 0$ the last stable orbit in GR is at $6m$, while in pc-GR it is further in. The dark gray shaded area describes stable orbits in pc-GR and the light gray area describes unstable orbits. The pc-GR follows closely the GR with a greater deviation for larger a. At about $a = 0.45m$ (for $n = 3$, for $n = 4$ its value is a little bit larger) all orbits in pc-GR are stable up to the surface of the star, which is estimated to lie at approximately $(4/3)m$. For $a = m$, in GR the last stable orbit is at $r = m$.

3.2. Accretion Discs. In order to connect to actual observations [26–31], one possibility is to simulate accretion discs

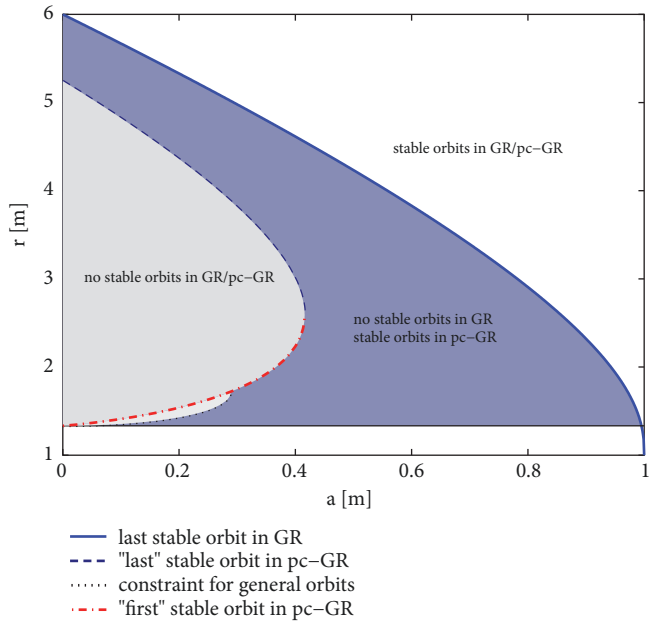

FIGURE 2: The position of the *Innermost Stable Circular Orbit* (ISCO) is plotted versus the rotational parameter a. The upper curve corresponds to GR and the lower curves correspond to pc-GR. The light gray shaded region corresponds to a forbidden area for circular orbits within pc-GR. For small values of a the ISCO in pc-GR follows more or less the one of GR, but at smaller values of r. From a certain a on stable orbits they are allowed until to the surface of the star (for $n = 3$ this limit is approximately $0.4\,m$ and for $n = 4$ it is at $0.5\,m$).

around massive objects as the one in the center of the elliptical galaxy M87. The underlying theory was published by D. N. Page and K. S. Thorne [32] in 1974. The basic assumptions are (see also [33]) the following:

(i) A thin, infinitely extended accretion disc. This is a simplifying assumption. A real accretion disc can be a torus. Nevertheless, the structure in the emission profile will be similar, as discussed here. These discs are easier to calculate.

(ii) An energy-momentum tensor is proposed which includes all main ingredients, as mass and electromagnetic contributions.

(iii) Conservation laws (energy, angular momentum, and mass) are imposed in order to obtain the flux function, the main result of [32].

(iv) The internal energy of the disc is liberated via shears of neighboring orbitals and distributed from orbitals of higher frequency to those of lower frequency.

How to deduce finally the flux is described in detail in [16].

In order to understand within pc-GR the structure of the emission profile in the accretion disc, we have to get back to the discussion in the last subsection. The local heating of the accretion disc is determined by the gradient of orbital frequency, when going further inward (or outward). At the maximum, neighboring orbitals have nearly the same orbital frequency; thus, friction is low. On the other hand, above and especially below the position of the maximum the change in orbital frequency is large and the disc gets heated. At the maximum the heating is minimal which will be noticeable by a dark ring. Further inside, the heating increases again and a bright ring is produced.

The above consideration is relevant for a larger than approximately 0.4, as can be seen from Figure 2 (for explanations, see the figure caption) and [23]. For lower values of a, in pc-GR the last stable orbit follows the one of GR, but with lower values for the position of the ISCO. As a consequence, the particles reach further inside and, due to the decrease of the potential, more energy is released, producing a brighter disc. However, the last stable orbit in pc-GR does not reach $r_{\omega_{\max}}$. This changes when a is a bit larger than 0.4. Now, $r_{\omega_{\max}}$ is crossed and the existence of the maximum of ω has to be taken into account as explained above.

Some simulations are presented in Figure 3. The line of sight of the observer to the accretion disc is 80° (near to the edge of the accretion disc), where the angle refers to the one between the axis of rotation and the line of sight. Two rotation parameters of the Kerr solution are plotted, namely, $a = 0$ (no rotation of the star, corresponding to the Schwarzschild solution) and nearly the maximal rotation $a = 0.9$ m.

As a global feature, the accretion disc in pc-GR appears brighter, which is due to the fact that the disc reaches further inside where the potential is deeper, thus releasing more gravitational energy, which is then distributed within the disc.

The reason for the dark fringe and bright ring was explained above due to the variability of the friction. The dark ring is the position of the maximum of the orbital frequency. An observed position of a dark ring can, thus, be used to determine n.

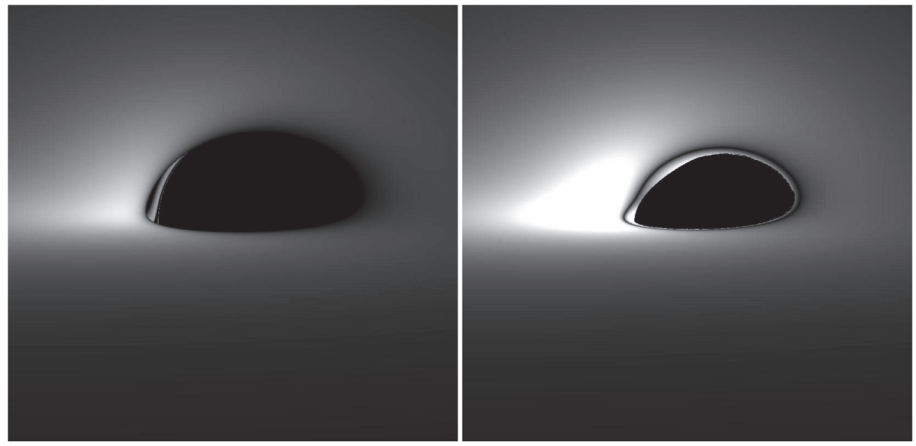

Figure 3: Infinite, counterclockwise rotating geometrically thin accretion disc around static and rotating compact objects viewed from an inclination of 80°. The left panel shows the disc model by [32] in pc-Gr, with $a = 0$. The right panel shows the modified model, including pc-GR correction terms as described in the text.

The differences in the structure of an accretion disc give us clear observational criteria to distinguish between GR and pc-GR. There are still others, maybe more realistic disc models, e.g., a thick disk as described in [36]. In case there is no disk present, as is probably the case in SgrA*, then the synchrotron model of infalling and emitted gas [37] may be more realistic. However, in all of those models the above discussed ring structure of the disc will not change. Unfortunately, this is for the moment the only clear prediction to differentiate pc-GR from GR. In the next subsection we will discuss gravitational waves and we will see pc-GR and GR give different interpretations of the source, though the final outcome is the same.

Finally, in Figure 4 we compare a disc simulation for GR (left panel) with pc-GR (right panel), for $a = 0.6$ and a 60° inclination angle. The intensity in GR is smaller while in pc-GR it is much stronger. Also, the maximum of the intensity is more in line with the EHT data, which reports the maximum at approximately 3-4m. Otherwise, the ring structure in pc-GR is lost due to the low resolution of 20μas and the cross-structure of pc-Gr is the same as in GR.

3.3. Gravitational Waves in pc-GR. In [4] the first observed gravitational wave event was reported. In [5] this gravitational event was investigated within the pc-GR, for $n = 3$.

Using GR and the mass-point approximation for the two black holes, before the merging, a relation is obtained between the observed frequency and its temporal change to the chirping mass $\mathcal{M}_c$, namely [38],

$$\mathcal{M}_c = \widetilde{\mathcal{M}}_c F_\omega(r) = \frac{c^3}{G}\left[\frac{5}{96\pi^{8/3}}\frac{df_{\mathrm{gw}}}{dt} f_{\mathrm{gw}}^{-11/3}\right]^{3/5}. \quad (20)$$

Substituting on the right hand side the observed frequency and its change and using $F_\omega(r) = 1$ for GR, the interpretation of the source of the gravitational waves is of two black holes of about 30 solar masses each which fuse to a larger one of less than 60 solar masses. The difference in energy is radiated away as gravitational waves. However, these changes are in pc-GR, where the two black holes can come very near to each other. Unfortunately, the point mass approximation is not applicable, though in [5] this approximation was still used in order to show in which direction the interpretation of the source changes. In pc-GR ($n = 3$) $F_\omega(r) = [1-(3b_3/4)(m/r)^2]$, which for b_n given by the right hand side of Eq. (16) is exactly zero. Therefore, a range of the last possible distances of the two black holes before merging was assumed. On the left hand side of Eq. (20), the function $F_\omega(r)$ becomes very small near where the two in-spiraling black holes merge. Thus, the chirping mass $\widetilde{\mathcal{M}}_c$ must be much larger than the chirping mass $\mathcal{M}$ deduced in GR. For $n = 4$, the function $F_\omega(r)$ changes to $[1-(b_4/3)(m/r)^3]$; thus, the main conclusions are the same, though the r-dependence has changed. We have not yet made explicit calculations, for one reason: The model applied in [5] has to be modified, because the point approximation is not very good.

The main result is that the source in pc-GR corresponds to two black holes with several thousand solar masses. This may be related to the merger of two primordial galaxies whose central black hole subsequently merges. One way to distinguish the two predictions is to look for light events very far way. If, for observed gravitational wave events in future, there is a consistent appearance of light events much farther away as the distance deduced from GR, then this might be in favor for pc-GR. However, all the prediction depends on the assumption that the point mass approximation is still more or less valid when the two black holes are near together, which is not very good! In [14] the inspiral frequency was determined within pc-GR, for various values of n, which is related to the one used in [14] by $n_N = n - 1$. As demonstrated, the wave form cannot be reproduced satisfactorily for $n = 3$; thus, it has to be increased and let us investigate the dependence of the results as a function in n.

In [6] the Schwarzschild case was considered and the Regge-Wheeler, for negative parity solutions, [39] and Zerrilli equations, for positive parity solutions, [40] were solved,

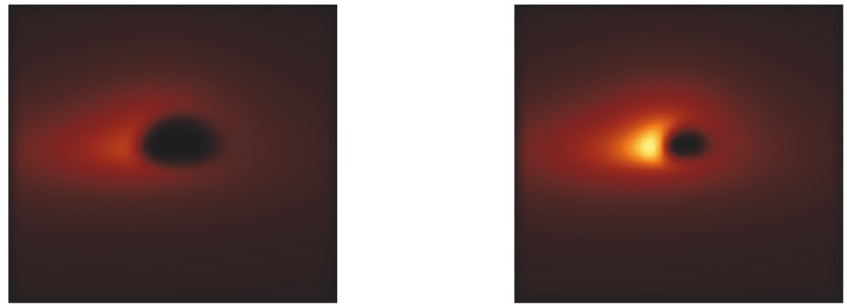

Figure 4: Infinite, counterclockwise rotating geometrically thin accretion disc around static and rotating compact objects viewed from an inclination of 60° and $a = 0.6$. The left panel is GR and the right one is pc-GR. A resolution of $20\mu as$ was assumed. A resolution of $20\mu as$ is assumed.

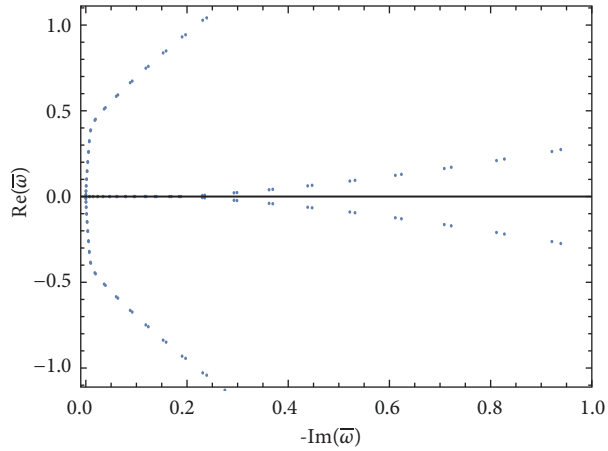

Figure 5: Axial gravitational modes in pc-GR. The vertical axis gives the real part of $\tilde{\omega} = m\omega$ while the horizontal axis depicts the negative of its imaginary part.

using an iteration method [41]. Due to a symmetry, in GR the two types of solutions have *the same* frequency spectrum [40], which unfortunately is lost in pc-GR. For pc-GR, the spectrum of frequencies for *axial modes* shows a convergent behavior for the frequencies, which is shown in Figure 5. A negative imaginary part indicates a stable mode, which turns out to be the case. For an increasing imaginary part the convergence is less sure. Unfortunately, for the polar modes no convergences for the polar modes were obtained up to now.

Another problem is to distinguish between GR and pc-GR. It depends very much on the observation of the ring-down frequency of the merger [6], which is not very well measured yet. Without it, we are not able to distinguish between both theories and various possible scenarios can be obtained in pc-GR [6, 12].

3.4. Dark Energy in the Universe. The pc-Robertson-Walker model is presented in detail in [12, 34]. The main results will be resumed in this subsection.

The line element in gaussian coordinates has the form

$$d\omega^2 = (dt)^2 - a(t)^2 \frac{1}{\left(1 + ka(t)^2/4a_0^2\right)^2} \left(dR^2 + R^2 d\vartheta^2 + a(t)^2 \sin^2\vartheta d\varphi^2\right), \tag{21}$$

where R is the radius of the universe and k is a parameter and the energy density of matter was assumed to be homogeneous. The value $k = 0$ corresponds to a flat universe, which will be taken here.

The corresponding Einstein equations were solved and an equation for the radius $a(t)$ if the universe was deduced [12]:

$$a(t)'' = \frac{4\pi G}{3}(3\beta - 1)\Lambda a(t)^{3(\beta-1)+1} - \frac{4\pi G}{3}(1 + 3\alpha)\varepsilon_0 a(t)^{-3(1+\alpha)+1}, \tag{22}$$

where G is the gravitational constant and β, Λ are parameters of the theory. The equation of state is set as $p = \alpha\varepsilon$, where ε is the matter density and α is set to zero for *dust*.

Two particular solutions are shown in Figure 6. Shown is the acceleration of the universe as a function of the radius $a(t)$. The left panel shows the result for $\beta = 1/2$ and $\Lambda = 3$ and on the right hand side the parameters β and Λ are set to 2/3 and 4, respectively. The left figure corresponds to a solution where the acceleration tends to a constant; i.e., the

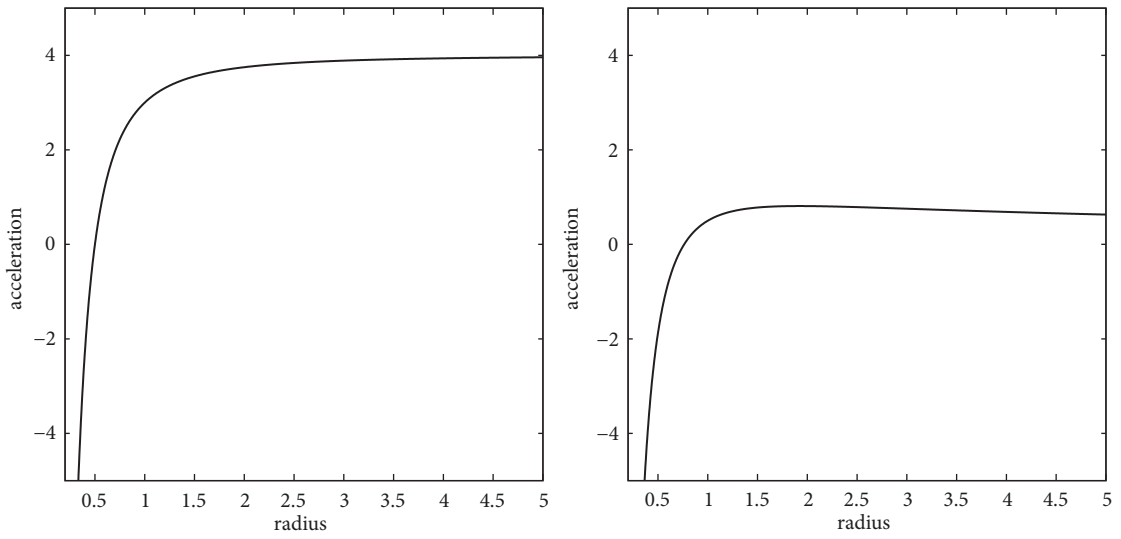

Figure 6: The left panel shows a case where the acceleration of the universe approaches a constant value and the right panel shows a case where the acceleration slowly approaches zero for $t \longrightarrow \infty$. The figures are taken from [12, 34].

universe will expand forever with an increasing acceleration, while in the right figure the acceleration tends slowly to zero for very large $a(t)$. In both examples the universe expands forever. These are not the only solutions; also one where the universe collapses again is possible.

These results are not very predictive, because one can obtain several possible outcomes, depending on the values of β and Λ. Nevertheless, they show that possible scenarios for the future of our universe are still possible.

3.5. Interior of Stars. For the description of the interior of a star one needs the equation of state of matter and the coupling of the dark-energy with the matter. For the equation of state one can use the model presented in [42], which also takes into account nuclear and meson resonances. However, these approximations will lose their validity when the matter density is too large. The situation is worse for the dark-energy contribution and it is twofold: (i) one has to know how the dark-energy evolves within the star (presence of matter) and (ii) how it is coupled to the matter itself. Both are not known and we have to rest on incomplete models. Alternatively, one can approach the problem with a very interesting and distinct model to simulate the dark energy, as done in [43–46], where compact and dense objects were investigated within the pc-GR and maximal masses were also deduced.

In [18] a simple coupling model of dark-energy to the mass density was proposed:

$$\varepsilon_\Lambda = \alpha \rho_m, \tag{23}$$

where the index Λ refers to the dark energy and ρ_m refers to the mass density. In this proposal the dark energy follows neatly the mass distribution. The Tolman-Oppenheimer-Volkoff (TOV) equations have to be solved, which are doubled in number, one treating the mass part and the other the dark-energy part (for more details see [12, 18]).

A particular result is shown in Figure 7, showing the mass of the star versus its radius. Curves are depicted for various values of the proportionality factor α. As can be seen, the model can reproduce stable stars up to 6 solar masses, which shows that the dark-energy stabilizes stars with larger masses. However, no stars with larger masses can be constructed, because for larger values of α and/or larger masses the repulsion due to the dark energy becomes too large near the surface and outer surface layers are evaporated.

In [35] calculations in one-loop order, using the monopole approximation, were calculated with the intention to derive the coupling between the dark energy and matter density. In Figure 8 the lower curve shows the result of these calculations and the upper curve shows the approximation in terms of a polynomial, used in the final calculations.

Finally, in Figure 9 the mass of the star versus its radius R is depicted. As can be noted, now stars with up to 200 solar masses are possible. Higher masses cannot be obtained due to the limits the model of [42] reaches.

This model also suffers from the approximations made and a complete description cannot be given. Nevertheless, now stars with up to 200 solar masses can be stabilized, which shows that the inclusion of dark-energy in massive stars may lead to stable stars of any mass! (Though, only within a phenomenological model.)

4. Conclusions

A report on the recent advances of the pseudocomplex General Relativity (pc-GR) was presented. The theory predicts a nonzero energy-momentum tensor on the right hand side of the Einstein equation. The new contribution is related to vacuum fluctuations, but due to a missing quantized theory of gravitation one recurs to a phenomenological ansatz. Calculations in one-loop order, with a constant back-ground

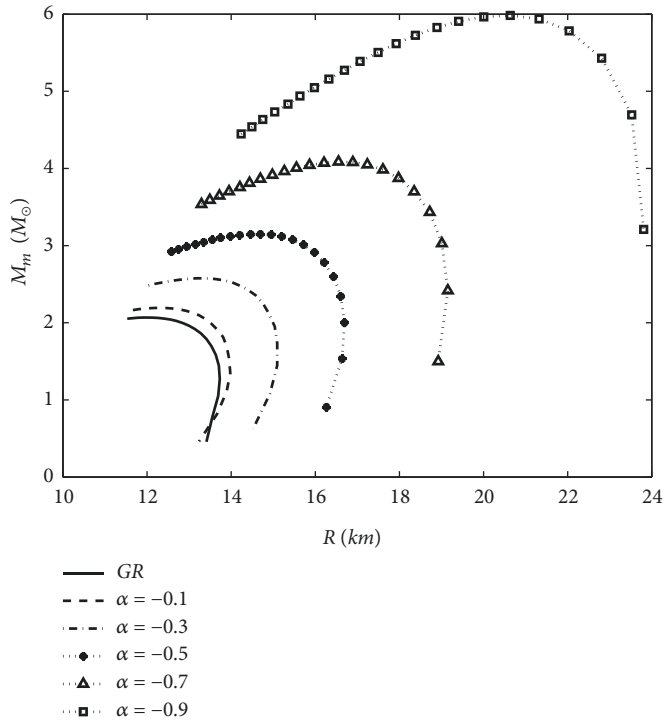

FIGURE 7: The figure shows the dependence of the mass of the star as a function of its radius (figure taken from [18]).

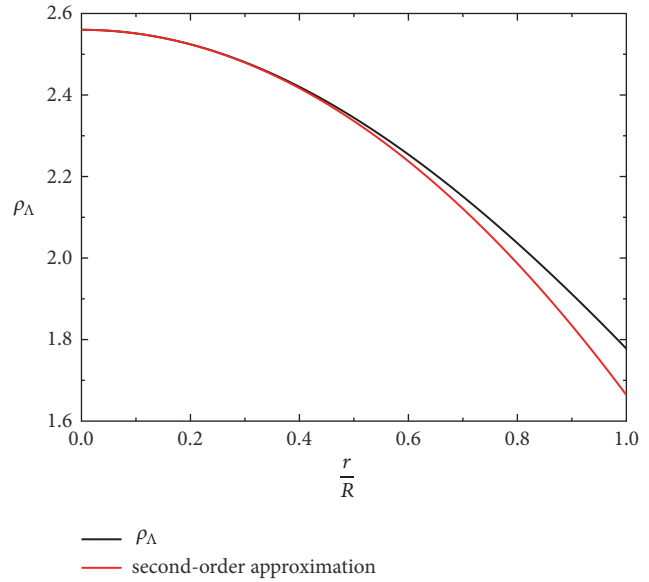

FIGURE 8: Dark energy density as a function of r/R, where R is the radius of the star. The upper curve depicts the result of the monopole approximation and the lower curve is an approximation for the upper one. The figure is taken from [35].

metric, show that the dark energy density has to increase toward smaller r.

Consequences of the theory were presented: (i) the appearance of a dark ring followed by a bright one in accretion discs around black holes, (ii) a new interpretation of the source of the first gravitational event observed, (iii) possible outcomes of the future evolving universe, and (iv) attempts to stabilize stars with large masses.

The only robust prediction is the structure in the emission profile of an accretion disc.

Conflicts of Interest

The author declares that they have no conflicts of interest.

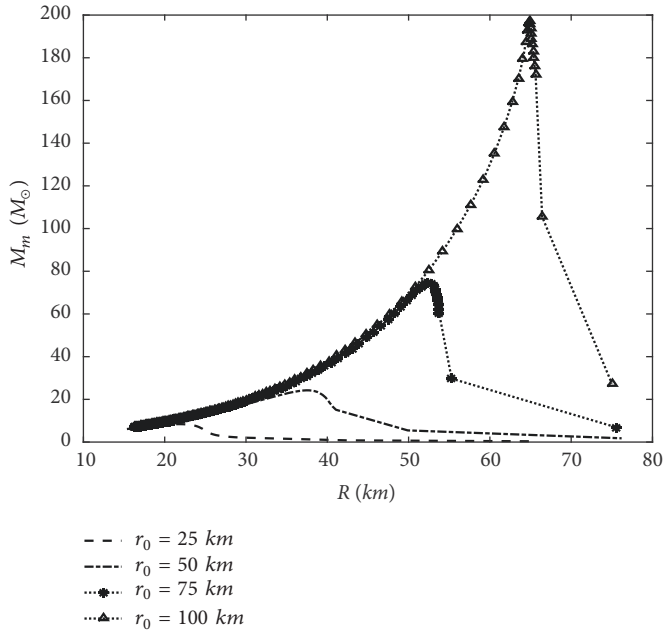

Figure 9: The mass of a star as a function on its radius R. With the modified coupling of the dark-energy to the mass density the maximal mass possible is now about 200. The figure is taken from [35].

Acknowledgments

Peter O. Hess acknowledges the financial support from DGAPA-PAPIIT (IN100418). Very helpful discussions with T. Boller (Max-Planck Institute for Extraterrestrial Physics, Garching, Germany) and T. Schönenbach are also acknowledged.

References

[1] C. W. Misner, K. S. Thorne, and J. A. Wheeler, *Gravitation*, W. H. Freeman and Company, San Francisco, Calif, USA, 1973.

[2] C. M. Will, "The confrontation between general relativity and experiment," *Living Reviews in Relativity*, vol. 9, no. 3, 2006.

[3] J. M. Weisberg, J. H. Taylor, and L. A. Fowler, "Gravitational waves from an orbiting pulsar," *Scientific American*, vol. 245, no. 4, p. 74, 1981.

[4] B. P. Abbott, R. Abbott, T. D. Abbott et al., "Observation of gravitational waves from a binary black hole merger," in *Physical Review Letters*, vol. 116, LIGO Scientific Collaboration and Virgo Collaboration, 2016.

[5] P. O. Hess, "The black hole merger event GW150914 within a modified theory of general relativity," *Monthly Notices of the Royal Astronomical Society*, vol. 462, no. 3, pp. 3026–3030, 2016.

[6] P. O. Hess, "Regge–wheeler and zerilli equations within a modified theory of general relativity," *Astron. Nachr*, vol. 340, no. 1-3, pp. 89–94, 2019.

[7] A. Einstein, "A generalization of the relativistic theory of gravitation," *Annals of Mathematics: Second Series*, vol. 46, pp. 578–584, 1945.

[8] A. Einstein, "A generalized theory of gravitation," *Reviews of Modern Physics*, vol. 20, pp. 35–39, 1948.

[9] M. Born, "A suggestion for unifying Quantum Theory and Relativity," *Proceedings of the Royal Society London. Series A: Mathematical and Physical Sciences*, vol. 165, no. 921, pp. 291–303, 1938.

[10] M. Born, "Reciprocity Theory of Elementary Particles," *Reviews of Modern Physics*, vol. 21, no. 3, pp. 463–473, 1949.

[11] E. R. Caianiello, "Is there a maximal acceleration?" *Lettere al Nuovo Cimento*, vol. 32, no. 3, pp. 65–70, 1981.

[12] P. O. Hess, M. Schäfer, and W. Greiner, *Psuedo-Complex General Relativity*, Springer, Heidelberg, Germany, 2016.

[13] P. F. Kelly and R. B. Mann, "Ghost properties of algebraically extended theories of gravitation," *Classical and Quantum Gravity*, vol. 3, no. 4, pp. 705–712, 1986.

[14] A. Nielsen and O. Birnholz, "Testing pseudo-complex general relativity with gravitational waves," *Astronomical Notes*, vol. 339, p. 298, 2018.

[15] P. O. Hess and W. Greiner, "Pseudo-complex general relativity," *International Journal of Modern Physics E*, vol. 18, p. 51, 2009.

[16] P. O. Hess and W. Greiner, *Centennial of General Relativity: A Celebration*, C. A. Z. Vasconcellos, Ed., World Scientific, Singapore, 2017.

[17] R. Adler, M. Bazin, and M. Schiffer, *Introduction to General Relativity*, McGraw-Hill, New York, NY, USA, 2nd edition, 1975.

[18] I. Rodríguez, P. O. Hess, S. Schramm, and W. Greiner, "Neutron stars within pseudo-complex General Relativity," *Journal of Physics G*, vol. 41, Article ID 105201, 2014.

[19] N. D. Birrell and P. C. W. Davies, *Quantum Fields in Curved Space*, Cambridge University Press, Cambridge, UK, 1986.

[20] M. Visser, "Gravitational vacuum polarization. III. Energy conditions in the (1+1)-dimensional Schwarzschild spacetime," *Physical Review D: Particles, Fields, Gravitation and Cosmology*, vol. 54, no. 8, pp. 5116–5122, 1996.

[21] G. Caspar, T. Schönenbach, P. O. Hess, M. Schäfer, and W. Greiner, "Pseudo-complex General Relativity: Schwarzschild, Reissner-Nordström and Kerr solutions," *International Journal of Modern Physics E*, vol. 21, Article ID 1250015, 2012.

[22] T. Schönenbach, PhD thesis, Universität Frankfurt am Main, Germany, 2014.

[23] T. Schönenbach, G. Caspar, P. O. Hess et al., "Experimental tests of pseudo-complex general relativity," *Monthly Notices of the Royal Astronomical Society*, vol. 430, no. 4, pp. 2999–3009, 2013.

[24] T. Boller, P. O. Hess, A. Müller, and H. Stöcker, "Predictions of the pseudo-complex theory of gravity for EHT observations – I. Observational tests," *Monthly Notices of the Royal Astronomical Society*, vol. 485, no. L34, 2019.

[25] P. O. Hess, T. Boller, A. Müller, and H. Stöcker, "Predictions of the pseudo-complex theory of Gravity for EHT observations – II: theory and predictions," *Monthly Notices of the Royal Astronomical Society*, vol. 482, no. L121, 2019.

[26] The Event Horizon Telescope collaboration, "First M87 event horizon telescope results. v. physical origin of the asymmetric ring," *The Astrophysical Journal Letters*, vol. 875, no. L1, 2019a.

[27] The Event Horizon Telescope collaboration, "First M87 event horizon telescope results. v. physical origin of the asymmetric ring," *The Astrophysical Journal Letters*, vol. 875, no. L2, 2019b.

[28] The Event Horizon Telescope collaboration, "First M87 event horizon telescope results. v. physical origin of the asymmetric ring," *The Astrophysical Journal Letters*, vol. L3, 2019c.

[29] The Event Horizon Telescope collaboration, "First M87 event horizon telescope results. v. physical origin of the asymmetric ring," *The Astrophysical Journal Letters*, vol. l4, 2019d.

[30] The Event Horizon Telescope collaboration, "First M87 event horizon telescope results. v. physical origin of the asymmetric ring," *The Astrophysical Journal Letters*, vol. 875, no. L5, 2019e.

[31] The Event Horizon Telescope collaboration, "First M87 event horizon telescope results. v. physical origin of the asymmetric ring," *The Astrophysical Journal Letters*, vol. 875, no. L6, 2019f.

[32] D. N. Page and K. S. Thorne, "Disk-accretion onto a black hole. time-averaged structure of accretion disk," *Astrophysical Journal*, vol. 191, pp. 499–506, 1974.

[33] T. Schönenbach, G. Caspar, P. O. Hess et al., "Ray-tracing in pseudo-complex General Relativity," *Monthly Notices of the Royal Astronomical Society*, vol. 442, no. 1, pp. 121–130, 2014.

[34] P. O. Hess, L. Maghlaoui, and W. Greiner, "The Robertson-Walker metric in a pseudo-complex General Relativity," *International Journal of Modern Physics E*, vol. 19, p. 1315, 2010.

[35] G. Caspar, I. Rodríguez, P. O. Hess, and W. Greiner, "Vacuum fluctuation inside a star and their consequences for neutron stars, a simple model," *International Journal of Modern Physics E*, vol. 25, Article ID 1650027, 2016.

[36] W. Kluzniak and S. Rappaport, "Magnetically torqued thin accretion disks," *The Astrophysical Journal*, vol. 671, no. 2, p. 1990, 2007.

[37] K. Dodds-Eden, D. Porquet, G. Trap et al., "Evidence For X-ray synchrotron emission from simultaneous mid-infrared to X-ray observations of a strong Sgr A* flare," *Astronomical Physical Journal*, vol. 698, p. 676, 2009.

[38] M. Maggiore, *Gravitational Waves*, vol. 1, Oxford Univ. Press, Oxford, UK, 2008.

[39] T. Regge and J. A. Wheeler, "Stability of a Schwarzschild singularity," *Physical Review A: Atomic, Molecular and Optical Physics*, vol. 108, no. 4, pp. 1063–1069, 1957.

[40] S. Chandrasekhar, *The Mathematical Theory of Black Holes*, The Clarendon Press, New York, NY, USA, 1st edition, 1983.

[41] H. Cho, A. S. Cornell, J. Doukas, T.-R. Huang, and W. Naylor, "A new approach to black hole quasinormal modes: a review of the asymptotic iteration method," *Advances in Mathematical Physics*, vol. 2012, Article ID 281705, 2012.

[42] V. Dexheimer and S. Schramm, "Proto-neutron and neutron stars in a Chiral SU(3) model," *The Astrophysical Journal*, vol. 683, p. 943, 2008.

[43] G. L. Volkmer, *Um Objeto Compacto Excotico na Relatividade Geral Pseudo-Complexa [Ph. D. thesis]*, Porto Alegre, Brazil, March 2018.

[44] M. Razeira, D. Hadjimichef, M. V. T. Machado, F. Köpp, G. L. Volkmer, and C. A. Z. Vasconcellos, "Effective field theory for neutron stars with WIMPS in the pc-GR formalism," *Astronomische Nachrichten*, vol. 338, p. 1073, 2017.

[45] D. Hadjimichef, G. L. Volkmer, R. O. Gomes, and C. A. Z. Vasconcellos, *Memorial Volume: Walter Greiner*, P. O. Hess and H. Stöcker, Eds., World Scientific, Singapore, 2018.

[46] G. L. Volkmer and D. Hadjimichef, "Mimetic dark matter in pseudo-complex General Relativity," *International Journal of Modern Physics: Conference Series*, vol. 45, Article ID 1760012, 2017.

Hindawi
Advances in High Energy Physics
Volume 2019, Article ID 1879568, 10 pages
https://doi.org/10.1155/2019/1879568

Research Article

Perihelion Advance and Trajectory of Charged Test Particles in Reissner-Nordstrom Field via the Higher-Order Geodesic Deviations

Malihe Heydari-Fard,[1] **Saeed Fakhry**,[2] **and Seyedeh Nahid Hasani**[1]

[1]*Department of Physics, The University of Qom, P.O. Box 37185-359, Qom, Iran*
[2]*Department of Physics, Shahid Beheshti University, G. C., Evin, Tehran 19839, Iran*

Correspondence should be addressed to Malihe Heydari-Fard; heydarifard@qom.ac.ir

Received 20 February 2019; Revised 4 May 2019; Accepted 20 May 2019; Published 3 June 2019

Guest Editor: Saibal Ray

By using the higher-order geodesic deviation equations for charged particles, we apply the method described by Kerner et.al. to calculate the perihelion advance and trajectory of charged test particles in the Reissner-Nordstrom space-time. The effect of charge on the perihelion advance is studied and we compared the results with those obtained earlier via the perturbation method. The advantage of this approximation method is to provide a way to calculate the perihelion advance and orbit of planets in the vicinity of massive and compact objects without considering Newtonian and post-Newtonian approximations.

1. Introduction

The problem of planets motion in general relativity is the subject of many studies in which the planet has been considered as a test particle moving along its geodesic [1]. Einstein made the first calculations in this regard for the planet Mercury in the Schwarzschild space-time which resulted in the equation for the perihelion advance

$$\Delta\varphi = \frac{6\pi GM}{a\left(1-e^2\right)}, \tag{1}$$

where G is the gravitational constant, M is the mass of the central body, a is the length of semi-major axis for planet's orbit, and e is eccentricity. Derivation of perihelion advance by using this method leads to a quasielliptic integral whose calculation is very difficult, which is then evaluated after expanding the integrand in a power series of the small parameter GM/rc^2. For the low-eccentricity trajectories of planets, one can obtain the following approximate formula for the perihelion advance:

$$\Delta\varphi = \frac{6\pi GM}{a\left(1-e^2\right)} \simeq \frac{6\pi GM}{a}\left(1+e^2+e^4+e^6+\cdots\right), \tag{2}$$

even for the case of Mercury up to second-order of eccentricity, the perihelion advance differs only by 0.18% error from its actual value [2]. It should be noted again that Einstein's method is only valid for the small values of GM/rc^2.

In what follows, we show that one can obtain the same results (without taking the complex integrals) only by considering the successive approximations around a circular orbit in the equatorial plane as the initial geodesic with constant angular velocity, which leads to an iterative process of the solving the geodesic deviation equations of first, second, and higher-orders [3–5]. Here, instead of the GM/rc^2 parameter the eccentricity, e, plays the role of the small parameter which is controlling the maximal deviation from the initial circular orbit. In this method, we have no constraint on GM/rc^2 anymore. So, one can determine the value of perihelion advance for large mass objects and write it in the higher-order of GM/rc^2.

The orbital motions of neutral test particles via the higher-order geodesic deviation equations for Schwarzschild and Kerr metrics are studied in [2] and [4], respectively. Also, for massive charged particles in Reissner-Nordstrom metric, geodesic deviations have been extracted up to first order [6].

In this paper, by using the higher-order geodesic deviations for charged particles [7], we are going to obtain the orbital motion and trajectory of charged particles. We also expect that our calculations reduce to similar one in Schwarzschild metric [2] by elimination of charge. In fact, we generalize the novel method used in [2] for neutral particles in the Schwarzschild metric to the charged particles in the Reissner-Nordstrom metric. Recently, an analytical computation of the perihelion advance in general relativity via the Homotopy perturbation method has been proposed in [8]. Also, one can study the perihelion advance of planets in general relativity and modified theories of gravity by using different methods in [8–21].

The structure of the paper is as follows. In Section 2, by using the approximation method introduced in [7], we derive the higher-order geodesic deviation for charged particles. By using the first-order geodesic deviation equations, the orbital motion of charged particles is found in Section 3. In Section 4, we obtain the second-order geodesic deviations and derive the semi-major axis, eccentricity, and trajectory using the Taylor expansion around a central geodesic. The obtained results are discussed in Section 5.

2. The Higher-Order Geodesic Deviation Method

As is mentioned above, the higher-order geodesic deviation equations for charged particles have been derived in [7] for the first time. In this section, we are going to derive the geometrical set-up used in our work. The geodesic deviation equation for charged particles is [6]

$$\frac{D^2n^\mu}{Ds^2} = R^\mu{}_{\lambda\nu\kappa}u^\lambda u^\nu n^\kappa + \frac{q}{m}F^\mu{}_\nu\frac{Dn^\nu}{Ds} + \frac{q}{m}\nabla_\lambda F^\mu{}_\nu u^\nu n^\lambda, \quad (3)$$

where D/Ds is the covariant derivative along the curve and n^μ is the separation vector between two particular neighboring geodesics (see Figure 1). Here, u^μ is the tangent vector to the geodesic, $R^\mu{}_{\lambda\nu\kappa}$ is the curvature tensor of space-time, q and m are charge and mass of particles (particles have the same charge-to-mass ratio, q/m), and $F^\mu{}_\nu$ is the electromagnetic force acting on the charged particles. For neutral particles, the above equation reduces to the following geodesic deviation [22, 23]:

$$\frac{D^2n^\mu}{Ds^2} = R^\mu{}_{\lambda\nu\kappa}u^\lambda u^\nu n^\kappa, \quad (4)$$

which is the well-known equation (Jacobi equation) in general relativity. We introduce the four-velocity $u^\alpha(s,p) = \partial x^\alpha/\partial s$ as the time-like tangent vector to the world-line and $n^\alpha(s,p) = \partial x^\alpha/\partial p$ as the deviation four-vector as well. Practically it is often convenient to work with the nontrivial covariant form. It can be obtained by replacement of the trivial expressions for the covariant derivatives, the Riemann curvature tensor, and use of the equation of motion in the left-hand side of (3) [6]

$$\frac{d^2n^\mu}{ds^2} + \left(2\Gamma^\mu{}_{\kappa\nu}u^\kappa - \frac{q}{m}F^\mu{}_\nu\right)\frac{dn^\nu}{ds} + \left(u^\kappa u^\sigma\partial_\nu\Gamma^\mu{}_{\kappa\sigma} - \frac{q}{m}u^\kappa\partial_\nu F^\mu{}_\kappa\right)n^\nu = 0. \quad (5)$$

The geodesic deviation can be used to compose geodesics $x^\mu(s)$ near a given reference geodesic $x_0^\mu(s)$, by an iterative method as follows. Considering this, one can write Taylor expansion of $x^\mu(s,p)$ around the central geodesic and obtain the first-order and higher-order geodesic deviations for charged particles

$$x^\mu(s,p) = x^\mu(s,p_0) + (p-p_0)\left.\frac{\partial x^\mu}{\partial p}\right|_{(s,p_0)} + \frac{1}{2!}(p-p_0)^2\left.\frac{\partial^2x^\mu}{\partial p^2}\right|_{(s,p_0)} + \cdots, \quad (6)$$

and our aim is to obtain an expression in terms of the deviation vector. As shown in the above equation, the second term, $\partial x^\mu/\partial p$, is the definition of deviation vector and shows the first-order geodesic deviation. But in the third term, $\partial^2x^\mu/\partial p^2$ is not vector anymore. Therefore, we define the vector b^μ as follows:

$$b^\mu = \frac{Dn^\mu}{Dp} = \frac{\partial n^\mu}{\partial p} + \Gamma^\mu_{\lambda\nu}n^\lambda n^\nu, \quad (7)$$

to change $\partial^2x^\mu/\partial p^2$ into the expression showing the second-order geodesic deviation. By substituting (7) into (6), one can obtain the expression in terms of the order of vector deviation

$$x^\mu(s,p) = x^\mu(s,p_0) + (p-p_0)n^\mu + \frac{1}{2!}(p-p_0)^2\left(b^\mu - \Gamma^\mu_{\lambda\nu}n^\lambda n^\nu\right) + \cdots \quad (8)$$

In the above expression, one can make some changes for simplification. We consider $\delta^n x^\mu(s)$ as n-th order of geodesic deviation and by assuming $(p-p_0)$ as a small quantity, ϵ; we rewrite (8) as follows:

$$x^\mu(s,p) = x_0^\mu(s) + \delta x^\mu(s) + \frac{1}{2}\delta^2x^\mu(s) + \cdots, \quad (9)$$

where $\delta x^\mu(s) = \epsilon n^\mu(s)$ is the first-order geodesic deviation and $\delta^2x^\mu(s) = \epsilon^2(b^\mu - \Gamma^\mu_{\nu\lambda}n^\nu n^\lambda)$ is the second-order geodesic deviation. In order to obtain the second-order geodesic deviation equation, one can apply the definition of the

covariant derivative on (7)(for more details see [7] and appendix therein)

$$\begin{aligned}
&\frac{D^2 b^\mu}{Ds^2} + R^\mu{}_{\rho\lambda\sigma} u^\rho u^\lambda n^\sigma \\
&\quad = \left(R^\mu{}_{\rho\lambda\sigma;\nu} - R^\mu{}_{\sigma\nu\rho;\lambda}\right) u^\lambda u^\sigma n^\rho n^\nu \\
&\qquad + 4R^\mu{}_{\rho\lambda\sigma} u^\lambda \frac{Dn^\rho}{Ds} n^\sigma + \frac{q}{m} R^\mu{}_{\sigma\rho\nu} F^\rho{}_\lambda n^\sigma u^\lambda n^\nu \\
&\qquad + \frac{q}{m} F^\mu{}_{\rho;\lambda\sigma} n^\lambda u^\rho n^\sigma + \frac{q}{m} F^\mu{}_\rho \frac{D^2 u^\rho}{Dp^2}.
\end{aligned} \tag{10}$$

Similar to the first-order geodesic deviation (5), we can write (10) in the nonmanifest covariant form

$$\begin{aligned}
&\frac{d^2 b^\mu}{ds^2} + \left(2\Gamma^\mu_{\kappa\nu} u^\kappa - \frac{q}{m} F^\mu{}_\nu\right) \frac{db^\nu}{ds} \\
&\quad + \left(u^\kappa u^\sigma \partial_\nu \Gamma^\mu_{\kappa\sigma} - \frac{q}{m} u^\kappa \partial_\nu F^\mu{}_\kappa\right) b^\nu = \\
&+ \left(\Gamma^\tau_{\sigma\nu} \partial_\tau \Gamma^\mu_{\lambda\rho} + 2\Gamma^\mu_{\lambda\tau} \partial_\rho \Gamma^\tau_{\sigma\nu} - \partial_\nu \partial_\sigma \Gamma^\mu_{\lambda\rho}\right) \\
&\quad \cdot \left(u^\lambda u^\rho n^\sigma n^\nu - u^\sigma u^\nu n^\lambda n^\rho\right) \\
&\quad + 4\left(\partial_\lambda \Gamma^\mu_{\sigma\rho} + \Gamma^\nu_{\sigma\rho} \Gamma^\mu_{\lambda\nu}\right) \frac{dn^\sigma}{ds} \left(u^\lambda n^\rho - u^\rho n^\lambda\right) + \frac{q}{m} \\
&\quad \cdot u^\nu n^\alpha n^\beta \left(\partial_\alpha \partial_\beta F^\mu{}_\nu - F^\mu{}_\rho \partial_\nu \Gamma^\rho_{\alpha\beta} - \partial_\sigma F^\mu{}_\nu \Gamma^\sigma_{\alpha\beta}\right) + 2\frac{q}{m} \\
&\quad \cdot n^\sigma \frac{dn^\nu}{ds} \left(\partial_\sigma F^\mu{}_\nu - F^\mu{}_\beta \Gamma^\beta_{\sigma\nu}\right).
\end{aligned} \tag{11}$$

As it clears, the left-hand side of the second-order geodesic deviation equation (11) is same to the left-hand side of (5). As in the case of the second-order geodesic deviation, the higher-order geodesic deviation equations have the same left-hand side and different right-hand side. A nonmanifest covariant form of the third-order geodesic deviation equation is given in Appendix A.

The successive approximations to the exact geodesic (b) have been shown in Figure 1. Lines (c) and (d) represent the first-order approximation, i.e., $x^\mu(s,p) = x^\mu(s,p_0) + (p-p_0)(\partial x^\mu/\partial p)|_{p_0}$, and the second-order approximation, i.e., $x^\mu(s,p) = x^\mu(s,p_0) + (p-p_0)(\partial x^\mu/\partial p)|_{p_0} + (1/2!)(p-p_0)^2(\partial^2 x^\mu/\partial p^2)|_{p_0}$, respectively.

In the next section, we are going to obtain the components of n^μ from the first-order geodesic deviation, (5), for a circular orbit of charged particles. Then by substituting them into (11), we can solve the second-order geodesic deviation equations, b^μ. Finally, by substituting n^μ and b^μ into (8), we will find the relativistic trajectory of charged particles in Reissner-Nordstrom space-time.

3. The First-Order Geodesic Deviation

3.1. Circular Orbits in Reissner-Nordstrom Metric. The Reissner-Nordstrom metric is a static exact solution of the

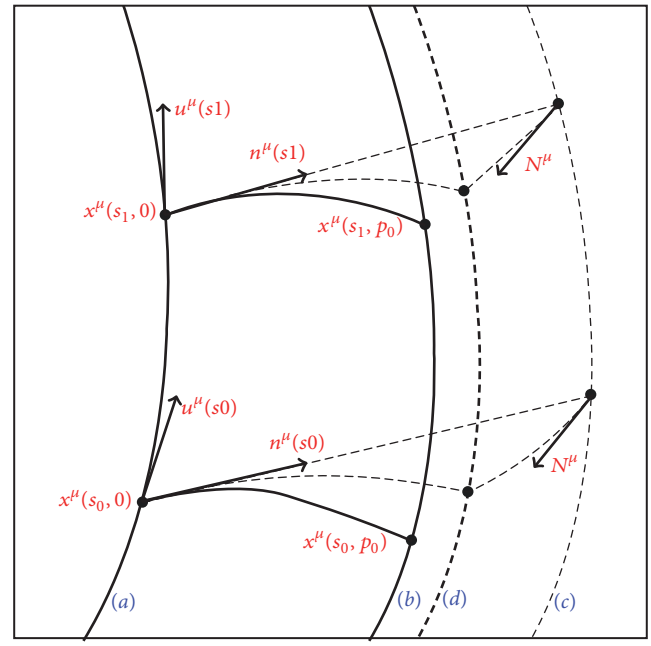

Figure 1: Deviation of two nearby geodesics in a gravitational field. Lines (a) and (b) represent the central geodesic $p = 0$ and the nearby geodesic $p = p_0$, respectively; lines (c) and (d) show the corresponding first and second-order approximations to the nearby geodesic (b). Also, u^μ is the unit tangent vector to the central world-line, n^μ is the separation vector to the curve $s = const$, and $N^\mu = b^\mu - \Gamma^\mu_{\lambda\rho} n^\lambda n^\rho$ is the second-order geodesic deviation [24].

Einstein-Maxwell equations which describes the space-time around a spherically nonrotating charged source with mass M and charge Q (in the natural coordinate with $c = 1$ and $G = 1$)

$$\begin{aligned}
ds^2 &= -B(r)\, dt^2 + \frac{1}{B(r)} dr^2 \\
&\quad + r^2 \left(d\theta^2 + \sin^2(\theta)\, d\varphi^2\right),
\end{aligned} \tag{12}$$

where

$$B(r) = 1 - \frac{2M}{r} + \frac{Q^2}{r^2}. \tag{13}$$

Also, the vector potential and the electromagnetic field of Maxwell's equations are [6]

$$\begin{aligned}
A &= A_\mu dx^\mu = -\frac{Q}{4\pi r} dt, \\
F &= dA = \frac{Q}{4\pi r^2} dr \wedge dt.
\end{aligned} \tag{14}$$

By assuming that $M^2 > Q^2$, we are going to obtain the equation of motion for test particles which have mass m and charge q. Now, we consider a circular orbit with a constant radius R. On the other hand, we know that the angular momentum of particles which are bounded to the spherically symmetric condition is limited to the equatorial plane. For

this purpose and for simplicity, we limit the space to the plane of $\theta = \pi/2$ in which the angular momentum is in the z direction. By using of the Euler-Lagrange equation, one can lead to the following constants of motion:

$$\frac{d\varphi}{ds} = \frac{l}{r^2}, \tag{15}$$

$$\frac{dt}{ds} = \frac{\varepsilon - qQ/4\pi mr}{1 - 2M/r + Q^2/r^2}, \tag{16}$$

where $l = J/m$ is the angular momentum per unit mass, $\dot{\varphi} = \omega$ is the angular velocity, and ε is the energy per unit mass.

Finally, from (12), (15), and (16) one obtains two constraints, namely, the conservation of the absolute four-velocity and the radial acceleration. Now, due to the fact that the radius of the circular orbit is constant ($r = R$), two mentioned constraints vanish at all times and this creates two relations between R, l, and ε as follows:

$$\left(\varepsilon - \frac{qQ}{4\pi MR}\right)^2 = \left(1 - \frac{2M}{R} + \frac{Q^2}{R^2}\right)\left(1 + \frac{l^2}{R^2}\right), \tag{17}$$

$$\left[\frac{l^2}{R} - M\left(1 + \frac{3l^2}{R^2}\right) + \frac{Q^2}{R}\left(1 + \frac{2l^2}{R^2}\right)\right]^2 = \left(\frac{qQ}{4\pi m}\right)^2\left(1 + \frac{l^2}{R^2}\right)\left(1 - \frac{2M}{R} + \frac{Q^2}{R^2}\right). \tag{18}$$

As we expect by eliminating charge, all obtained equations reduce to the similar equations in the Schwarzschild metric.

In summary, we obtain the following four-velocity vector for a circular orbit with radius R in an equatorial plane:

$$\begin{aligned} u^t &= \frac{dt}{ds} = \frac{\varepsilon - qQ/4\pi mR}{1 - 2M/R + Q^2/R^2}, \\ u^r &= \frac{dr}{ds} = 0, \\ u^\theta &= \frac{d\theta}{ds} = 0, \\ u^\varphi &= \frac{d\varphi}{ds} = \omega_0 = \frac{l}{R^2}. \end{aligned} \tag{19}$$

In the next subsection, we obtain the orbital motion by using the higher-order geodesic deviation method and compare the results with the perturbation method.

3.2. First-Order Geodesic Deviation around the Circular Orbits. Now let us calculate the first-order geodesic deviation for the components n^t, n^r, n^θ, and n^ϕ, by using of (5) in a matrix form

$$\begin{pmatrix} m_{11} & m_{12} & m_{13} & m_{14} \\ m_{21} & m_{22} & m_{23} & m_{24} \\ m_{31} & m_{32} & m_{33} & m_{34} \\ m_{41} & m_{42} & m_{43} & m_{44} \end{pmatrix} \begin{pmatrix} n^t \\ n^r \\ n^\theta \\ n^\varphi \end{pmatrix} = \begin{pmatrix} 0 \\ 0 \\ 0 \\ 0 \end{pmatrix}, \tag{20}$$

where the matrix elements are given by

$$\begin{aligned} m_{11} &= \frac{d^2}{ds^2}, \\ m_{12} &= \frac{2R\varepsilon\left(M/R - Q^2/R^2\right) - \left(qQ/4\pi m\right)\left(1 - Q^2/R^2\right)}{R^2\left(1 - 2M/R + Q^2/R^2\right)^2}\frac{d}{ds}, \\ m_{13} &= m_{14} = 0, \\ m_{22} &= \frac{d^2}{ds^2} - \frac{l^2}{R^4}\left(1 - \frac{Q^2}{R^2}\right) + \frac{\left(-2M/R + 6M^2/R^2 + 3Q^2/R^2 - 12MQ^2/R^3 + 5Q^4/R^4\right)\left(\varepsilon - qQ/4\pi mR\right)^2}{R^2\left(1 - 2M/R + Q^2/R^2\right)^2} - \frac{q}{m}F^r_{t,r}u^t, \\ m_{21} &= \frac{2}{R}\left(\frac{M}{R} - \frac{Q^2}{R^2}\right)\left(\varepsilon - \frac{qQ}{4\pi mR}\right)\frac{d}{ds} - \frac{q}{m}F^r_t\frac{d}{ds}, \\ m_{23} &= 0, \\ m_{24} &= -\frac{2l}{R}\left(1 - \frac{2M}{R} + \frac{Q^2}{R^2}\right)\frac{d}{ds}, \\ m_{31} &= m_{32} = m_{34} = 0, \\ m_{33} &= \frac{d^2}{ds^2} + \frac{l^2}{R^4}, \\ m_{41} &= m_{43} = 0, \\ m_{42} &= \frac{2l}{R^3}\frac{d}{ds}, \\ m_{44} &= \frac{d^2}{ds^2}. \end{aligned} \tag{21}$$

As can be seen, the geodesic deviation equation of θ component represents a harmonic oscillator equation with the angular frequency of $\omega_\theta = \omega_0 = l/R^2$. So we consider n^θ as follows:

$$n^\theta(s) = n_0^\theta \cos(\omega_0 s), \tag{22}$$

which is similar to the Schwarzschild case. So in this case we can neglect this solution ($n^\theta = 0$), because the new plane of orbit is a new one inclined, or just a change of coordinate system [4]. Now, by eliminating the derivatives of n^t and n^ϕ in the differential equation of n^r, we obtain the following oscillating equation:

$$\frac{d^2 n^r}{ds^2} + w^2 n^r = 0, \tag{23}$$

with the characteristic frequency

$$\omega^2 = \omega_0^2 \left(1 - \frac{6M}{R} + \frac{Q^2}{MR} + \frac{3Q^2}{R^2} + \cdots\right). \tag{24}$$

By considering $n_0^r > 0$, we choose the following solution for n^r:

$$n^r = -n_0^r \cos(\omega s). \tag{25}$$

Also, from the n^t and n^φ geodesic deviation equations, the solutions for n^t and n^φ are given by

$$n^t = n_0^t \sin(\omega s), \tag{26}$$

$$n^\varphi = n_0^\varphi \sin(\omega s), \tag{27}$$

where the amplitudes depend on n_0^r

$$n_0^t = \frac{2\sqrt{MR - Q^2}}{R\left(1 - 2M/R + Q^2/R^2\right)\sqrt{1 - 6M/R + Q^2/MR}} n_0^r, \tag{28}$$

$$n_0^\varphi = \frac{2}{R\sqrt{1 - 6M/R + Q^2/MR}} n_0^r. \tag{29}$$

In this way, the trajectory and the law of motion are obtained by

$$r = R - n_0^r \cos(\omega s), \tag{30}$$

$$\varphi = \omega_0 s + n_0^\varphi \sin(\omega s), \tag{31}$$

$$t = \frac{\varepsilon - qQ/4\pi mR}{1 - 2M/R + Q^2/R^2} s + n_0^t \sin(\omega s), \tag{32}$$

where the argument phase of the cosine function is taken by $s = 0$ for perihelion and $s = \pi/\omega$ for aphelion. Now, (30) can be written as

$$r = R\left[1 - \frac{n_0^r}{R}\cos(\omega s)\right]. \tag{33}$$

By direct solution of the Euler-Lagrange equations, the trajectory of motion for particles is obtained in terms of centrifugal inertia [25]

$$r(t) = \frac{a\left(1 - e^2\right)}{1 + e\cos(\omega_0 t)} \simeq a\left[1 - e\cos(\omega_0 t)\right]. \tag{34}$$

Obviously, (33) and (34) show that we have the same results. It means that if we bring up the eccentricity e to n_0^r/R and the semimajor axis a to R, the same results are extracted, but there is also a difference that the circular frequency, ω, is lower than the circular frequency of the unperturbed circular motion, ω_0. So, if the circular frequency decreases, the period increases. Then we obtain an expression for the periastron shift per one revolution as

$$\triangle\varphi = 2\pi\left(\frac{\omega_0}{\omega} - 1\right) = 2\pi\left(\frac{3M}{R} + \frac{27}{2}\frac{M^2}{R^2} + \frac{135}{2}\frac{M^3}{R^3} - \frac{Q^2}{2MR} - \frac{6Q^2}{R^2} + \cdots\right). \tag{35}$$

It can be seen from the above equation that the charge parameter, Q, decreases the perihelion advance. In the perturbation method (Einstein's method), the orbital motion for charged particles moving in the equatorial plane of the Reissner-Nordstrom source is given by [20]

$$\triangle\varphi = \frac{6\pi M}{R} - \frac{\pi Q^2}{MR}, \tag{36}$$

and comparing (35) with (36) shows that the presented method can be used in the vicinity of very massive and compact objects which is having a nonnegligible ratio of M/R.

When the source is neutral and for the small values of M/R, (35) reduces to the standard formula for Perihelion advance of planets [23]. If we also compare (35) to (2), it is clear that, in the first-order deviation, we hold only the terms up to e^2. In order to obtain $\triangle\varphi$ for the higher values of the eccentricity, we must go beyond the first-order deviation equations. Therefore in the next section, we solve the second-order geodesic deviation equations in Reissner-Nordstrom space-time.

4. The Second-Order Geodesic Deviation

In this section, by using the first-order geodesic deviation equation and inserting (25), (26), and (27) into (10) and also doing a set of hard calculations, a linear equations system for the second-order geodesic deviation vector b^μ is obtained

$$\begin{pmatrix} m_{11} & m_{12} & m_{14} \\ m_{21} & m_{22} & m_{24} \\ m_{41} & m_{42} & m_{44} \end{pmatrix} \begin{pmatrix} b^t \\ b^r \\ b^\varphi \end{pmatrix} = \left(n_0^r\right)^2 \begin{pmatrix} C^t + C_q^t \\ C^r + C_q^r \\ C^\varphi + C_q^\varphi \end{pmatrix}, \tag{37}$$

where the constants C^t, C^t_q, C^r, C^r_q, C^φ, and C^φ_q contain quantities depending on M, R, ω, ω_0, q, and Q

$$C^t = -\frac{6M\sqrt{MR-Q^2}\left(2-7M/R+31Q^2/3R^2-5Q^2/3MR-4Q^4/3MR^3-Q^4/M^2R^2\right)}{R^5\left(1-2M/R+Q^2/R^2\right)\left(1-3M/R+2Q^2/R^2\right)\sqrt{1-6M/R+Q^2/MR}}\sin(2\omega s), \tag{38}$$

$$\begin{aligned} C^r = &-\frac{3M\left[6-27M/R+6M^2/R^2+158Q^2/3R^2-22Q^2/3MR-14MQ^2/R^3-16Q^4/3R^4-4Q^4/M^2R^2\right]}{2R^4\left(1-3M/R+2Q^2/R^2\right)\left(1-6M/R+Q^2/MR\right)}\cos(2\omega s)\\ &+\frac{3M\left[2-5M/R+18M^2/R^2+6Q^2/R^2-10Q^2/3MR-34MQ^2/R^3+4Q^4/M^2R^2\right]}{2R^4\left(1-3M/R+2Q^2/R^2\right)\left(1-6M/R+Q^2/MR\right)}, \end{aligned} \tag{39}$$

$$C^\varphi = -\frac{6M\omega_0\left[1-3M/R+2M^2/R^2+5Q^2/R^2-4Q^2/3MR-8MQ^2/3R^3-Q^4/R^4-Q^4/MR^3\right]}{\omega R^5\left(1-3M/R+2Q^2/R^2\right)\left(1-2M/R+Q^2/R^2\right)}\sin(2\omega s), \tag{40}$$

$$C^t_q = \frac{qQ\sqrt{M/R-Q^2/R^2}\sqrt{1-6M/R+Q^2/R^2}\left[3M/R-31M^2/2R^2+15M^3/R^3+Q^2/R^2+3MQ^2/R^3-7M^2Q^2/R^4\right]}{4\pi mMR^3\sqrt{1-3M/R+2Q^2/R^2}\left(1-2M/R+Q^2/R^2\right)^2\left(1-6M/R+Q^2/MR\right)}\sin(2\omega s), \tag{41}$$

$$\begin{aligned} C^r_q = &\frac{qQ\sqrt{1-3M/R+2Q^2/R^2}\left[7M/R-61M^2/R^2+169M^3/R^3-150M^4/R^4+3Q^2/R^2+11MQ^2/R^3-130M^2Q^2/R^4+198M^3Q^2/R^5\right]}{4\pi mMR^3\left(1-3M/R+2Q^2/R^2\right)\left(1-6M/R+Q^2/MR\right)\left(1-2M/R+Q^2/R^2\right)}\\ &\cdot\cos(2\omega s)\\ &-\frac{qQ\sqrt{1-3M/R+2Q^2/R^2}\left[M/R+5M^2/R^2-45M^3/R^3+54M^4/R^4-3Q^2/R^2+21MQ^2/R^3-2M^2Q^2/R^4-54M^3Q^2/R^5\right]}{4\pi mMR^3\left(1-3M/R+2Q^2/R^2\right)\left(1-6M/R+Q^2/MR\right)\left(1-2M/R+Q^2/R^2\right)}, \end{aligned} \tag{42}$$

$$C^\varphi_q = 0. \tag{43}$$

Here we have not used any approximation in C^i, $(i = r, \theta, \phi)$ but in what follows we neglect terms of higher order of the small parameters M/R, Q/M, and q/m. Solving the matrix equation (10) for b^μ is similar to the approach used in the previous section (for the first-order geodesic deviation vector n^μ) which contains the terms with characteristic frequency ω. Here we are only interested in a particular solution because of the oscillating general solution with the angular frequency ω already taken into account for $n^\mu(s)$. The particular solution of the above equation which is containing the oscillating terms with the angular frequency 2ω, the linear terms in the proper time s, and constants. To obtain the trajectory x^μ according to (9), we need to calculate $(1/2)\delta^2 x^\mu$. Also for x^μ, the perihelion is extracted by $\omega s = 2k\pi$ and the aphelion is derived by $\omega s = (1+2k)\pi$, where $k \in Z$.

In Appendix B, we have put the particular solution of the above equation, b^μ, the second-order geodesic deviation $\delta^2 x^\mu$, and the semimajor axis a and eccentricity e, respectively.

Finally, successive approximation brings us to trajectory by substituting $s(\varphi)$ to $\varphi(s)$

$$\begin{aligned} \frac{r}{R} = &1-\left(\frac{n^r_0}{R}\right)\cos\left(\frac{\omega}{\omega_0}\varphi\right)+\left(\frac{n^r_0}{R}\right)^2\left[\frac{\left(3-5M/R-30M^2/R^2+72M^3/R^3+7Q^2/R^2-7Q^2/MR\right)}{2\left(1-2M/R+Q^2/R^2\right)\left(1-Q^2/MR\right)\left(1-6M/R+Q^2/MR\right)^2}\right.\\ &+\frac{\left(1-7M/R+10M^2/R^2+61Q^2/2R^2-8Q^2/3MR\right)}{2\left(1-2M/R+Q^2/R^2\right)\left(1-6M/R+Q^2/MR\right)}\cos\left(\frac{2\omega}{\omega_0}\varphi\right)\\ &+\frac{(3/2)\,Qq}{32\pi Mm\left(1-Q^2/MR\right)\left(1-2M/R\right)\left(1-3M/R\right)^{3/2}\left(1-6M/R+Q^2/MR\right)^2}\\ &\left.+\frac{(19/2)\,Qq}{32\pi Mm\left(1-Q^2/MR\right)\left(1-2M/R\right)\left(1-3M/R\right)^{3/2}\left(1-6M/R+Q^2/MR\right)^2}\cos\left(\frac{2\omega}{\omega_0}\varphi\right)\right]+\cdots \end{aligned} \tag{44}$$

In the Schwarzschild limit, we have an elliptical orbit with [2]

$$a = R + \frac{\left(n_0^r\right)^2}{R}\left[\frac{\left(2 - 9M/R + 11M^2/R^2 + 6M^3/R^3\right)}{(1-2M/R)(1-6M/R)^2}\right], \tag{45}$$

$$e = \frac{n_0^r (1-2M/R)(1-6M/R)^2}{R(1-2M/R)(1-6M/R)^2 + \left(\left(n_0^r\right)^2/R\right)\left(2 - 9M/R + 11M^2/R^2 + 6M^3/R^3\right)} = \frac{n_0^r}{R} + \mathcal{O}\left(\frac{\left(n_0^r\right)^3}{R^3}\right). \tag{46}$$

Also, for the Schwarzschild case the shape of the orbit is described up to second-order of (n_0^r/R) as

$$\begin{aligned}\frac{r(\varphi)}{R} &= 1 - \left(\frac{n_0^r}{R}\right)\cos\left(\frac{\omega}{\omega_0}\varphi\right) + \left(\frac{n_0^r}{R}\right)^2 \\ &\cdot\left[\frac{3 - 5M/R - 30M^2/R^2 + 72M^3/R^3}{2(1-2M/R)(1-6M/R)^2}\right. \\ &\left. + \frac{(1-5M/R)}{2(1-6M/R)}\cos\left(\frac{2\omega}{\omega_0}\varphi\right)\right] + \cdots.\end{aligned} \tag{47}$$

which is in agreement with equation (62) of reference [2].

5. Third-Order Geodesic Deviation and Poincaré-Lindstedt's Method

In the previous section, we have calculated the trajectory of charged particles up to second-order. To find a more accurate trajectory, we need to obtain the higher-order terms of expansion (9). Using the first and second-order solutions and third-order equation (A.2) for $\delta^3 x^\mu$, we have

$$\begin{pmatrix} m_{11} & m_{12} & m_{14} \\ m_{21} & m_{22} & m_{24} \\ m_{41} & m_{42} & m_{44} \end{pmatrix}\begin{pmatrix} \delta^3 t \\ \delta^3 r \\ \delta^3 \varphi \end{pmatrix} = \epsilon^3 \begin{pmatrix} D^t \\ D^r \\ D^\varphi \end{pmatrix}, \tag{48}$$

where m_{ij} are defined in (20) and the coefficients D_0^i, D_{0q}^i, D_1^i, D_{1q}^i, D_3^i, and D_{3q}^i, $(i = t, r, \varphi)$ are functions of M, R, q, and Q

$$\begin{aligned} D^t &= \left(D_1^t + D_{1q}^t\right)\cos(\omega s) + \left(D_3^t + D_{3q}^t\right)\cos(3\omega s) \\ &\quad + D_0^t + D_{0q}^t, \\ D^r &= \left(D_1^r + D_{1q}^r\right)\cos(\omega s) + \left(D_3^r + D_{3q}^r\right)\cos(3\omega s) \\ &\quad + D_0^r + D_{0q}^r, \\ D^\varphi &= \left(D_1^\varphi + D_{1q}^\varphi\right)\cos(\omega s) + \left(D_3^\varphi + D_{3q}^\varphi\right)\cos(3\omega s) \\ &\quad + D_0^\varphi + D_{0q}^\varphi. \end{aligned} \tag{49}$$

As one can see the right-hand side of (48) has a frequency that is the same as the eigenvalues of the differential matrix in the left-hand side (resonant terms). This makes a new problem, i.e., infinite solution for $\delta^3 r$ which is called the secular term (growing without bound). For avoiding these unbounded deviations we use the Poincaré's method. In this method by replacing ω by infinite series in power of the infinitesimal parameter $\epsilon = n_0^r/R$ as

$$\omega \longrightarrow \omega_p = \omega + \epsilon\omega_1 + \epsilon^2\omega_2 + \epsilon_3\omega^3 + \cdots, \tag{50}$$

the correction frequencies $\omega_1, \omega_2, \omega_3, \cdots$ can be chosen such that Poincaré's resonances vanish, by considering a differential equation for x^μ as

$$\begin{aligned} &\frac{d^2}{ds^2}\left(\delta r + \frac{1}{2}\delta^2 r + \frac{1}{6}\delta^3 r\right) + \omega^2\left(\delta r + \frac{1}{2}\delta^2 r + \frac{1}{6}\delta^3 r\right) \\ &= C_0^r + C_{0q}^r + \left(C^r + C_q^r\right)\cos\left(2\omega_p s\right) \\ &\quad + \left(D_1^r + D_{1q}^r\right)\cos\left(\omega_p s\right) \\ &\quad + \left(D_3^r + D_{3q}^r\right)\cos\left(3\omega_p s\right) + D_0^r + D_{0q}^r. \end{aligned} \tag{51}$$

Now, by developing both of the sides in terms of a series of the parameter ϵ, for avoiding the secular terms, we find some algebraic relations on $\omega_1, \omega_2, \omega_3, \cdots$. In the Schwarzschild limit, we have [4]

$$\begin{aligned} \omega_p &= \frac{M^{1/2}\sqrt{1-6M/R}}{R^{3/2}\sqrt{1-3M/R}} \\ &\quad - \epsilon^2\frac{3M^{3/2}(6 - 37M/R)}{4R^{5/2}\sqrt{1-3M/R}\,(1-6M/R)^{3/2}}, \end{aligned} \tag{52}$$

where $\epsilon^2 = (n_0^r)^2/R^2$. The resonant terms will also appear at the fifth-order approximation; by terms $\cos^5(ws), \sin^3(ws)\cos^2(ws)$, etc., this problem can be solved in a similar way.

Finally, we note that the electric charge of any celestial body is practically close to zero anyway. Therefore, it is worth investigating the geodesic deviation and higher-order geodesic deviations in a more realistic background such as the Schwarzschild metric in a strong magnetic dipole field or magnetized black holes [26–28]. The study of them will be the subject of the future investigations.

6. Conclusion and Discussion

Many of significant successes in general relativity are obtained by approximation methods. One of the most

important approximation scheme in general relativity is the post-Newtonian approximation, an expansion with a small parameter which is the ratio of the velocity of matter to the speed of light. A novel approximation method was also proposed by Kerner et al. which is based on the world-line deviations [2].

The calculation of the perihelion advance by means of the higher-order geodesic deviation method for neutral particles in different gravitational fields such as Schwarzschild and Kerr metric was first studied in several papers [2, 4]. In the present paper by using of the higher-order geodesic deviation method for charged particles [7], we applied this approximation method to charged particles in the Reissner-Nordstrom space-time.

We first started with an orbital motion which is close to a circular orbit with constant angular velocity which is considered as zeroth-approximation (unperturbed circular orbital motion) with the orbital frequency ω_0. In the next step, we solved the first- and second-order deviation equations which reduced to a system of the second-order linear differential equations with constant coefficients. The solutions are harmonic oscillators with characteristic frequency. From (37), the first- and second-order corrections are oscillating terms with angular frequency ω and 2ω, respectively.

Finally, we have obtained the new trajectory by adding the higher-order geodesic deviations (nonlinear effects) to the circular one (44). The advantage of this approach is to get the relativistic trajectories of planets without using Newtonian and post-Newtonian approximations for arbitrary values of quantity M/R.

Appendix

A.

For solving the third-order geodesic deviation equation, we should invoke to Poincare's method. For this purpose, it is better to write the third-order geodesic deviation as $\delta^3 x^\mu$. The third-order geodesic deviation equation $\delta^3 x^\mu$ is related to the third-order geodesic deviation vector h^μ

$$\begin{aligned}&\delta^3 x^\mu \\ &\quad = \epsilon^3 \left[h^\mu - 3\Gamma^\mu_{\lambda\rho} n^\lambda b^\nu + \left(\partial_\kappa \Gamma^\mu_{\lambda\nu} - 2\Gamma^\mu_{\lambda\sigma}\Gamma^\sigma_{\kappa\nu}\right) n^\kappa n^\lambda n^\nu \right],\end{aligned} \tag{A.1}$$

where $h^\mu = Db^\mu/Dp$. We derive the third-order geodesic deviation equation as

$$\begin{aligned}&\frac{d^2\delta^3 x^\mu}{ds^2} + \left(2\Gamma^\mu_{\lambda\nu}u^\lambda - \frac{q}{m}F^\mu{}_\nu\right)\frac{d\delta^3 x^\nu}{ds} + \left(\partial_\sigma \Gamma^\mu_{\lambda\rho}u^\lambda u^\rho \right. \\ &\left. - \frac{q}{m}u^\nu \partial_\sigma F^\mu{}_\nu\right)\delta^3 x^\sigma = \\ &-6\Gamma^\mu_{\lambda\rho}\frac{d\delta x^\lambda}{ds}\frac{d\delta^2 x^\rho}{ds} - 3\delta x^\sigma \left(\partial_\tau\partial_\sigma\Gamma^\mu_{\lambda\rho}\right)u^\lambda\left(\delta^2 x^\tau u^\rho \right. \\ &\left. + 2\delta x^\tau \frac{d\delta x^\rho}{ds}\right) - 6\left(\partial_\sigma\Gamma^\mu_{\lambda\rho}\right)\left(\delta x^\sigma u^\lambda \frac{d\delta^2 x^\rho}{ds}\right. \\ &\left. + \delta x^\sigma \frac{d\delta x^\lambda}{ds}\frac{d\delta x^\rho}{ds} + \delta^2 x^\sigma u^\lambda \frac{d\delta x^\rho}{ds}\right) \\ &- \delta x^\sigma \delta x^\tau \delta x^\nu \left(\partial_\tau\partial_\sigma\partial_\nu\Gamma^\mu_{\lambda\rho}\right)u^\lambda u^\rho + \frac{q}{m} \\ &\cdot \frac{dn^\nu}{ds}\left[\left(\partial_\sigma F^\mu{}_\nu\right)\delta^2 x^\sigma + \left(\partial_\sigma\partial_\tau F^\mu{}_\nu\right)n^\sigma n^\tau\right] + \frac{q}{m} \\ &\cdot n^\sigma\left[\frac{d\delta^2 x^\nu}{ds}\left(\partial_\sigma F^\mu{}_\nu\right) + \left(\partial_\sigma\partial_\tau F^\mu{}_\nu\right)\delta^2 x^\tau u^\nu\right],\end{aligned} \tag{A.2}$$

and by substituting $\delta^3 x^\mu$ in term of h^μ into above equation, we obtain (72) for case $q = 0$ [2].

B.

The second-order geodesic deviation vector b^μ is

$$\begin{aligned}b^t = {} & \frac{\left(n_0^r\right)^2 M\left(\varepsilon - qQ/4\pi mR\right)}{R^3\left(1 - 6M/R + Q^2/MR\right)\left(1 - 2M/R\right)^2}\left[-\frac{3\left(2 - 5M/R + 18M^2/R^2 - (10/3)\left(Q^2/MR\right)\right)}{\left(1 - 6M/R + Q^2/MR\right)}s\right. \\ & \left. + \frac{\left(2 - 13M/R + (79/6)\left(Q^2/MR\right)\right)\sin(2\omega s)}{\omega} - \frac{6qQ\omega s + 19qQ\sin(2\omega s)}{32\pi mM\omega\left(1 - 6M/R + Q^2/MR\right)\left(1 - 2M/R\right)\left(1 - 3M/R\right)^{3/2}}\right],\end{aligned} \tag{B.1}$$

$$\begin{aligned}b^r = {} & \frac{\left(n_0^r\right)^2 M}{2R^2\left(M/R - Q^2/R^2\right)\left(1 - 6M/R + Q^2/MR\right)}\left[\frac{3\left(2 - 5M/R + 18M^2/R^2 - (10/3)\left(Q^2/MR\right)\right)}{\left(1 - 6M/R + Q^2/MR\right)}\right. \\ & \left. + \left(2 + \frac{5M}{R} - \frac{28}{3}\frac{Q^2}{MR}\right)\cos(2\omega s) + \frac{3qQ + 19qQ\cos(2\omega s)}{16\pi mM\left(1 - 6M/R + Q^2/MR\right)\left(1 - 2M/R\right)\left(1 - 3M/R\right)^{3/2}}\right],\end{aligned} \tag{B.2}$$

$$\begin{aligned}b^\varphi = {} & \frac{\left(n_0^r\right)^2 \omega_0 M}{R^3\left(M/R - Q^2/R^2\right)\left(1 - 6M/R + Q^2/MR\right)}\left[-\frac{3\left(2 - 5M/R + 18M^2/R^2 - (10/3)\left(Q^2/MR\right)\right)}{\left(1 - 6M/R + Q^2/MR\right)}s\right. \\ & \left. + \frac{(1 - 8M/R)\sin(2\omega s)}{2\omega} - \frac{6qQs + qQ\,(31 - 196M/R)\sin(2\omega s)}{32\pi mM\left(1 - 6M/R + Q^2/MR\right)\left(1 - 2M/R\right)\left(1 - 3M/R\right)^{3/2}}\right].\end{aligned} \tag{B.3}$$

As explained in Section 2 the second-order geodesic deviation, $(\delta^2 x = b^\mu - \Gamma^\mu_{\nu\lambda} n^\nu n^\lambda)$, is given by

$$\begin{aligned}\delta^2 t = {} & \frac{\left(n_0^r\right)^2 M\left(\varepsilon - qQ/4\pi mR\right)}{R^3}\left[-\frac{3\left(2-5M/R+18M^2/R^2-10Q^2/3MR\right)}{\left(1-2M/R\right)^2\left(1-6M/R+Q^2/MR\right)}s\right.\\ & + \frac{\left(2-15M/R+14M^2/R^2-79Q^2/6MR\right)\sin\left(2\omega s\right)}{\omega\left(1-2M/R\right)^3\left(1-6M/R+Q^2/MR\right)}\\ & \left. - \frac{6qQ\omega + 19qQ\sin\left(2\omega s\right)}{32\pi mM\omega\left(1-2M/R\right)^3\left(1-3M/R\right)^{3/2}\left(1-6M/R+Q^2/M\mathrm{R}\right)^2}\right],\end{aligned} \tag{B.4}$$

$$\begin{aligned}\delta^2 r = {} & \frac{\left(n_0^r\right)^2 M}{R^2\left(M/R-Q^2\right)\left(1-6M/R+Q^2/MR\right)}\left[\frac{\left(5-33M/R+90M^2/R^2-72M^3/R^3+5Q^2/R^2-5Q^2/MR\right)}{\left(1-2M/R+Q^2/R^2\right)\left(1-6M/R+Q^2/MR\right)}\right.\\ & + \frac{\left(-1+9M/R+33Q^2/2R^2-19M^2/R^2-(23/2)\left(MQ^2/R^3\right)-8Q^2/3MR\right)\cos\left(2\omega s\right)}{\left(1-2M/R+Q^2/R^2\right)}\\ & \left. + \frac{3qQ+19Qq\cos\left(2\omega s\right)}{32\pi mM\left(1-2M/R\right)\left(1-3M/R\right)^{3/2}\left(1-6M/R+Q^2/MR\right)}\right],\end{aligned} \tag{B.5}$$

$$\begin{aligned}\delta^2\varphi = {} & \frac{\left(n_0^r\right)^2 M\omega_0}{R^3\left(M/R-Q^2/R^2\right)\left(1-6M/R+Q^2/MR\right)}\left[-\frac{3\left(2-5M/R+18M^2/R^2-10Q^2/3MR\right)}{\left(1-6M/R+Q^2/MR\right)}s\right.\\ & + \frac{\left(5-32M/R\right)\sin\left(2\omega s\right)}{2\omega} - \left.\frac{6qQs + qQ\left(31-196M/R\right)\sin\left(2\omega s\right)}{32\pi mM\left(1-2M/R\right)\left(1-3M/R\right)^{3/2}\left(1-6M/R+\mathrm{Q}^2/MR\right)}\right],\end{aligned} \tag{B.6}$$

and, also, the semimajor axis a and eccentricity e are

$$a = R + \frac{\left(n_0^r\right)^2}{R}\left[\frac{\left(2-9M/R+11M^2/R^2+6M^3/R^3+15Q^2/R^2-13Q^2/3MR-235MQ^2/4R^3\right)}{\left(1-2M/R+Q^2/R^2\right)\left(1-Q^2/MR\right)\left(1-6M/R+Q^2/MR\right)^2}\right], \tag{B.7}$$

$$e = \frac{n_0^r\left(1-2M/R+Q^2/R^2\right)\left(1-Q^2/MR\right)\left(1-6M/R+Q^2/M\mathrm{R}\right)^2}{R\left(1-2M/R+Q^2/R^2\right)\left(1-Q^2/MR\right)\left(1-6M/R+Q^2/MR\right)^2+\left(\left(n_0^r\right)^2/R\right)\left(2-9M/R+11M^2/R^2+6M^3/R^3+15Q^2/R^2-13Q^2/3MR-235MQ^2/4R^3\right)}, \tag{B.8}$$

in which for massive central objects we have neglected all terms of order $qQ/4\pi mM$.

Data Availability

The data findings of this study are available within the article and could be open access.

Conflicts of Interest

The authors declare that they have no conflicts of interest.

References

[1] A. Einstein, "Die Grundlage der allgemeinen relativitätstheorie [AdP 49, 769 (1916)]," in *Annalen der Physik*, vol. 14, 2005.

[2] R. Kerner, J. W. van Holten, and J. Colistete, "Relativistic epicycles: another approach to geodesic deviations," *Classical and Quantum Gravity*, vol. 18, p. 4725, 2001.

[3] R. Kerner, J. Martin, S. Mignemi, and J.-W. van Holten, "Geodesic deviation in Kaluza-KLEin theories," *Physical Review D: Particles, Fields, Gravitation and Cosmology*, vol. 63, Article ID 027502, 2001.

[4] J. Colistete, C. Leygnac, and R. Kerner, "Higher-order geodesic deviations applied to the Kerr metric," *Classical and Quantum Gravity*, vol. 19, p. 4573, 2002.

[5] J. W. van Holten, "World-Line deviations and epicycles," *International Journal of Modern Physics A*, vol. 17, no. 20, p. 2764, 2002.

[6] A. Balakin, J. W. van Holten, and R. Kerner, "Motions and worldline deviations in Einstein-Maxwell theory," *Classical and Quantum Gravity*, vol. 17, p. 5009, 2000.

[7] M. Heydari-Fard and S. N. Hasani, "Higher-order geodesic deviation for charged particles and resonance induced by gravitational waves," *International Journal of Modern Physics D*, vol. 27, p. 1850042, 2018.

[8] V. K. Shchigolev, "Analytical computation of the perihelion precession in general relativity via the homotopy perturbation method," *Universal Journal of Computational Mathematics*, vol. 3, p. 45, 2015.

[9] Y. P. Hu, H. Zhang, J. P. Hou, and L. Z. Tang, "Perihelion precession and deflection of light in the general spherically symmetric spacetime," *Advances in High Energy Physics*, vol. 2014, Article ID 604321, 7 pages, 2014.

[10] H. Arakida, "Note on the perihelion/periastron advance due to cosmological constant," *International Journal of Theoretical Physics*, vol. 52, pp. 1408–1414, 2013.

[11] R. R. Cuzinatto, P. J. Pompeia, M. de Montigny, F. C. Khanna, and J. M. Silva, "Classic tests of General Relativity described by brane-based spherically symmetric solutions," *The European Physical Journal C*, vol. 74, p. 3017, 2014.

[12] H. J. Schmidt, "Perihelion precession for modified Newtonian gravity," *Physical Review D*, vol. 78, Article ID 023512, 2008.

[13] T. J. Lemmon and A. R. Mondragon, "Alternative derivation of the relativistic contribution to perihelic precession," *American Journal of Physics*, vol. 77, p. 890, 2009.

[14] M. K. Mak, C. S. Leung, and T. Harko, "Computation of the general relativistic perihelion precession and of light deflection via the laplace-adomian decomposition method," *Advances in High Energy Physics*, vol. 2018, Article ID 7093592, 15 pages, 2018.

[15] V. K. Shchigolev, "Variational iteration method for studying perihelion precession and deflection of light in general relativity," *International Journal of Physical Research*, vol. 4, no. 2, p. 52, 2016.

[16] C. M. Will, "New general relativistic contribution to mercury's perihelion advance," *Physical Review Letters*, vol. 120, Article ID 191101, 2018.

[17] G. V. Kraniotis and S. B. Whitehouse, "Compact calculation of the perihelion precession of Mercury in general relativity, the cosmological constant and Jacobi's inversion problem," *Classical and Quantum Gravity*, vol. 20, p. 4817, 2003.

[18] M. L. Ruggiero, "Perturbations of Keplerian orbits in stationary spherically symmetric spacetimes," *International Journal of Modern Physics D*, vol. 23, Article ID 1450049, 2014.

[19] C. Jiang and W. Lin, "Post-Newtonian dynamics and orbital precession in Kerr-Newman field," *The European Physical Journal Plus*, vol. 129, p. 200, 2014.

[20] A. Avalos-Vargas and G. Ares de, "The precession of the orbit of a charged body interacting with a massive charged body in General Relativity," *The European Physical Journal Plus*, vol. 127, p. 155, 2012.

[21] A. Avalos-Vargas and G. Ares de Parga, "The precession of the orbit of a test neutral body interacting with a massive charged body," *The European Physical Journal Plus*, vol. 126, p. 117, 2011.

[22] C. W. Misner, K. S. Thorne, and J. A. Wheeler, "Gravitation," Freeman, San Francisco, Calif, USA, 1970.

[23] S. Weinberg, "Gravitation and Cosmology: Principles and Applications of the General Theory of Relativity," New York, NY, USA, John Wiley and Sons, 1972.

[24] D. Baskaran and L. P. Grishchuk, "Components of the gravitational force in the field of a gravitational wave," *Classical and Quantum Gravity*, vol. 21, p. 4041, 2004.

[25] J. Kepler, "Astronomia nova," (Pragae) 1609 (2015).

[26] Y.-K. Lim, "Motion of charged particles around a magnetized/electrified black hole," *Physical Review D: Particles, Fields, Gravitation and Cosmology*, vol. 91, Article ID 024048, 2015.

[27] D. B. Papadopoulos, I. Contopoulos, K. D. Kokkotas, and N. Stergioulas, "Radiation from charged particles on eccentric orbits in a dipolar magnetic field around a Schwarzschild black hole," *Journal of Mathematical Physics*, vol. 47, no. 4, 49 pages, 2015.

[28] M. Kološ, Z. Stuchlk, and A. Tursunov, "Quasi-harmonic oscillatory motion of charged particles around a Schwarzschild black hole immersed in a uniform magnetic field," *Classical and Quantum Gravity*, vol. 32, Article ID 165009, 2015.

Hindawi
Advances in High Energy Physics
Volume 2019, Article ID 3709472, 9 pages
https://doi.org/10.1155/2019/3709472

Research Article

Cosmological Analysis of Modified Holographic Ricci Dark Energy in Chern-Simons Modified Gravity

Sarfraz Ali[1,2] **and M. Jamil Amir**[1,2]

[1]*Department of Mathematics, University of Education Lahore, Faisalabad Campus, Pakistan*
[2]*Department of Mathematics, Government Post Graduate College (Boys), Taunsa, DG Khan, Pakistan*

Correspondence should be addressed to Sarfraz Ali; sarfraz270@ue.edu.pk

Received 4 April 2019; Accepted 19 May 2019; Published 28 May 2019

Guest Editor: Farook Rahaman

In this paper, we study the cosmological analysis of the modified holographic Ricci dark energy model and reconstruct different scalar field models in the context of Chern-Simons modified gravity. We investigate the deceleration parameter, which shows that the universe is in the accelerating expansion phase. The equation of state parameter in this case also favors the fact that dark energy is the dominant component of universe, which is responsible for the accelerated expansion. A number of scalar fields, such as quintessence, tachyon, K-essence, and dilaton models, are reconstructed using modified holographic Ricci dark energy model in the context of dynamical CS modified gravity. The quintessence and K-essence models represent exponentially increasing behaviors, while tachyon model shows decreasing behavior. Unfortunately, the dilaton model has no numerical solution for modified holographic Ricci dark energy model in the framework of dynamical Chern-Simons modified gravity.

1. Introduction

A large number of evidences have been provided in the favor of accelerated expansion of the universe by Type Ia supernovae [1, 2], Cosmic Microwave Background (CMB) [3], weak lensing [4], Large Scale Structures [5, 6], and integrated Sachs-Wolfe effect [7, 8]. It is postulated that there exists a component in the universe which has negative pressure and is responsible for the accelerated expansion of the universe, called dark energy (DE). The most familiar candidate of DE model is cosmological constant Λ which satisfies the cosmological observations [9, 10] but fails to resolve the fine tuning problem and cosmic coincidence [11]. In literature, there are many DE models such as an evolving canonical scalar field [12, 13] quintessence, the phantom energy [14, 15], and quintom energy [16–18].

In recent studies, to understand the nature of universe, a new DE model has been constructed in the context of quantum gravity on holographic principle named holographic dark energy (HDE) model [19–22]. This principle is extensively used to study the quantum behavior of black holes. The energy density of HDE is defined as $\rho = 3c^2 M_{pl}^2 L^{-2}$, where c is constant, M_{pl} is Plank mass, and L is supposed to be size of the universe. For Hubble radius H^{-1}, this HDE model's density is very similar to the observational results. Gao et al. [23], motivated by the holographic principle, introduced a new DE model, which was inversely proportional to Ricci scalar curvature called Ricci dark energy (RDE). Their investigation shows that RDE model solves the causality problem and the evolution of density perturbations of matter power spectra and CMB anisotropy is not much affected by such modification. Granda and Oliveros [24] introduced a new infrared cut-off for HDE model and reconstructed the potentials and fields for different DE models such as the quintessence, tachyon, K-essence, and dilaton for FRW universe. Karami and Fehri [25] using Granda and Oliveros cut-off studied the nonflat FRW universe to find the DE density, deceleration parameter, and equation of state (EoS).

Jackiw and Pi [26] introduced Chern-Simons (CS) modified gravity, in which the Einstein-Hilbert action is modified as the sum of parity-violating CS term and scalar field. Silva and Santos [27] analyzed the RDE of FRW universe and found it to be similar to GCG in the context of CS modified gravity. Jamil and Sarfraz [28] did the same for amended FRW universe and presented their results graphically. Jawad and Sohail [29] considering modified QCD ghost dark energy

model investigated the dynamics of scalar field and potentials of various scalar field models in the framework of dynamical CS modified gravity. Jamil and Sarfraz [30] considering HDE model found the accelerated expansion behavior of the universe under certain restrictions on the parameter α. We studied the correspondence between quintessence, K-essence, tachyon, and dilaton field models and holographic dark energy model. Pasqua et al. [31] investigated the HDE, modified holographic Ricci dark energy (MHRDE), and another model, which is a combination of higher-order derivatives of the Hubble parameter in the framework of CS modified gravity.

In this paper, working on same lines using the MHRDE model, we explored the energy density, deceleration parameter, EoS parameter, and correspondence between different models. The paper is organized in following order. The basic formalism of CS modified gravity is discussed in Section 2. Section 3 is devoted for the investigation of energy density, deceleration parameter, and EoS parameter. The correspondence between scalar field models such as quintessence, tachyon, K-essence, and dilaton model is given in Section 4. Summery and concluding remarks are in the last section.

2. ABC of Chern-Simons Modified Gravity

Jackiw and Pi [26] modify the 4-dimensional GR theory introducing a Chern-Simons term in Einstein-Hilbert action given by [32, 33]

$$S = \int d^4x\sqrt{-g}\left[\chi R + \frac{\zeta}{4}\Theta\, {}^*RR - \frac{\eta}{2}\left(g^{\mu\nu}\nabla_\mu\Theta\nabla_\nu\Theta + 2V[\Theta]\right)\right] + S_{mat}, \tag{1}$$

where the terms used in this relation are defined as $\chi = (16\pi G)^{-1}$, R is the usual Ricci scalar, the term ${}^*RR$ is defined as ${}^*RR = {}^*R^a{}_b{}^{cd}R^b{}_{acd}$, is topological invariant, called Pontryagin term where ${}^*R^a{}_b{}^{cd}$ is the dual of Riemann tensor $R^b{}_{acd}$ can be expressed as ${}^*R^a{}_b{}^{cd} = (1/2)\epsilon^{cdef}R^a{}_{bef}$, ∇_μ is titled as covariant derivative, the dimensionless parameters ζ and η are treated here as coupling constants, and $V[\Theta]$ is potential and in the context of string theory it is assumed that $V[\Theta] = 0$. The most important term Θ, called CS coupling field, works as a deformation function of the space-time which is always other than constant (if Θ is constant function, then the CS theory reduces to GR).

The variation of Einstein-Hilbert action S corresponding to metric tensor $g_{\mu\nu}$ and scalar field Θ resulted into a set of field equations of CS modified gravity given by

$$G_{\mu\nu} + lC_{\mu\nu} = \chi T_{\mu\nu}, \tag{2}$$

$$g^{\mu\nu}\nabla_\mu\nabla_\nu\Theta = -\frac{\zeta}{4}\, {}^*RR, \tag{3}$$

where $G_{\mu\nu}$, $C_{\mu\nu}$, l, and $T_{\mu\nu}$ are called Einstein tensor, Cotton tensor (C-tensor), coupling constant, and energy-momentum tensor, respectively. The energy-momentum tensor is a combination of matter part $T^m_{\mu\nu}$ and the external field part $T^\Theta_{\mu\nu}$. The mathematical expressions for these terms are as follows:

$$C^{\mu\nu} = -\frac{1}{2\sqrt{-g}}\left[\upsilon_\sigma\epsilon^{\sigma\mu\zeta\eta}\nabla_\zeta R^\nu_\eta + \frac{1}{2}\upsilon_{\sigma\tau}\epsilon^{\sigma\nu\zeta\eta}R^{\tau\mu}_{\zeta\eta}\right] + (\mu \longleftrightarrow \nu), \tag{4}$$

$$T^m_{\mu\nu} = (\rho + p)u_\mu u_\nu - pg_{\mu\nu}, \tag{5}$$

$$T^\Theta_{\mu\nu} = \zeta\left(\partial_\mu\Theta\right)\left(\partial_\nu\Theta\right) - \frac{\zeta}{2}g_{\mu\nu}\left(\partial^\lambda\Theta\right)\left(\partial_\lambda\Theta\right). \tag{6}$$

Here ρ is energy density, p is pressure, and $u_\mu = (1, 0, 0, 0)$ denotes standard time-like 4-velocity, respectively. The terms $\upsilon_\sigma \equiv \nabla_\sigma\Theta$ and $\upsilon_{\sigma\tau} \equiv \nabla_\sigma\nabla_\tau\Theta$. On the basis of choice of ($\zeta \neq 0$ and $\chi \neq 0$) and ($\chi \neq 0$ and $\zeta = 0$), this theory is divided into two distinct theories named dynamical and nondynamical Chern-Simons modified gravity, respectively.

3. Modified Holographic Ricci Dark Energy Model

In this paper, we studied FRW universe in the framework of dynamical CS modified gravity. By the 00-component of field equation for FRW universe using (2), we get

$$H^2 = \frac{1}{3}\rho_D + \frac{1}{6}\dot{\Theta}^2. \tag{7}$$

Here $H = \dot{a}/a$ is called Hubble parameter and $\dot{a}$ is time derivative of scale factor $a(t)$. The Pontryagin term ${}^*RR$ vanishes for FRW metric identically, so (3) takes the form

$$g^{\mu\nu}\nabla_\mu\nabla_\nu\Theta = g^{\mu\nu}\left[\partial_\mu\partial_\nu\Theta - \Gamma^\rho_{\mu\nu}\partial_\rho\Theta\right] = 0. \tag{8}$$

Keeping in view the fact that Θ is a function of space-time, we consider $\Theta = \Theta(t)$; (8) turns out to be

$$\ddot{\Theta} = Ca^{-3}. \tag{9}$$

C is constant of integration other than zero (as if this C is zero then the function Θ becomes constant which reduces the CS theory to GR).

Using holographic principle, Hooft [34] proposed very simple and convenient model to investigate the issues raised in DE, named as HDE model. This model is used in different scenarios such as Hubble radius and cosmological conformal time of particle horizon [35, 36]. An interesting holographic RDE model defined as $L = |R|^{-1/2}$, where R is Ricci curvature scalar, was proposed by Gao et al [37].

In this paper, we use HDE model suggested by Granda and Oliveros in [22] defined as

$$\rho_{MHRDE} = \frac{2}{\alpha - \beta}\left(\dot{H} + \frac{3\alpha}{2}H^2\right), \tag{10}$$

and here α and β are constants. It is worth mentioning here, in limiting case ($\alpha = 4/3, \beta = 1$), that the Granda and Oliveros IR cut-off reduces to Gao et al.'s IR cut-off. Using (9) and (10) in (7), we arrive at

$$H^2 = \frac{2}{3(\alpha - \beta)}\left(\dot{H} + \frac{3\alpha}{2}H^2\right) + \frac{1}{6}C^2a^{-6} \tag{11}$$

and solving the differential equation, the scale factor $a(t)$ is explored as

$$a(t) = \left[\frac{12C_1}{C(\alpha-4)} - \frac{3C(\alpha-4)}{4}t^2\right]^{1/6}. \quad (12)$$

To avoid the singular solution, it is provided that $\alpha \neq 4$. The Hubble parameter $H(t) = \dot{a}/a$ can be evaluated as

$$H(t) = -\frac{Ct(\alpha-4)}{4\left(12C_1/C(\alpha-4) - (3/4)Ct^2(\alpha-4)\right)}. \quad (13)$$

Since the scale factor has been explored by assuming $\beta = 4$ in (10), it takes the form

$$\rho_{MHRDE} = \frac{2}{\alpha-4}\left(\dot{H} + \frac{3\alpha}{2}H^2\right), \quad (14)$$

and using corresponding values of $H(t)$ and $\dot{H}(t)$, the expression for MHRDE density turned out to be

$$\rho_{MHRDE} = \frac{(\alpha-4)\left(C^4t^2(\alpha-4)^2(\alpha-2) - 32C^2C_1\right)}{3\left(C^2t^2(\alpha-4)^2 - 16C_1\right)^2}. \quad (15)$$

In terms of redshift parameter, the density is given as

$$\rho(z) = \frac{1}{4}(1+z)^6\left[-C(\alpha-2) + 12C_1(1+z)^6\right]. \quad (16)$$

The energy density of this model is increasing for all values of C, $\alpha < 2$, and $C_1 > 0$. We plot a graph for different values of these parameters.

The graphical behavior of the density is exponentially increasing after $z > 0$ in the context of CS gravity using this MHRDE model.

3.1. Deceleration Parameter. The rate of expansion of the universe remained unchanged at constant values of $\dot{a}(t)$ and deceleration term q along with condition imposed on scale factor $a(t)$, that is, $a(t) \propto t$, where t is cosmic time. The Hubble parameter H remains constant and deceleration term $q = -1$, when de Sitter and steady-state universes are under consideration. Furthermore, the deceleration parameter varies with time for some universes available in literature. Using the variational values of H and q, we can classify all the defined universe models whether they are in expansion or contraction mode and acceleration or deceleration mode:

(1) $H > 0$, $q > 0$, expanding and decelerating
(2) $H > 0$, $q = 0$, expanding, zero deceleration
(3) $H < 0$, $q = 0$, contracting, zero deceleration
(4) $H < 0$, $q > 0$, contracting and decelerating
(5) $H < 0$, $q < 0$, contracting and accelerating
(6) $H = 0$, $q = 0$, static.

The deceleration parameter q in terms of Hubble parameter H is defined as

$$q(t) = -1 - \frac{\dot{H}}{H^2}, \quad (17)$$

where $\dot{H}$ represents the derivative of H with respect to t, termed as

$$\dot{H}(t) = -\frac{C^2(\alpha-4)^2\left(C^2t^2(\alpha-4)^2 + 16C_1\right)}{3\left(C^2t^2(\alpha-4)^2 - 16C_1\right)^2}. \quad (18)$$

Substituting these values in (17), we find deceleration parameter q:

$$q(t) = 2 + \frac{48C_1}{(\alpha-4)^2C^2t^2}. \quad (19)$$

Representing in the form of redshift, it becomes

$$q(z) = \frac{2\left[C(\alpha-4) - 30C_1(1+z)^6\right]}{C(\alpha-4) - 12C_1(1+z)^6} \quad (20)$$

It is obvious that the deceleration parameter depends on C, C_1, α, and redshift parameter z. At present epoch $z = 0$, the deceleration parameter $q < 0$ for each case given below:

$$\begin{aligned}
&(1)\quad \alpha < 4,\\
&\qquad C_1 < 0,\\
&\qquad \frac{12C_1}{\alpha-4} < C < \frac{30C_1}{\alpha-4},\\
&(2)\quad \alpha > 4,\\
&\qquad C_1 < 0,\\
&\qquad \frac{30C_1}{\alpha-4} < C < \frac{12C_1}{\alpha-4},\\
&(3)\quad \alpha < 4,\\
&\qquad C_1 > 0,\\
&\qquad \frac{30C_1}{\alpha-4} < C < \frac{12C_1}{\alpha-4},\\
&(4)\quad \alpha > 4,\\
&\qquad C_1 > 0,\\
&\qquad \frac{12C_1}{\alpha-4} < C < \frac{30C_1}{\alpha-4}.
\end{aligned} \quad (21)$$

For all these conditions, the model under consideration in CS gravity advocates that the universe is in accelerated expansion phase.

3.2. Equation of State Parameter. The nature of component which is dominating universe can be studied with the EoS parameter ω. In fact, it illustrates the era of dominance of universe by certain component. For example, $\omega = 0, 1/3$, and 1 predict that the universe is under dust, radiation, and stiff fluid influence, respectively. Meanwhile, $\omega = -1/3, -1$, and $\omega < -1$ stand for quintessence DE, ΛCDM, and Phantom

eras, respectively. Now, differentiating (15) with respect to time t,

$$\dot{\rho}(t) = -\frac{2C^4 t(\alpha-4)^3\left(C^2t^2(\alpha-4)^2(\alpha-2)+16C_1(\alpha-6)\right)}{3\left(C^2t^2(\alpha-4)^2-16C_1\right)^3}. \quad (22)$$

The conservation equation in CS modified gravity is given by [38]

$$\dot{\rho}+3H(\rho+p)=0. \quad (23)$$

The expression for EoS parameter ω can be explored using (23) such that

$$\omega(t) = -1-\frac{\dot{\rho}(t)}{3H(t)\rho(t)}. \quad (24)$$

Making use of (13), (18), and (22) in (24), we found analytic solution of EoS parameter as given below:

$$\omega(t) = -1-\frac{-2C^2t^2(\alpha-4)^2(\alpha-2)-32C_1(\alpha-6)}{C^2t^2(\alpha-4)^2(\alpha-2)-32C_1}. \quad (25)$$

The EoS parameter ω in terms of redshift parameter z looks like

$$\omega(z) = \frac{C(\alpha-2)-36C_1(1+z)^6}{C(\alpha-2)-12C_1(1+z)^6}. \quad (26)$$

Obviously, EoS parameter ω is a function of variable redshift parameter z depending on C, C_1, and α. At the present epoch $z=0$ the EoS is $\omega<-1$ for each of the cases described below:

$$\begin{aligned}
&(1)\quad C<0,\\
&\qquad C_1<0,\\
&\qquad \frac{12C_1+2C}{C}<\alpha<\frac{24C_1+2C}{C},\\
&(2)\quad C<0,\\
&\qquad C_1>0,\\
&\qquad \frac{24C_1+2C}{C}<\alpha<\frac{12C_1+2C}{C},\\
&(3)\quad C>0,\\
&\qquad C_1<0,\\
&\qquad \frac{24C_1+2C}{C}<\alpha<\frac{12C_1+2C}{C},\\
&(4)\quad C>0,\\
&\qquad C_1>0,\\
&\qquad \frac{12C_1+2C}{C}<\alpha<\frac{24C_1+2C}{C}.
\end{aligned} \quad (27)$$

For different values of these parameters, the EoS $\omega<-1$ favors the fact that the universe is dominated by DE.

4. Study of MHRDE Model Using Scalar Field Models

In this section, we discuss different scalar field models like quintessence, tachyon, K-essence, and dilaton models in the framework of CS modified gravity. To study the behavior of quantum gravity, we explore the potential and scalar field.

4.1. Quintessence Model. A DE model is developed to explain the late-time cosmic acceleration called quintessence, which is a simplest scalar field that has no theoretical problem like ghosts and Laplacian instabilities appearance [11]. This model is useful to settle down the issue of fine-tuning in cosmology considering the time-dependent EoS. Using this model, we can explain the cosmic acceleration having negative pressure when potential energy dominates the kinetic energy. The energy and pressure densities are defined as

$$\begin{aligned}
\rho_Q &= \frac{1}{2}\dot{\phi}^2+V(\phi),\\
p_Q &= \frac{1}{2}\dot{\phi}^2-V(\phi),
\end{aligned} \quad (28)$$

where the scalar field ϕ is differentiated with respect to t. The EoS parameter for the quintessence is

$$\omega_\phi = \frac{(1/2)\dot{\phi}^2-V(\phi)}{(1/2)\dot{\phi}^2+V(\phi)}. \quad (29)$$

The comparison of EoS ω_ϕ formulated for quintessence model given in (29) and EoS ω calculated for MHRDE modal given in (25) turned as

$$\frac{(1/2)\dot{\phi}^2-V(\phi)}{(1/2)\dot{\phi}^2+V(\phi)} = \frac{C^2t^2(\alpha-4)^2(\alpha-2)+32C_1(\alpha-5)}{C^2t^2(\alpha-4)^2(\alpha-2)-32C_1}. \quad (30)$$

Now, equating density of quintessence model given in (28) and density evaluated from MHRDE model represented in (15) are expressed as

$$\frac{1}{2}\dot{\phi}^2+V(\phi) = \frac{(\alpha-4)\left(C^4t^2(\alpha-4)^2(\alpha-2)-32C^2C_1\right)}{3\left(C^2t^2(\alpha-4)^2-16C_1\right)^2}. \quad (31)$$

Using (30) and (31), we arrive at

$$\dot{\phi}^2 = \frac{2C^2(\alpha-4)\left(C^2t^2(\alpha-4)^2(\alpha-2)+16C_1(\alpha-6)\right)}{3\left(C^2t^2(\alpha-4)^2-16C_1\right)^2} \quad (32)$$

and integrating the last equation with respect to t,

$$\begin{aligned}\phi(t) &= \sqrt{\frac{2}{3}}\left[-\sqrt{2}\tanh^{-1}\left(\frac{\sqrt{2}Ct(\alpha-4)^{3/2}}{\sqrt{C^2t^2(\alpha-4)^2(\alpha-2)+16C_1(\alpha-6)}}\right)\right.\\ &\quad+\sqrt{\frac{\alpha-2}{\alpha-4}}\ln\left[C\left(Ct\left(\alpha^2-2\alpha+8\right)+\sqrt{\alpha-2}\right.\right.\\ &\quad\left.\left.\left.\times\sqrt{C^2t^2(\alpha-4)^2(\alpha-2)+16C_1(\alpha-6)}\right)\right]\right].\end{aligned} \tag{33}$$

In terms of redshift parameter z, it turns out to be

$$\begin{aligned}\phi(z) &= -\frac{2}{3(\alpha-4)}\tanh^{-1}\left[\frac{(\alpha-4)^{3/2}\sqrt{4C/(1+z)^6+48C_1/(4-\alpha)}}{\sqrt{8-2\alpha}\sqrt{(\alpha-4)\left(-c(\alpha-2)+24(1+z)^6C_1\right)/(1+z)^6}}\right]+(\alpha-4)\sqrt{\frac{2(\alpha-2)}{3}}\\ &\quad\cdot\log\left[\frac{2C}{\sqrt{3}}\left(\sqrt{\alpha-2}\sqrt{\frac{(\alpha-4)\left(-c(\alpha-2)+24(1+z)^6C_1\right)}{(1+z)^6}}+\frac{\sqrt{c}\left(8-6\alpha+\alpha^2\right)\sqrt{4/(1+z)^6+48C_1/C(4-\alpha)}}{2\sqrt{4-\alpha}}\right)\right].\end{aligned} \tag{34}$$

Again using (30) and (31), the potential for quintessence model can be explored as

$$V(t) = -\frac{16C^2C_1(\alpha-4)^2}{3\left(C^2t^2(\alpha-4)^2-16C_1\right)^2}. \tag{35}$$

And making it convenient to discuss, we change into redshift parameter

$$V(z) = -3C_1(1+z)^{12}. \tag{36}$$

It is obvious that the potential of quintessence model depends on the values of constant of integration C_1 only. It shows the increasing behavior for all $C_1 < 0$ and decreasing behavior for $C_1 > 0$. It is interesting that the parameters C and α do not appear in the final expression of potential in the framework of CS Modified gravity.

4.2. Tachyon Model. Much attention has been given to tachyon field models in the last few decades in string theory and cosmology [39–45]. In fact, isotropic cosmological models whose radius depends on time and their potential can be constructed using minimally coupled scalar field model [46]. The same procedure for the correspondence between minimally coupled scalar field models and tachyon can be utilized to study the similar cosmological evolution [45]. The energy and pressure densities for the tachyon fields model are expressed as

$$\begin{aligned}\rho &= \frac{V(\phi)}{\sqrt{1-\dot{\phi}^2}},\\ p &= -V(\phi)\sqrt{1-\dot{\phi}^2}.\end{aligned} \tag{37}$$

Since $p = \rho\omega$, using the above expressions, the EoS parameter can be evaluated as

$$\omega = \dot{\phi}^2 - 1 \tag{38}$$

The comparison of (25) with (38) gives kinetic energy $\phi(t)$ such that

$$\begin{aligned}\phi(t) &= \sqrt{\frac{C_1(6-\alpha)}{C^2(\alpha-4)^2(\alpha-2)}}E\left[\arcsin\left(t\sqrt{\frac{C^2(\alpha-4)^2(\alpha-2)}{32C_1}}\right);\right.\\ &\quad\left.\frac{2}{\alpha-6}\right].\end{aligned} \tag{39}$$

The tachyon potential in this case is

$$V(t) = \frac{C^2(\alpha-4)}{3\left(C^2t^2(\alpha-4)^2-16C_1\right)^2}\times\sqrt{\left[C^2t^2(\alpha-4)^2(\alpha-2)-32C_1\right]\left[C^2t^2(\alpha-4)^2(\alpha-2)+32C_1(\alpha-5)\right]}. \tag{40}$$

Now, the kinetic and potential energies of tachyon model in terms of redshift parameter z, respectively, are

$$\phi(z) = \frac{4\sqrt{2C_1(\alpha-6)}}{\sqrt{C^2(\alpha-2)(\alpha-4)^2}} EllipticE\left[\sin^{-1}\left[\frac{\sqrt{C^2(\alpha-2)(\alpha-4)^2/C_1}\sqrt{4/(1+z)^6+48C_1/C(4-\alpha)}}{4\sqrt{6C(4-\alpha)}}\right], -\frac{2}{\alpha-6}\right], \quad (41)$$

$$V(z) = -\frac{1}{4}(1+z)^6\left(C(\alpha-2)-12(1+z)^6C_1\right)\sqrt{1-\frac{1}{2}(1+z)^6\left(-c(\alpha-2)+24(1+z)^6C_2\right)}. \quad (42)$$

To investigate the behavior of potential, we plot a graph of $V(z)$ versus z.

The graph plotted for the potential $V(z)$ of tachyon model against redshift parameter z shows the decreasing behavior irrespective of the values of parameters α, C, and C_1. This graph is plotted by taking particular values of these parameters to elaborate the result.

4.3. K-Essence. Armendariz et al. [47] introduced the dynamical concept of k-essence to explain the fact of accelerated expansion of universe. This model solves the fine-tuning problem of parameters. Actually, k-essence is developed on the principle of dynamical attractor solution; that is why it works as cosmological constant at the onset of matter domination. The energy and pressure densities of this model are given as

$$\rho = V(\phi)\left(-X+3X^2\right), \qquad p = V(\phi)\left(-X+X^2\right). \quad (43)$$

$X = \dot{\phi}^2/2$; the EoS parameter for this model is

$$\omega = \frac{1-X}{1-3X} \quad (44)$$

Equating (25) and (44), we obtain

$$X(t) = \frac{16C_1(\alpha-4)}{C^2t^2(\alpha-4)^2(\alpha-2)+16C_1(3\alpha-14)}. \quad (45)$$

Since $X(t) = \dot{\phi}^2/2$, the integration of the above equation provides $\phi(t)$:

$$\phi(t) = \frac{4C_1}{\sqrt{(\alpha-4)(\alpha-2)}}\ln\left[C\left(Ct\left(\alpha^2-6\alpha+8\right)+\sqrt{\alpha-2}\sqrt{C^2t^2(\alpha-4)^2(\alpha-2)+16C_1(3\alpha-14)}\right)\right]. \quad (46)$$

The kinetic energy ϕ in terms of redshift parameter z is turned as

$$\phi(z) = \frac{4C_1}{c\sqrt{\alpha-2}\sqrt{(\alpha-4)C_1}} \times \log\left[\frac{2C}{\sqrt{3}}\sqrt{\frac{(\alpha-4)\left(-C(\alpha-2)+48(1+z)^6C_1\right)}{(1+z)^6}} + \frac{\sqrt{C}\left(8-6\alpha+\alpha^2\right)\sqrt{4/(1+z)^6+48C_1/C(4-\alpha)}}{2\sqrt{4-\alpha}}\right]. \quad (47)$$

The k-essence potential is calculated using (43), (44), and (25) as

$$V(t) = -\frac{C^2\left(C^2t^2(\alpha-4)^2(\alpha-2)+16C_1(3\alpha-14)\right)^2}{48C_1\left(C^2t^2(\alpha-4)^2-16C_1\right)^2}. \quad (48)$$

Now, we convert this function in terms of redshift parameter z and investigate its behavior.

$$V(z) = -\frac{\left(c(\alpha-2)-48(1+z)^6C_1\right)^2}{48C_2}. \quad (49)$$

The potential $V(z)$ is increasing function for all values of C and α at value of constant of integration $C_1 = -1$. We plot a graph for particular values of these parameters just for example. After present epoch $z = 0$, it increases exponentially.

4.4. Dilaton Model. The negative kinetic energy of the phantom field creates the problem of quantum instability. To resolve this puzzle of instability, dilaton model is proposed and further used to study the nature of DE. The dilaton model is defined as 4-dimensional effective low-energy model in the context of string theory. The pressure and energy densities are presented as

$$\rho = -X + c_1e^{\lambda\phi}X^2, \qquad p = -X + 3c_1e^{\lambda\phi}X^2. \quad (50)$$

$X = \dot{\phi}^2/2$, and c_1 and λ are positive constants. The EoS parameter $\omega = p/\rho$ for these densities is calculated as

$$\omega = \frac{1-c_1e^{\lambda\phi}}{1-3c_1e^{\lambda\phi}}. \quad (51)$$

The comparison of (25) with (51) yields

$$c_1e^{\lambda\phi}\dot{\phi}^2 = \frac{16C_1(\alpha-4)}{C^2t^2(\alpha-4)^2(\alpha-2)+16C_1(3\alpha-14)}. \quad (52)$$

Solving for $\phi(t)$, we arrive at

$$\phi(t) = \frac{2}{\lambda}\ln\left[\frac{\lambda}{2}\cdot\sqrt{\frac{16C_1}{C^2(\alpha-4)}}\sinh^{-1}\left(t\sqrt{\frac{C^2(\alpha-4)^2(\alpha-2)}{16C_1(3\alpha-14)}}\right)\right]. \quad (53)$$

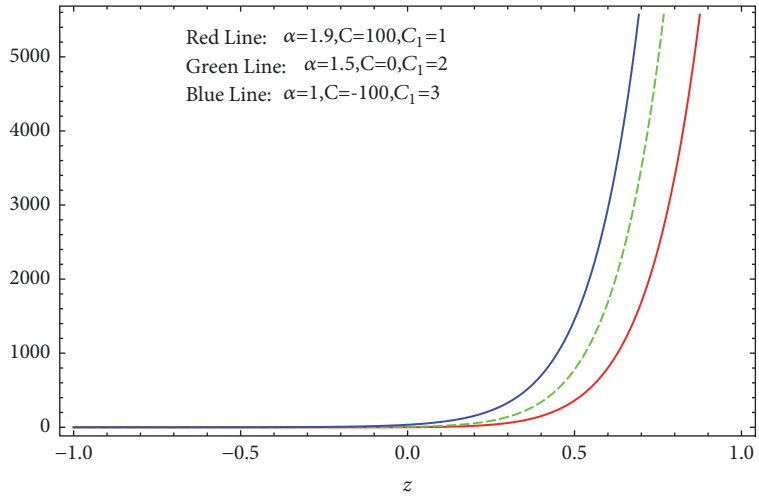

Figure 1: Density versus redshift parameter.

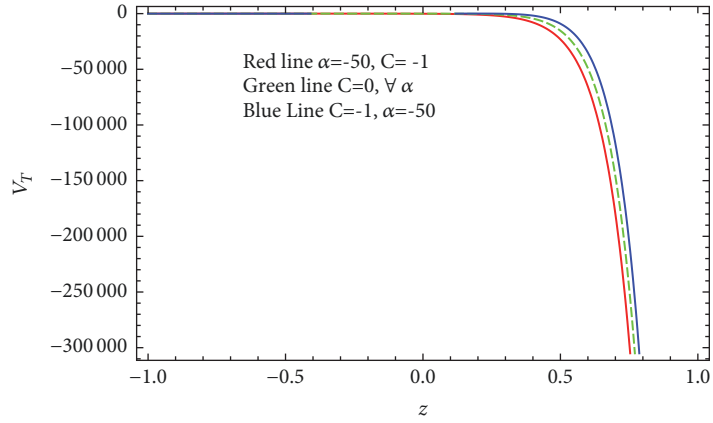

Figure 2: Potential versus redshift parameter.

In terms of redshift parameter z,

$$\phi(z) = \frac{2}{\lambda}\log\left[\sqrt{\frac{16C_1}{C^2(\alpha-2)}}\sinh^{-1}\frac{\left(\sqrt{C^2(\alpha-4)^2(\alpha-2)/C_1(3\alpha-14)}\sqrt{4/(1+z)^6+48C_1/C(4-\alpha)}\right)}{4\sqrt{3C(4-\alpha)}}\right]. \quad (54)$$

Analytically, it is found that there is no combination of parameters α, C, C_1 for which this function is defined.

5. Summary and Discussion

This work is devoted to study the cosmological analysis of MHRDE model in the context of CS modified gravity. The energy density for this model is calculated and observed in Figure 1. From the graph, it is obvious that density of the universe for MHRDE model is increasing for all values of CS modified gravity constants C, $\alpha < 2$, and $C_1 > 0$. The deceleration parameter $q < 0$ for the different combination of C, C_1, and α which advocates the accelerating expansion. The EoS parameter $\omega < -1$ is found, which favors the fact that DE is dominant at present epoch in case of MHRDE model in the context of CS modified gravity.

Furthermore, we reconstructed different scalar filed models using MHRDE in the context of dynamical CS modified gravity and found interesting results plotting them graphically. It is obvious that the potential of quintessence model depends only on the value of constant of integration C_1. It shows the increasing behavior for all $C_1 < 0$ and decreasing behavior for $C_1 > 0$. It is interesting that the potential in (36) is independent of CS parameter C and MHRDE parameter α identically, although we are working in the framework of CS modified gravity using MHRDE model. The graph plotted in Figure 2 for the potential of tachyon model shows the exponentially decreasing behavior irrespective of the values

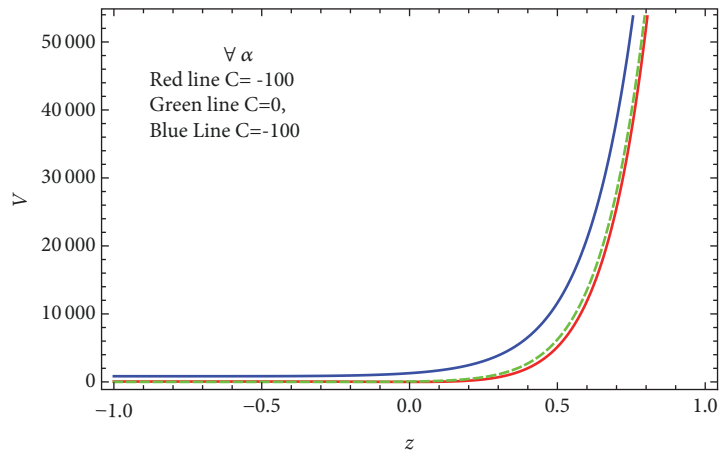

Figure 3: Potential versus redshift parameter.

of parameters α, C, and C_1. In case of k-essence, the potential is increasing function for all values of C and α at particular value of $C_1 = -1$. After present epoch $z = 0$, the graph increases exponentially as given by Figure 3. Analytically, it is found that there is no combination of parameters α, C, C_1 for which $\phi(z)$ is defined in case of dilaton model.

Data Availability

No data were used to support this study; these are the general results obtained mathematically using Mathematica software.

Conflicts of Interest

The authors declare that they have no conflicts of interest.

Acknowledgments

The authors acknowledge the remarkable assistance of the Higher Education Commission Islamabad, Pakistan. Sarfraz Ali would like to acknowledge Department of Physics and Astronomy, University of British Columbia, Canada, for giving me space in their Astro Lab for six months as Visiting International Research Scholar. Sarfraz Ali really thankful to Dr. Douglas Scott for his supervision and valuable suggestions on this work.

References

[1] A. G. Riess, A. V. Filippenko, P. Challis et al., "Observational evidence from supernovae for an accelerating universe and a cosmological constant," *The Astronomical Journal*, vol. 116, no. 3, article 1009, 1998.

[2] S. Perlmutter, G. Aldering, G. Goldhaber et al., "Measurements of Ω and Λ from 42 high-redshift supernovae," *The Astrophysical Journal*, vol. 517, no. 2, pp. 565–586, 1999.

[3] D. N. Spergel, R. Bean, O. Doré et al., "Three-year Wilkinson microwave anisotropy probe (WMAP) observations: implications for cosmology," *The Astrophysical Journal*, vol. 170, no. 2, article 377, 2007.

[4] C. R. Contaldi, H. Hoekstra, and A. Lewis, "Joint cosmic microwave background and weak lensing analysis: constraints on cosmological parameters," *Physical Review Letters*, vol. 90, no. 22, Article ID 221303, 2003.

[5] M. Colless, G. Dalton, S. Maddox et al., "The 2dF galaxy redshift survey: spectra and redshifts," *Monthly Notices of the Royal Astronomical Society*, vol. 328, no. 4, pp. 1039–1063, 2001.

[6] M. Tegmark, M. A. Strauss, M. R. Blanton et al., "Cosmological parameters from SDSS and WMAP," *Physical Review D: Particles, Fields, Gravitation and Cosmology*, vol. 69, no. 10, Article ID 103501, 2004.

[7] S. Cole, W. J. Percival, J. A. Peacock et al., "The 2dF galaxy redshift survey: power-spectrum analysis of the final data set and cosmological implications," *Monthly Notices of the Royal Astronomical Society*, vol. 362, no. 2, pp. 505–534, 2005.

[8] S. Boughn and R. Crittenden, "A correlation between the cosmic microwave background and large-scale structure in the Universe," *Nature*, vol. 427, no. 6969, pp. 45–47, 2004.

[9] S. Weinberg, "The cosmological constant problem," *Reviews of Modern Physics*, vol. 61, no. 1, pp. 1–23, 1989.

[10] V. Sahni and A. Starobinsky, "The case for a positive cosmological λ-term," *International Journal of Modern Physics D*, vol. 9, no. 4, pp. 373–443, 2000.

[11] E. J. Copeland, M. Sami, and S. Tsujikawa, "Dynamics of dark energy," *International Journal of Modern Physics D: Gravitation, Astrophysics, Cosmology*, vol. 15, no. 11, pp. 1753–1935, 2006.

[12] I. Zlatev, L. Wang, and P. J. Steinhardt, "Quintessence, cosmic coincidence, and the cosmological constant," *Physical Review Letters*, vol. 82, no. 5, pp. 896–899, 1999.

[13] X. Zhang, "Coupled quintessence in a power-law case and the cosmic coincidence problem," *Modern Physics Letters A*, vol. 20, no. 33, pp. 2575–2582, 2005.

[14] R. R. Caldwell, "A phantom menace? cosmological consequences of a dark energy component with super-negative equation of state," *Physics Letters B*, vol. 545, no. 1-2, pp. 23–29, 2002.

[15] R. R. Caldwell, M. Kamionkowski, and N. N. Weinberg, "Phantom energy: dark energy with $w <;;; -1$ causes a cosmic doomsday," *Physical Review Letters*, vol. 91, Article ID 071301, 2003.

[16] T. Qiu, "Theoretical aspects of quintom models," *Modern Physics Letters A*, vol. 25, no. 11-12, pp. 909–921, 2010.

[17] Y.-F. Cai, E. N. Saridakis, M. R. Setare, and J.-Q. Xia, "Quintom cosmology: theoretical implications and observations," *Physics Reports*, vol. 493, no. 1, pp. 1–60, 2010.

[18] M. R. Setare and E. N. Saridakis, "Quintom dark energy models with nearly flat potentials," *Physical Review D: Particles, Fields, Gravitation and Cosmology*, vol. 79, no. 4, Article ID 043005, 2009.

[19] C-H Chou and K-W Ng, "Decaying superheavy dark matter and subgalactic structure of the universe," *Physics Letters B*, vol. 594, no. 1-2, pp. 1–7, 2004-2007.

[20] A. G. Cohen, D. B. Kaplan, and A. E. Nelson, "Effective field theory, black holes, and the cosmological constant," *Physical Review Letters*, vol. 82, no. 25, pp. 4971–4974, 1999.

[21] M. Li, "A model of holographic dark energy," *Physics Letters B*, vol. 603, no. 1-2, pp. 1–5, 2004.

[22] L. N. Granda and A. Oliveros, "Infrared cut-off proposal for the holographic density," *Physics Letters B*, vol. 669, no. 5, pp. 275–277, 2008.

[23] C. Gao, F. Wu, X. Chen, and Y.-G. Shen, "Holographic dark energy model from Ricci scalar curvature," *Physical Review D: Particles, Fields, Gravitation and Cosmology*, vol. 79, no. 4, article 043511, 2009.

[24] L. N. Granda and A. Oliveros, "New infrared cut-off for the holographic scalar fields models of dark energy," *Physics Letters B*, vol. 671, no. 2, pp. 199–202, 2009.

[25] Y. C. Hong, T. H. Lho, D. H. Shin et al., "Removal of fluorinated compound gases by an enhanced methane microwave plasma burner," *Japanese Journal of Applied Physics*, vol. 49, no. 1R, Article ID 017101, 2010.

[26] R. Jackiw and S.-Y. Pi, "Chern-simons modification of general relativity," *Physical Review D particles, fields, gravitation, and cosmology*, vol. 68, no. 10, Article ID 104012, 2003.

[27] J. G. Silva and A. F. Santos, "Ricci dark energy in Chern-Simons modified gravity," *The European Physical Journal C*, vol. 73, article 2500, 2013.

[28] M. J. Amir and S. Ali, "Ricci dark energy of amended FRW universe in chern-simon modified gravity," *International Journal of Theoretical Physics*, vol. 54, no. 4, pp. 1362–1369, 2015.

[29] A. Jawad and A. Sohail, "Cosmological evolution of modified QCD ghost dark energy in dynamical Chern-Simons gravity," *Astrophysics and Space Science*, vol. 359, article 55, 2015.

[30] S. Ali and M. J. Amir, "A study of holographic dark energy models in Chern-Simon modified gravity," *International Journal of Theoretical Physics*, vol. 55, no. 12, pp. 5095–5105, 2016.

[31] A. Pasqua, R. da Rocha, and S. Chattopadhyay, "Holographic dark energy models and higher order generalizations in dynamical Chern-Simons modified gravity," *The European Physical Journal C*, vol. 75, article 44, 2015.

[32] S. Alexander and N. Yunes, "Parametrized post-newtonian expansion of chern-simons gravity," *Physical Review D*, vol. 75, no. 12, Article ID 124022, 2007.

[33] S. Alexander and N. Yunes, "Chern-Simons modified general relativity," *Physics Reports*, vol. 480, no. 1-2, pp. 1–55, 2009.

[34] G. 't. Hooft, "Dimensional reduction in quantum gravity," in *Proceedings of the Highlights of Particle and Condensed Matter Physics (SALAMFEST)*, pp. 284–296, Trieste, Italy, 1993.

[35] S. Thomas, "Holography stabilizes the vacuum energy," *Physical Review Letters*, vol. 89, no. 8, Article ID 081301, 2002.

[36] R. G. Cai, B. Hu, and Y. Zhan, "Holography, UV/IR relation, causal entropy bound, and dark energy," *Communications in Theoretical Physics*, vol. 51, Article ID 954, 2009.

[37] C. Gao, F. Wu, X. Chen, and Y.-G. Shen, "Holographic dark energy model from Ricci scalar curvature," *Physical Review D: Particles, Fields, Gravitation and Cosmolog*, vol. 79, no. 4, article 043511, 2009.

[38] C. Furtado, J. R. Nascimento, A. Y. Petrov, and A. F. Santos, Dynamical Chern-Simons modified gravity and Friedmann-Robertson-Walker metric, 2010, https://arxiv.org/abs/1005.1911v3.

[39] A. Sen, "Rolling tachyon," *Journal of High Energy Physics*, vol. 2002, article 048, 2002.

[40] A. Sen, "Tachyon matter," *Journal of High Energy Physics*, vol. 2002, article 065, 2002.

[41] A. Sen, "Field theory of tachyon matter," *Modern Physics Letters A*, vol. 17, no. 27, pp. 1797–1804, 2002.

[42] G. W. Gibbons, "Cosmological evolution of the rolling tachyon," *Physics Letters B*, vol. 537, no. 1-2, pp. 1–4, 2002.

[43] S. Mukohyama, "Brane cosmology driven by the rolling tachyon," *Physical Review D: Particles, Fields, Gravitation and Cosmology*, vol. 66, no. 2, Article ID 024009, 2002.

[44] A. Feinstein, "Power-law inflation from the rolling tachyon," *Physical Review D: Particles, Fields, Gravitation and Cosmology*, vol. 66, no. 6, Article ID 063511, 2002.

[45] T. Padmanabhan, "Accelerated expansion of the universe driven by tachyonic matter," *Physical Review D: Particles, Fields, Gravitation and Cosmology*, vol. 66, no. 2, Article ID 021301, 2002.

[46] A. A. Starobinsky, "How to determine an effective potential for a variable cosmological term," *Journal of Experimental and Theoretical Physics Letters*, vol. 68, no. 10, pp. 757–763, 1998.

[47] C. Armendariz-Picon, V. Mukhanov, and P. J. Steinhardt, "Dynamical solution to the problem of a small cosmological constant and late-time cosmic acceleration," *Physical Review Letters*, vol. 85, no. 21, pp. 4438–4441, 2000.